AVIDAN, AMOS A.

BED EXPANSION AND SOLID MIXING IN HIGH VELOCITY FLUIDIZED BEDS

City University of New York PH.D. 1980

PLEASE NOTE:

In all cases this material has been filmed in the best possible way from the available copy. Problems encountered with this document have been identified here with a check mark ✓.

1. Glossy photographs _____
2. Colored illustrations _____
3. Photographs with dark background _____
4. Illustrations are poor copy _____
5. Print shows through as there is text on both sides of page _____
6. Indistinct, broken or small print on several pages ✓
7. Tightly bound copy with print lost in spine _____
8. Computer printout pages with indistinct print _____
9. Page(s) _____ lacking when material received, and not available from school or author
10. Page(s) _____ seem to be missing in numbering only as text follows
11. Poor carbon copy _____
12. Not original copy, several pages with blurred type _____
13. Appendix pages are poor copy _____
14. Original copy with light type _____
15. Curling and wrinkled pages _____
16. Other _____

BED EXPANSION AND SOLID MIXING IN HIGH VELOCITY FLUIDIZED BEDS

by

Amos A. Avidan

A dissertation submitted to the Graduate Faculty in Engineering in partial fulfillment of the requirements for the degree of Doctor of Philosophy , The City University of New York.

1 9 8 0

This manuscript has been read and accepted for the Graduate Faculty in Engineering in satisfaction of the dissertation requirement for the degree of Doctor of Philosophy.

26 June 1980
date

Chairman of Examining Committee

July 1, 1980
date

Executive Officer

Prof. R.A.Graff (Chairman)

Dr. J.Yerushalmi

Prof. H.Weinstein

Prof. L.Jiji

City University of New York

Abstract

High velocity gas fluidization is a unit operation which brings gas and solid into intimate contact. It includes the turbulent and fast fluidization regimes which lie beyond the low velocity bubbling or slugging regimes. Bed expansion and solid mixing were studied in 15.2 - cm I.D. rigs, of high aspect ratios: a circulating system 8.5 m tall, and an expanded top bed, 3.5 m tall. Fine cracking catalysts of Geldart's group A classification were used and air at ambient conditions served as the fluidizing medium. The gas velocities investigated were in the range 0.075 - 6.5 m/s and the solid rate in the upper end of the fast fluidization regime topped 150 $kg/m^2.s$.

The Two-Phase Theory is shown not to apply when the gas velocity is raised beyond the slugging regime: the bed structure becomes more homogeneous. Particulate like fluidization describes these high velocity regimes. A modified Richardson-Zaki approach is used to correlate bed expansion. It is shown to confirm the more homogeneous nature of the turbulent and fast regimes, and the validity of the concept of clusters - or the tendency of fine particles to aggregate. This clustering phenomenon is quite complex.

Solid mixing was studied with a ferromagnetic tracer and modelled by a turbulent eddy diffusivity dispersion model. Results in the low velocity expanded top bed show a maximum for the axial dispersion coefficient in the slugging regime. The dispersion coefficients in the turbulent regime are uniform throughout the bed and depend on the mode of solid recirculation - they are higher than those in the slugging regime when

the recirculation is from the top (the expanded top bed). The axial Péclet number goes through a minimum in the fast fluidization regime (a gas velocity of 3.5 m/s, a solid rate of 100 $kg/m^2.s$ and a voidage of 0.82), qualitatively in agreement with results from liquid - solid systems. The dependence of the axial dispersion coefficient on bed diameter is shown to be linear by a steady state density fluctuation analysis. Some implications for heat transfer in a high velocity fluidized bed are discussed.

Acknowledgements

I want to express my sincere thanks and appreciation to Dr. Joseph Yerushalmi for his help and trust.

I am also thankful to Professor R.A.Graff for his constant encouragement. Helpful discussions with Professors H. Weinstein and R. Shinnar are gratefully acknowledged.

Special thanks to Professor T. Fitzgerald from Oregon State University for his help in setting up the solid mixing experiments. Some of the experimental results were obtained with the help of A. Chau and J.J. Louis.

The work was supported by the U.S. Department of Energy under contract EX-76-S-01-2340.

"Notte e giorno faticar
per chi nulla sa gradir;
piova e vento sopportar,
mangiar male , e mal dormir."

Mozart, "Don Giovanni"

Table of Contents

Table of Contents (cont.)

List of Figures

List of Figures (cont.)

List of Figures (cont.)

List of Figures (cont.)

List of Figures (cont.)

List of Tables

List of Tables (cont.)

Nomenclature

c - Local volume fraction of tracer (downflow phase).

C - Local volume fraction of tracer (upflow phase).

$c(t)$ - Tracer concentration at a solid mixing probe (mV).

c^{∞} - Tracer concentration in the expanded top bed at steady state.

d_p - Volume-surface mean diameter; $d_p = 1/\Sigma(x_i/d_i)$

d_i - Particle diameter in a given size cut

D_t - Column diameter.

D_c - Effective cluster diameter.

D_{SA} - Axial solid dispersion coefficient based on total cross-sectional area.

D_{Sp} - Axial solid dispersion coefficient based on solid phase area.

f - Volume fraction (downflow phase).

F - Volume fraction (upflow phase).

g - Acceleration due to gravity.

Ga - Galilleo Number, $Ga = \dfrac{\rho_g(\rho_s-\rho_g)gd_p^3}{\mu^2}$

G_s - Solid rate per bed unit area.

H - Height of the bed (Stationary Bed).

h_{AB} - Renewal density.

kg - Gas transfer coefficient.

k_s - Solid transfer coefficient

K - Volume of aggregates per unit volume of solid.

L - Length of bed.

m - Volume fraction of tracer injected.

n - Index in the Richardson-Zaki equation.

n' - The effective index n if the suspension is considered to be large clusters (i.e. $n' \cong 2.4$).

Pe - Péclet number.

q - Volumetric flow rate of gas (downflow).

Q - Volumetric flow rate of gas (upflow).

Re - Reynolds number, $Re = \frac{U\rho_g d_p}{\mu}$

Re_t - Reynolds number based on the single particle terminal velocity.

Re_c - Reynolds number based on cluster size.

t - Time

T - Period of oscillation (the distance between two successive peaks).

U - Superficial velocity.

U_c - the velocity at which the pressure fluctuations across a bubbling bed begin to diminish from their peak value.

U_k - The onset of the turbulent regime.

U_s - Mean solid velocity.

U_T - Terminal velocity of a particle of size $\bar{d}_p$.

U_{TR} - Transport velocity.

U_{slip} - Slip velocity.

U_T^* - Effective cluster terminal velocity.

v - Linear velocity (downflow).

V - Linear velocity (upflow).

W_B - Local flux of solids

x - Axial coordinate.

X - Non-dimensional spacing between slugs (distance/D_t) in eq. 4.41.

Greek Symbols

ϵ - Void fraction (porosity).

$\bar{\epsilon}$ - Average void fraction.

ϵ_a - Apparent voidage (eq. 3.9).

ϵ_c - Cluster voidage.

ϵ_e - Effective voidage (eq. 3.8).

ϕ_s - Sphericity of particles.

ρ - Density

$\bar{\rho}$ - Bed density.

K - Effective axial thermal conductivity.

$\left(\frac{\Delta P}{\Delta L}\right)$ - Pressure drop per unit length.

τ - Characteristic time.

μ - Gas viscosity.

Subscripts

g - gas

s - solids

0 - minimum fluidization

T,t - terminal

P - particle

Chapter 1: Introduction *

1.1 Historical

Gas fluidization is a unit operation which brings gas and solid into intimate contact. Although references bearing on the fluidized technique can be found as far back as 1878, fluidization as it is known today was born from the pioneering work of Standard Oil Development Company, the M.W. Kellog Company, and Standard Oil of Indiana in their efforts to find a better catalytic cracking process than the fixed-bed process which was introduced commercially in 1937.

The first commercial fluid catalytic cracking plant operated in the fast bed mode. The plant, whose reactor and regenerator measured, respectively, 4.5 and 5.9 m in inside diameter, was erected at the Baton Rouge refinery of the Standard Oil of New Jersey (now Exxon). It was placed in operation on May 25, 1942 "with surprisingly little difficulty" (Murphree, et al., 1943). That research enjoyed the input of MIT Professors Lewis and Gilliland. Along with the fast fluidized bed they considered two other options. The then new bubbling fluidized bed offered the advantage of a large surface of contact between gas and solid per unit reactor volume and temperature uniformity throughout the bed. However, its characteristic low gas velocities implied low gas-treating capacities. High gas throughputs could be achieved by contacting a high-velocity

*Large portions of this chapter are based on Yerushalmi (1980,a) and Cankurt et al. (1980).

gas stream with solid in dilute-phase flow, but the low solid concentrations typical to this condition would have required, save in cases of unusual catalyst activity, very tall vessels or use of multiple-tube coiled reactors. Also, dilute-phase reactors often exhibited a temperature gradient along the flow path.

Operation in the fast bed regime was thus chosen since, in the words of Lewis and Gilliland (1950), it could "secure in large degree the advantages of both types of operation just described, and at the same time eliminate or greatly reduce the disadvantages."

The name fast bed was coined much later (Yerushalmi, et al., 1976). Lewis and Gilliland and Standard Oil's engineers simply regarded the fast fluid bed as just another mode of fluidization, and referred to it as the "upflow" operation to distinguish it from low-velocity bubbling fluidization which they termed "downflow" operation (Fig.1.1). Lewis and Gilliland (1950) described it in this way:

"If one will operate at a gas velocity sufficient to blow all or substantially all of the solid material out of the reactor in a relatively short time, provided no fresh solid material be introduced during this time, but will feed into the reactor simultaneously solid material at a sufficiently high rate, one can maintain in the reactor a high concentration of solid granules approaching that of the 'liquid state' [of the bubbling fluid bed]....and yet be blowing the solid particles out of the top of the reactor at a corresponding rate." Lewis and Gilliland reported the results of experiments with a pulverized clay catalyst (with a settled density of 560 kg/m^3) in which a fluidized density as high as 160 kg/m^3 was maintained at a gas velocity of

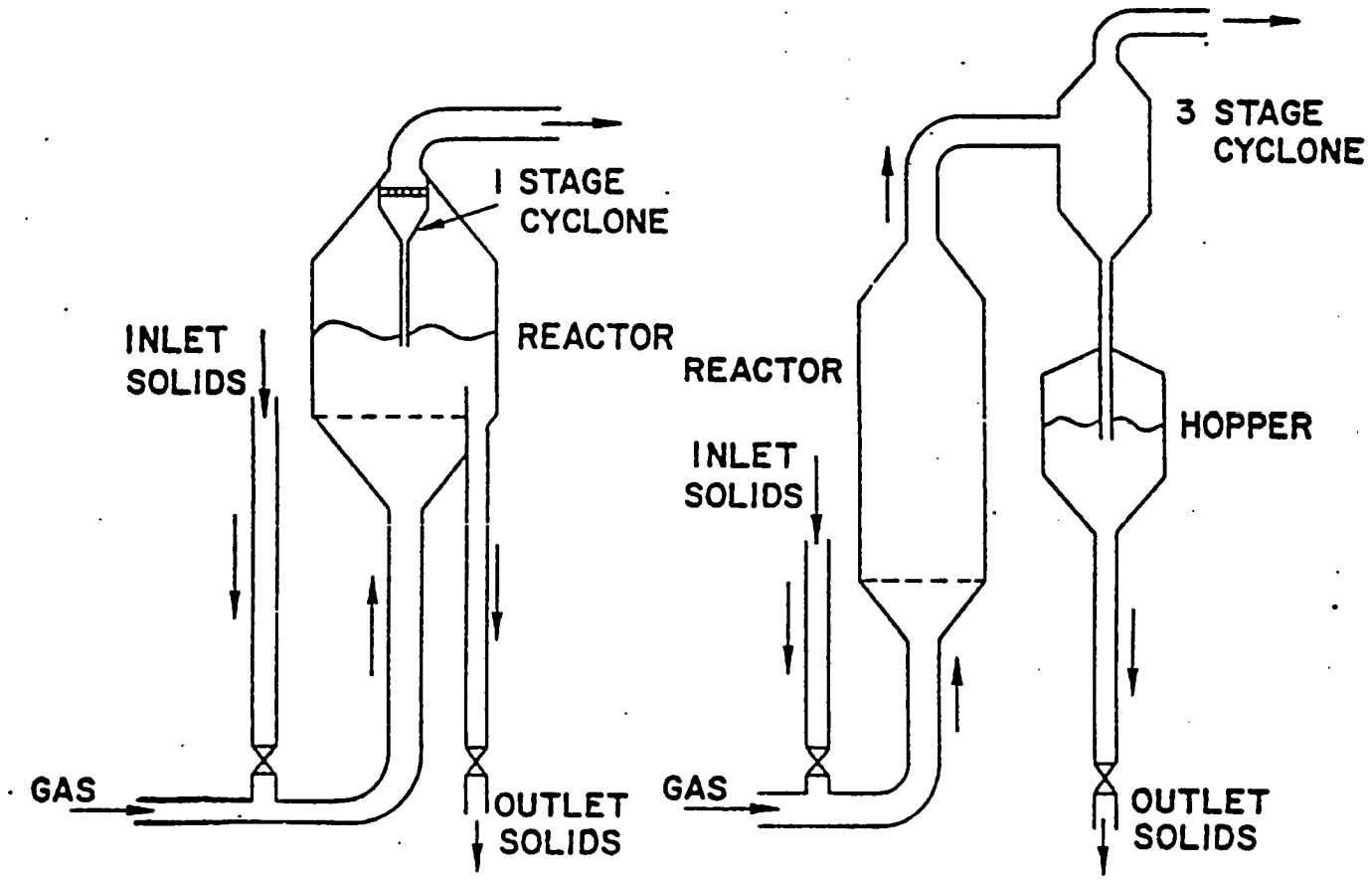

Fig. 1.1. The upflow (fast bed) design used in the first fluid cat cracker, and the downflow (bubbling bed) design used in later models (Murphree, et al., 1944).

2.4 m/sec.

The success of the first fluid cat cracker led the way to additional installations, and by the end of 1943 several upflow plants had gone into production. The operation of these plants, however, was not free of difficulty. Dust collection, and control of solid holdup in the reactor and regenerator posed problems. From today's vantage point, these plants appear to have been poorly designed, particularly insofar as the cyclones and standpipes are concerned. As a result, and on the spur of the war effort, industry switched to the bubbling fluid where carryover rates were kept low and dust recovery was accordingly easier, the height of the solid interface could be set at will, and where the mechanical design was on the whole simpler (Murphree, et al., 1944). Those who had earlier expounded the qualities of the upflow plants (Murphree, et al., 1943) were now singing the praise of "the new improved" downflow technique.

When the war ended, it was the bubbling bed that emerged as fluidization's archetype, and the upflow plants and the principles they embodied were all but forgotten.

The process engineer, however, often turns toward higher gas velocities not only for higher throughputs, but also as possible means of improving performance, smoothing instabilities, and overcoming the tendency of sticky particles to agglomerate. Over the years, one by one it seems, few fluid bed processes employing high velocity beds emerged. Today, industry can offer an ample catalogue of these processes, which beacon several advantages on the part of high velocity fluid bed over the bubbling bed. Among these

advantages are higher processing capacities, more efficient contact between gas and solid, and a capability to receive and handle cohesive solids.

1.2 High Velocity Fluidization Regimes

Research in the Clean Fuels Institute of The City College of New York has delineated the various high velocity fluidization regimes. These regimes start with the turbulent regime, which results from raising the gas velocity in a heterogeneous, bubbling fluidized bed (fig. 1.2a). The two-phase character of the bed first peaks, then gradually changes giving way to a condition of increasing uniformity culminating in the turbulent state (fig. 1.2b) in which large discrete bubbles or voids are on the whole absent.

In the turbulent fluidized bed, there is an upper bed surface though it is considerably more diffuse than in a bubbling fluidized bed because of the greater freeboard activity attending operation at higher gas velocities.

The turbulent regime extends to the so-called transport velocity. As the transport velocity is approached, there is a sharp increase in the rate of particle carryover, and in the absence of solid recycle, and the bed would empty in short order. Beyond the transport velocity, solid fed to the bottom of the column or vessel traverses it in fully entrained transport flow, and the concentration or density of the resulting suspension depends not only on the velocity of the gas, but also on the solid flow rate. If the solid rate is low, dilute-phase flow will result. If, on the other hand, solid is fed to the column at a sufficiently high rate -- for example, by circulating solid carried over from the column to its bottom via external cyclones and a standpipe -- then it is possible to maintain

in the column a relatively large solid concentration typical to the fast fluidized bed condition (Fig. 1.2c).

1.3 Transition from Bubbling to Turbulent Fluidization

Lanneau (1960) was the first to quantitively describe the transition from bubbling to turbulent fluidization. He represented the degree of non-uniformity by a "heterogeneity" parameter defined as the mean deviation of the instantaneous point density from the time-averaged bed density (fig. 1.3). Kehoe and Davidson (1971), working in transparant equipment and utilizing capacitance probes, reported that the transition to the turbulent regime occurred at

$$U_g > 3U_{T,min} \qquad (1.1)$$

where $U_{T,min}$ is the terminal velocity of particles belonging to the smallest cut. Since then, the transition from bubbling to turbulent fluidization has been the subject of a number of investigations (Carotenuto, et al., 1974, Crescitelli, et al., 1978, Thiel and Potter, 1977; at General Electric, Canada, et al., 1976, and Staub and Canada, 1978; and at The City College of New York, Yerushalmi, et al., 1976, 1978a, Cankurt and Yerushalmi, 1978, Yerushalmi and Cankurt, 1978, 1979, and Turner, 1978). The test conditions, experimental methods, and the results of these investigations are summarized in Table 1.1.

While the phenomenon of bubble breakup and transition to a more homogeneous regime is very complex some trends are evident:

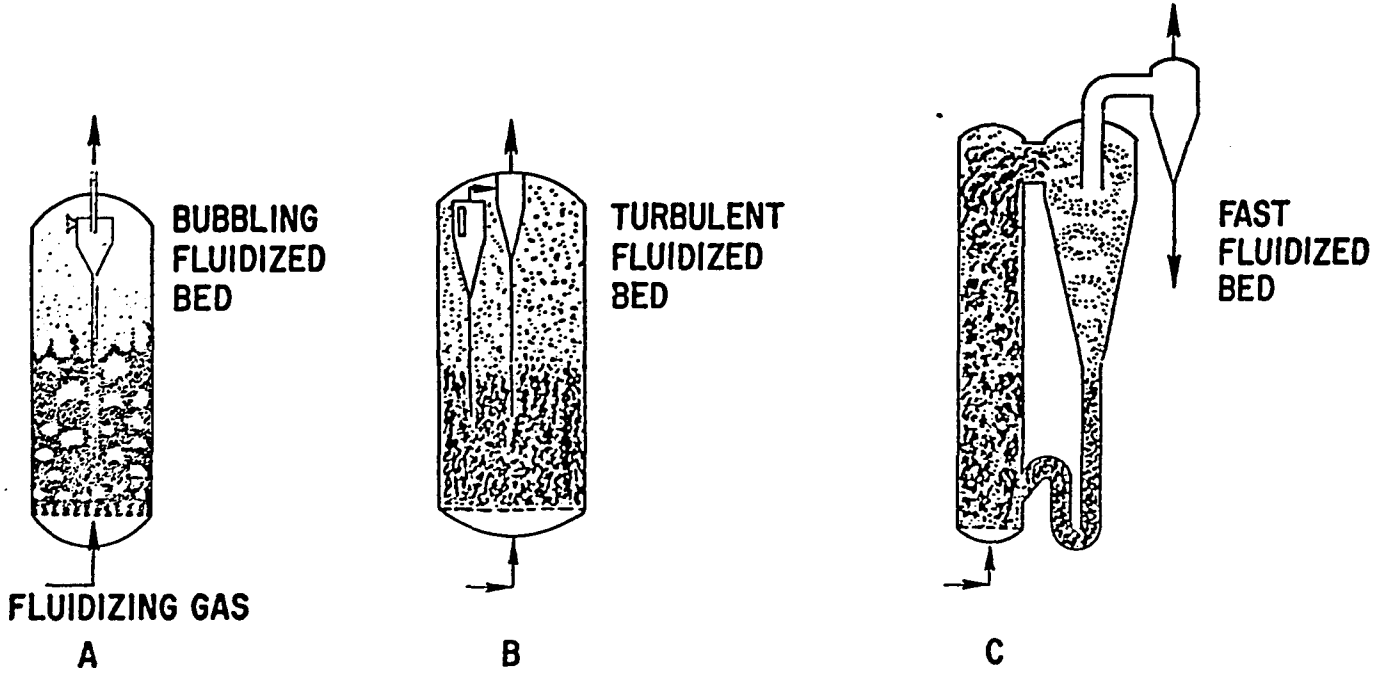

Fig. 1.2 Schematics of (A) bubbling, (B) turbulent, and (C) fast fluidized beds.

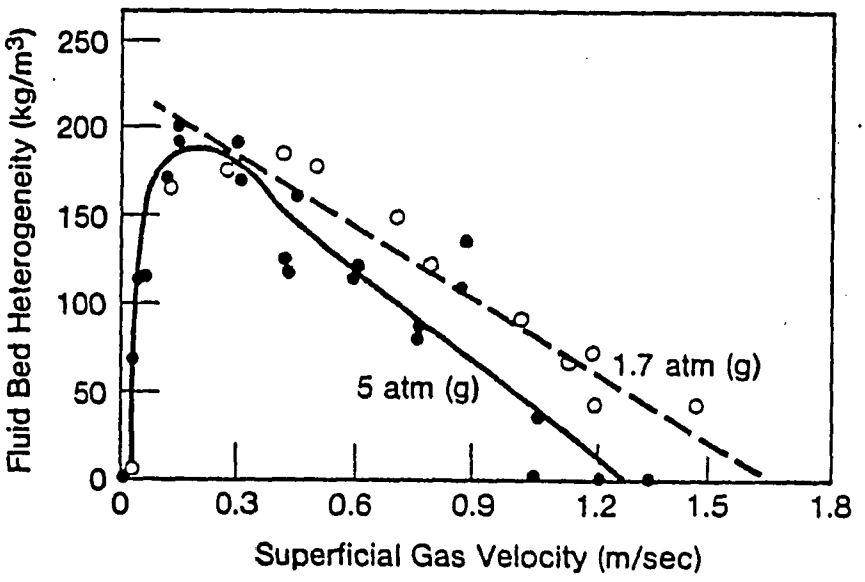

Fig. 1.3 Lanneau's heterogeneity - the mean deviation of the instantaneous point density from the time-averaged bed density (from Lanneau, 1960).

Table 1.1 Transition from bubbling to turbulent fluidization.
Summary of test conditions and results.

Solids	Size Range (microns)	Mean Diameter[1] (microns)	Particle Density (gm/cc)	Particle Sphericity	Experimental Methods[2]	Apparatus	Pressure Level (atm.)	U_t (cm/s)	U_c (cm/sec)	U_k (cm/sec)	U_k/U_t
					LANNEAU (1960)						
Catalyst	30-150	70	2.0	NA	C	7.5-cm I.D.	1.7	27	30	uncertain	--
"	"	"	"	"	"	"	5.0	21	30	"	--
					KEHOE AND DAVIDSON (1971)						
Catalyst A	15-43	22[3]	1.1	NA	X	10-cm I.D.	1.0	1.6	--	11.0	6.8
Ballotini	15-43	22[3]	2.2	NA	X	"	"	3.2	--	35.0	11.0
"	"	"	"	"	C	5-cm I.D.	"	"	--	40.0	12.5
"	"	"	"	"	"	6.2x0.6 cm	"	"	--	35.0	11.0
Catalyst B	15-90	26[3]	1.1	"	C,X	10-cm I.D.	"	2.3	--	18.0	7.8
"	"	"	"	"	C	6.2x0.6 cm	"	"	--	17.0	7.4
"	"	"	"	"	C	10-cm I.D.[4]	"	"	--	32.0[4]	14.0
Catalyst	40-90	55[3]	1.1	"	X	"	"	10.0	--	44.0	4.0
"	"	"	"	"	C	5-cm I.D.	"	"	--	50.0	5.0
"	"	"	"	"	C	10-cm I.D.[4]	"	"	--	>>50.0	>>5.0

Table 1.1 (cont.)

MASSIMILLA (1971)											
Catalyst	NA	56	1.9[5]	.	C	15.6-cm I.D.	1.0	9.5	--	30-40.0	31.-4.2
THE CITY COLLEGE STUDIES											
Dicalite	0-160	33	1.67	0.4	PDF	15.2-cm I.D.	1.0	2.3	53.0	107.0	47.1
FCC[6]	0-130	49	1.07	1.0	"	"	"	7.8	61.0	61.0	7.8
HFZ-20	0-130	49	1.45	1.0	"	"	"	10.6	91.0	137.0	12.9
"	"	"	"	"	PT	5 x 51 cm	"	"	61.0	107.0	10.9
Alumina	40-200	103	2.46	1.0	PDF	15.2-cm I.D.	"	58.2	122.0	274.0	4.7
"	"	"	"	"	PT	5 x 51 cm	"	"	137.0	255.0	4.4
Sand	80-670	268	2.65	0.8	PDF	15.2-cm I.D.	"	116.0	274.0	550.0	4.7
"	"	"	"	"	PT	5 x 51 cm	"	"	150-215	Uncertain[7]	--
Glass	105-210	157	2.42	1.0	PT	"	"	95	150-215	"	--
CANADA ET AL. (1976)											
Glass	550-750	650	2.48	1.0	PT,C	0.3x0.3 m and 0.61x0.61 m	1-10.0	varies with pressure	NA		0.5-0.65
Glass	2500-2700	2600	2.92	1.0	"	"		"	NA		0.3-0.35

Table 1.1 (cont.)

THIEL AND POTTER (1977)												
FCC	0-180	60	0.93	NA	V	5.1-cm I.D.	1.0	10	--	41	4.1
"	"	"	"	"	"	10.2-cm I.D.	"	"	--	22	2.2
"	"	"	"	"	"	21.8-cm I.D.	"	"	--	2.5	0.25
CARETENUTO ET AL. (1974), CRESCITELLI ET AL. (1978)												
Catalyst	NA	60	0.94	NA	PT,C	15.2-cm I.D.	1.0	10.0	--	20.0	2.0
Alumina	"	95	1.55	"	"	"	"	36.0	--	100.0	2.8
Ludox	"	60	1.4	"	"	"	"	15.0	--	33.0	2.2

[1] Unless otherwise indicated, the volume-surface mean diameter, $\bar{d}$, is used.

[2] C = Capacitance probes; X = X-ray photography; PDF = Pressure drop fluctuations; PT = Pressure transducers; V = Visual

[3] The mean diameter was computed from $\frac{1}{0.5/\text{smallest cut} + 0.5/\text{largest cut}}$

[4] The bed depth was 255 cm; in all other experiments conducted by Kehoe and Davidson, bed heights ranged below 170 cm.

[5] Assumed, see table 3.3

[6] FCC = Fluid cracking catalyst

[7] Owing to wall effects

Transition velocities. The transition from bubbling to turbulent fluidization is gradual and spans a range of gas velocities which depend on the properties of gas and solids and on equipment scale as well. The transition may be bracketed and thus characterized by two velocities: U_c the velocity at which the pressure fluctuations peak, and U_k, the velocity at which the fluctuations, having decayed from their peak value, beging to level off. U_k marks the end of the transition and the onset of the turbulent regime. Results for four solids investigated in the CCNY test stand (described in Chapter 3) are shown in fig. 1.4. Fig. 1.4 gives the relative pressure fluctuations -- i.e., the fluctuations of the pressure drop across the bed divided by the mean pressure drop -- as a function of the superficial gas velocity. Corresponding to each data point, the figure also displays the fluidized density reckoned from the mean pressure drop across the bed and the bed depth. Unlike the City College investigators, most results reported in table 1.1 represent a single transition velocity, and often it is not clear how it was defined.

The ratio U_k/U_T. The last column of table 1.1 shows the ratios of the transition velocity U_k to the terminal velocity, U_T, of a particle of size $\bar{d}_p$. The ratios are strongly dependent on the particle's size and density. The ratios approach and even exceed 10 for the finer solids, and decrease sharply with particle size and density. For the coarse glass beads tested by Canada, et al., U_k/U_T falls below unity and lies in the range of 0.5 - 0.65 for the 650 microns glass, and 0.3 - 0.35 for the coarser, 2600 microns solid.

Effect of particle size and size distribution. Although the results summarized in table 1.1 do not lend themselves

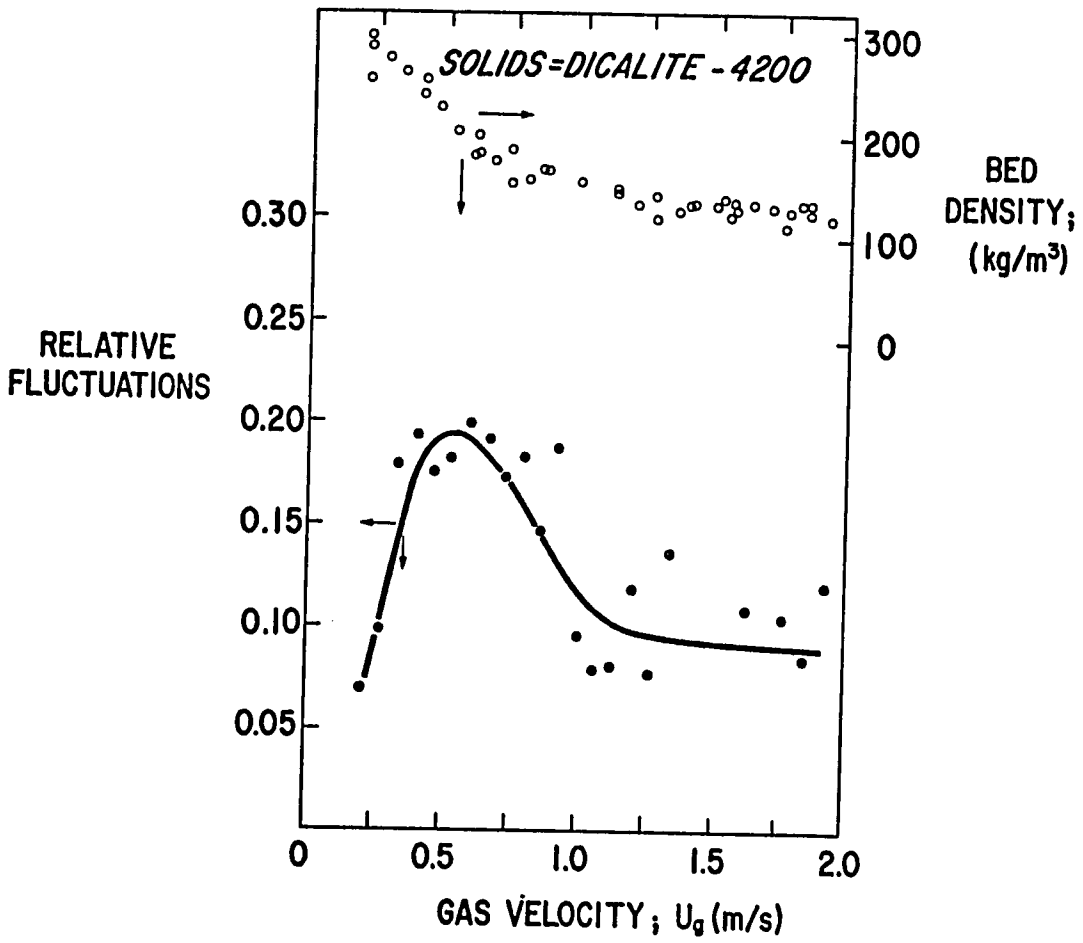

Fig. 1.4a. Pressure fluctuations relative to the mean pressure drop across a fluid bed of Dicalite. The upper curve gives the corresponding mean pressure drop across the bed.

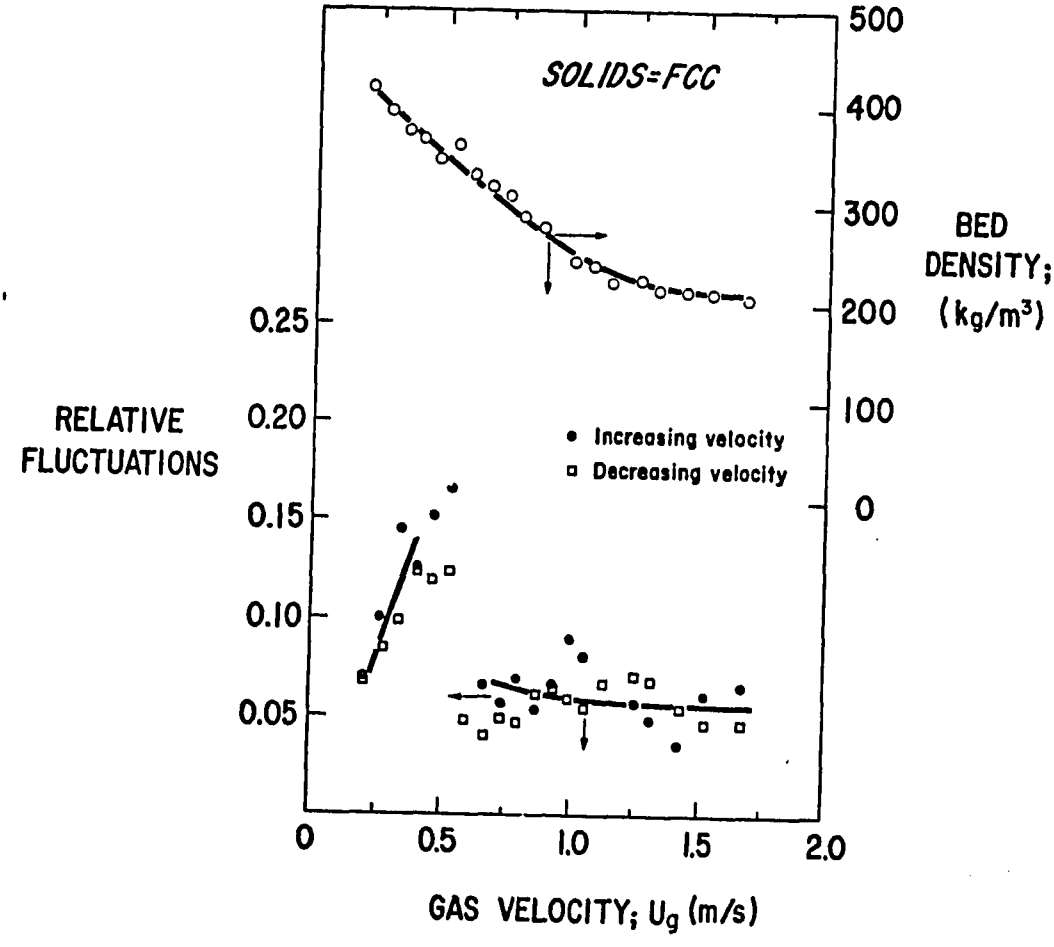

Fig. 1.4b. Pressure fluctuations relative to the mean pressure drop across a fluid bed of fluid cracking catalyst (FCC). The upper curve gives the corresponding mean pressure drop across the bed.

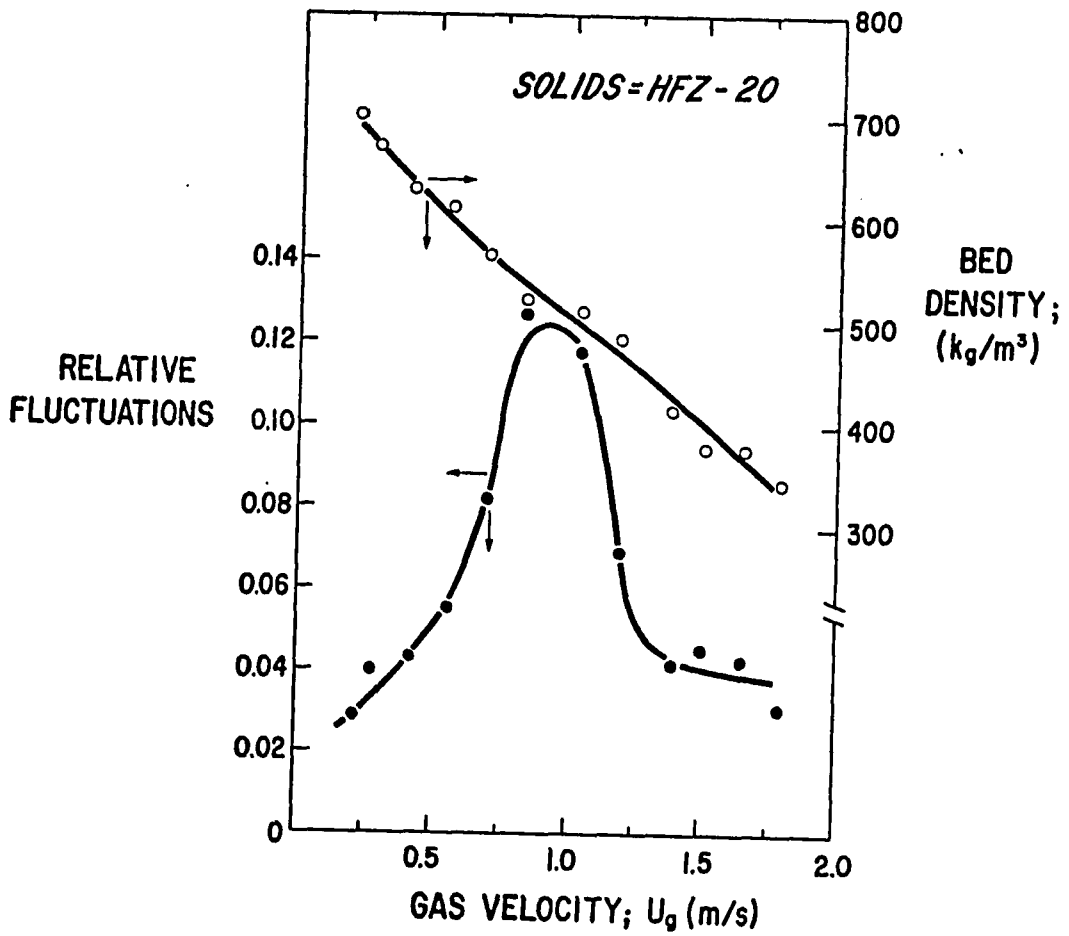

Fig. 1.4c. Pressure fluctuations relative to the mean pressure drop across a fluid bed of HFZ-20. The upper curve gives the corresponding mean pressure drop across the bed.

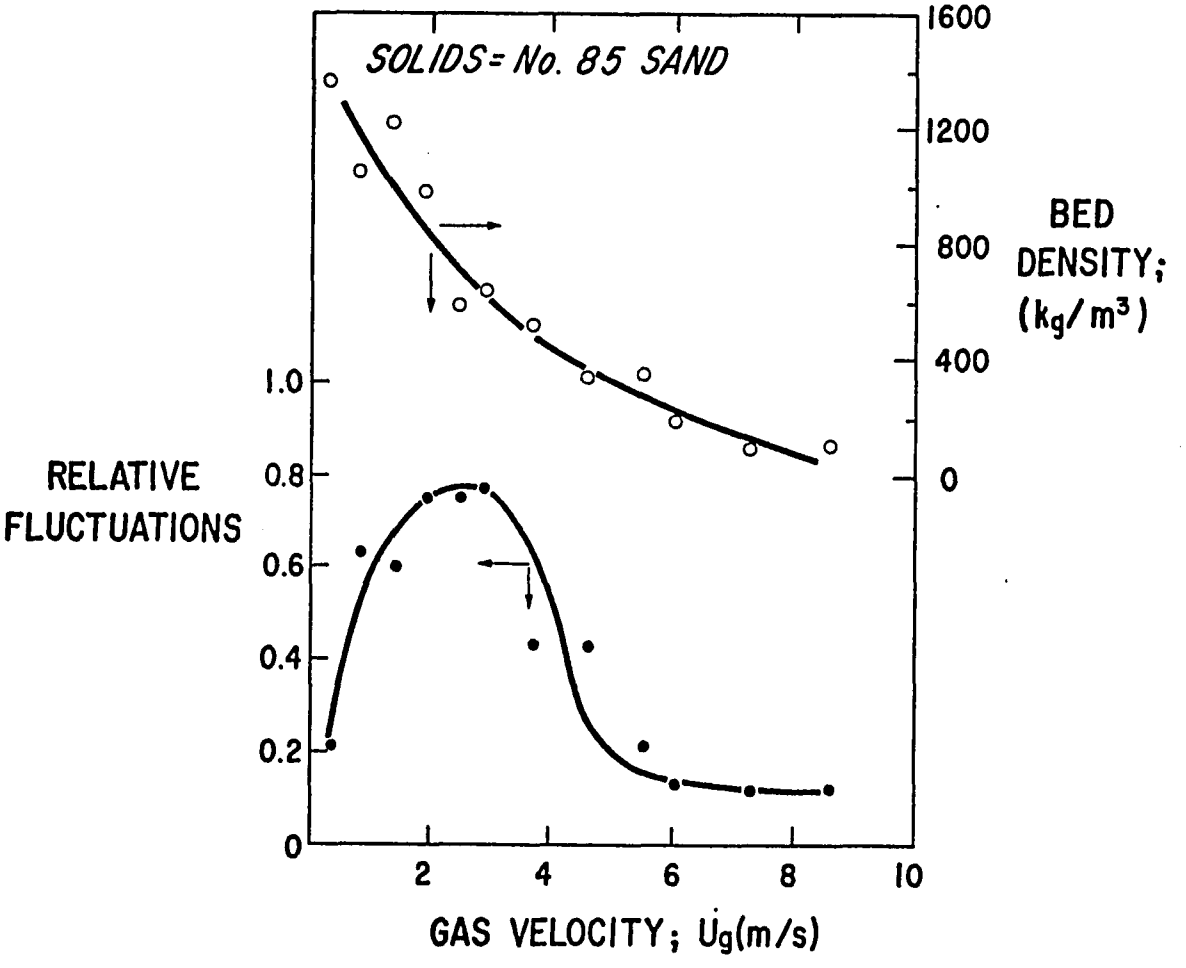

Fig. 1.4d. Pressure fluctuations relative to the mean pressure drop across a fluid bed of sand. The upper curve gives the corresponding mean pressure drop across the bed.

to exact correlations, they do clearly indicate that both U_c and U_k increase with particle size and density.

Little information, however, is available on the effect of particle size distribution. Kehoe and Davidson added the finest catalyst (A) to catalyst C to obtain catalyst B, and noted that as a result the transition velocity was lowered significantly. This is not surprising since the mean size of catalyst B is considerably smaller than that of catalyst C. Information on the effect of size distribution for solids having comparable mean size is lacking. The effect of size distribution on the transition to turbulence is further discussed in section 3.4.4.

Effect of bed height. Canada, et al. report no apparent effect of bed height over a range of 25 to 70 cm. Kehoe and Davidson, on the other hand, report that (for catalyst B and C) a bed 255 cm in height gave rise to transition velocities higher than those recorded in beds of the same solids ranging in heights to only 170 cm. The shallower beds, they argue, support a greater degree of slugs coalescence and the approach to the "breakdown" velocity is accordingly faster. Lanneau (1960) conducted his experiments in a bed 4.6 m deep and he notes that the bed structure could vary significantly with bed height. Our work with the experimental test stand described in Chapter 3 conforms this observation, and table 3.4 includes different values of the superficial gas velocity at which transition to turbulence is observed for different positions in the bed. Figure 1.5 shows the pressure fluctuation for FCC in the circulating system (described in Chapter 3) at two locations in the bed. The transition to turbulence is taking place at a lower gas velocity in the middle section

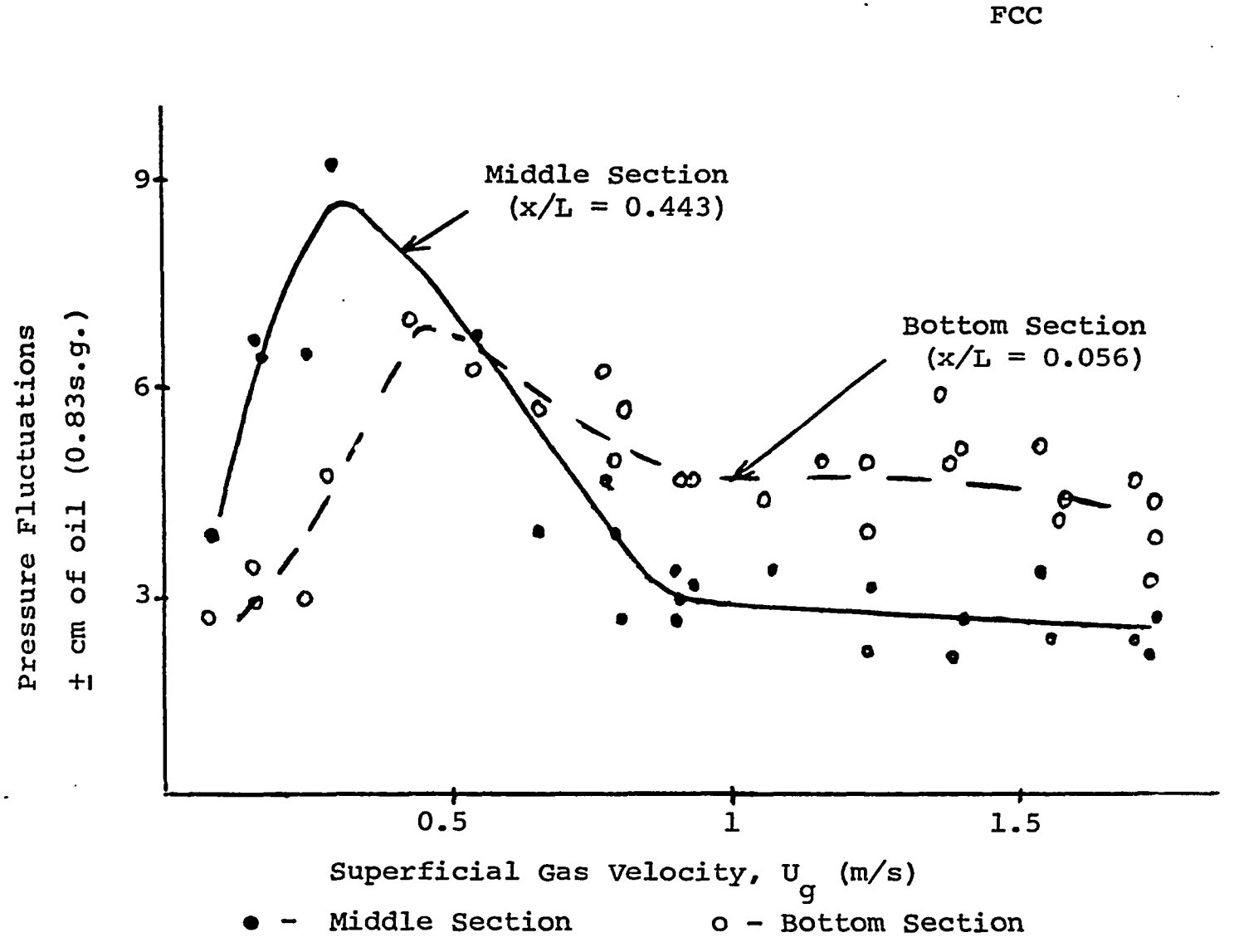

Fig. 1.5. Pressure fluctuations for FCC in the circulating 15.2-cm I.D. system at two locations.

of the bed than in the bottom section.

Effect of pressure. Canada, et al. report that, at the same gas velocity, the fluidization grows smoother, as reckoned from the relative pressure fluctuations, as the pressure is raised. For a given solid, the transition velocity U_k decreases with increasing pressure, but over the range of 1 - 10 atm., the ratio of U_k to the particle's terminal velocity, v_t, remained essentially constant, 0.5 - 0.65 for the 650 microns glass, and 0.3 -0.35 for the coarser 2400 microns solid.

Effect of bed size. The results of Kehoe and Davidson, and especially of Thiel and Potter indicate that for a given solid the transition velocity U_k decreases with increasing bed size. The City College results corroborate this if comparison is drawn between the data from the 15.2 cm column and from the two-dimensional bed. In the latter, the transition generally came into play at lower gas velocities. Now, the two-dimensional bed is comparable in cross-sectional area to the 15.2 cm column, but it does afford growth of bubbles larger than 15.2 cm and in that respect could be regarded as effectively larger. The effect of bed diameter is also illustrated in the results of Zenz and Othmer (1960), shown in fig. 3.7. As the bed diameter is increased, the absolute rise velocity of slugs increases and the bed expands to a lesser degree. In large bed diameters slugs have more freedom to coalesce and twist, accelerate each other, and thus bring about a transition to turbulence at a lower superficial gas velocity. This mechanism is discussed further in chapter 3.

In summary, the transition to turbulent fluidization involves the gradual breakdown of large bubbles (or slugs) into smaller bubbles and voids. The process of bubble splitting

is to some extent counterbalanced by coalescence of the resulting smaller bubbles, but the net effect is a progressive change toward a structure of greater homogeneity, culminating in the turbulent state where on the whole large discrete bubbles are absent, and traces from capacitance probes no longer register a clear periodic element. To be sure, a relatively large void or slug will occasionally form, travel some distance up, and soon disperse. This and the recurring process in which the small voids split, coalesce and accelerate do lend the phenomena some apparent periodic character. To one viewing a turbulent fluid bed this impression may be particularly strong when the bed is narrow and where accordingly the voids tent to segregate toward the center leaving the wall region fairly dense, and when the bed material is coarse.

1.4 The Turbulent Regime

The change that takes place as the velocity of the gas spans the transition from bubbling to turbulent fluidization may be described as a process of dispersion. Large bubbles and slugs split dispersing as smaller voids in the solid. Simultaneously, the dense phase expands, but the expansion is not uniform. Instead, the solid too disperses, dividing by the action of the lean phase into clusters and streamers. As a result, the structure of a turbulent fluid bed is more homogeneous consisting of two phases, of which neither can be viewed as either continuous or discontinuous.

The steady process of coalescence and splitting of the lean phase voids sets into motion a similar phenomenon in the dense phase. Together these lend the regime its "turbulent" character. Solid mixing is vigorous, the interaction of the two phases is strong, and the contact between gas and

solid, as Massimilla's experiment (fig. 1.6) plainly shows, is highly efficient. The relatively high solid concentration coupled with the high degree of solid mixing are likely to result in high heat transfer rates to immersed surfaces, especially in beds of fine solids, but I know of no relevant data.

The structure of the turbulent fluid bed depends strongly on the transition velocity U_c. If U_c is small, as the case would be in beds of small particles, the size of the bubbles (slugs) attained before the onset of the transition would be relatively small, and the scale of the demixing of gas and solid in the resulting turbulent bed would be fine. In beds of coarse solids, on the other hand, U_c would be relatively high, the size of the bubbles attained before the transition commenced would be correspondingly larger, and the structure of the resulting turbulent bed would be more open, marked by wider channels and by a grosser scale of the demixing patterns of gas and solid. These observations are borne out by photographs of the transitions in two-dimensional beds presented by Kehoe and Davidson (1971).

The existence of clusters and the concept which attaches to them some effective size are useful in understanding the range of the turbulent regime for a fine solid. First, however, consider a fluidized bed of closely sized coarse particles, such as those which figured in the experiments of Canada, et al. (1976). The turbulent regime for the 2600 μm glass, for example, extends from around $(0.3 - 0.35)U_T$ up to a velocity at least equal to U_T. Over this range, since the gas velocity lies below the terminal velocity of the individual particle no carryover will be experienced provided

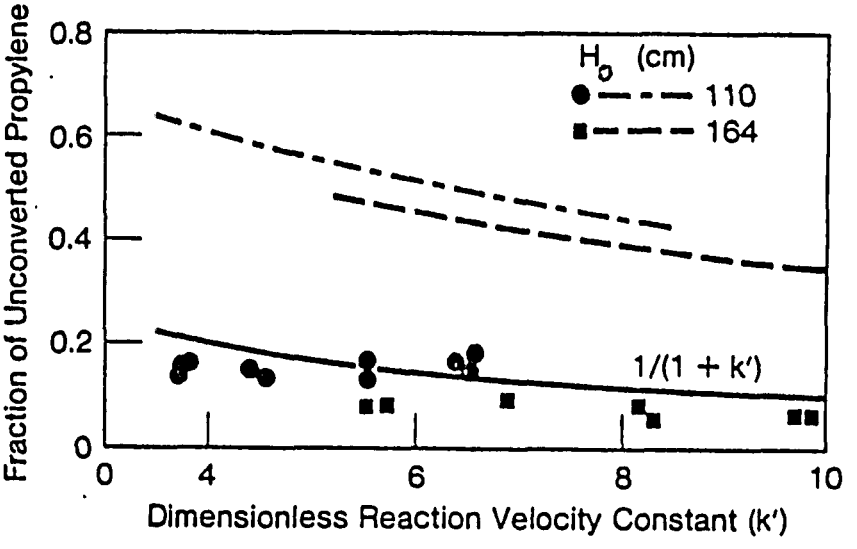

Fig.16. Ammonoxidation of propylene to acrylonitrile in a turbulent fluid bed (from Massimilla, 1973). $k' = \beta H_o / U_g$ where β is the reaction velocity constant, sec^{-1}. The upper dashed curves are predictions based on a slug flow model (Hovmand and Davidson, 1971).

the freeboard is sufficiently high.

A somewhat analogous situation holds for a turbulent bed of a fine solid, except that here the focus has shifted from large individual particles to large clusters of small particles. From the ratios of U_k/U_T presented in the last column of table 1.1 it appears that the effective size of these aggregates relative to the size of the individual particles increases with decreasing size of the individual particles. The mean effective size and density of these clusters at any gas velocity is such that their terminal velocities remain greater than the velocity of the gas. That is why a bed of a fine solid can be maintained at gas velocities that are 10 to 20 times the terminal velocity of its median particle. Entrainment of particles will of course take place owing to particles swept from the lean phase near the top of the bed, and the erosion of clusters by the surrounding lean phase. Clustering is a complex phenomenon, and is discussed in detail, in view of our expansion experiments, in the last two sections of chapter 3.

The turbulent regime extends from U_k to the transport velocity, U_{TR}. The approach to the transport velocity is accompanied by a sharp increase in the rate of carryover. It is difficult, without having made suitable measurements, to associate the transport velocity with some mean cluster size. By analogy to the behavior of beds of closely sized coarse particles, one may only surmise that when the transport velocity is reached, the terminal velocities of a large proportion of the clusters are smaller than the velocity of the gas. For fine solids, the transport velocity is typically an order of magnitude greater than the terminal

velocity of the individual median particle. For coarse particles, the transport velocity lies closer to the terminal velocity of the median particle. Though they differ in structure, the turbulent and the bubbling fluid beds are similar in several respects. Over the turbulent regime, though particle carryover rates are relatively high, the fluidized density of the bed remains quite high, and an upper bed level is present though it is, of course, more diffused than in a bubbling fluidized bed. As in the bubbling bed, when solid is fed to the turbulent bed at a rate matching the saturation carrying capacity, the concentration of solid above the bed would decay through the transport disengaging height and approach a constant level. If solid were fed to the bed at a rate beyond the saturation carrying capacity, the bed level would then rise until the new solid rate is matched by solid carried out of the bed. The gas exit point would now lie within the transport disengaging height. But unless the slip velocity - that is, the relative velocity of gas and solid - changed significantly, the fluidized density of the bed itself would remain virtually the same.

Some of the general points made above may be illustrated by experimental results reported by Yerushalmi and Cankurt (1979) for the fluid cracking catalyst (FCC). The experiments were conducted in the 15.2 cm column of the apparatus described in chapter 3. As will be presently demonstrated, the transport velocity for the FCC lies around 1.2 - 1.5 m/sec. For this solid, the turbulent regime accordingly stretches from about 0.6 m/sec to a velocity around 1.2 - 1.5 m/sec. Over this range, the fluidized density measured at the bottom of the bed remains rather high -- ranging from about 335 kg/m^3 to around 190 - 208 kg/m^3. Throughout the

turbulent regime, if solid is recirculated to the bed at a rate equal to the carryover, it is possible to perceive distinctly can upper bed surface. This surface is becoming more diffuse as the gas velocity is raised. Work with different powders shows a clear axial density gradient in the turbulent bed, becoming more pronounced in the fast bed. For a light powder, such as our FCC, this gradient is slight and the bottom of the bed is not much denser than the top. The heavier the powder, the more pronounced is this density gradient. Experiments are undertaken now at The City College test stand to quantify this phenomenon.

1.5 The Fast Bed Regime

The transport velocity may be regarded as the boundary which divides vertical gas-solid flow regimes into two groups of states. Below it lie the bubbling and the turbulent fluid beds where, save for some carryover, the bed in general experiences no net flow and remains at the bottom of the holding vessel. These are, to use Lanneau's description, the captive states. Above lie the transport regimes which encompass a wide range of states from dilute-phase flow to the fast bed condition.

As noted earlier, the transport velocity for the fluid cracking catalyst lies around 1.2 - 1.5 m/sec (which is nearly 20 times the terminal velocity of a single particle with a size equal to the mean diameter of the solid, 49 microns). As this velocity is approached, there is a sharp increase in the rate of particle carryover and in the absence of solid recycle, the bed would empty in short order.

Beyond the transport velocity, solid traverses the column in fully entrained flow and the density or concentration of the resulting suspension depends not only on the gas

velocity but also on the solid rate. If the solid rate is low, dilute-phase flow results. As its name is meant to suggest, solid concentration is low in the dilute-phase flow regime, the particles stream upwards in relatively straight paths, and slip velocities lie in the neighborhood of the free-all velocities of the individual particles. As the solid rate increases, the suspension becomes progressively denser, and at a sufficiently high solid rate, the fast fluidized bed (Yerushalmi, et al., 1976) is established. The fast bed condition is marked by relatively high solid concentrations, aggregation of the particles in clusters and strands which break apart and reform in rapid succession, extensive backmixing of solid, and slip velocities that are an order of magnitude greater than the free-fall velocities of the individual particles. As noted earlier, a way to create the dense suspension typical to the fast bed condition is simply to circulate the very solid emerging from the top of the reactor back to its bottom by means of cyclones and a standpipe (fig. 1.2c).

Fig. 1.7 presents fluidization data for FCC obtained in the 15.2 cm column mostly over the fast bed range. The figure gives the pressure gradient measured across the middle section of the column as a function of the solid rate at different gas velocities. Over this range, wall-solid friction is relatively small (Van Swaaij, et al., 1970; Turner, 1978), and the pressure gradient can essentially be regarded as the fluidized density, $\bar{\rho}$, in the section of the bed in question. Fig. 1.7 attests to the high solid concentrations that can be maintained in the fast bed at gas velocities that are an order of magnitude greater than those normally employed in a bubbling fluidized bed of the same solid.

Effect of bed size. It is of interest to compare the data for FCC obtained in the 15.2 cm column with similar data obtained in a 7.5 cm column (Yerushalmi, et al., 1976). Fig. 1.8 provides this comparison. There is obviously a discrepancy between the two sets of data. At a given solid rate, a higher gas velocity must be employed in the narrower, 7.5 cm bed to register the same pressure drop. Two factors may contribute to this difference: wal phenomena, and wall-solid friction. The results of Van Swaaij, et al. (1970) and Turner (1978) indicate that friction effects, being relatively small, could not alone be the cause of the observed discrepancy, but wall phenomena could. Segregation of solid along the wall has been observed in the narrower, 7.5 cm column to a degree clearly greater than in the 15.2 cm unit. With the core somewhat more dilute, gas in the 7.5 cm bed can stream relative to the solid at higher velocities than in the 15.2 cm bed, for the same solid rate and solid holdup. That is, slip velocities are higher in the 7.5 cm bed. A little reflection suggests that, in the extreme case, if the entire solid segregated along the wall in a dense layer, leaving the core empty, slip velocities would be even higher.

The bed diameter at which wall phenomena ceases to exert a significant influence, for a given solid, has not been determined.

The transport velocity should in principle not be dependent on bed size. But in laboratory experiments, it might appear so to the extent that wall phenomena influence the structure of the bed in narrow columns and in tests with coarse or heavy particles.

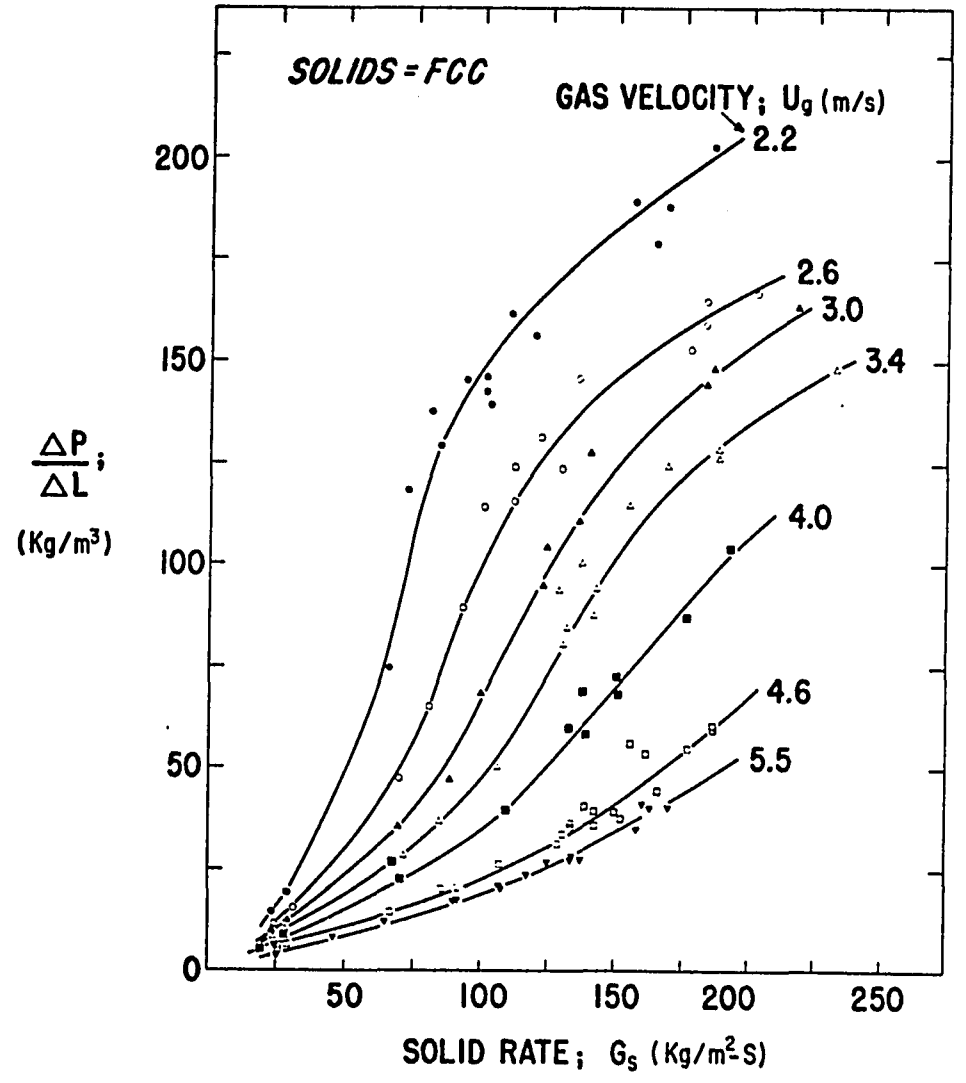

Fig. 1.7. Pressure gradient vs. the solid rate at different gas velocities. Data were taken with the fluid cracking catalyst (FCC) in the 15.2-cm column across a section extending from 3.14 to 6.28 m from the bottom of the column.

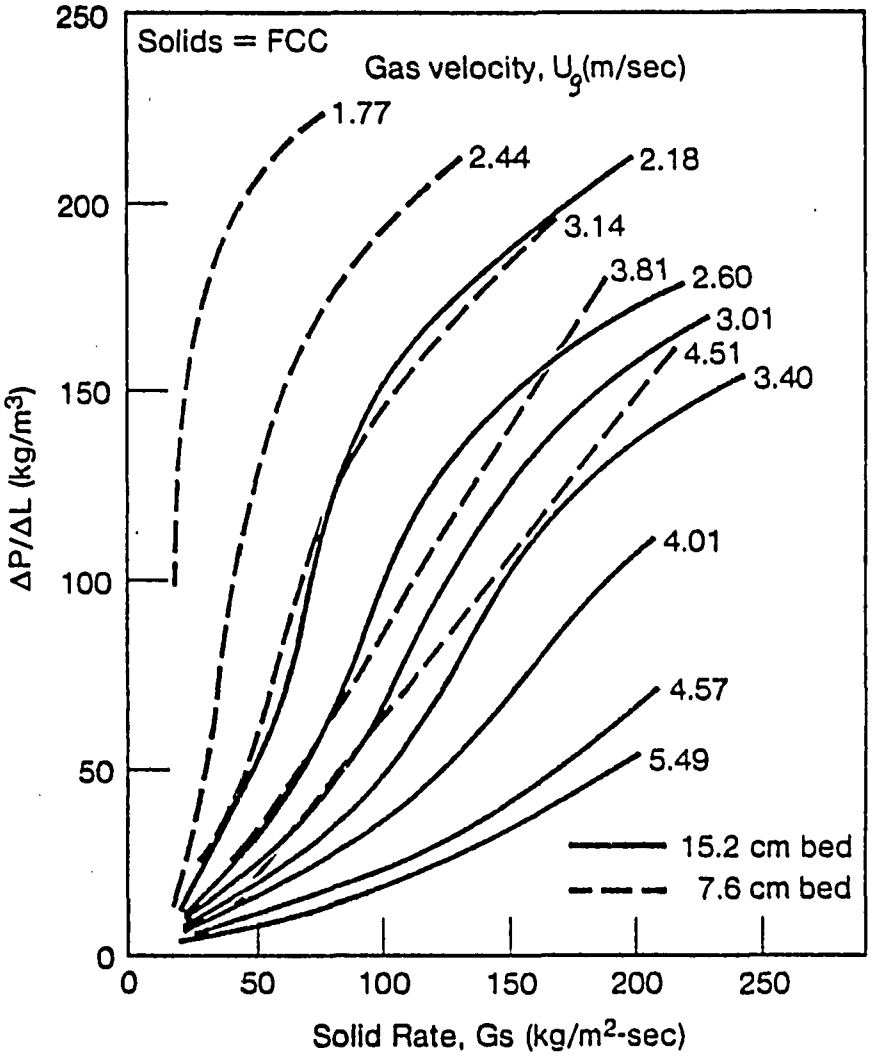

Fig. 1.8. Comparison between the data for FCC obtained in the 15.2-cm column (circulating system) and corresponding data for the same solid obtained in a 7.6-cm column.

Effect of pressure. There is essentially no fundamental information on the effect of pressure on the phenomena discussed here. Pressure may exert its well-known smoothing effect, and in one known instance involving highly concentrated suspensions maintained at velocities around 7-10 m/sec, this has indeed been reported to be the case (Horsler, et al., 1969).

Pressure may also diminish the degree of aggregation in the fast bed, and thus reduce the extent of solid backmixing. By stability considerations Grace and Tout (1979) verify the concept of cluster formation in the fast bed, and one gathers from their results that pressure may lead to reduction in cluster size.

Similar arguments lead to the speculation that the transport velocity will decrease with pressure.

The flooding point. Following the practice of students of vertical gas-liquid flow, Yerushalmi and Cankurt (1979) used the data shown in Fig. 1.7 to prepare plots of the volumetric gas flux, in $m^3/m^2 s$ versus the volumetric solid flux at constant bed densities. The results are shown in Fig. 1.9. Note that $\epsilon(U_g/\epsilon) = U_g$ is in fact the volumetric gas flux, and $G_s/\rho_s = (1 - \epsilon)U_s$ is the volumetric solid flux; $(1 - \epsilon)$ is the volumetric solid concentration.

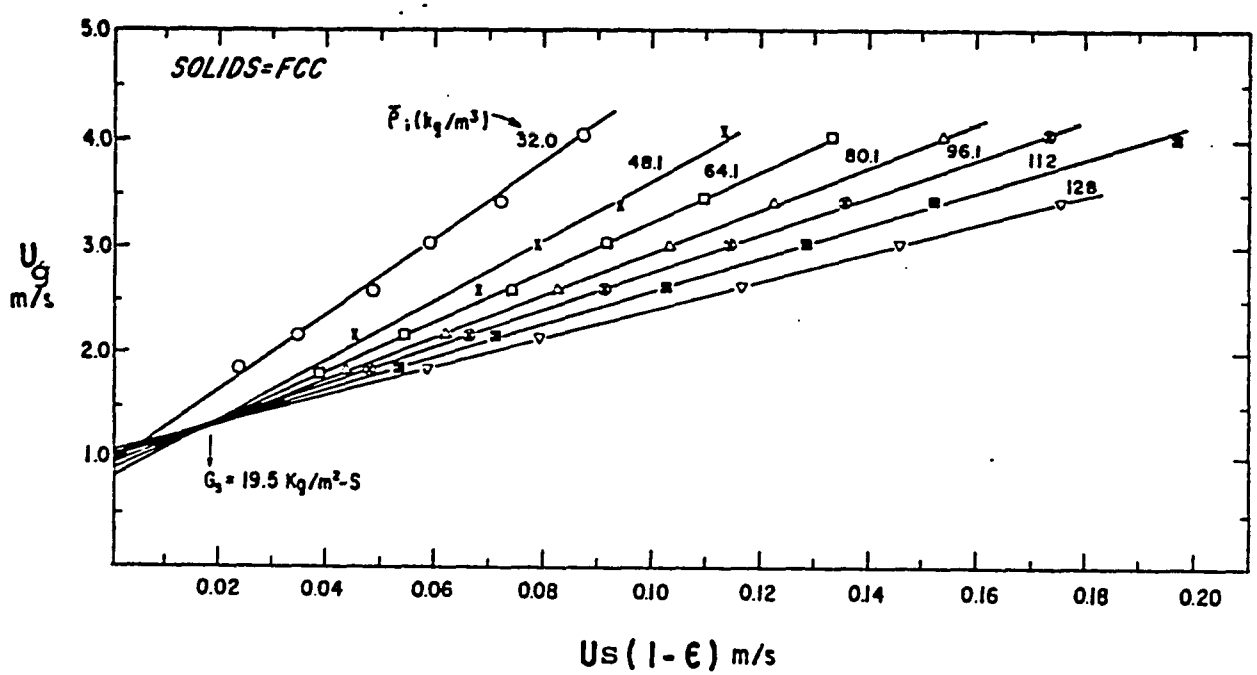

Fig. 1.9. Volumetric flux of gas, Ug. vs. the solid flux $U_s(1 - \varepsilon)$ at constant bed densities.

The curves of fig. 1.9 are straight lines converging, with one exception, on the point defined by $U_g = 1.37$ and $U_s(1 - \epsilon) = 0.02$. The line corresponding to $\bar{\rho} = 32$ kg/m^3 does not converge on this point probably due to predominance of wall phenomena at this relatively low suspension density. The intersection is the so-called flooding point (Wallis, 1969) marking as it does the onset of cocurrent flow of both phases, and $U_g = 1.37$ m/sec is accordingly the transport velocity. The flooding point will always have a positive coordinate for $U_s(1 - \epsilon)$ because of particle carry-over from a turbulent bed. Indeed, $U_s(1 - \epsilon) = 0.02$ reflects the fluidized density (about 192 kg/m^3) and the saturation carrying capacity (about 20 kg/m^2-s) from a turbulent bed maintained just below the transport velocity.

Determination of the flooding point provides a method for fixing the transport velocity. Other methods are described by Yerushalmi (1980).

Chapter 2 : Scope

The bulk of this work deals with two of the main properties of a fluidized bed: its voidage and the degree of solid mixing. Both properties are important to the design of fluid bed reactors. One needs to understand the underlying principles governing each of these phenomena, as well as to be able to predict them. Given the properties of a certain powder, bed geometry, and the fluidizing medium properties, one would like to be able to predict bed expansion and solid mixing as a function of both fluid and solid fluxes.

This work is concerned with high velocity fluidized beds, in the turbulent and fast regimes. A large volume of data is available in the literature concerning bed expansion and solid mixing for the low velocity regimes, bubbling and slugging. Data are scarce in the published literature for the higher velocity regimes. Our approach is to take published data and theory from low velocity fluidization, together with some of our own experimental data in this region, as a starting point in the investigation of higher velocity regimes. Information from low velocity regimes is extended into the high velocity regimes, where applicable, and new approaches are also suggested.

This investigation focuses primarily on fine cracking catalysts, of Geldart's group A classification. Most experimental data were obtained using two such powders, FCC and HFZ, whose mean particle diameter is 49μm, and particle densities are 1.07 and 1.45 g/cm^3, respectively. These data are compared with data for similar powders from the literature.

Some comparisons and comments concerning coarser powders are also made where appropriate. The experiments were conducted in fluidized bed columns 15.2 cm I.D., with ambient air as the fluidizing medium. Some comments concerning different bed geometries and different fluidizing medium conditions and their effect on the present study's conclusions are made.

2.1 Bed Expansion

The main distinguishing feature of high velocity beds is their greater homogeneity, when compared to low velocity aggregative systems. Thus, the Richardson-Zaki approach, which is used for particulate systems, is considered in section 3.1, as well as its application to other systems which are homogeneous otherwise. This approach has not been applied to low velocity fluidization, where the classical two phase theory applies. The application of two phase theory to slugging beds, which are at the lower limit of high velocity fluidization, is considered in section 3.2. The major point suggested by this section is that for most fine powders, the two phase approach becomes less applicable as the gas velocity is raised and the slug velocity is not easily predicted anymore.

Section 3.3 describes the experimental apparatus and procedure, as well as the properties of the powders used. Section 3.4 describes our results for high velocity, as well as for the slugging regimes, compares them with other published data, and discusses them. It is divided into seven subsections. The first presents our results for the slugging regime and the second compares these results with the literature. It is shown that in a few cases, where slugs are axisymmetric (especially for light fine solids) the two phase

approach accurately predicts bed expansion, while in most other cases, deviations from this theory occur. The connection between these deviations and particle properties and bed diameter is discussed.

In subsection 3.4.3 we show that the Richardson-Zaki approach, suitably modified, can also be used to correlate the expansion data of a fluid cracking catalyst (FCC) in most fluidization regimes. Some comments on the transitions among the expansion regimes as a function of bed height and size distribution are made, and a new "dense conveying regime" is postulated for $\varepsilon > 0.945$.

Subsection 3.4.4 extends the modified Richardson-Zaki correlation to other powders used by us, as well as different size distributions, and subsection 3.4.5 compares our results to data from the literature. In the penultimate subsection, the significance of the index n is discussed. It is thought of as a measure of segregation, being high in the slugging regime, and low in the turbulent regime. The last subsection describes the postulated significance of U_T^*, an "effective" cluster terminal velocity.

2.2 Solid Mixing

The importance of solid mixing to catalytic and non-catalytic gas-solid reactions is discussed in section 4.1. Various experimental techniques to study solid mixing are presented in the following section. These techniques are classified into disruptive techniques, which require the introduction of equipment into the bed, and non-disruptive techniques. The former are discussed in sub-section 4.2.1 and the latter in sub-section 4.2.2.

The experimental technique chosen here, the ferromagnetic tracer method, is described in section 4.3. The experimental apparatus constructed, the solid tracer used and some experimental difficulties are described. The results were obtained in both 15.2 cm I.D. systems: the expanded top bed and the circulating system. The expanded top bed results are presented in subsection 4.4.1 and circulating system results in subsection 4.4.2.

Section 4.5 serves as an introduction to the various models previously used to describe solid mixing in fluidized beds. Two phase models, mainly the one due to van Deemter, are described in section 4.6. The results of our previous gas mixing experiments are described by such a model, and it is shown how to model solid mixing as well. The main disadvantage of such a model, the difficulty in obtaining the phase velocities is elaborated upon, and the probability theory approach of Naor, Shinnar and Katz is presented. This difficulty prevents us from using the two phase model, except at all but the lowest gas velocities investigated.

A modified turbulent dispersion model is presented, along with the reasons for using it, in section 4.7. It is applied to the expanded top bed results in sub-section 4.7.1, and the results are presented in the form of apparent axial diffusivities. The next sub-section treats the results of the expanded top bed in a more precise way, utilizing the Aris method for the difference in the second moments of concentration histories at two adjacent probes.

The implications of the solid mixing results as far as heat transfer is concerned are discussed in subsection 4.7.3. The mixing results from the two upstream channels are also

presented. Section 4.8 presents a fluctuation method to determine the axial dispersion coefficients from the steady state response of the probes. Some results, especially in the slugging regime, are found in good agreement with the dispersion coefficients obtained previously. This method leads us to examine the effect of bed diameter on solid mixing. The chapter concludes with some qualitative remarks about the analogy between the high velocity states of gas-solid systems and liquid-solid systems. It is shown that the same minimum for the Péclet number is observed for both systems and a simple way to estimate the voidage at the point of maximum mixing is presented.

Chapter 3 : Bed Expansion

3.1 Introduction

Bed expansion is one of the most important, as well as one of the most reported properties in a fluidized bed. Most of the published data on bed expansion deal with the low velocity regimes (bubbling and slugging) and little is known about the expansion of gas fluidized beds of fine particles, of Geldart's group A, as the superficial gas velocity is increased, and the fluidized bed passes through different regimes of fluidization: slugging (in small diameter units), turbulent and fast fluidization, and pneumatic transport. As an example, one of the most striking features of the fast fluidized bed is the fact that the voidage is no longer a unique function of the slip velocity, and the solid feed rate has to be taken into account as well (Yerushalmi and Cankurt, 1979).

Traditionally, a distinction is made between particulate (mostly liquid systems) and aggregative fluidization to which the two phase theory of fluidization is usually applied.

Liquid-solid fluidized beds generally exhibit smooth expansion, often represented by the well known Richardson-Zaki (1954) equation.

$$\frac{U_g}{U_T} = \varepsilon^n \qquad (3.1)$$

The index n is a function of the particle diameter to tube diameter ratio, and the particle Reynolds number.

$$n = f\,(Re, d_p, D_t) \qquad (3.2)$$

The Richardson-Zaki equation has proven to be quite accurate in predicting bed expansion of liquid-solid systems even though it is purely empirical in nature.

Leva (1959) suggested that equation 3.1 also applies to uniform gas-solid beds such as those slightly above minimum fluidization conditions or when homogenized with baffles. Another homogenizing influence is higher pressure, and indeed Mogan et al. (1969) show how the Richardson-Zaki equation applies to cracking catalyst at 2.17-5.79 MP_a (300-800 psig). The Beranek method was used to calculate the terminal velocity of the "largest significant particles."

For aggregative fluidization the picture is more complicated. In the discussion following the Richardson and Zaki (1954) presentation, Mr. W.L. Lom noted that in the case of gaseous fluidization the "increase of velocity eventually led to a change in the characteristics of the bed, and disperse phase fluidization set in." It would seem intuitively that the higher gas velocity, producing the more homogeneous turbulent and fast fluidization regimes, would bring about an analogy to particulate systems and thus the Richardson-Zaki equation should apply. It is the intention of the present study to show that this is indeed the case. Moreover, it will be shown that the modified Richardson-Zaki approach is a better representation of bed expansion for fine powders, even in the rather aggregative state of slugging.

A number of authors (for example, Richardson (1971) and Capes (1974) commented on the higher values of the exponent n for fine powders than those predicted by equation 3.2. These deviations are attributed in the present study to the phenomenon of agglomeration.

3.2 Expansion of Slugging Beds

At the lower limit of high velocity fluidization, one encounters the phenomenon of slugging only in small diameter tubes. Using the two phase theory of fluidization, Matsen et al. (1969) arrived at the following relationship for bed expansion:

$$\frac{H_{max}}{H_o} = 1 + \frac{U_g - U_o}{0.35(gD_t)^{\frac{1}{2}}} \qquad (3.3)$$

where the maximum bed height rather than the average height is used. When trying to correlate the data of Kehoe (1969) they point out that their correlation did not fit at higher gas velocities. The explanation given was that slugs tend to travel asymmetrically at the higher velocities. Birkhoff and Carter (1957) suggested that slugs might be moving as if they were in a column of twice the actual width, changing the square root term in equation 3.3. to be $(2gD_t)^{\frac{1}{2}}$.

$$\frac{H_{max}}{H_o} = 1 + \frac{U_g - U_o}{0.35(2gD_t)^{\frac{1}{2}}} \qquad (3.4)$$

This has been validated for Kehoe's data by Hovmand and Davidson (1971). Slugs tend to coalesce and accelerate appeciably in the process, and as pointed out by Massimilla (1971), the deviation from equation 3.3 and its corrected form, 3.4, becomes even larger. One of Massimilla's curves is reproduced in Figure 3.1. At low velocities, equation 3.3 underestimates bed expansion because the bubbles have not reached their maximum size yet, and consequently, their velocity is lower. At $X = \left(\frac{U_g - U_o}{0.35\sqrt{gD_t}}\right)$ value of 0.2 bed expansion deviates from equation 3.3 and is more closely

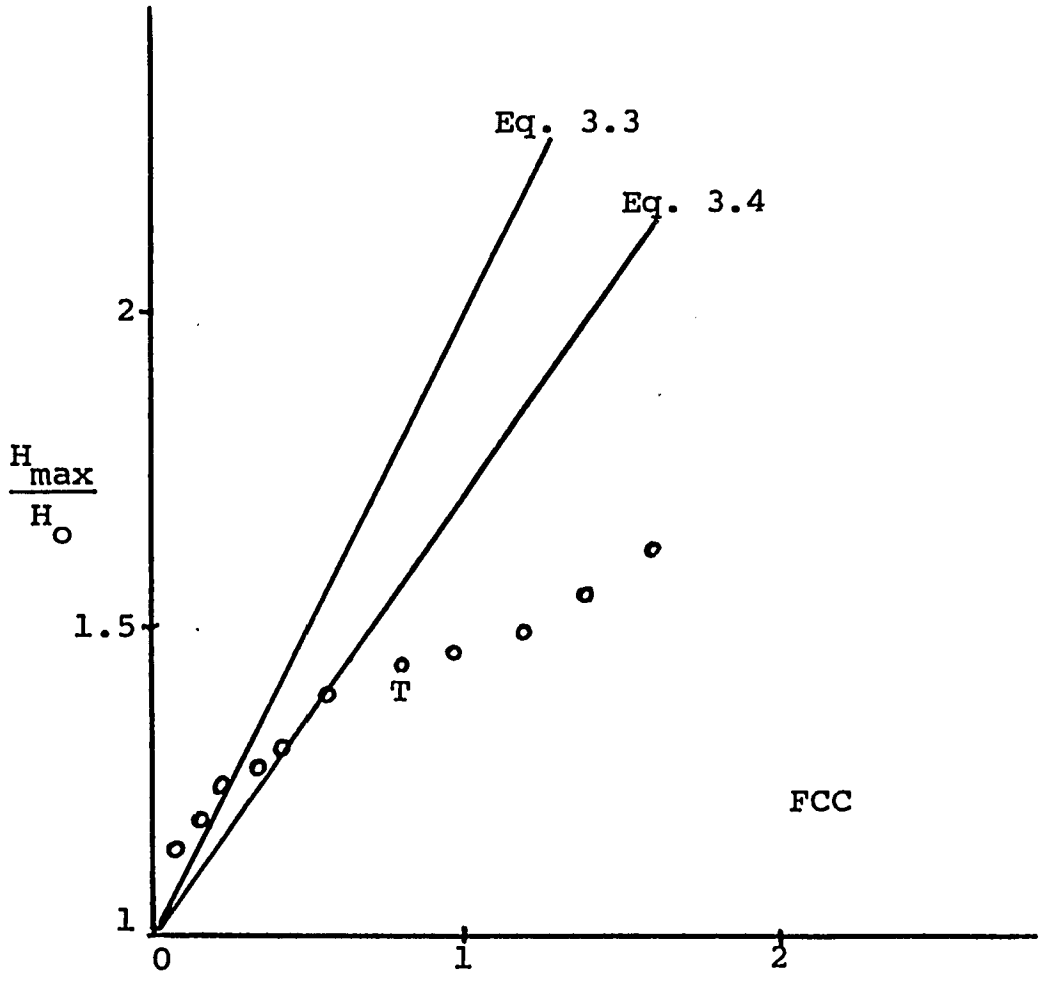

$$X = \frac{U_g - U_o}{0.35(gD_t)^{\frac{1}{2}}}$$

T - Transition from slugging to turbulence.

H_o = 110cm, D_t = 15.6, d_p = 56μm

Figure 3.1: Bed expansion in the slugging and turbulent regimes, Massimilla (1971).

approximated by equation 3.4, up to values of X=0.6. As the onset of turbulence (X=0.8) is approached equation 3.4 over-estimates bed expansion. The slugs break down into smaller voids which are vigorously mixed, formed and destroyed, having an equivalent rise velocity higher than the slug velocity. Another feature worth noting in Massimilla's data is the presence of an inflection point in the beginning of the turbulent region (X≅1.0) where H/H_o begins to grow faster with increasing gas velocity. This phenomenon, of a more pronounced bed expansion in the turbulent regime, is corroborated later by our own results.

The difficulty in predicting these deviations from ideal slug flow behavior is caused by being unable to predict bubble sizes and velocities. While for ideal slug flow behavior, the two-phase behavior, the two phase theory does accurately predict bed expansion, extrapolation to a higher velocity region is not always accurate.

3.3 Experimental

3.3.1 The Circulating System

All the experiments have been conducted at room conditions, with air as the fluidizing medium, in two 15.2cm I.D. systems: a circulating system and expanded top bed. A schematic of the circulating system is shown in figure 3.2. The 15.2cm column is shown on the left: it is 8.5m tall. On the right is a 34.3cm I.D. round vessel in which the test solid is maintained in low-velocity, bubbling fluidization. This so-called "slow" bed doubles as a standpipe and as a storage for the solid. Fluidizing air to the 15.2cm column is provided at its bottom. Solid can be maintained in the 15.2cm column

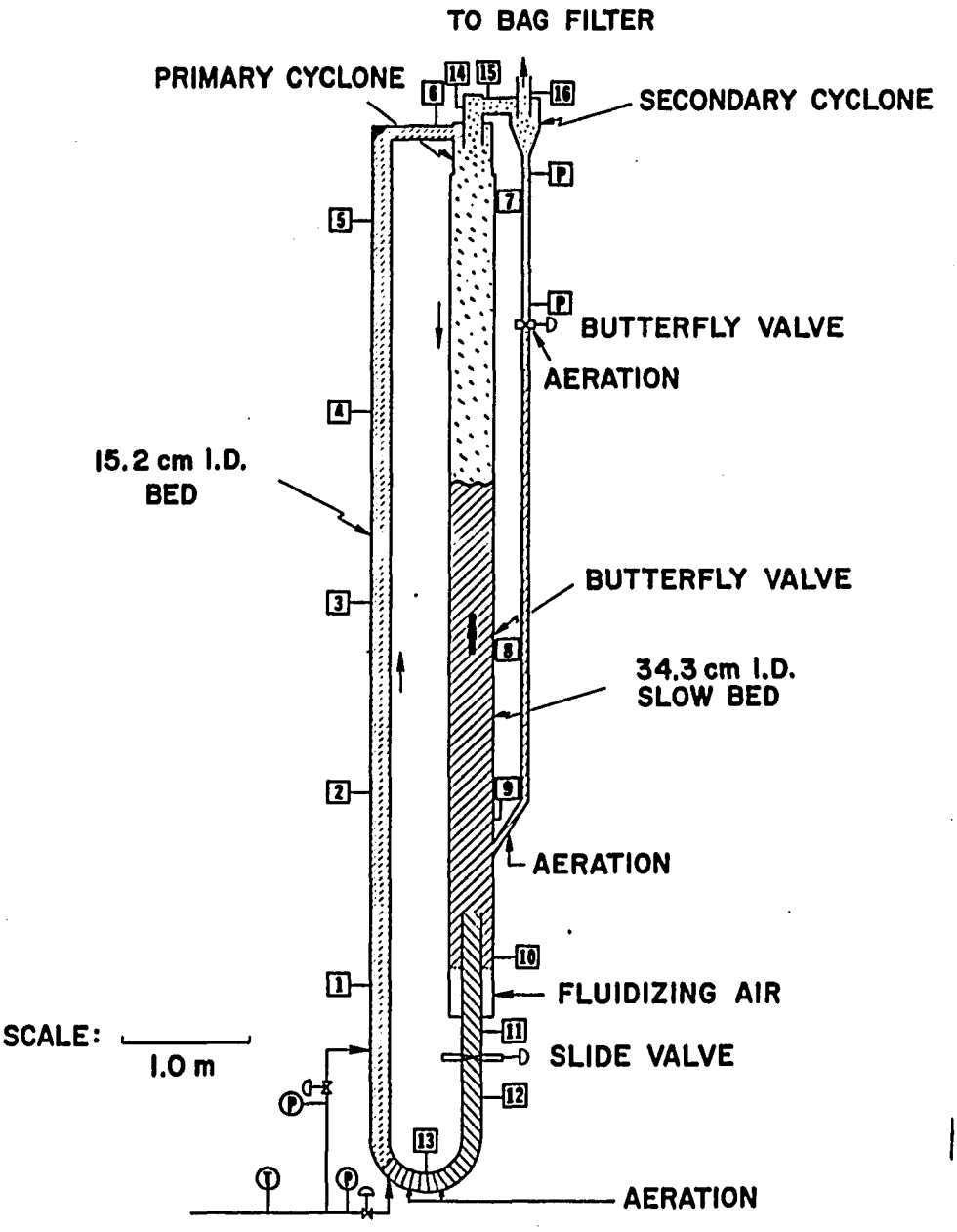

Figure 3.2: The 15.2cm I.D. circulating system.

at any desired fluidization condition through independent control of the gas velocity and of the solid rate from the slow bed to the bottom of the 15.2cm column. The solid rate is controlled by a slide valve installed in the U-tube just below the bottom of the slow bed. Solid traversing the 15.2cm column is separated from the gas in a primary cyclone which form an extension of the vessel that houses the slow bed. The primary cyclone does not have an inverted conical button. A smaller cyclone acts as the secondary cyclone, and gas leaving it flows to a bag filter. Pressure taps have been installed liberally around the system and are indicated by the numbers shown in Fig. 3.2. Our previous work has shown solid friction to be less than 10% of the total pressure drop in a given section for the turbulent and fast fluidization regimes. Consequently, the pressure drop is taken to be due primarily to the static head of the solid in the suspension, and this allows the average voidage between two pressure taps to be calculated. For light powders, such as our FCC, the voidage is a slight function of the height and taking ε_{1-2} (between pressure taps 1 and 2) well represents the average bed voidage. Some deviation is apparent for FCC at the higher solid rates and gas velocities of the fast regime, where the lower part of the bed is denser than the top. This phenomenon is more pronounced for heavier powders, such as HFZ-20. We are currently engaged in measuring this axial density profile by using the system shown in Figure 3.2 outfitted with 17, instead of 5 pressure taps.

Solid circulation rates are measured with the aid

of a sintered plate butterfly valve installed in the middle of the 34.3-cm I.D. slow bed.

3.3.2 The Expanded Top Bed

The expanded top bed is shown in Figure 3.3. The lower part is a 15.2cm I.D. column, 3.5m tall, equipped with 6 pressure taps. The second pair of pressure taps from the bottom is of the aerated type (much like the pressure taps in the circulating system) allowing for the pressure drop as well as the pressure fluctuations to be measured. The rest of the pressure taps are of the filter head type which, due to their higher resistance, average the pressure drop between any two points with less oscillations. The 15.2cm I.D. section ends with a 23cm long cone, which leads to the 34.3cm I.D. and 1.4m long expanded top section. The expanded top bed was designed to give accurate expansion data at lower velocities (bubbling, slugging and the beginning of the turbulent regime) and to set up the solid mixing experiments. Because of the area increase by a factor of 5, the superficial gas velocity is reduced by that factor in the expanded section, allowing entrained particles to fall back into the bed. Any entrained particles are returned by an external cyclone. The solid recirculation mode of this system (from the top) is inherently different from the one of the 15.2cm I.D. circulating system (from the bottom). This leads to significant differences in the behavior of the two systems as the gas solid rate becomes appreciable, and these differences are discussed in the appropriate sections.

3.3.3 The Powders Used

The properties of the powders used are given in Table 3.1 and their size distributions are given in Table 3.2. These size distributions are for "used" powders, or powders that have been fluidized for a few

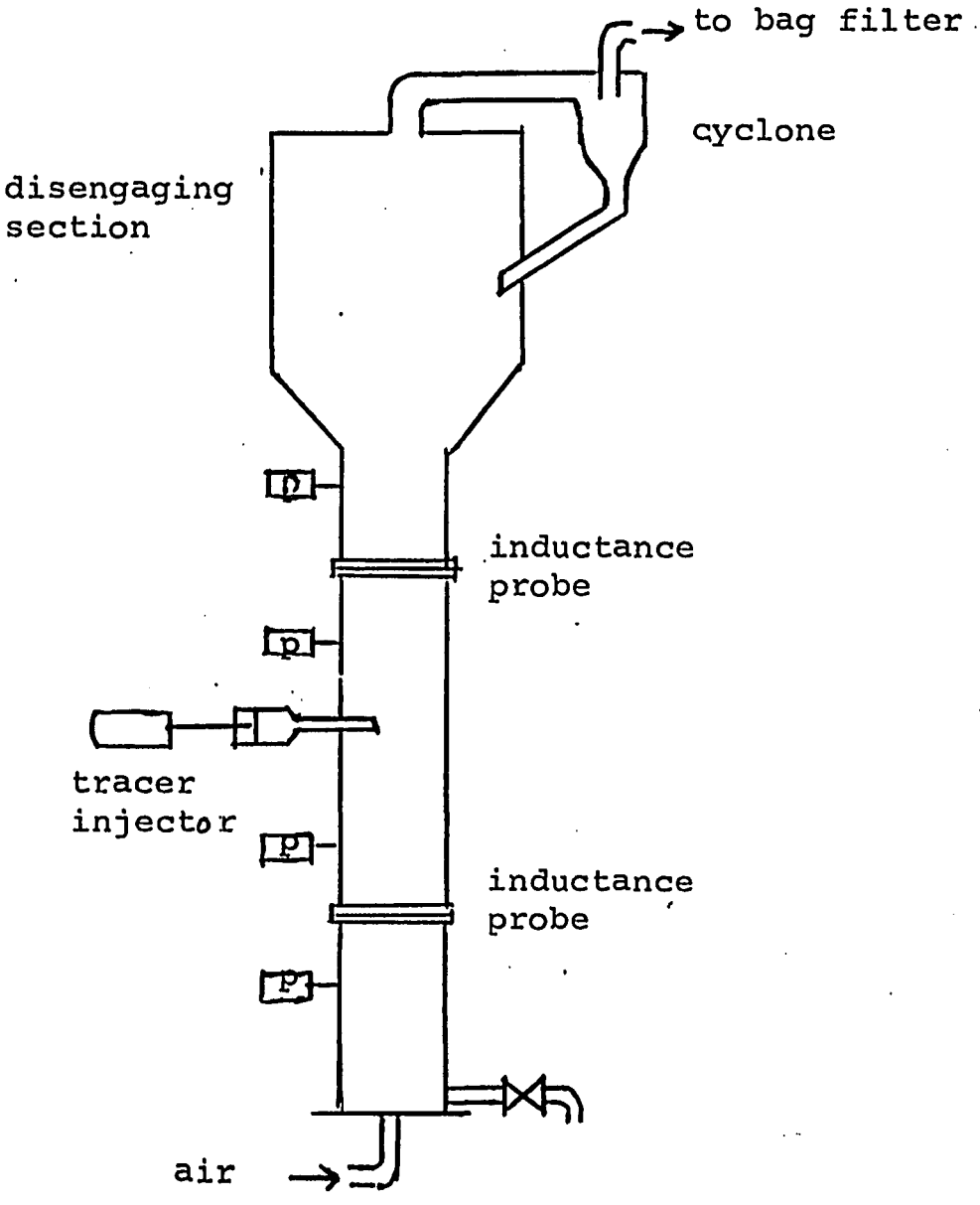

Figure 3.3: The 15.2 cm Expanded Top Bed

hours and have reached a "steady state" size distribution after an initial loss of fines. This is a crucial and poorly understood factor. The presence of fines has far reaching effects on bed expansion, transition to turbulence, and the "quality" of fluidization. The difference between the "used" and "fresh" catalysts used here is mainly in the fines fraction. Typically a "used" catalyst as described in this report has half the amount of fines as a "fresh" catalyst. For example, "fresh" FCC contains 24.5% by weight of particles with a diameter less than 37μm. The "used" catalyst contains 12% by weight of the same fraction.

Table 3.1 Properties of Powders Used

Solid	Size Range (μm)	$\overline{d_p}$ (μm)	Density, ρ_s (g/cm^3)	Sphericity ϕ_s	U_o (cm/s)	ε_o	G_a $\times 10^{-8}$
Dicalite 4200	0-160	33	1.67	0.4	0.15	0.71	1.88
Fluid Cracking Catalyst (FCC)	0-130	49	1.07	1.0	0.12	0.45	1.84
HFZ-20	0-130	49	1.45	1.0	0.09	0.48	2.49

Table 3.2 Size Distributions of Powders Used

a) Dicalite 4200

Particle Diameter (Microns)			Volume %
0	to	12.7	1.8
12.7	to	16	3.1
16	to	20.2	7.0
20.2	to	25.4	10.5
25.4	to	32	13.4
32	to	40.3	14.7
40.3	to	50.8	14.9
50.8	to	64	13.0
64	to	80.6	9.4
80.6	to	101.6	5.4
101.6	to	128	3.2
128	to	161	1.6
> 161			2.0
			100.0

Table 3.2 (cont.)

b) FCC

Particle Diameter (Microns)	Volume %
0 to 16	0.6
16 to 20.2	0.4
20.2 to 25.4	1.4
25.4 to 32	5.5
32 to 40.3	12.9
40.3 to 50.8	22.4
50.8 to 64	27.1
64 to 80.6	19.7
80.6 to 101.6	7.5
101.6 to 128	1.6
> 128	0.9
	100.0

c) HFZ-20

Diameter in microns	Weight %
0 - 1	1.1
20 - 40	20.1
40 - 64	47.5
64 - 80	22.0
80 - 130	9.0
> 130	0.3
	100.0

3.4 Results and Discussion

3.4.1 The Slugging Bed

Bed expansion results in the slugging regime were obtained in the expanded top bed. The data is plotted as H/H_o which is obtained from the measured voidage by:

$$\frac{H}{H_o} = \frac{1 - \varepsilon o}{1 - \varepsilon} \qquad (3.5)$$

Strictly speaking, $Hmax/H_o$ should be used to describe the expansion of a slugging bed, as was shown by Matsen et al. (1969). However, bed top fluctuations are moderate for fine powders. Massimilla (1971) reports $\frac{Hmax-Hmin}{H_o} = 0.10 - 0.15$, and in the present study H_o values used are at least twice those in the former study. Consequently, the H/H_o obtained from equation 3.5 is used.

Figure 3.4 depicts bed expansion for HFZ-20. The expansion behavior is qualitatively similar to Massimilla's (1971) cracking catalyst, with deviation from equation 3.3 at low values of X. An inflection point is also noted at the onset of the turbulent regime. "Fresh" catalyst expands more than used catalyst, as expected, and thus is better described by equation 3.4 at low values of X. One can qualitatively state that the "fresh" catalyst having more fines gives rise to more "regular" slugs; while the lower "quality" of fluidization for "used" catalyst causes more gas-solid segregation, and consequently higher velocity slugs. Note also that transition to the turbulent regime takes place for "fresh" catalyst at a lower gas velocity than for "used" catalyst. Figure 3.5 describes bed expansion for FCC. Again one notes the difference between "fresh" and "used" catalyst, qualitatively similar to the HFZ behavior. At low X values, equation 3.3 underestimates bed expansion, especially for "fresh" catalyst, because the

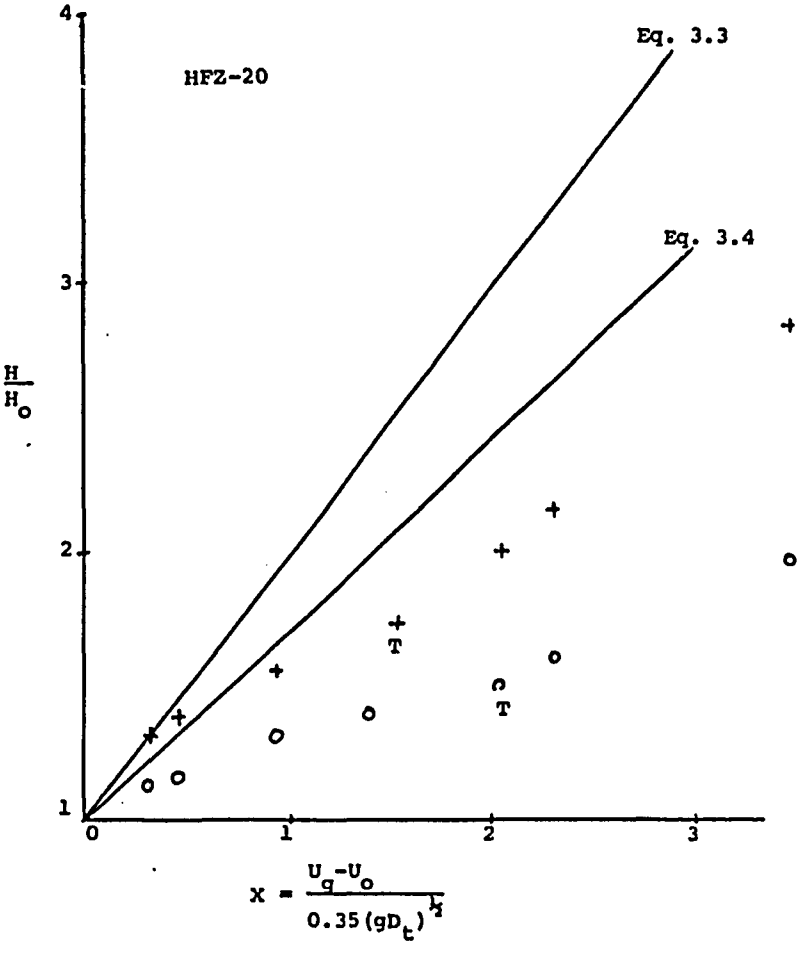

T - Transition from slugging to turbulence

\+ - "Fresh" HFZ-20 o = "used" HFZ-20

Figure 3.4: Bed expansion in the slugging and turbulent regimes, expanded top bed, HFZ-20.

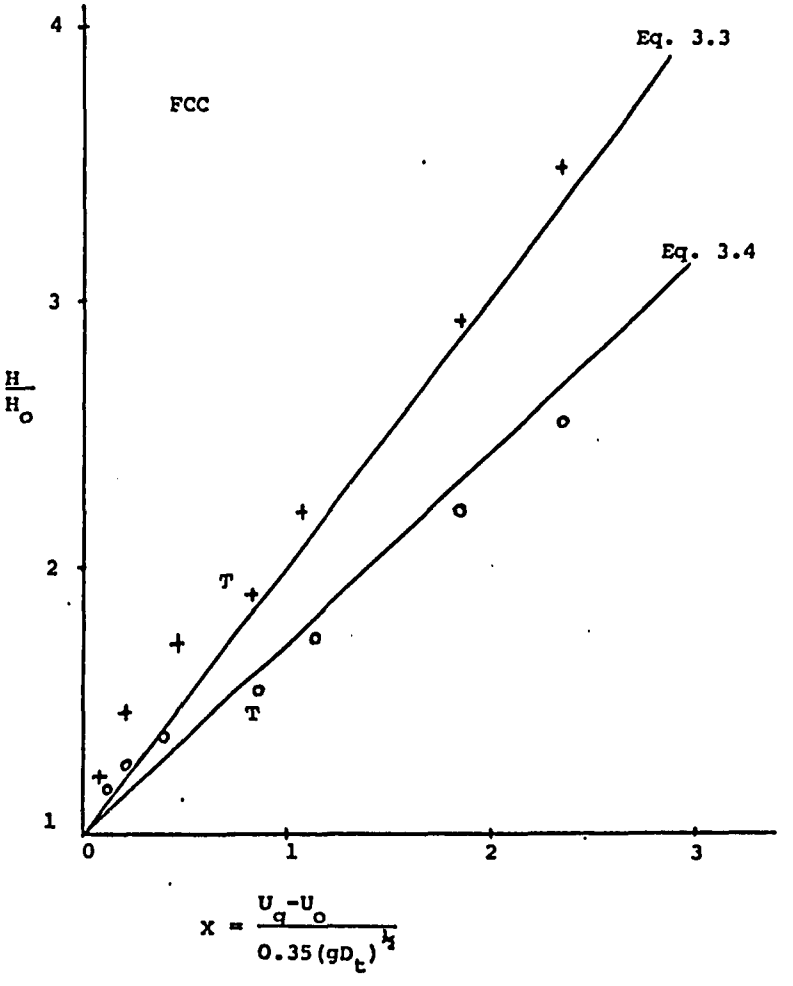

T - Transition from slugging to turbulence

\+ - "Fresh" FCC o - "used" FCC

Figure 3.5: Bed expansion in the slugging and turbulent regimes, expanded top bed, FCC.

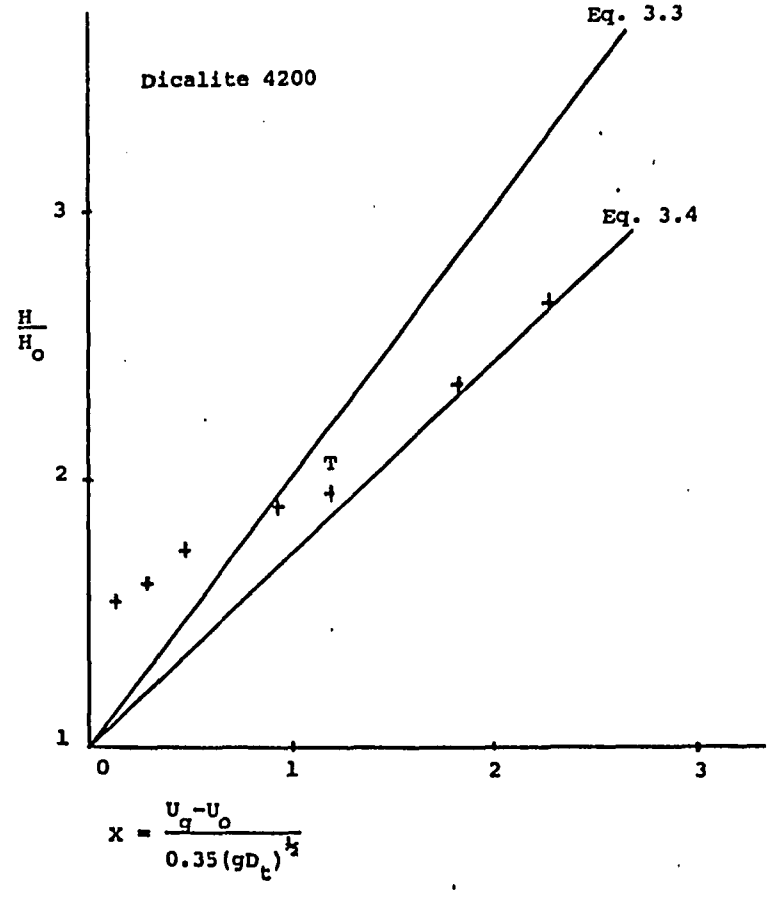

T = Transition from slugging to turbulence

Figure 3.6: Bed expansion in the slugging and turbulent regimes, expanded top bed, Dicalite 4200.

bubbles did not reach their maximum size (and velocity) yet. However, no deviation from equation 3.3 is noted for "fresh" FCC in the turbulent regime, while equation 3.4 describes "used" FCC rather well. This should be viewed more as coincidence than verification of the two phase theory, because equations 3.3 and 3.4 do not obviously hold on theoretical grounds in the turbulent regime.

3.4.2 The Effect of Particle Properties and Bed Diameter in the Slugging Regime

The pattern shown by figures 3.1, 3.4, 3.5 and 3.6 shows that deviation from equations 3.3 and 3.4 is a function of size distribution and density. For relatively heavy particles like HFZ-20 and probably Massimilla's (1971) cracking catalyst, the deviation from equation 3.3 is strong and void velocities are generally higher than those predicted by the two phase theory. The lighter the particles, the smaller this deviation is. The same trend is reported by Crescitelli et al. (1978). A slight deviation from equation 3.3 is noted for their "Ludox" catalyst (ρ_s = 1.4 g/cm^3) while no deviations are reported for a light FCC (similar to our own).

Figure 3.6 shows bed expansion for Dicalite. Throughout its slugging regime there is a strong deviation from equation 3.3. This points to the fact that bubble velocities are lower than those predicted by the two phase theory. While part of this deviation can be attributed to bubble growth, just as was shown for FCC, the deviation is more pronounced here, suggesting even lower bubble velocities. Indeed, visual observations of Dicalite do not show smooth fluidization, such as is clear for "fresh" FCC. Instead one sees a

greater degree of segregation and tortuous distribution of slug/bubbles which seems to slow their ascend velocities. After transition to turbulence, equation 3.4 is followed closely.

Table 3.3 summarizes our, as well as some results from the literature that show deviation from equation 3.3.

Table 3.3. Summary of Bed Expansion Data in the Slugging Regime

Solid	Average Particle Size (μm)	ρ_s (g/cm^3)	D_t (cm)	Deviation from Eq. 3.3 at X=*	Source
Dicalite	33	1.67	15.2	1.0	
FCC-Fresh	49	1.07	15.2	No	Present
FCC-Used	49	1.07	15.2	0.4	Study
HFZ-Fresh	49	1.45	15.2	0.3	
HFZ-Used	49	1.45	15.2	~0.1	
Ballotini	68	2.55	5	0.53	Kehoe
"	77	2.6	5	0.69	and
"	113	2.63	5	~0.8	Davidson
"	113	2.63	10	0.26	(1970)
"	212	2.71	10	0.26	
Sand	145	2.65	10	0.29	
Iron	100	4.8**	5	1.6	Zenz and
Ore	100	4.8**	15.2	1.0	Othmer
	100	4.8**	30.5	0.65	(1960)
FCC	60	0.94	15	No	Carotenuto et
Alumina	95	1.55	15	0.8	al. (1974)
FCC	56	1.9**	15.6	0.25	Massimilla (1971)

Notes - (continued on next page)

Notes:

*Most data deviates from Eq. 3.3 at low values of X. Here we present deviation at high X values.

**Assumed - From similarity to HFZ-20 data and the value of U_T^*.

While no clear trends are evident from Table 3.3, some tentative general remarks can be deduced.

(1) While there is no clear dependence of the deviation from Eq. 3.3 on $\rho_s dp$, for powders of similar size distribution in similar diameter beds, the heavier powders will deviate more and at lower X values than lighter powders. This was noted in the beginning of this section.

(2) In general, bed expansion data seems to deviate at lower values of X from equation 3.3, as the bed diameter is increased. The reason for this seems to relate to the fact that at larger bed diameters the slugs have more freedom to twist, coalesce and break and thus, have higher velocities.

Summary

The behavior of a slugging bed is complicated by the fact that slug velocity is not always easy to predict. For axisymmetric slugs, in medium diameter beds and light powders, Eq. 3.3 adequately describes bed expansion, and is surprisingly extendable to the turbulent regime (Figure 3.5 and the results of Carotenuto et al. (1974). For situations where wall slugs persist, Eq. 3.4 is applicable. Both equations are in general not applicable to situations where slugs accelerate appreciably due to coalescence (e.g. heavy fine powders, larger diameter beds). It is not easy to predict when deviations from Equation 3.3 will begin (Table 3.3). Thus, except for

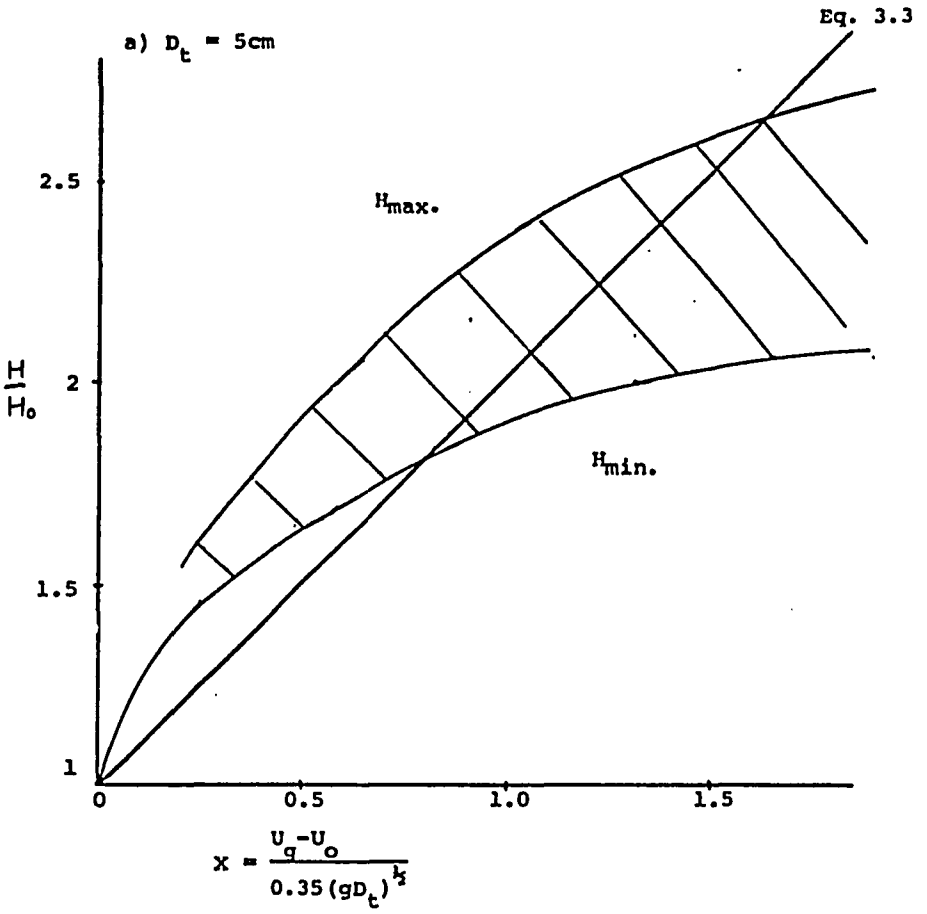

Figure 3.7: Bed expansion in three bed diameters, iron ore in the slugging regime, Zenz and Othmer (1960).

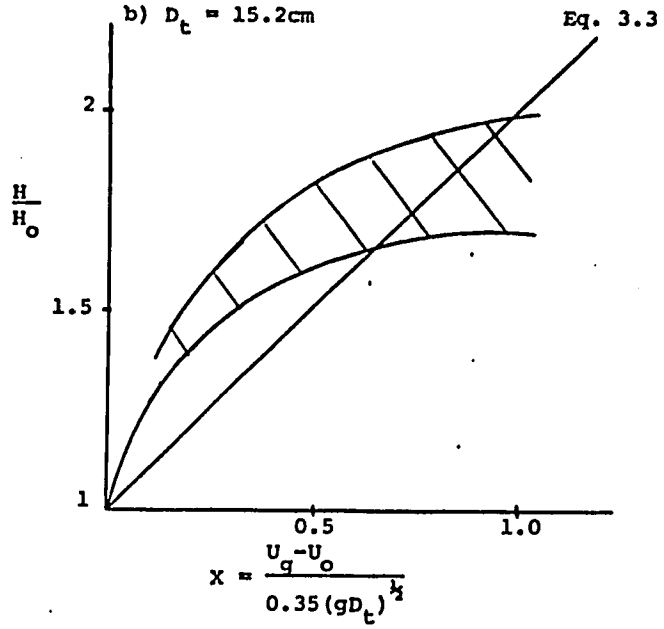
b) D_t = 15.2cm
Eq. 3.3
2
1.5
1
$\frac{H}{H_o}$
0.5
1.0
$X = \frac{U_g - U_o}{0.35(gD_t)^{\frac{1}{2}}}$

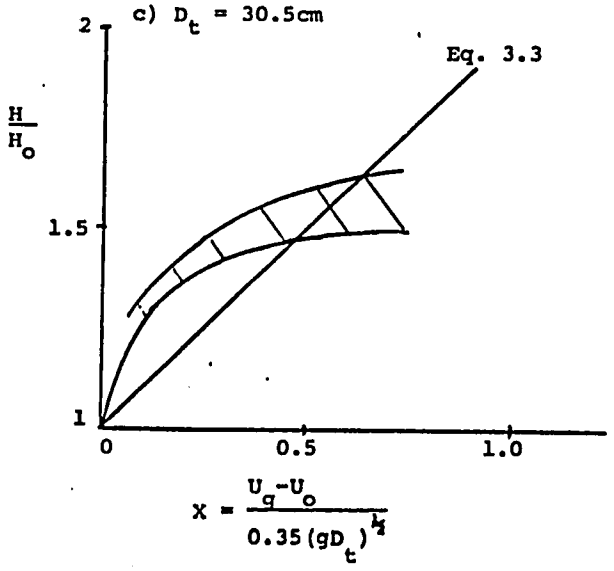
c) D_t = 30.5cm
Eq. 3.3
2
1.5
1
$\frac{H}{H_o}$
0
0.5
1.0
$X = \frac{U_g - U_o}{0.35(gD_t)^{\frac{1}{2}}}$

the noted exceptions, bed expansion in the high velocity regimes does not follow from knowledge of bed expansion at the lower velocity regimes. It should also be noted that bed expansion strongly depends on bed diameter especially for heavy particles such as iron ore (Table 3.3). Zenz and Othmer's (1960) results are shown in Figure 3.7 for three bed diameters: 5, 15.2, and 30.5 cm I.D. The shaded region represents the fluctuations in pressure and the upper line corresponds to $\frac{Hmax}{H_o}$. They suggest that bed expansion for iron ore (or for coarse particles) should vary little, if any, beyond D_t = 30 cm. For fine powders a 15 cm I.D. bed might be large enough for scale-up of bed expansion data. (Note that this is not the case for transition to turbulence.)

3.4.3 Bed Expansion in High Velocity Fluidization - the Modified Richardson-Zaki Approach - FCC ("Used")

Noting that the turbulent and fast fluidization regimes are more homogeneous in nature, we represent our expansion results in the Richardson-Zaki form by plotting log Ug vs. log ε. A complete expansion curve for FCC ("used") is shown in Figure 3.8. For completeness, the curve is extended into the slugging regime, and gives a surprisingly good representation of bed expansion there. The bubble/slug regime extends from a velocity of 0.076 m/s to 0.4 m/s where a sharp change in slope is noted. This point is close to the observed transition to turbulence (U_c - see Chapter 1). Thus, data from the expanded top bed is used, and while the resulting correlation line averages the circulating system data, there is a slight change in the transition velocities. This change is attributed to the use of a porous plate distributor (in the expanded top system) vs. several

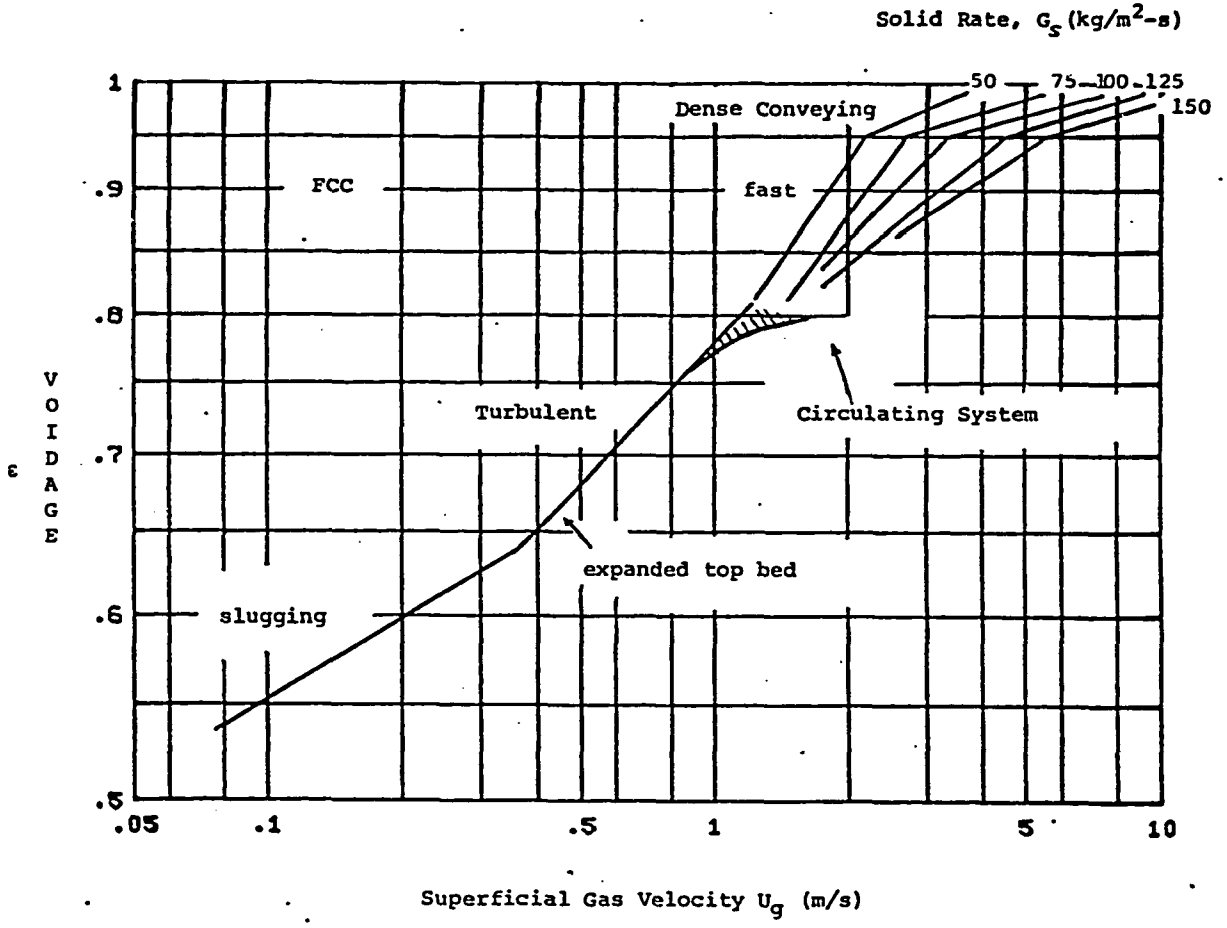

Figure 3.8: A complete expansion curve for FCC ("used").

nozzles in the circulating system. Moreover, the circulating system bed is taller and the transition to turbulence is also a function of height, coming into play at the top first then progressing downwards.

Table 3.4. Transition to Turbulence

Solid	Circulating System			Expanded Top Bed	
	U_C (m/s)	U_k (m/s)	Expansion* Slope Change (m/s)	U_c (m/s)	Expansion Slope Change (m/s)
Fresh HFZ	-	-	-	-	0.67
Used HFZ	0.91	1.37	-	-	0.88
Fresh FCC	Bottom 0.52 of bed	0.91	-	-	-
	Middle 0.37 of bed	0.91	0.43	0.3	0.38
Used FCC	0.61	0.61	0.53	0.3	0.37
Dica-lite	0.53	1.07	-	-	0.52

*Velocity at which the expansion curve experiences a change in slope.

The curve for the turbulent regime is also from the expanded top bed data and it extends from U_c (~0.4 m/s) to the end of the turbulent regime, U_{TR} = 1.28 m/s which agrees quite well with U_{TR} obtained by other means (Yerushalmi and Cankurt, 1979). The expanded top bed data agrees with the circulating bed data well up to Ug = 0.91 m/s.

Beyond this velocity the solid rate becomes appreciable and points from the circulating system fall within the shaded region in Figure 3.8.

Another change in slope is noted at the transition velocity. The data for the fast regime are from the circulating system and now the voidage is not a unique function of the superficial gas velocity. The solid rate enters into the picture and lines for five different solid rates are shown. The fast fluidization regime ends at a voidage of 0.945, for all solid rates. At this point all expansion curves show a dramatic change in slope, indicating that another change in regime might be taking place.

This new regime, if it does indeed exist, is tentatively termed the "dense conveying regime," and it extends from a voidage of 0.945 to approximately 0.99 where dilute pneumatic conveying takes over. There is an analogy between the limiting voidage for gas-solid fast fluidization and liquid systems. The Richardson-Zaki equation applies up to a voidage of 0.95 for liquid systems where a marked change was observed. In most reported data (for example Lewis and Blowerman (1952) the slope of the expansion curve increases for $\varepsilon > 0.95$, much like our own results. Happel (1958) and Adler and Happel (1962) have shown that the Richardson-Zaki approach underestimates particle-to-particle interactions for $\varepsilon > 0.95$. They suggest a correlation of the form:

$$\frac{U_q}{U_t} = 1 - \text{constant} \times (1 - \varepsilon)^{1/3} \qquad (3.6)$$

which does correlate their data and is equivalent to using a higher value for the exponent n.

The fact that the Richardson-Zaki equation can be used for gas solid systems has been mentioned in the introduction to this chapter, especially where homogenizing influences such as internals, high pressure, etc. are evident. Canada, McLaughlin and Staub (1978) also demonstrate the use of the Richardson-Zaki equation for coarse particles, 650μm and 2600μm in diameter. They note a change in slope of the expansion curve in going from n = 3.4 (in the slugging regime) to n - 1.85 (in the turbulent regime) for the 650μm particles in a 0.61 x 0.61 m and a 0.305 x 0.305 m bed. A similar change for the 2600μm particles (from 3.7 to 3.3) is noted for the 0.61 x 0.61 bed. For these heavier particles in the 0.305m column, however, n changes from 2.71 to 3.3, but they note that a different regime piston like movement was present in the lower section of the bed. Another important observation, made previously by Brzozowski, McLaughlin and Staub (1976) is that the value of n changes continuously and is apparently a function of U_g/U_T. Thus, they propose a volumetric flux plot method which utilizes a mean drift velocity and a void fraction profile, C_o.

In the case of fine powders the change to the index n is sharp, from region to region and, moreover, it stays relatively constant in any given regime. Thus, the use of the Richardson-Zaki equation is justified, with the modification of U_T*, an "apparent" terminal velocity used instead of the single particle terminal velocity.

The equations of the lines shown in Figure 3.8 are given in Table 3.5.

Table 3.5. Expansion Correlation for FCC ("Used")

$$\frac{U_g}{U_T^*} = \varepsilon^n$$

Regime	U_T^* (m/sec)	n	Transition Velocity to Next Regime (m/s)
Bubble/Slugging	22.6	9.2	0.4
Turbulent	3.4	5	1.4
Fast G_s= 50 Kg/m^2-s	2.5	2.9	2.1
75	3.3	3.6	2.7
100	4.5	5.2	3.4
125	5.6	5.9	4.3
150	7.2	7.2	5.0
Dense G_s = 50	4.6	14.2	4.0
75	6.4	14.6	5.5
Conveying 100	9.4	17	7.9
$0.945 < \varepsilon < 0.99$ 125	11.6	19	9.4
150	13.7	20	11.3

These equations predict the voidage for used FCC, in both the expanded top bed and the circulating system rather well. Most of the experimental points are within 1% of the correlation line and more than 95% of the points fall within a 5% band.

3.4.4. The Modified Richardson-Zaki Approach for Other Powders

Experiments were also conducted in the circulating and expanded top systems for the other two group A powders, HFZ-20 and Dicalite 4200. The results for the fast fluidization region suffer from too much scatter for these two powders and so only a comparison to FCC in the slugging, turbulent, and dense conveying regime will be attempted. A comparison for the slugging and turbulent regimes for the three powders (all "used") is shown in Table 3.6.

There seems to be a good deal of similarity between FCC and HFZ-20. Their n values are very close in both the slugging and turbulent regimes, and their U_T^*/U_T values seem to be linearly proportional to their respective $\rho_s d_p$ (or Ga) values. This indicates that powders similar in size distribution behave similarly in the slugging and turbulent regimes, their n values are ~9 (slugging) and ~4.7 (turbulent). Their U_T^* values are proportional to particle properties, as shown for HFZ-20 and FCC.

Dicalite, on the other hand, exhibits a markedly different behavior, both visually and as indicated in Table 3.6. The much higher values of U_T^* and n for Dicalite in the lower gas velocities (slugging and turbulent regimes) are attributed to its cohesiveness, especially when in a humid atmosphere. Dicalite is on the border between group A and C of Geldart's classification and in these two regimes its cohesive properties predominate.

The size distribution of the particles has a large effect on U_T^* and a small effect on n. This was shown in our expanded top bed when one compares "fresh" catalyst (with a large fines fraction) to "used" catalyst that has been run in the recirculating system for several hours and thus lost one half of the smaller particles.

Table 3.6. Expansion Properties of Three Group A Powders ("Used") in the Slugging and Turbulent Regimes

Powder	$\rho_s d_p$ (g/cm^2 $x10^3$)	Ga $x10^{-8}$	Slugging Regime			Transition to Turbulence Velocity (m/s)	Turbulent Regime			Transition to Fast Fluidization (m/s)
			n	U_T^* (m/s)	$\frac{U_T^*}{U_T}$		n	U_T^* (m/s)	$\frac{U_T^*}{U_T}$	
FCC	5.24	1.84	9.2	22.6	290	0.37	5	3.4	43.7	1.4
HFZ-20	7.11	2.49	8.3	38.7	365	0.88	4.4	6.3	59.4	1.8-2.1
Dicalite	5.51	1.88	46	853	$3.8x10^4$	0.52	14	5.0	220	1.1

All our reported results, so far, save for the comparison in Table 3.7, are for "used" catalyst.

Table 3.7. Comparison between "Fresh" and "Used" Catalyst

Powder	Slugging Regime		Turbulent Regime	
	U_T^* (m/s)	n	U_T^* (m/s)	n
FCC ("Fresh")	12.2	10.2	2.8	6
FCC ("Used")	22.6	9.2	3.4	5
HFZ ("Fresh")	30.5	10	4.5	5.1
HFZ ("Used")	38.7	8.3	6.3	4.4

Little effect on n is shown for both FCC and HFZ. However a considerable difference in U_T^* is noted: "Fresh" catalyst has a lower value than used catalyst indicating better fluidization of a powder that contains a larger fines fraction. The "used" powder has less fines, thus clusters to a larger degree than the "smooth" fresh catalyst, causing a large effective U_T^*.

All three powders behave similarly in the dense conveying regime. This is shown in Figure 3.9. Figure 3.9a shows the variation in the index n, with the solid rate in the dense conveying regime. Despite some scatter, there seems to be no statistically significant difference between the three powders, which is surprising in the case of Dicalite. Figure 3.9b, which shows U_T^* vs. G_s, shows an even better correlation.

If one considers U_T^* to be a measure of cluster size

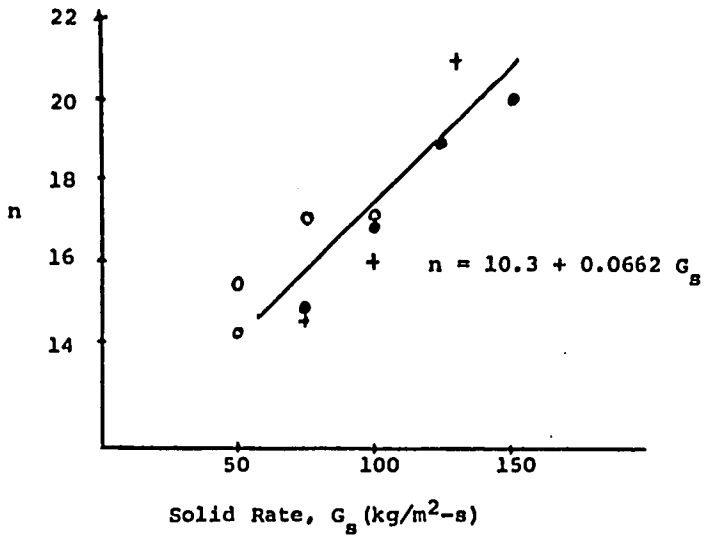

Figure 3.9a: The index n in the dense conveying regime for three Group A powders.

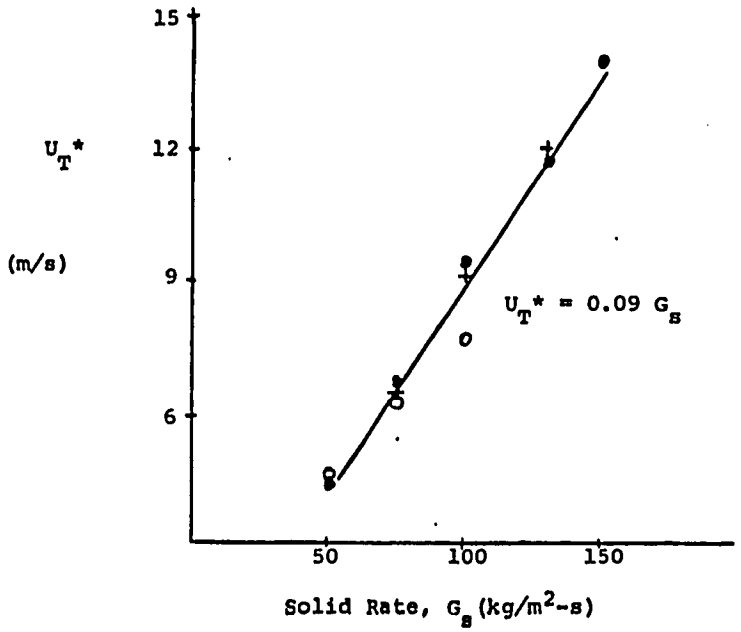

Figure 3.9b: U_T* in the dense conveying regime for three Group A powders.

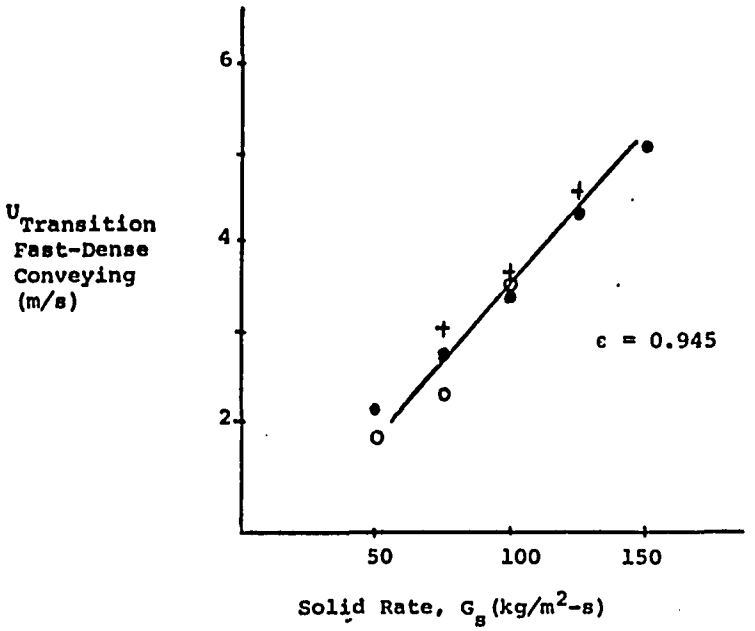

Figure 3.9c: Transition velocity from fast fluidization to dense conveying for three Group A powders.

Symbols used in Fig. 3.9

+ - HFZ-20

o - Dicalite

● - FCC

and density (an "effective" terminal velocity), it seems that all three powders give rise to similar clusters for $\varepsilon > 0.945$. Figure 3.9c shows the transition velocity from fast fluidization to dense conveying (i.e., the gas velocity at $\varepsilon = 0.945$) vs. solid rate, and again, all three powders behave similarly.

3.4.5. The Modified Richardson-Zaki Approach Applied to Data from the Literature

It is much riskier to represent other investigators' results in the Richardson-Zaki form, without access to the original data. However, some tentative comparisons will be tried. The results of Massimilla (Figure 3.1) are represented in Figure 3.10, assuming $\varepsilon_o = 0.45$. The index n has a value 11.7 in the slugging regime, which agrees with the values for our two cracking catalysts, FCC and HFZ-20. U_T^* for Massimilla's data is rather high, 102 m/s, possibly indicating a heavier solid than HFZ-20, or a much narrower size distribution without a substantial fines fraction. The change in slope in Massimilla's expansion curve seems to be around 0.6 m/s, while a transition velocity of between 0.3 - 0.4 m/s is reported. It is not clear, however, how this transition was measured. It seems that the capacitance probe was located near the bed top, where transition to turbulence takes place much earlier than in the lower section.

Another comparison seems to exist between our data for FCC and the FCC used by Carotenuto et al. (1974). Assuming $\varepsilon_o = 0.45$, one can transform their expansion data to the Richardson-Zaki form. This is shown in Figure 3.11. The slugging regime is represented by $U_T^* = 9.8$ m/s and $n = 8$, which is close to our results. The transition to turbulence is observed to be at 0.2 m/s by capacitance probes while the change in the expansion curve slope occurs at $U_g = 0.18$ m/s - slightly before the observed transition, which well agrees with our results.

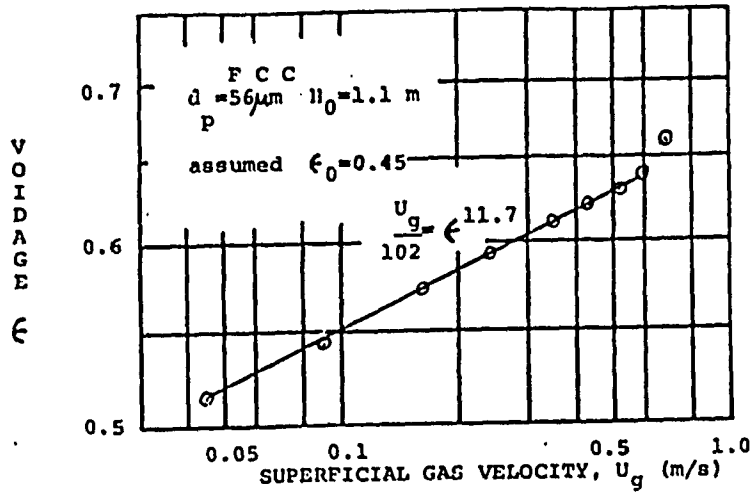

Figure 3.10: Bed expansion in the slugging and turbulent regimes, Massimilla (1971)

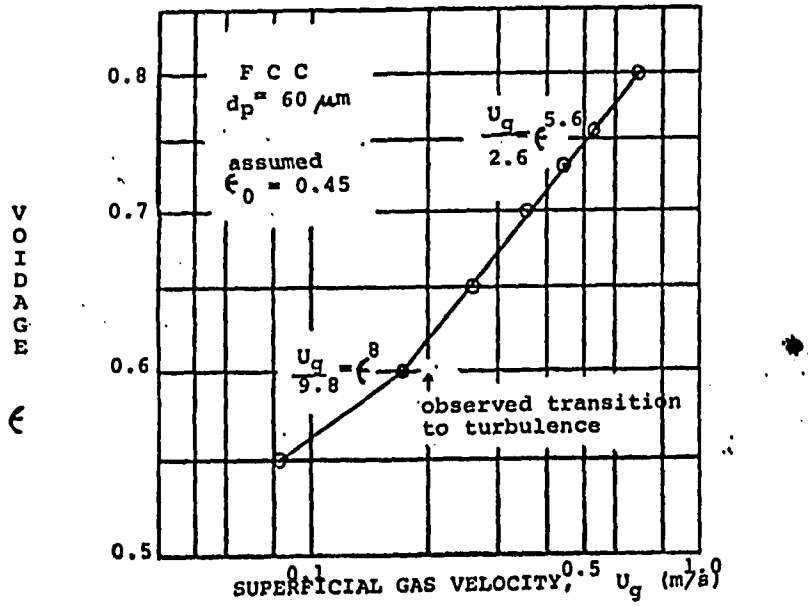

Figure 3.11: Bed expansion in the slugging and turbulent regimes, Carotenuto(1974).

In the turbulent regime, Carotenuto et al. results yield $U_T^* = 2.6$ and $n = 5.6$, and again this agrees rather well with our own observations. The other two powders used by Carotenuto et al., fine alumina and coarse alumina, yield $U_g/17 = \varepsilon^{9.3}$ and $U_g/1.0 = \varepsilon^{3.5}$ for the slugging regime.

Other data can also be reduced to the Richardson-Zaki form, but it should be stressed again that without the original data only qualitative agreement can possibly be pointed out.

Some observations are summarized in Table 3.8.

For fine powders the results of Table 3.8 compare favorably with the CCNY results of Table 3.6. It is clear that for these "regular" cracking catalysts the index n is 8-11 in the slugging regime, and half this value range, at around 5 in the turbulent regime. The variations in U_T^* are not so clear. In our work, where similar size distributions were employed, U_T^*/U_T for FCC and HFZ was shown to be linearly proportional to $\rho_s d_p$. This can no longer be claimed for the data represented idn Table 3.8. Noting the strong and even predominant effect of size distribution as shown in Table 3.7, one is led to believe that the different size distributions employed by the investigations summarized in Table 3.8 are responsible for the apparent non-dependence of U_T^* (or U_T^*/U_T) on particle properties. Indeed, it is conceivable that if U_T^* is viewed as a measure of an "effective" terminal velocity (incorporating cluster size and voidage) there is reason to believe that the particle size distribution is the most crucial parameter that would determine this degree of agglomeration.

Table 3.8 The Richardson-Zaki Representation for the Slugging and Turbulent Regimes - Data from the Literature

a) Fine Powders

Powders	ρ_s (g/cm^3)	$\bar{d}_p$ (μm)	$\rho_s \bar{d}_p$ (g/cm^2) x10^3	Slugging Regime U_T*/ (m/s)	Slugging Regime n	Transition Velocity (m/s)	Turbulent U_T* (m/s)	Turbulent n	Source
FCC	0.94	60	5.64	9.8	8	0.2	2.6	5.6	Carotenuto et al. (1974)
D_t=0.15m fine alumina	1.55	95	14.7	17	9.3	1.0			
FCC D_t=0.156m	1.9*	56	10.64	102	11.7	0.3-0.4			Massimilla (1971)
b) Coarse powders									
Iron ore D_t=0.05m	4.8*	100	48	5.6	15				Zenz** and Othmer (1960)
0.152m				30	18				
0.305m				505	24.4				

*Notes

* assumed

**no transition to turbulence is noted in Zenz and Othmer's data. It is interesting to note though, that the expansion curves for these data do predict closely the transition from bubbling to slugging in the 0.05m I.D. and 0.152m I.D. bed using the Stewart and Davidson (1967) criterion: $U_{\text{Transition bubble-slug}} = U_o + 0.07(gD_t)^{1/2}$

Tube diameter (m)	Transition to slugging $U_{TR}=U_{mf}+0.07(gD)^{1/2}$ (m/s)	Transition to slugging, expansion curves (m/s)
0.05	0.101	0.12
0.152	0.065	0.072
0.305	0.137	0.06-0.14

3.4.6. The Index n in the Modified Richardson-Zaki Approach

The index n should assume the value of 4.65 for fine powders, according to equation 3.2, which applies to particulate systems. Indeed, for FCC and HFZ, as well as for the cracking catalysts used by Canotenuto (1974) and Massimilla (1971), $n \cong 5$ in the turbulent regime. This view of the turbulent regime is supported by visual observations in our transparent equipment. The transition to turbulence is associated with the break-up of the slugs. On the whole the voids are smaller, and moreover, they appear and disappear in contrast to the slugging regime where usually one can follow a single slug from the bottom of the bed to the top.

Thus the index n can be viewed as a measure of the homogeneity of the fluidized bed. For fine cracking catalysts it seems to be only slightly dependent on particle properties or size distribution, which strongly affect U_T^*. In the slugging regime, our data as well as the above-mentioned data from the literature yield values of the index n which average around 10, or twice its value in the turbulent regime. Mogan, Taylor and Booth (1970/71) summarize data from several investigators showing n values from 4 - 10 for fine solids. Analysis of the Data of Zenz and Othmer (1960) shows a change in slope, or in the index n, which a transition from bubbling to slugging occurs. Thus, the range 4 - 10 reported by Morgan et al. can be viewed as representing data from the two regimes, the lower values in the bubbling regime, and the higher n values in the slugging regime. This reinforces the notion that the index n is a degree of segregation showing the greatest degree of inhomogeneity for the slugging regime.

Capes (1974) has suggested that high values of n

reported by Morgan et al. may be due to increased particle volume caused by agglomeration or irregular particle shape. This can be tied to our representation of segregation in the slugging regime, since the formation of slugs is probably enhanced by the agglomerative nature of the particles. Capes presents an approach that takes this agglomeration into account, and by making use of an "effective" porosity represents bed expansion by:

$$\frac{U_g}{U_T^*} = (1-KC)^n. \qquad (3.7)$$

where: $(1-KC) = \varepsilon_e$ effective porosity (3.8)

$(1-C) = \varepsilon_a$ apparent porosity (3.9)

Values of K > 1 indicates clustering and indeed this causes the effective porosity to be less than the apparent one. It is interesting to compare this approach to Yerushalmi et al. (1978), shown in equation 3.10:

$$(1 - \varepsilon_a) = (1 - \varepsilon_e)\ (1 - \varepsilon_c) \qquad (3.10)$$

where ε_c, the cluster voidage is not assumed to be ε_{mf} for the moment. Substituting equations 3.8 and 3.9 into equation 3.10 one gets:

$$K = \frac{1}{1-\varepsilon_c} \quad (3.11) \quad \text{or} \quad \varepsilon_c = 1 - \frac{1}{K} \qquad (3.12)$$

Let us examine the K values reported by Capes:

Table 3.9: Cluster Voidage from K Values Reported by Capes (1974)

K	ε_c
0.8	-0.25
1	0
1.2	0.17
1.4	0.29
1.7	0.41

In this analysis it is hard to attach physical sense to K < 1, which gives negative values to ε_c. For spherical values of K > 1.3 should be used, and if one assumes minimum fluidization voidage for the clusters, one should use K > 1.7, which is the highest value reported by

Capes. It is clear that the "clusters" reported by Capes and the same concept as used by us are different. While Capes reports cluster size of 100-260 μm, which is in the range of the largest particles used by Morgan et al., much larger clusters are evident in our work.

The results of Mogan, Taylor and Booth (1969), are important because of the limited high pressure data available, but a 1.75 cm ID. tube was used. They observed a "predominately downward motion at the tube wall", which raises questions as to the magnitude of wall effects. The dependence of bed expansion on bed diameter was shown (see Figure 3.7) to be quite strong. In general, the voidage will decrease strongly in going from D_t = 1.75 cm to D_t say, of 15 cm. This would offer an alternative explanation to the high value of n as being a small diameter phenomenon in this case.

We applied the Capes approach to our FCC data in the slugging regime, with the help of equation 3.13

$$U_t^* = \left\{\frac{4}{225} \frac{(\rho_s-\rho_g)^2 g^2}{\rho_g \mu}\right\}^{1/3} D_c \qquad (3.13)$$

This gives D_c = 0.21 cm.

Our approach, on the other hand, is to view the index n as a degree of segregation in a slugging bed of fine solids caused largely by particle agglomeration. Thus, large values of the index n arise naturally and need not be corrected. These values of n can be obtained from the Richardson-Zaki equation (3.2) if one uses D_c, or an "equivalent" cluster diameter, instead of D_p, the single particle diameter.

For FCC and HFZ the appropriate equation is:

$$n = \left(4.35 + 17.5 \frac{D_c}{D_t}\right) R_{e_t}^{-0.03} \qquad (3.14)$$

Note that the single particle Reynolds number is used in

choosing the appropriate Reynolds number range and in equation 3.14, while D_c is used for dp. The rationale for this choice is that clustering is a dynamic phenomenon, particles move in and out of clusters - a phenomenon that is supported by high velocity movies taken at CCNY and by DeLasa and Gau (1973). Thus the single particle properties, as well as its Reynolds number are still important. Clustering is taken into account as a segregation causing phenomenon, which is relative to D_t, the tube diameter. Obviously, equation 3.14 is only a first approximation, but some order of magnitude values of D_c can be obtained from it (and experimental values of n) and compared to the cluster diameter calculated by Yerushalmi et al. (1978).

Table 3.10. Cluster Diameters for FCC

Regime	D_c from Eq. 3.14 (cm)	D_c from Yerushalmi et al. (cm)
Slugging	3.9	~ 3.0
Turbulent	0.4	0.7-1.5

An order of magnitude agreement and the same trend are shown for the cluster diameter calculated by both methods in Table 3.10. The same trend continues into the fast fluidization regime, n values are getting smaller, and so is D_c as calculated by Yerushalmi et al. While this can be viewed as encouraging, one should not forget that we refer to clusters as a concept rather than as hard spheres of a diameter D_c. As was pointed out before, clustering is a complex dynamic phenomenon. One should

keep in mind the following important features of clusters:

a) A size distribution rather than a single diameter is more likely to represent cluster size.

b) The cluster voidage, ε_i, as well as the cluster size affects the "effective terminal velocity". This voidage can vary with cluster size, time, and gas and solid fluxes. The effect of this cluster voidage on the slip velocity is elaborated upon in the next subsection.

c) Clustering is a dynamic phenomenon, particles move into clusters, are stripped off by the rising gas; smaller clusters coalesce to large ones, which in turn break up. DeLasa and Gau (1973) found that this observed clustering does not affect conversion in a catalytic reaction. This would seem to indicate that clustering is not a segregative phenomenon as far as gas-solid contact is concerned. It would seem plausible to assume that either or both of the following is taking place: more gas than previously assumed is traveling through the cluster phase (causing larger cluster voidages than minimum fluidization; the characteristic time distribution associated with a particle being in a cluster is small when compared to the average gas residence time.

d) Our visual observations and high velocity movies support the dynamic picture presented above. It also seems that most rising clusters are elongated in shape, explaining the observed drag reduction by the shielding effect of long chains of spheres. This has been discussed by the author (1979).

All of these factors help illustrate the complexity of the clustering phenomenon. It is clear that a simple "hard sphere" picture is inadequate when describing clustering. A more quantitative comparison between the

"hard sphere" model and the actual slip velocity is presented in the following subsection.

In the fast fluidization and dense conveying regimes both n and U_T^* become dependent on solid rate, as is shown in Table 3.5. The dependence of the index n on solid rate was shown to be linear for all three group A powders (Figure 3.9a) investigated in the dense conveying regime, and can be described by:

dense conveying fine powders

$$n = 10.3 + 0.0662G_s \qquad (3.15)$$

The same linear dependence is shown for FCC in the fast fluidization regime (Figure 3.12a).

FCC fast fluidization

$$n = 0.0482G_s \qquad (3.16)$$

Both regimes show an increase in the value of n, or the degree of segregation, with increasing the solid rate.

An Alternative Representation of the Index n:

In the first part of this subsection the index n was presented as a measure of the degree of segregation. It was assumed that because clustering can be viewed as a dynamic phenomenon, thus causing gas to come into contact with the individual particles, single particle properties come into play even when the overall effective terminal velocity indicates much larger aggregations of particles. Thus Equation 3.14 predicts large values of n.

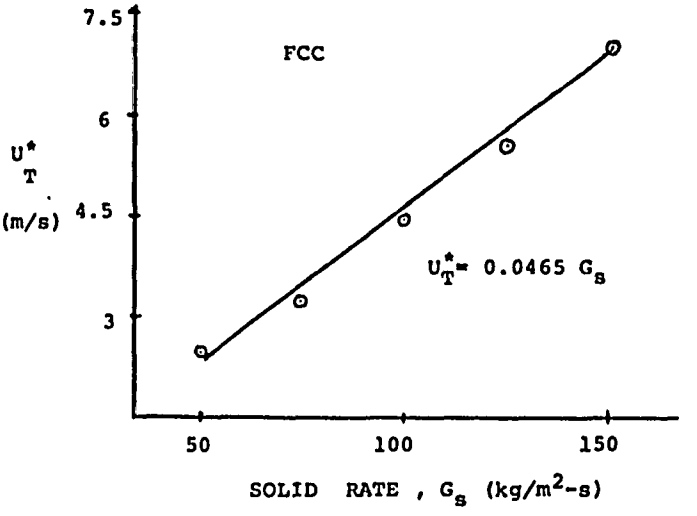

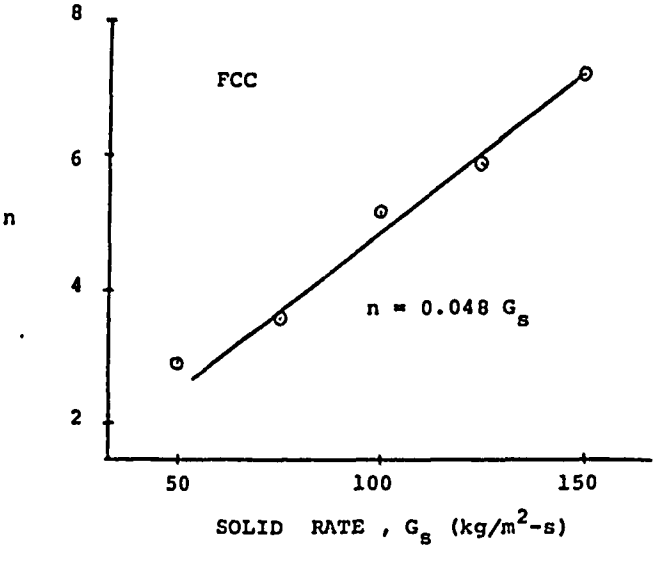

Figure 3.12: The index n and U_T^* for FCC ("used") in the fast fluidization regime.

On the basis of available information an equally plausible explanation has been suggested by Yerushalmi (1980,b). In this approach the clusters are considered more "tightly packed", so that their cluster size and voidage would cause an effective behavior similar to large particle fluidization, i.e., n values from Equation 3.2 would be in the 2.4 - 3 range. An effective, rather than the apparent voidage should then be used to represent bed expansion (in the form of Equation 3.7). Both voidages are represented in Figure 13, which is similar to the curves presented by Capes (1974).

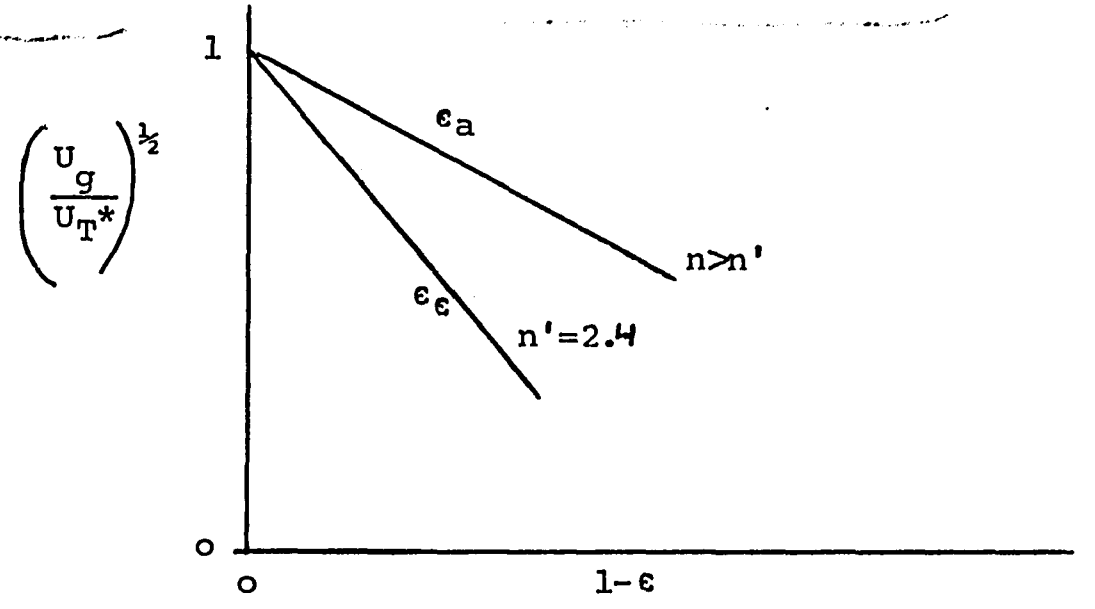

Figure 3.13. Schematic representation of bed expansion in one fluidization regime.

Thus, the Yerushalmi-Capes approach would consider n values to be those of large particles, of the same diameter as D_c, The connection between the apparent and effective voidages is through the cluster voidage, Equation 3.10. The cluster diameter is calculated from

$$\epsilon_c = 1 - \frac{1-\epsilon_a}{1-\epsilon_a^{n/n'}} \qquad (3.15)$$

If n' = 2.4 would have been used throughout all fluidization regimes, the following cluster voidages are calculated.

Table 3.11 - Cluster Voidage Calculated from Equation 3.15

Regime	n	Apparent Voidage ε_a	Cluster Voidage ε_c	Effective Voidage ε_ε
Slugging	9.2	0.54	0.49	0.09
		0.6	0.53	0.14
Turbulent	5	0.64	0.41	0.39
		0.7	0.43	0.48
		0.75	0.45	0.55

Fast Fluidization

G_s = 50 kg/m^2-s			G_s = 100 kg/m^2-s			G_s = 150 kg/m^2-s		
n = 2.9			n = 9.5			n = 7.2		
ε_a	ε_c	ε_ε	ε_a	ε_c	ε_ε	ε_a	ε_c	ε_ε
0.82	0.16	0.79	0.84	0.43	0.72	0.86	0.62	0.64
0.87	0.16	0.85	0.90	0.44	0.82	0.90	0.63	0.73
0.95	0.17	0.94	0.95	0.45	0.91	0.95	0.65	0.86

Dense Conveying n = 14.2			n = 9.4			n = 20		
ε_a	ε_c	ε_ε	ε_a	ε_c	ε_ε	ε_a	ε_c	ε_ε
0.97	0.82	0.84	0.97	0.73	0.89	0.97	0.87	0.78

The following features are presented by Table 3.11:

a) The values of the effective voidage are very low in the slugging regime. It can be concluded that this method is not suitable for the slugging regime where the index n represents gross segregation into the slug and dense phases rather than clustering.

b) For the more homogeneous higher velocity regimes reasonable values for the cluster voidage are obtained. It should be noted that the cluster voidage remains relatively constant in each fluidization regime, increasing slightly as the gas velocity is raised.

c) In the turbulent regime, the cluster voidage is close to minimum fluidization voidage, an assumption which is often made.

d) In the fast and dense conveying regimes the cluster voidage is a function of the solid rate, being very low for G_s = 50 kg/m^2-s.

For this low solid rate it is hard to attach physical significance to ϵ_c = 0.16 unless one can assume very small clusters, or an almost uniform suspension. The higher solid rates present reasonable cluster voidages, from minimum fluidization voidage (G_s = 100 kg/m^2-s) to ϵ_c = 0.63 for G_s = 150 kg/m^2-s. The higher slip velocity associated with the higher solid rate is causing a higher cluster voidage. All three voidages, ϵ_a, ϵ_c, and ϵ_ϵ approach one when the dilute transport regime is approached.

3.4.7 U_T^* in the Modified Richardson-Zaki Approach

The value of U_T^* is thought to represent the size and density of clustering in the suspension. It has a high value,

many times the single particle terminal velocity, in the slugging regime and it decreases considerably once transition to turbulence takes place. For both HFZ-20 and FCC ("used") U_T^*/U_T values in the turbulent and slugging regime are linearly dependent on their respective $\rho_s d_p$ products, or Galileo numbers. This relationship shown in Table 3.6 cannot be taken to include our "fresh" catalysts, Dicalite, or the fine solids used by other investigators (Table 3.8). The culprit seems to be the effect of the size distribution shown in Table 3.7. "Fresh" catalysts show markedly lower values of U_T^* in both the slugging and turbulent regimes than "used" catalysts. Thus, unless the effect of the size distribution, which seems stronger than particle properties, can be taken into account, no general dependence on $\rho_s d_p$ can be suggested. The strong dependence of bed expansion on size distribution was shown by Rowe et al. (1978) and qualitatively their results show the same trend: the higher the fines fraction, the higher the voidage at the same gas velocity. Since the index n does not vary much, this causes a much lower value for U_T^*. A reduction in the effective cluster size seems to take place when more gas flows in the dense phase.

Much like the index n, U_T^* seems to decrease in going to the turbulent regime, suggesting more homogeneity. U_T^* increases with increasing solid rate in both the fast and dense conveying regimes (Table 3.5), qualitatively agreeing with the picture of increased clustering as the solid rate increases. It is not clear how an "equivalent" cluster diameter can be calculated from U_T^*. As an exercise, a simple approach is illustrated in Table 3.12 where a cluster diameter is calculated by using:

$$U_T^* = \left(\frac{3.1g(\rho_s - \rho_g) D_c}{\rho_g} \right)^{\frac{1}{2}} \qquad (3.16)$$

$$R_{e_c} = \frac{D_c \rho_g U_T^*}{\mu} > 500 \quad \text{(Kunii and Levenspiel, 1969)}$$

The qualitative agreement with D_c values, calculated from the index n, is shown for the slugging and turbulent regimes (Tables 3.10, 3.12). The variation of U_T^* with solid rate in the fast fluidization regime for FCC is shown in Figure 3.12b where it is shown that $U_T^* = 0.0465\ G_s$. In the dense conveying regime, all three powders investigated seem to follow the same linear relationship $U_T^* = 0.09\ G_s$, possibly suggesting that all three cluster to the same degree in that regime. This relationship is shown in Figure 3.9b.

Table 3.12: Cluster Diameter Calculated from U_T^* for "Used" FCC

Regime	U_T^* (m/s)	D_c (cm)
Slugging	22.6	1.92
Turbulent	3.4	0.0435
Fast G_s=50 $\frac{kg}{m^2-s}$	2.5	0.0235
75	3.3	0.0410
100	4.5	0.0763
125	5.6	0.118
150	7.2	0.195
Dense Conveying		
G_s = 50 kg/m^2-s	4.6	0.080
75	6.4	0.154
100	9.4	0.333
125	11.6	0.507
150	13.7	0.707

It is interesting to look at the connection between the effective terminal velocity and the slip velocity. When one starts with a single particle conveyed by a gas with a superficial velocity, U_g, the slip velocity is close to the single particle terminal velocity. This is illustrated in Figure 3.14a. Upon adding more particles, but keeping the suspension dilute one can observe uniformly dispersed particles - especially when wall effects are negligible. For this situation, depicted in Figure 3.14b, the slip velocity is <u>less</u> than the single particle terminal velocity, and the phenomenon is known as hindered settling. While no data is presented here for pneumatic conveying, visual observations lead us to believe that particles are not truly uniformly dispersed and one can always detect some clustering and recirculating especially in the vicinity of the walls. This deviation from a uniformly dispersed suspension is more pronounced at higher solid rates, or lower gas velocities. As a voidage of approximately 0.98 or lower, the uniform suspension structure breaks down and the agglomerative nature of the suspension is evident. Particles rise in center, in the form of twisting chains, of varying lengths and widths. These chains or strands are broken and reformed and some are falling back, especially in the vicinity of the walls. Some agglomerations of particles seem to be almost stagnant at the wall, they creep down (or up at higher gas velocities) and are constantly stripped of particles and then replaced by new clusters, seemingly thrown off the center region of the tube. This picture is typical of the proposed dense conveying regime, and is represented schematically in Figure 3.14c.

Both clustering and solid recirculation are causing a reversal in the magnitude of the slip velocity, and one obtains slip velocities much <u>higher</u> than the single

a) A single particle

$U_{slip} = U_g - U_p = U_T$

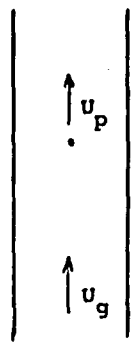

b) Uniformly dispersed dilute suspension

$\frac{U_g}{\epsilon} - U_p = \epsilon^n U_T$

$U_{slip} < U_T$

"hindered settling"

c) "dense conveying"

$U_{slip} \gg U_T$

$\frac{U_g}{\epsilon} - U_p < \epsilon^n U_T^*$

clustering and recirculation

d) Fast fluidization

$\frac{U_g}{\epsilon} - U_p \leq \epsilon^n U_T^*$

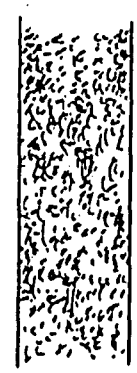

Figure 3.14: Slip Velocity in various fluidization regimes.

particle terminal velocity. The suspension "effective terminal velocity" U_T^* was calculated, along with the index n, from the expansion data and they were given previously in Table 3.5. It is evident that all values of U_T^*, in the dense conveying regime, are more than an order of magnitude greater than the single particle terminal velocity. These values of U_T^* lead to cluster sizes in the range of 0.08-0.707 cm as opposed to a particle mean diameter of 0.0049 cm. If one can consider these clusters as rigid spheres one would expect a modified equation for the slip velocity to hold.

$$\frac{U_g}{\varepsilon} - U_p = \varepsilon^n U_T^* \qquad (3.17)$$

The average slip velocity is calculated and compare to the right hand side of Equation (3.17) in Figure 3.15 for three solid rates. It is clear that throughout the dense conveying regime Equation 3.17 overestimates the actual (average) slip velocity -

$$U_{slip} < \varepsilon^n U_T^* \qquad (3.18)$$

Moreover, while Equation 3.17 predicts an increase in the slip velocity as the voidage is increased (because of an increase in the value of ε^n, i.e., a decrease in the magnitude of the hindered settling effect) the actual slip velocity peaks at around $\bar{\varepsilon} = 0.97$ and then decreases approaching U_T as the voidage approaches the value 1.0. It seems then that as was pointed out before, the phenomenon of clustering is much more complex than a single model of rigid spheres would predict. One possible explanation would seem to be as follows: while U_T^* is a measure of cluster size, one has to take the cluster voidage into account as well. It stands to reason that when voidage is increased (by increasing the superficial gas velocity)

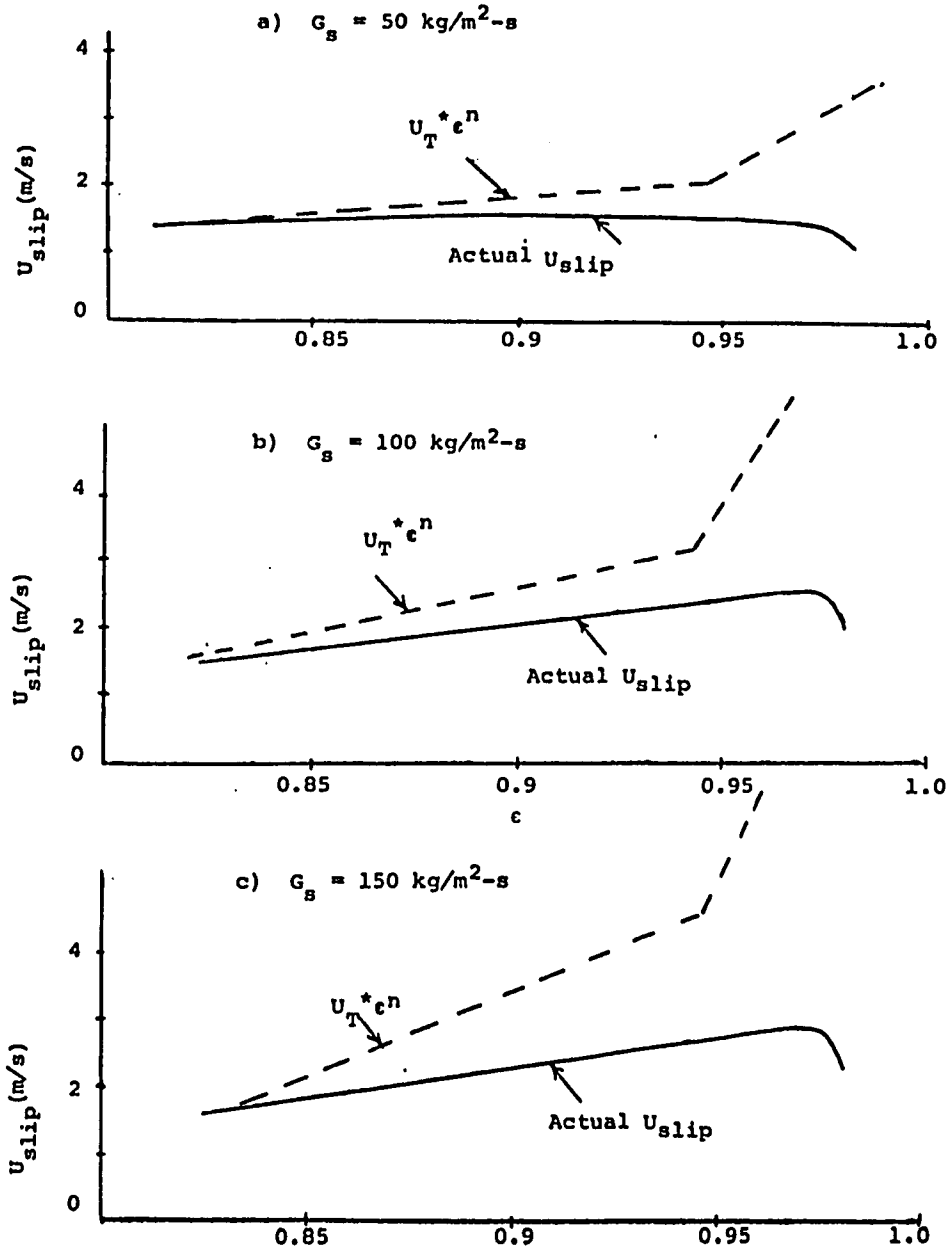

Figure 3.15: The slip velocity in the dense conveying and fast regime.

the clusters have mor "room" to move. Two parallel phenomena might be takding place: a) the clusters expand and their voidage ε_c is larger than at lower bed voidage values. Thus, more gas passes in the interstitial voidage of the cluster, causing the single particle properties to come more into play. This was alluded to before, in the use of Equation 3.14. The overall slip velocity then would lie between the high value caused by $\varepsilon^n U_T^*$ and the much lower value predicted by $\varepsilon^n U_T^*$.
b) The higher gas velocity is exerting a larger shearing stress on the down-flowing phase. Thus, clusters would recirculate less than at lower gas velocities. This phenomenon of decreased down-flow velocity at superficial gas velocities higher than 3 m/s is corroborated later by our solid mixing results.

These two factors, a lower down-flow velocity and a higher cluster voidage offer one possible explanation for the deviation of the actual slip velocity from that predicted by Equation 3.17.

When one goes into the fast fluidization regime, depicted in Figure 3.14d, the voidage decreases and solid recirculation becomes predominant. The actual slip velocity approaches the theoretical prediction of Equation 3.17 (Figure 3.15) and seems to equal it exactly at the onset of the fast fluidization regime for all solid rates investigated. Note that different values of n and U_T^* are used in the fast fluidization regime. Following the same logic one may presume that clusters behave more as tightly packed spheres in the denser fast fluidization regime. The denser the suspension - the denser are the clusters and thus their terminal velocity, corrected for the voidage, approximately equals the actual slip velocity. It is interesting to note that Equation 3.17 seems to be exactly satisfied at U_{T_R}, the transport velocity, for all

solid rates investigated. This seems to offer another method for calculating U_{TR} and it agrees well with the picture of this transition as presented in the introduction to this work.

The transport velocity is thought of as the velocity which would cause the entrainment of the largest possible clusters. As the voidage is increased beyond the voidage at U_{TR} the actual slip velocity is less than that predicted by Equation 3.17 for the same reasons discussed before: the clusters expand, allowing more gas to percolate through them, and less recirculation is taking place at the higher gas velocities.

Chapter 4 : Solid Mixing

4.1 Introduction

Gas and solid mixing can be of interest to the design of fluidized bed reactors. Gas mixing and the residence time distribution of the gas in the bed are especially important in solid-catalyzed gas phase reactions, but they can also be of interest in non-catalytic processes. For example, in flash-hydrogenation of coal, the gas residence time is of primary interest. Our previous experiments (Cankurt and Yerushalmi, 1978) have touched upon the phenomenon of gas mixing in high velocity fluidized beds, and these results will also be discussed here insofar as they are connected to the phenomenon of solid mixing. Our gas mixing studies seem to indicate considerable mixing (or backflow) of gas at low superficial gas velocities. This relative backflow seems to decrease linearly in the turbulent fluidization regime, and to decay to virtually plug flow of gas in the fast fluidization regime.

In situations where the solid is being treated, as in non-catalytic gas-solid reactions, roasing of ores, and in coal conversion processes solid mixing and residence time distribution are important. In catalytic gas-solid reactions solid mixing can still be of interest as it is thought of as the primary mechanism for heat transfer in the bed.

Solid mixing is a complex phenomenon and despite a large number of investigations in the low velocity fluidization regimes, considerable disagreements are reported. This is due both to experimental difficulties and to the limited predictive powers of the various models used to describe solid mixing. Scarce information is available

about solid mixing in the high velocity regimes where the above mentioned problems are probably compounded. Low velocity fluidization data and theory are used as the starting point for treatment of solid mixing in the high velocity regimes. The direct approach to investigate solid mixing seems to be (and indeed has usually been) to measure local velocities of solid particles. This information can then be used in combination with an appropriate physical model, for example the two phase countercurrent flow model, or the Kunii and Levenspiel bubbling model to predict local and overall solid fluxes in the bed. These fluxes however do not seem to be of primary interest and usually the results would have to be translated into dispersion coefficients which are subsequently used to predict conversions and heat transfer coefficients. (It should be noted that one of the solid mixing experimental techniques, namely, the heat transfer method, gives heat transfer coefficients directly.) A dispersion model has also been used (May (1959) and others) to predict dispersion coefficients but it was generally discarded in favor of the two-phase models in the past two decades. The main reason for this seems to be in its inability to predict lower conversion than the completely mixed model (as the dispersion coefficient can only vary from zero for plug flow, to infinity for CSTR behavior.) Lower conversions than a completely mixed model would predict have been observed for low velocity fluidized beds, particularly for shallow ones.

The two-phase models, while quite successful in correlating experimental results, seem to be of limited predictive value. The problem lies in the rather large (2 to 6) number of parameters which cannot be easily determined, much less extrapolated. Chief among them is the problem of bubble

size and velocity, especially in large diameter vessels and higher gas velocities. This problem was discussed in Chapter 3, where it was shown to cause large deviations in bed expension from two-phase models predictions. These various models will be discussed and compared in this chapter.

4.2 Solid Mixing Experimental Techniques

The direct approach to investigate solid mixing is to measure local velocities of solid particles, either directly or by labeling some of the particles with some detectable property. Oki et al. (1977) review several methods for measuring solid velocities at high solid loadings. The main approaches reported are: the drag force method, the heat transfer method, the tracer method, and the optical fiber method. All experimental techniques can be classified in two general categories, disruptive and non-disruptive.

4.2.1 Disruptive Techniques

Defluidization

Disruptive techniques require either the introduction of probes into the fluidized bed or abrupt defluidization of the bed and laborious layer by layer analysis. The latter method is described by Babu et al. (1973) and others. Besides being time consuming, defluidization techniques suffer from large uncertainties as the bed requires a few seconds to defluidize, and in that time the particles can move significantly. Naturally, this technique introduces a larger error as the gas velocity is increased and thus is probably unsuitable for high velocities. Other disruptive techniques include direct sampling, isokinetic or otherwise, and introducing various probes into the bed.

Isokinetic Sampling

Isokinetic sampling is a well-known technique which uses suction probes positioned parallel to the main stream. The underlying assumption is that if the velocity in the nozzle is equal to that of the surrounding stream, the main flow will not be disturbed. This technique was used by van Breugel et al. (1970) and others. A large number of factors influence the accuracy of isokinetic sampling in a dense suspension. A careful analysis of this technique is presented by van Breugel et al. and the following factors are mentioned:

1) turbulence
2) acceleration by deflection around the probe
3) friction and entrance losses
4) partial plugging
5) unbalance of the static pressures inside and outside the probe.

Keeping these factors in mind van Breugel et al. claim a 10% accuracy at low solids concentrations and 20-30% accuracy at high concentrations. These values apply to a probe pointing in the upstream direction. If one wants to obtain the true solids flux, one has to measure the flux of solids flowing backwards as well. This situation arises near the wall region for the "riser" condition described by van Breugel et al. (1970) and by Gajdos and Bierl (1978) or throughout the whole cross-section in the turbulent or fast bed regimes. However, turning the probe upwards seems to violate isokinetic sampling conditions as gas is still being sucked by the probe.

Additional factors, not easily quantified, make isokinetic sampling less accurate for high velocity fluidization where the solid concentration is higher than a few percent.

1) As mentioned before, turning the probe to face the downstream direction can no longer be considered isokinetic. To be truly isokinetic, gas would have to be blown out of the probe. Thus, it can be suspected that even if some suction is provided, the results for the backflow are underestimated and little backmixing in a high velocity region will be detected.

2) Isokinetic sampling, used traditionally for low density systems, relies on smooth streamline flow. This is not the case for the turbulent eddy nature of high velocity-high solid loading flow, and one can only speculate how much of the flux is actually measured.

3) The phenomenon of clustering of fine particles at high solid loadings is well documented (Yousfi and Gau (1976), Chapter 3). High speed movies of the fast fluidized bed reveal that fine particles aggregate, and long strands of particles can be seen rising in the center and descending predominantly near the wall. This behavior further complicates isokinetic sampling techniques since it is not known how long it takes to give true averaging of a flux nor in what manner clusters are deflected or broken in the immediate vicinity of the probe.

The solid flux is calculated from the solid velocity and the local bed density which can vary significantly both in time and location in the bed. Unless some density probe is used along with the main probe, using the average bulk density introduces a large error.

We thus conclude that isokinetic sampling is unsuitable for flow situation in which particle trajectories depart strongly from streamline flow, and involving high solid loadings. Notwithstanding the foregoing considerations, which they fully recognized, Gajdos and Bierl (1978) have

used the results of isokinetic sampling obtained in a narrow 3-inch column to draw conclusions regarding the nature of the fast bed condition vis-a-vis riser flow.

Other Disruptive Techniques

Collecting solid samples can be performed in a non-isokinetic way. One solid is used as a tracer, and simultaneous samples are being withdrawn from multiple points in the bed. This technique, used by Brekken et al. (1970) and others, is disruptive of the flow patterns just before sampling. Although this effect can be minimized by making the samples small enough, it is still necessary to use automatic sampling techniques. As the gas velocity is raised, the time interval between two consecutive samples has to decrease, and obviously this technique becomes impractical for high velocity fluidization.

Other disruptive techniques use various probes inserted in the bed; for example, thermistor integrator probes are used widely (Avidan, 1979). Solid particles are heated in one part of the bed and their temperature is measured at various points above. The results are an average for groups of particles and the mass flow can be correlated by the heat transfer rate. The use of capacitance probes to measure bubble frequency, and thus correlate solid mixing, is described by Werther (1976). Two probes are positioned vertically, one above the other and the signals interpreted to give both mean bubble rise velocity and bubble size distribution.

Two main problems are always present in probe sampling methods. The measurement of solid particle velocity is not always direct, and the probes disrupt the local flow pattern in their immediate vicinity. The latter problem is more serious at higher solid loadings and we believe it is prohibitive at high velocity fluidization conditions. Probe

methods have a high degree of accuracy at low solid loadings, for example, in pneumatic conveying. Mendies et al. (1973) report three percent reproducibility in axial particle velocities using electrostatic charge transducers.

Another technique which can be classified as disruptive is the radio pill method used by Merry and Davidson (1973) and others. A hollow perspex shell, containing a transistorized oscillator, is used as a "tracer" and is detected by inductance probes. Even though the pill is neutrally buoyant, it is much larger than the individual particles, and it could not be expected to follow the random movements of particles. Further, at high velocity a disrupted flow pattern develops around the pill.

4.2.2 Non-Disruptive Techniques

Non-disruptive techniques do not disrupt the flow pattern in the bed and usually employ a tracer. The tracer has to have the same density and size distribution as the bed material to give the actual solid particle flow patterns. While photographic methods are used to follow colored particles (Merry and Davidson, (1973), they are naturally limited to two-dimensional configurations or to observation of wall phenomena only, so usually a radioactive tracer is used. While some useful data were obtained by the latter method (van Zuillichen et al. (1973), Kondukov et al. (1964) and others) it still involves some disadvantages. Besides the obvious disadvantages involving the hazards of handling radioactive materials, this method gives rather noisy data. Strong gamma radiation has to be used because of shielding by bed material and this means that adjacent probes pick up signals from particles far from them. As demonstrated by Fitzgerald, et al. (1977), even at steady state the tracer signal would fluctuate by at least one order of magnitude.

The only other non-disruptive technique known to us involves use of a ferro-magnetic tracer. The first use of this technique is to our knowledge reported by Razumov, et al. (1968). The details are sketchy and despite the fact that the probes used were patented, very scattered experimental data are presented. Cranfield (1972) reports using the ferro-magnetic tracer method in a fluidized bed of large particles. An important observation reported by Cranfield is the observation that the inductance probes used did not initiate the flow of particles or attract the particles, the high frequency alternating magnetic field being closely confined to the immediate vicinity of the probe.

A ferro-magnetic tracer system adopted for use in the present study is based on a sensitive bridge circuit developed by Fitzgerald et al. (1977) and is described in the next section.

4.3 Experimental

The solid mixing experiments were conducted in the 15.2 cm I.D. expanded top bed and the 15.2 cm I.D. circulating system described in section 3.3. The solid used in both systems was fresh HFZ-20 whose properties are given in Tables 3.1 and 3.2. The schematic layout of the ferro-magnetic tracer system is described in Figure 4.1. Ferro-magnetic tracer is injected into the center section of the bed in a short time (0.5-1 sec) thus approximating an impulse disturbance. The concentration of ferro-magnetic particles is monitored by four outside probes, positioned 0.76 m and 1.42 m downstream and 0.53 m and 1.2 m upstream from the injection point. The signal from each probe is processed by a bridge element developed by Prof. T. Fitzgerald and his associates at Oregon State University and is recorded on a Hewlett Packard strip

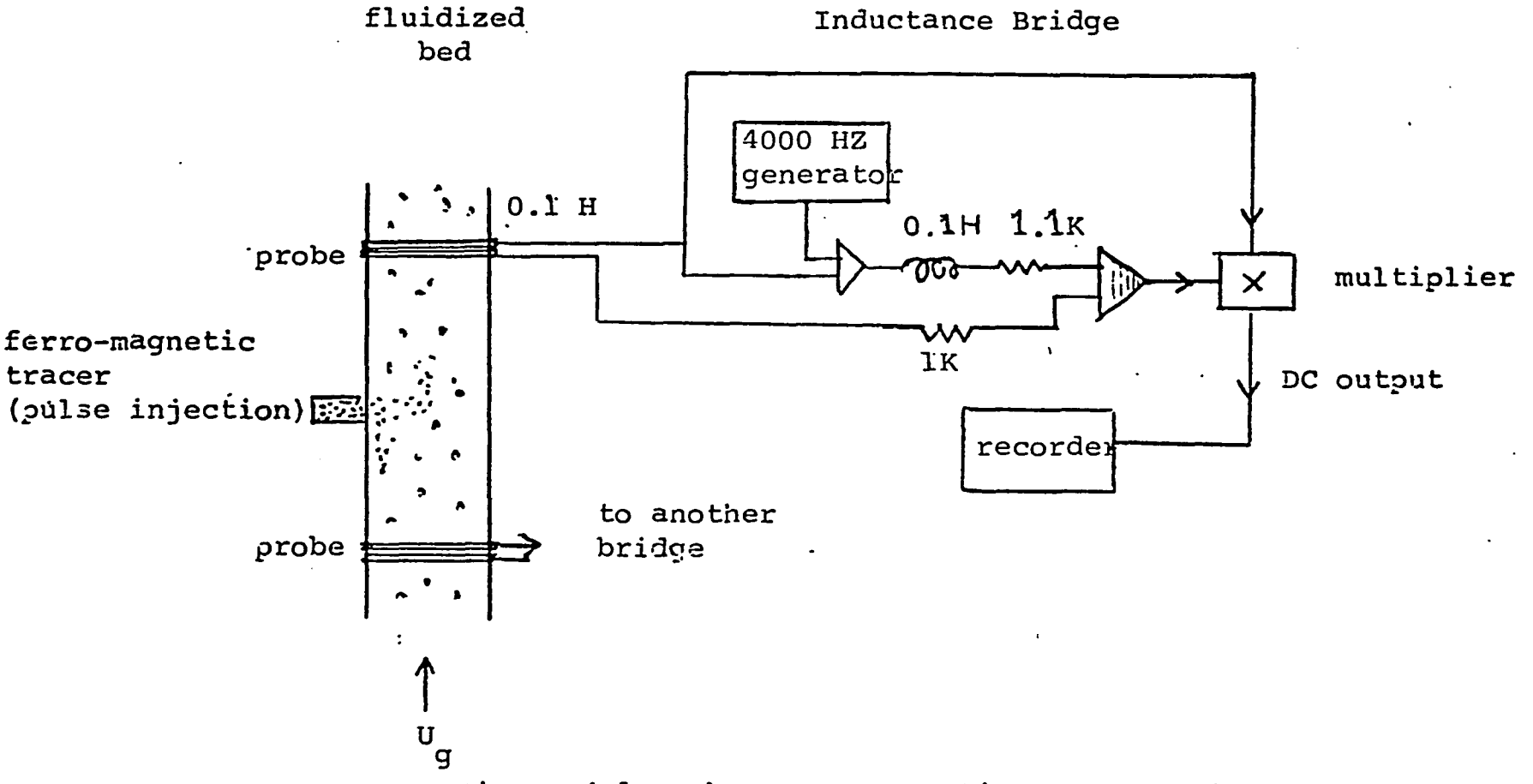

Figure 4.1: The Ferro-magnetic Tracer System

chart recorder.

Inductance Bridge

The bridge, shown in Figure 4.2, makes use of a function multiplier to obtain a linear signal whose change is directly proportional to inductance changes and virtually independent of resistance changes in the probe. A 4000 HZ sine wave is used to excite the bridge, one of its legs being the 0.1 Henry torroid and the other, the 0.1 Henry inductance of the probe. Small changes in the resistance of the bridge legs produce an output 90° out of phase with the excitation voltage. Hence, their integrated average is zero. An imbalance of the inductance, however, gives rise to a signal at the output of the amplifier which has a non-zero average value. Further details of the bridge element are given by Fitzgerald et al. (1977).

Solid Tracer Injector

The injector was designed to inject up to 150 g of tracer (corresponding to ~ 1% of the bed solid inventory) in 0.5-1 sec. This is considered as satisfactory as far as approximating an impulse injection is concerned. One would not want to reduce this time interval further, as the entering tracer particles would have too high a kinetic energy, thus cause serious disruption of the local flow patterns. The mechanical injector first used is illustrated in Fig. 4.3. It was found to give slightly different injection as the "O" ring teflon seal wore out. Thus, the design shown in Figure 4.3 was modified to a pneumatic injector by removing the piston and air cylinder arrangement and introducing a 200 kPa pressure line. This pressure was found to be acceptable in a series of experiments in the expanded top bed. At a superficial gas velocity of 0.5 m/s a difference in bed behavior was observed in going from an injection pressure of 380 kPa

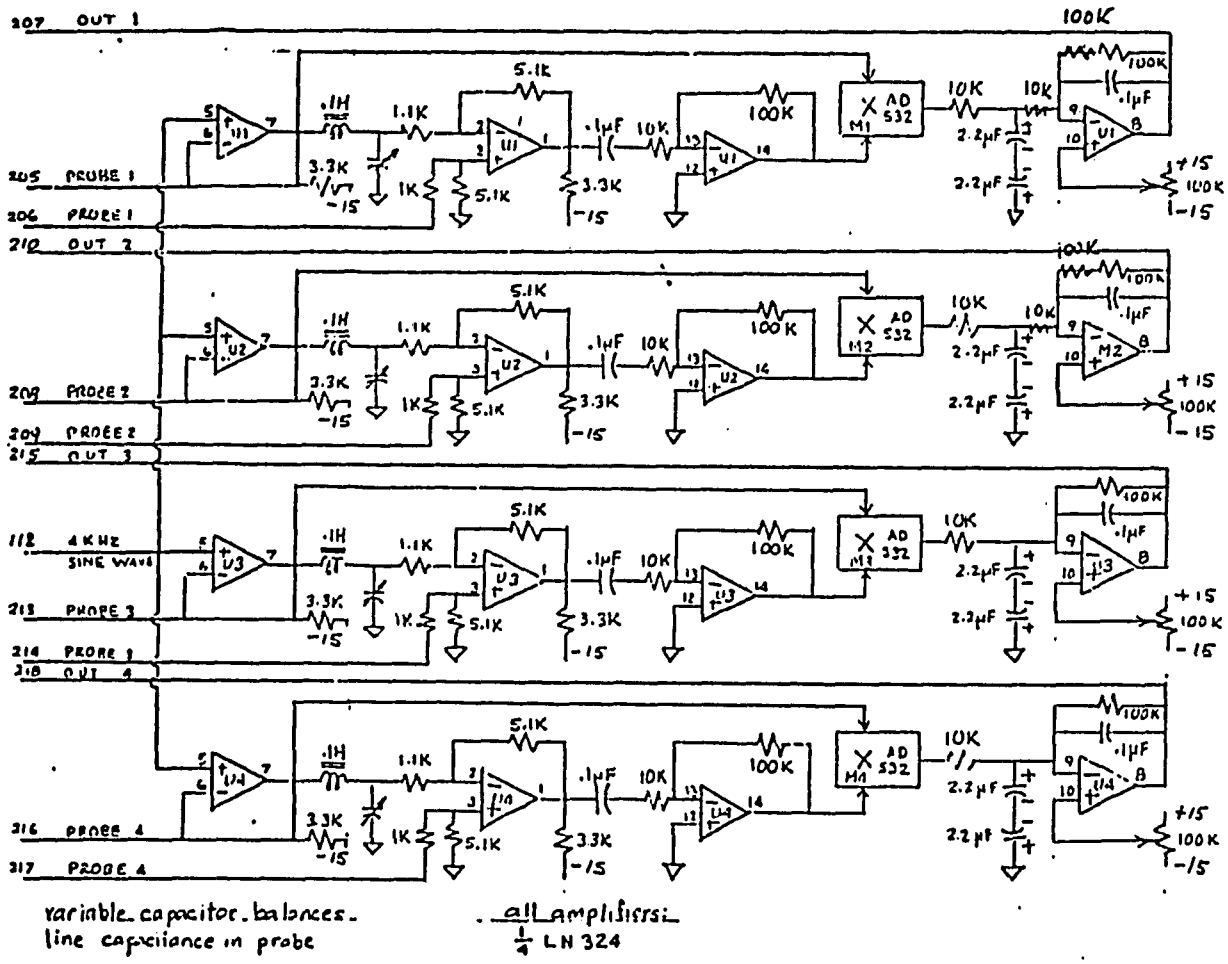

Figure 4.2: Schematic drawing of an inductance bridge card. There are four separate inductance bridge amplifiers on a card.

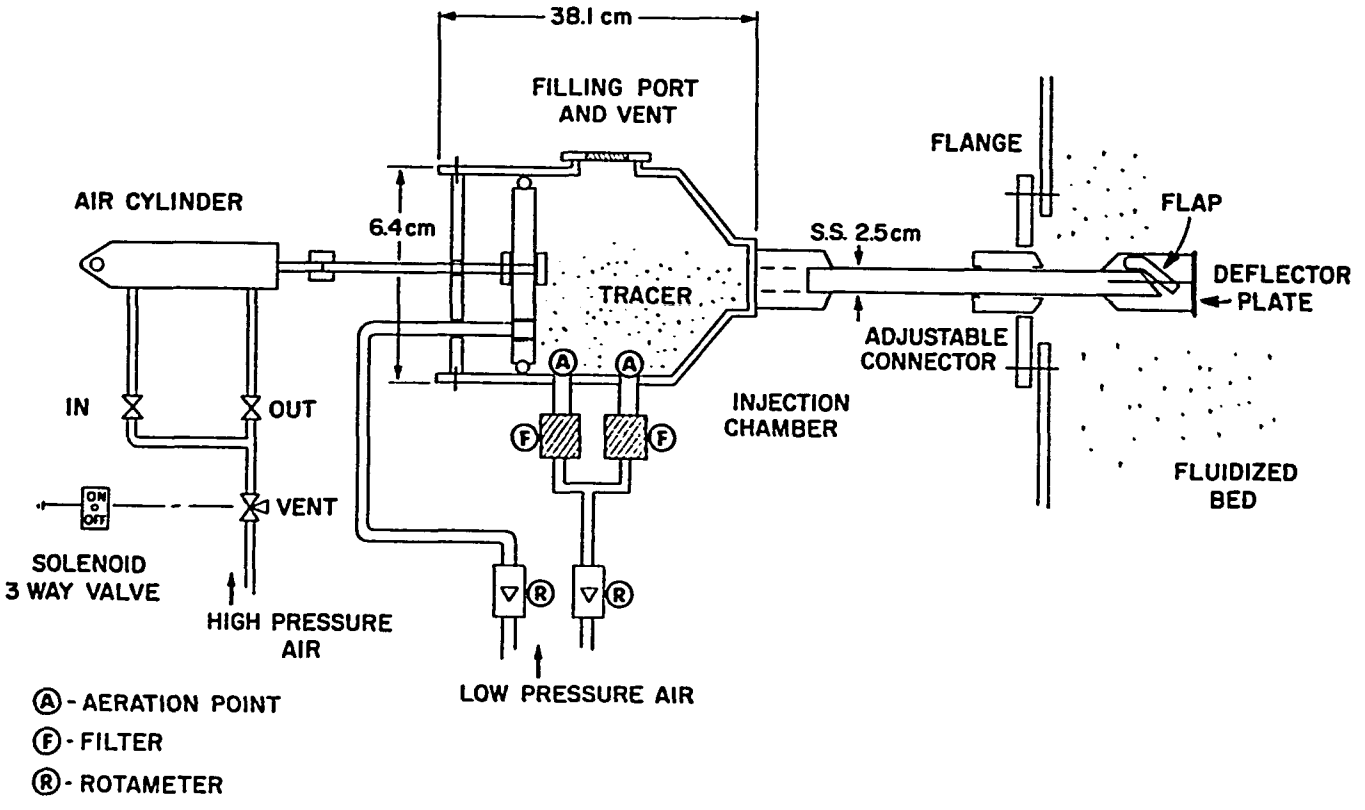

Figure 4.3: Tracer Injector

to 240kPa. However, no further change was observed for an injection pressure of 170 kPa, thus an air pressure of 200 kPa was chosen as the injection pressure for all experiments reported here.

Tracer

To be considered a tracer the ferro-magnetically tagged solid has to have the same terminal velocity as the bed material, i.e., the same solid density and the same size distribution. The procedure for preparing the tracer is as follows:

1) The ferrite material (manganese-zinc scrap transformer parts from Indiana General) is crushed to -400 mesh in a micronizer.
2) The resulting powder is incorporated in a polyurethane foam (kit supplied to Witco Chemical.) To prepare a tracer having the same bulk density as HFZ-20 (980 kg/m^3), 74% by weight of ferrite powder and 13% by weight of each of the two solutions in the polymer kit are used. The powder is first incorporated in liquid A (toluene diisocynate/polyester monomer) and then the catalyst (liquid B) is added while the solution is stirred at 2000 RPM for 60 seconds.
3) The dry tracer is crushed in a roller mill and sieved to the required HFZ-20 size distribution.

For the ferro-magnetic tracer method to be a nondisruptive technique, the measuring coils should produce no effect on the tracer particles, and there should be no interaction among the particles themselves. This indeed seems to be the case. The ferro-magnetic particles are well dispersed in the fluidized bed and do not seem to aggregate. Moreover, when the bed is slowly defluidized while the active inductance bridge is left on (i.e., the magnetic field created by the

probes is still active) no particles seem to concentrate in the area of the probe. This indicates that the attractive force between a tracer particle and the probe is negligible when compared to the other forces acting on the particle, drag, friction and gravity. The same conclusion was reached by Cranfield (1972). The bed material with the tracer was discarded after each run in the expanded top bed, so that each run was performed with fresh HFZ-20 and fresh tracer. In the circulating system it was found that because of the large inventory of solid in the slow bed, three or four consecutive solid mixing runs could be performed with the same bed material without giving excessive noise. This proved especially true at the higher gas velocities.

Special care had to be taken to avoid magnetic or ferro-magnetic materials in or near the fluidized bed. For example, the sintered steel porous plate used as an air distribution in the expanded top bed had to be replaced by a carborundum plate. The steel plate proved to be slightly magnetic thus trapping some fine tracer particles and causing a large pressure drop through the distributor.

Probes

The inductance probes used were copper wire coils (24 gauge) wrapped around a bed section. The average diameter of a coil was 16.5 cm and the height was 3.8 cm. Nine layers of copper wire were needed to give the required inductance of 0.1 Henry. The sensitivity of the probe seemed to be acceptable extending well into the center of the bed, and thus giving a cross-sectional average of the concentration of ferro-magnetic tracer particles in the effective volume influencing the probe, estimated to be 800 cm^3. The probe tends to give more weight to particles travelling near the wall than

to particles travelling in the center. This problem is common to most through-the-wall tracer sampling techniques (May, 1959) and the only way to overcome it would seem to be placement of an inside probe to measure center line concentrations. However, it is probable that the disruption of flow patterns in the bed is less desirable than the above-mentioned problem. Since the effective volume sensitive to the probe is large and contains $\sim 5 \times 10^7$ tracer particles, it seems reasonable to assume that the average reading from the probe is indeed proportional to the true concentration of ferro-magnetic tracer particles in that section. Since the exact value of this concentration is not needed (see the calculation of dispersion coefficients from the data) assuming linear dependence between the true and the measured concentration (in mV) is sufficient.

Shielding of the probes with lead sheets does not reduce the noise level (which for the tracer-free bed is usually within 5 mV). However, care had to be taken to remove external electrical fields such as an adjacent electrostatic filter, which increase the noise level of the probe. Adding ferro-magnetic rods to the outside of the probe does not seem to increase its sensitivity as it does for smaller probes where these rods are usually placed in the center of the probe (Fitzgerald, et al., 1977.) In the expanded top bed the probe is sensitive to quantities as low as 2-5 g of ferro-magnetic particles (1.3×10^{-4} - 3.3×10^{-4} percent of the bed material.)

In summary, it is claimed that the ferro-magnetic tracer technique is a nondisruptive tracer method linearly sensitive to relatively small amounts of tracer. It is reliable, relatively easy to use, applicable to both coarse and fine particles and could also prove feasible for high temperature and

high pressure applications.

4.4 Results

4.4.1 The Expanded Top Bed

The results of the solid mixing runs were recorded on two 2-channel strip chart recorders. The results from the expanded top bed are shown in Figure 4.4. The time scale is shown in the right hand side of the chart - the distance between two adjacent "boxes" is one second. The left hand side event marker records the injection of tracer. It is connected to the injection air solenoid and both were pressed at the same time. Zero time is chosen to approximate the mean of this injection time band. At the beginning and the end of the injection band, a jump in the recorder pen is sometimes evident and it should not be confused with the actual readings.

The conditions of the runs shown in Figure 4.4 are summarized in Table 4.1. Altogether, 24 runs were conducted in the expanded top bed, the first 16 were preliminary runs which were used to set up the experimental technique.

Run E1 The noise level before the injection of the tracer seems to be within $\pm$ 4 mV. The four probe channels are labeled from the bottom of the bed to the top. Channel 1 is located 0.15 m from the distributor and 1.2 m from the tracer injection point. Channel 2 is 0.67 m above channel 1 (0.53 m from the injector.) Channels 3 and 4 are 0.76 m and 1.42 m downstream from the injector respectively. The time and concentration scales are shown in Figure 4.4 for each channel. Both channels 1 and 2 show a large peak of tracer moving downward in the bed. Channel 1 shows an additional, smaller peak following the main one. This could possibly be the same

Table 4.1: Solid Mixing Experiments in the Expanded Top Bed

Run No.	H_o (m)	U_g (m/s)	$\bar{\epsilon}$	Regime
E1	2.6	0.075	0.51	bubbling
E2	2.2	0.24	0.56	bubbling[1]
E3	2.2	0.48	0.61	slugging
E4	2.2	0.48	0.61	slugging
E5	2.2	0.84	0.66	slugging/turbulent
E6	2.2	0.86	0.67	slugging/turbulent
E7	2.1	0.86	0.66	slugging/turbulent
E8	1.8	1.10	0.70	turbulent

Notes

1 slugging at the top

2 ~150 g of tracer injected in each run

3 injection pressure constant at 200 kPa

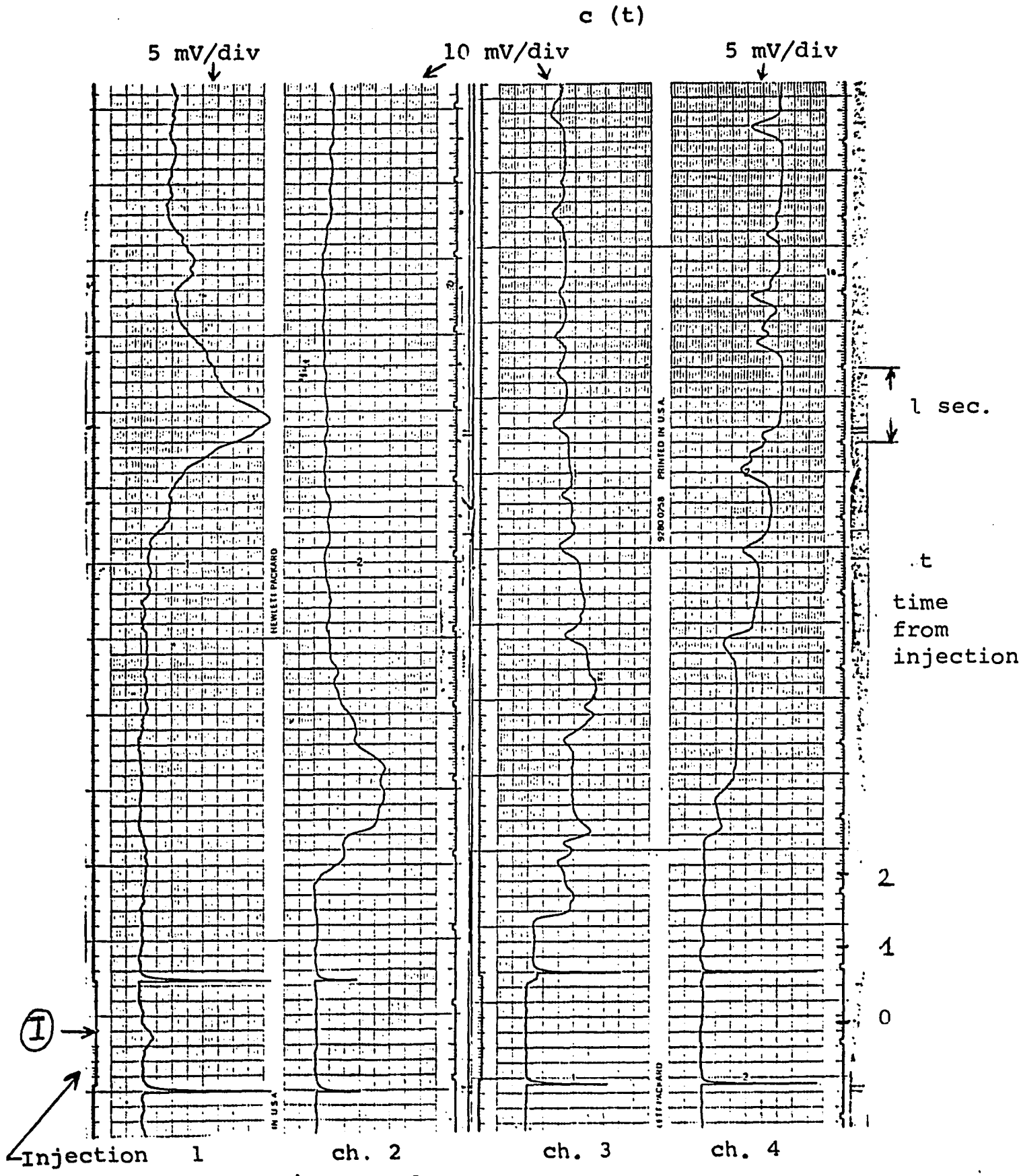

a) RUN E 1

Figure 4.4 : Solid mixing results in the expanded top bed.

peak "reflected" at the distributor plate and now moving upward in the bed. The concentration of tracer in the vicinity of probes 1 and 2 seems to decrease immediately following each peak and then slowly rise to the equilibrium position. The noise level at the equilibrium position is slightly higher than the one before the injection. Both downstream channels 3 and 4 show a markedly different behavior. While the response is still underdamped, it is more spread out. Moreover, periodic "dips" are evident and these correspond to the passage of bubbles. Whenever a bubble passes near a probe, the average voidage of that section increases and the total number of particles (including tracer particles) decreases too. It is seen that bubbles coalesce and grow larger as they pass through the bed. While of insignificant size near the distributor and channel 2, they are evident in channel 3 ane larger in channel 4. In this sense, these oscillations are not considered "noise" (or instrument noise) but rather as density fluctuations in the bed. These fluctuations are becoming more pronounced as the gas velocity is increased (slugging, runs E2 and E3) and more random at the higher velocities.

Run E2 The same qualitative behavior as in run E1 is demonstrated in run E2. The bubbles are still in the coalescing stage, while the top of the bed is slugging. This further illustrates the fact that regime transitions, as discussed in chapter 3, travel from the top of the bed to the bottom. The top of the main peak of channel 1 is unfortunately cut as it is not always easy to predict its maximum value. This, however, does not represent a difficulty for the analysis of the results. The "tails" of experiments E1 and E2 are rather long and thus omitted from Figure 4.4. They are later shown in the results analysis stage.

Fig. 4.4 b: RUN E 2

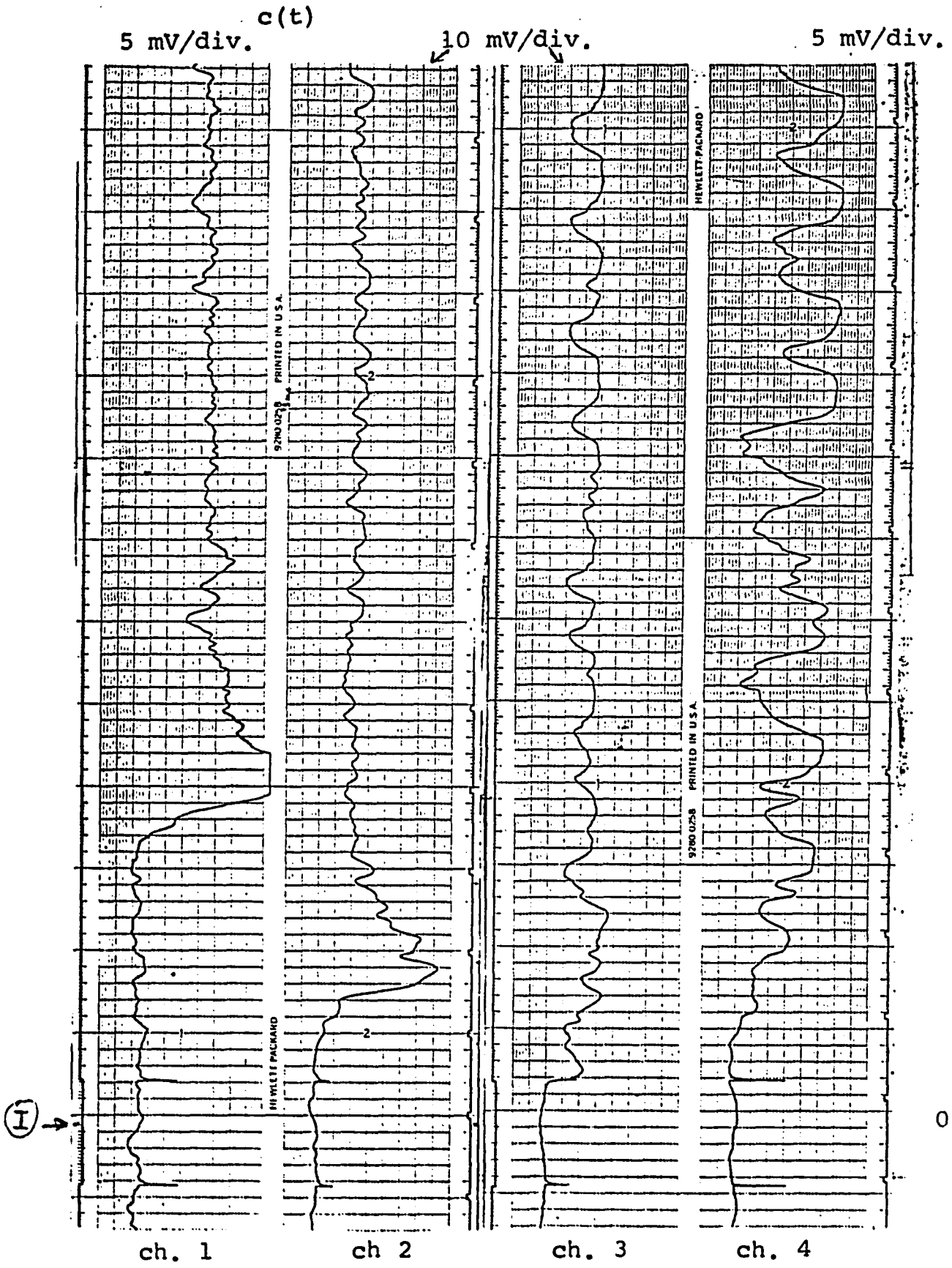

Runs E3 and E4 These two are repeat runs. The higher frequency of the density fluctuations, and their decreased magnitude should be noted. This agrees with the picture of transition to turbulence discussed in chapter 1. Another feature of this higher gas velocity is the difference in the response of the closer channels 2, 3 which is underdampled, and the response of the outer channels 1, 4 which is overdamped.

Runs E5, E6 and E7 These are repeat runs at the onset of the turbulent regime. Superposition of the results of these three runs shows the reproducibility of the results. The initial slopes of the responses are much alike but the void frequency might be out of phase, thus while the first part of the transient response is the same for all three runs, the steady state fluctuations are not. Their peaks and dips have the same magnitude though, and thus it strengthens our assumption that these are density fluctuations. The upper part of the curve connecting the peaks might be thought of as the dense phase response. Since the results of the expanded top bed experiments are interpreted as C/C_∞, one can take either the average of the fluctuations or the dense phase response and in this sense these density fluctuations do not contribute noise to the results.

Run E8 This run is in the midst of the turbulent regime, but one should keep in mind that as the gas velocity (and consequently the entrainment rate) is raised, there is a marked difference between the expanded top bed, where solid falling from the top is promoting a larger degree of mixing, and the circulating system. These differences were discussed in chapter 3.

Figure 4.4 c:

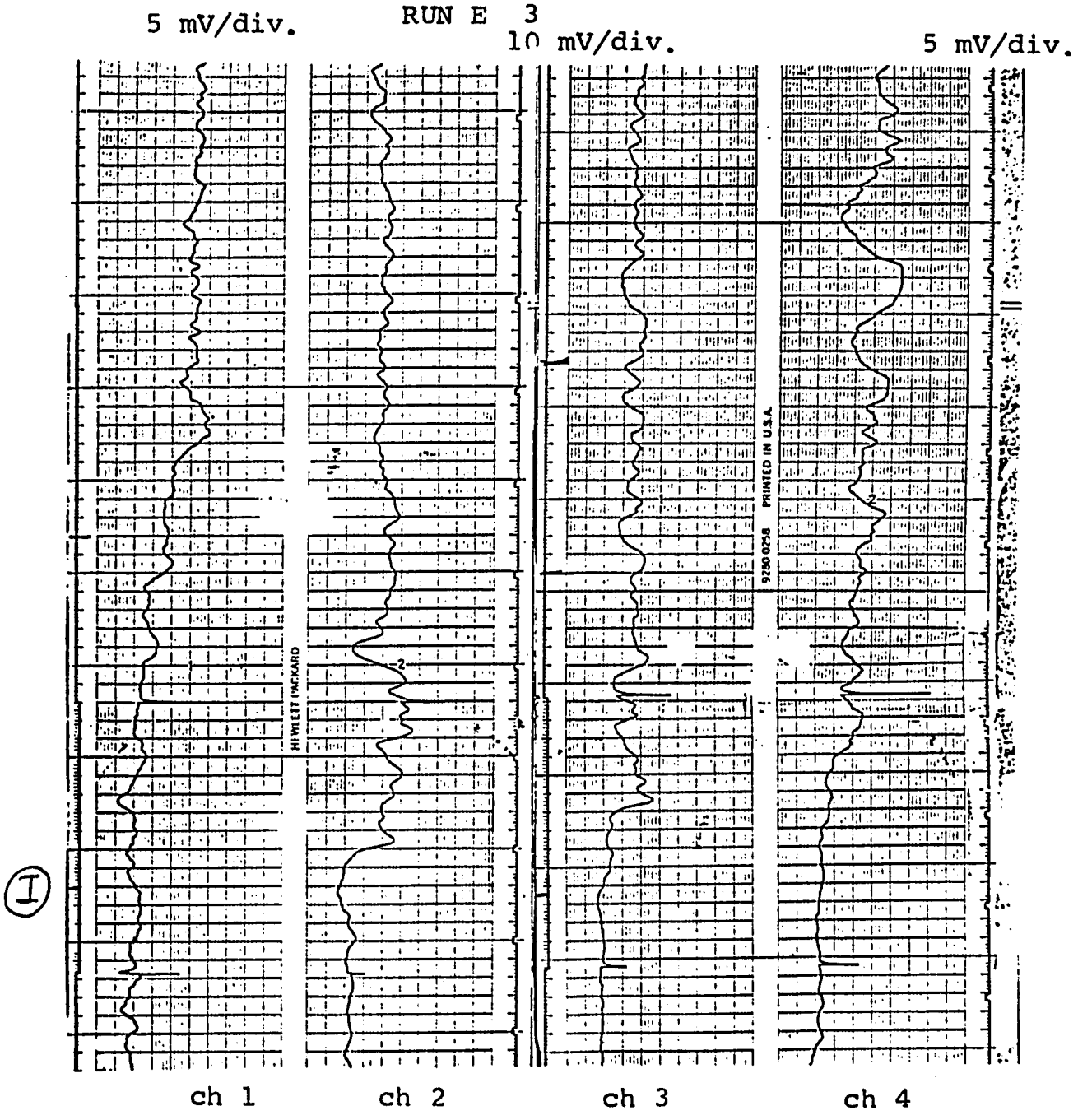
5 mV/div.
RUN E 3
10 mV/div.
5 mV/div.
HEWLETT PACKARD
9280-0258 PRINTED IN U.S.A.
ch 1
ch 2
ch 3
ch 4

Figure 4.4 d:

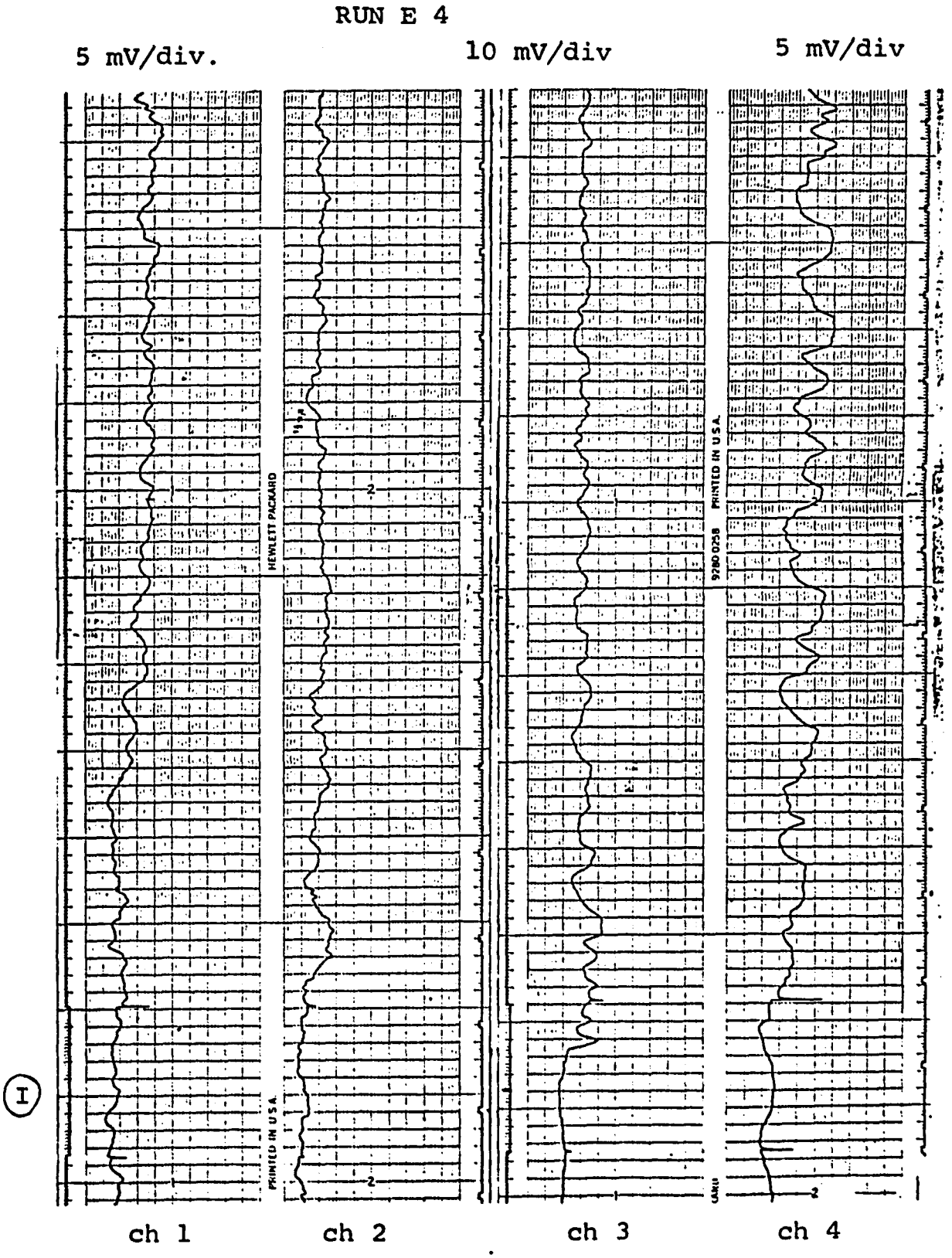
RUN E 4
5 mV/div.
10 mV/div
5 mV/div
HEWLETT PACKARD
PRINTED IN U.S.A.
9280-0258
PRINTED IN U.S.A.
I
ch 1
ch 2
ch 3
ch 4

Figure 4.4 e:

RUN E 5

5 mV/div

10 mV/div.

5 mv/div.

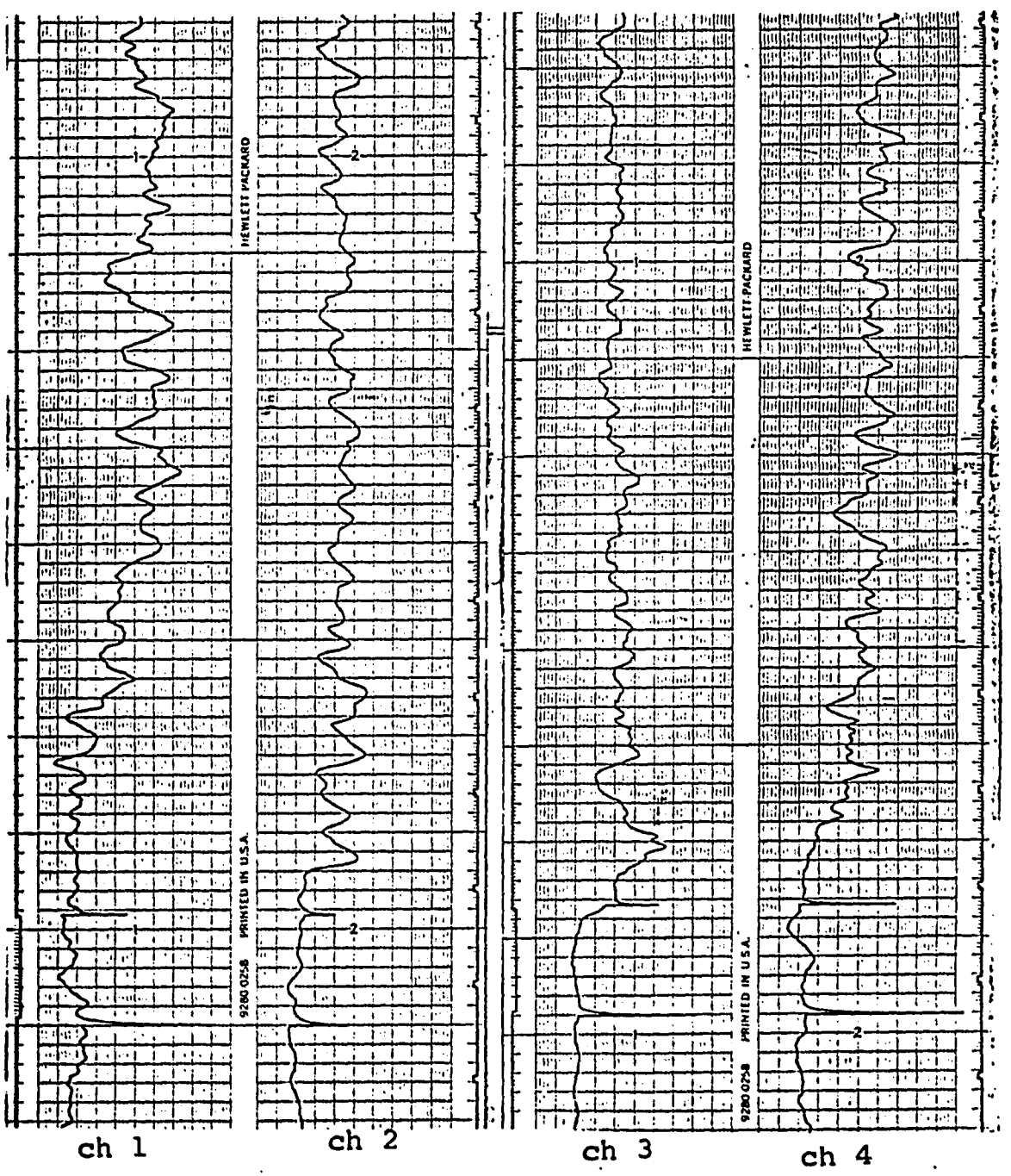

Figure 4.4 f:

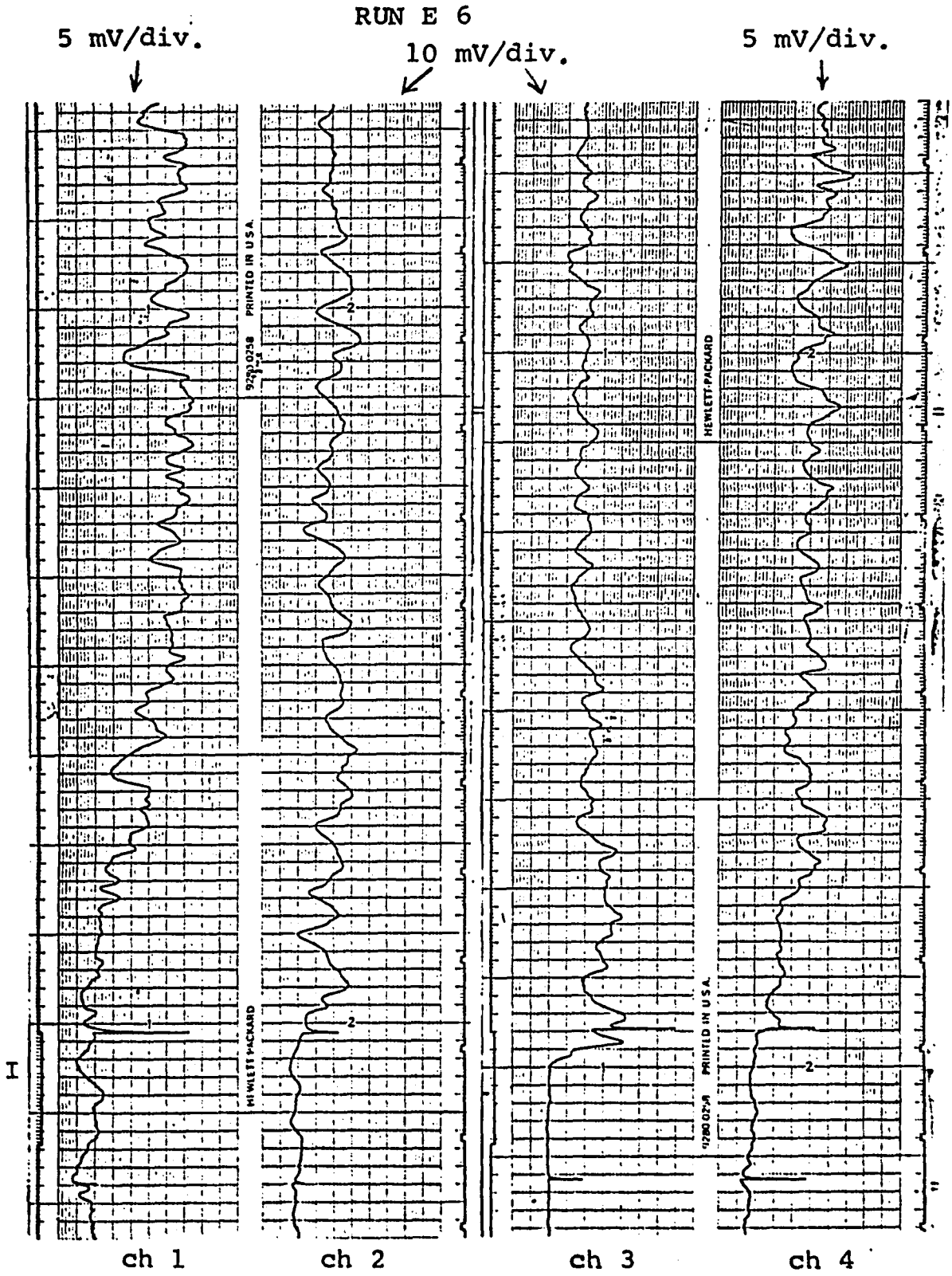

Figure 4.4 g:

RUN E 7
5 mV/div.

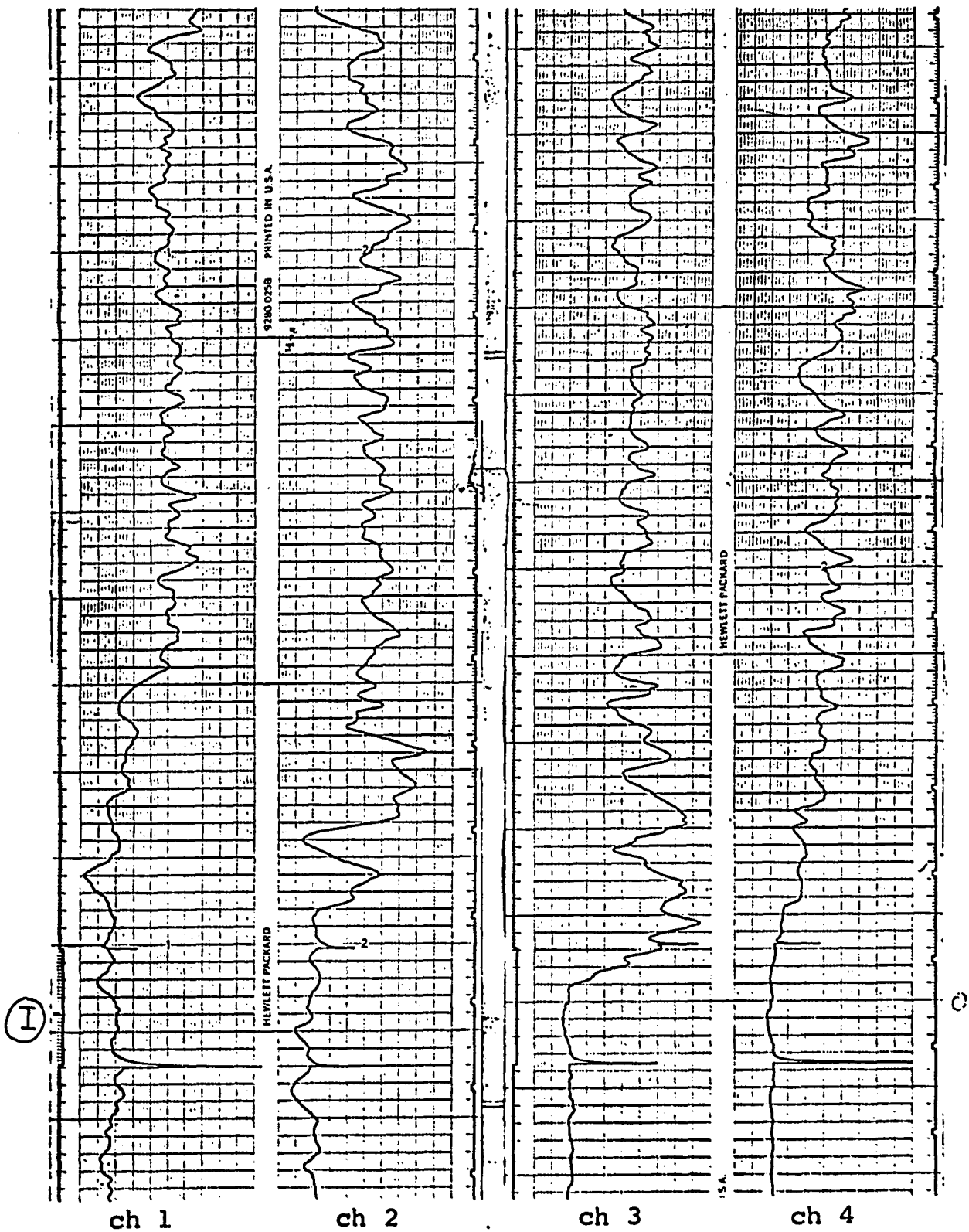

Figure 4.4 h: RUN E 8

5 mV/div.

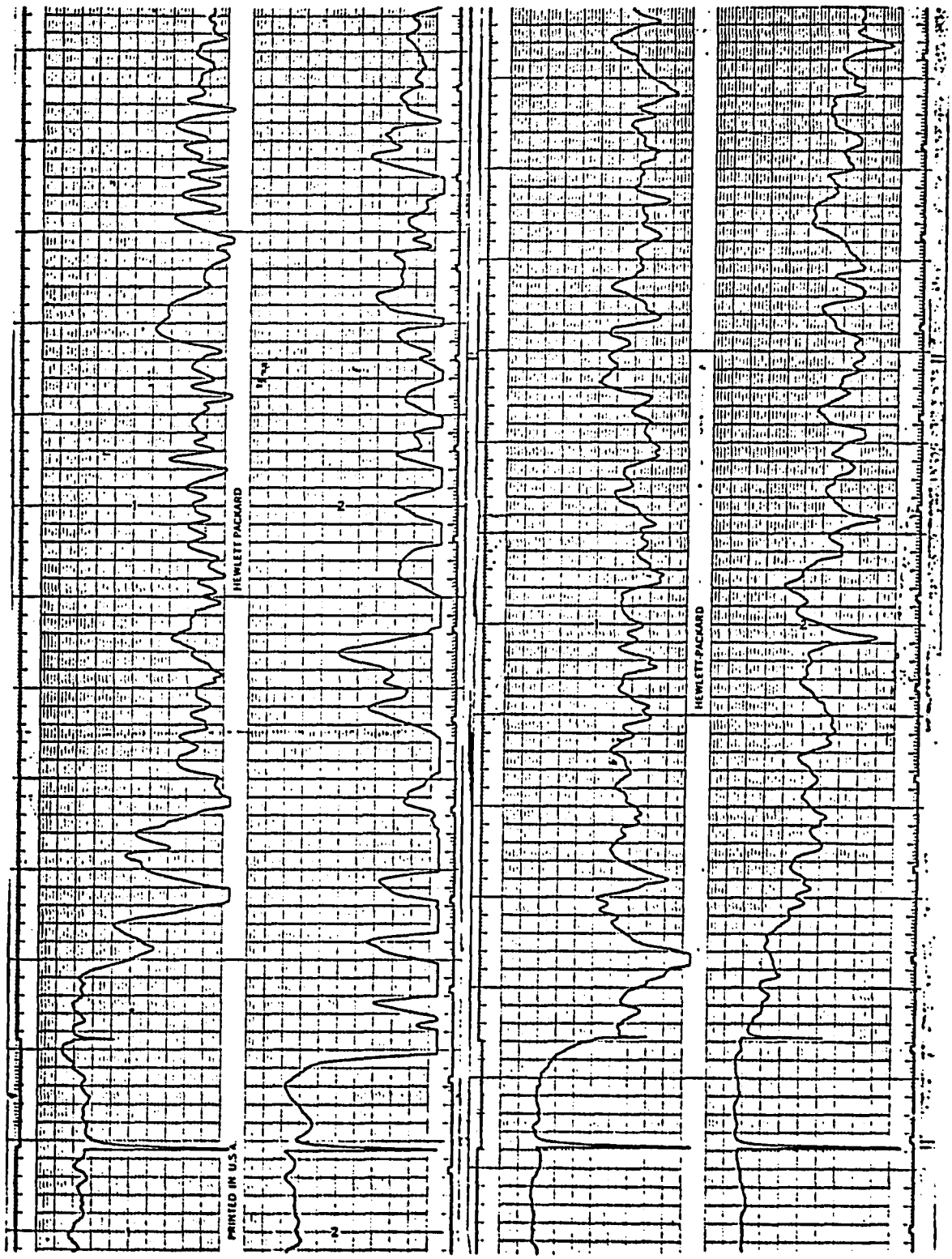

ch 1 ch 2 ch 3 ch 4

4.4.2 The Circulating System

The same experimental setup used in the expanded top bed was transferred as a whole to the circulating system, where it was positioned in the lower part of the bed. The reason for this was that at the lower velocities (the turbulent regime) high solid levels would be needed in the companion "slow" bed to maintain a high bed level in the "fast" bed. Entrance effects, as monitored by the pressure drop for fine powders throughout the turbulent and fast fluidization regimes are limited to a small region - typically of the order of 5-8 L/D. The first probe (channel 1) was positioned just above this distance, and indeed only the highest gas velocities investigated did it show some entrance pressure fluctuations. The conditions of the solid mixing run in the circulating system are shown in Table 4.2.

Table 4.2: Solid Mixing Experiments in the Circulating System

Run No.	U_g (m/s)	G_s (kg/m^2.s)	$\bar{\epsilon}$	Regime
C1	0.80	-	0.64	slugging
C2	1.08	5.8	0.70	slugging/turbulent
C3	1.43	16.5	0.74	turbulent
C4	1.46	14.3	0.74	turbulent
C5	1.48	18.4	0.73	turbulent
C6	2.00	47.8	0.78	turbulent/fast
C7	2.28	71.5	0.78	fast
C8	2.39	97.9	0.79	fast
C9	2.44	75.0	0.81	fast
C10	3.41	76.0	0.92	fast
C11	3.41	73.4	0.927	fast
C12	3.35	107	0.81	fast
C13	3.34	117	0.83	fast
C14	3.38	112	0.81	fast
C15	4.69	74.0	0.958	fast
C16	4.58	84.0	0.958	fast
C17	4.45	135	0.84	fast
C18	4.58	134	0.84	fast
C19	5.62	152	0.85	fast

The experimental results are shown in Figure 4.5 For the low velocity runs the decay to zero (which happens in the circulating system - which is open, as opposed to the expanded top bed where a new equilibrium level is achieved) can be slow and is not shown in Figure 4.5. It is later shown, when the results are analyzed.

a) RUN C 1 5mV/div.

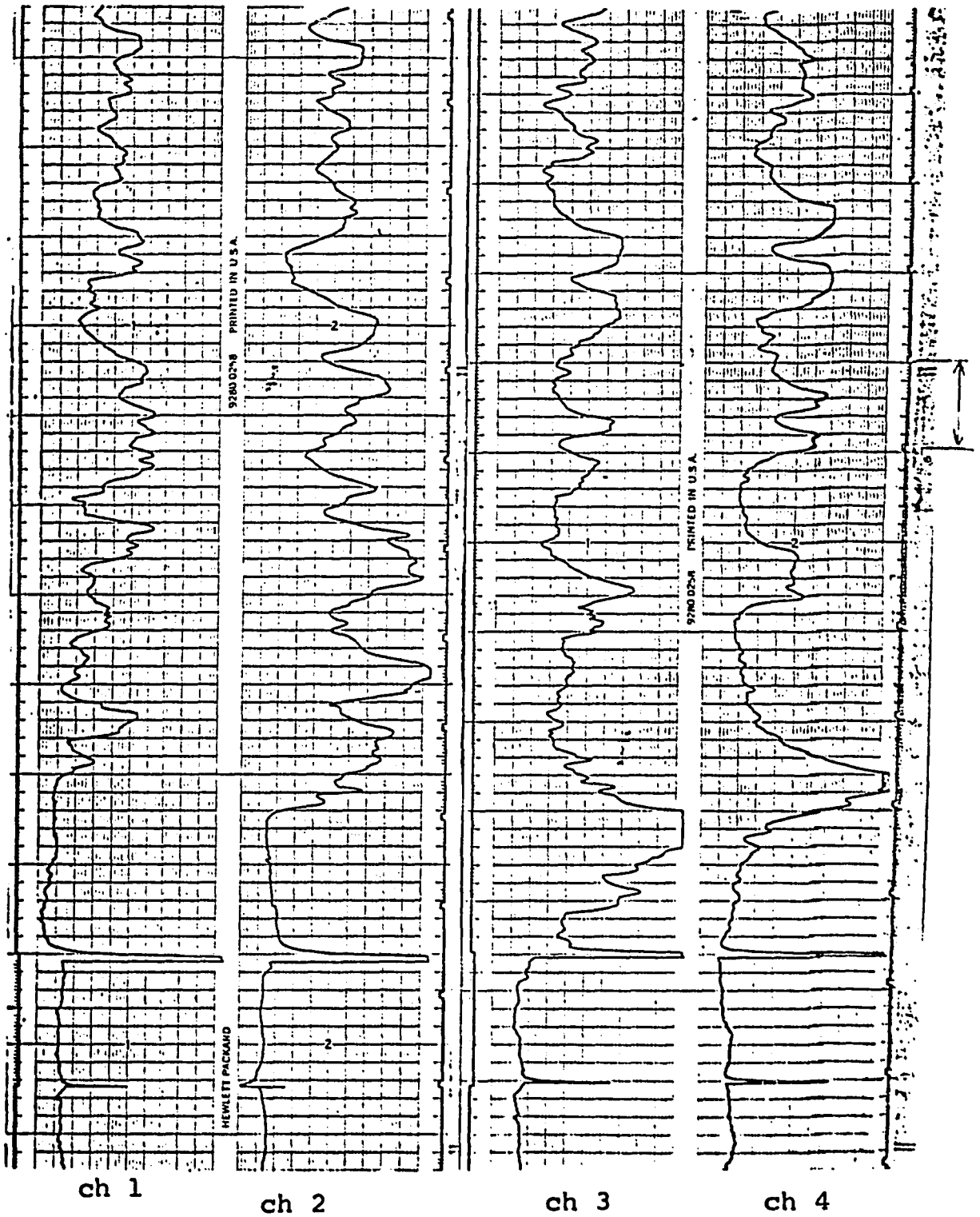

Figure 4.5: Solid mixing results in the circulating system.

Figure 4.5b RUN C 2

5 mV/div.

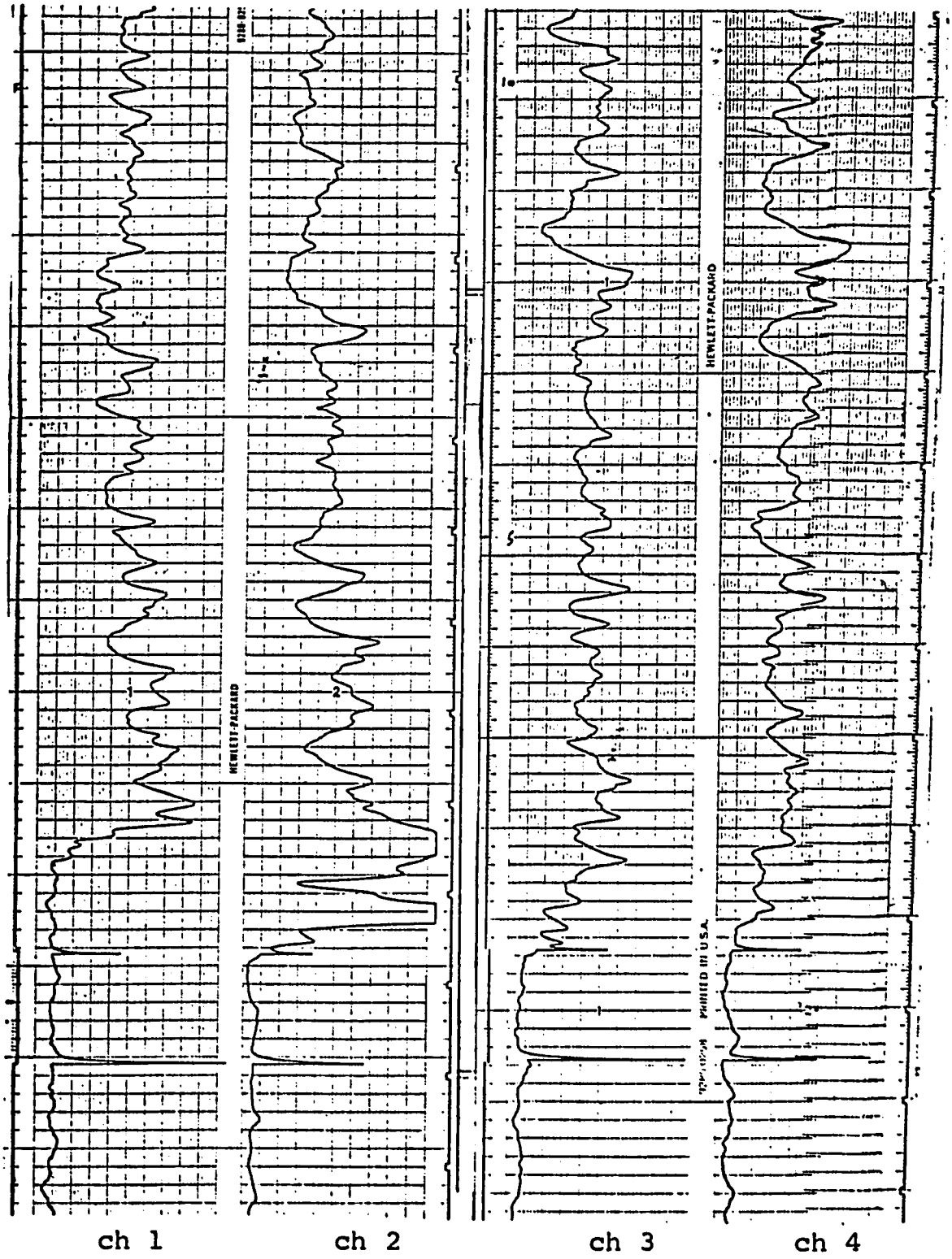

Figure 4.5 c: RUN C 4 5 mV/div.

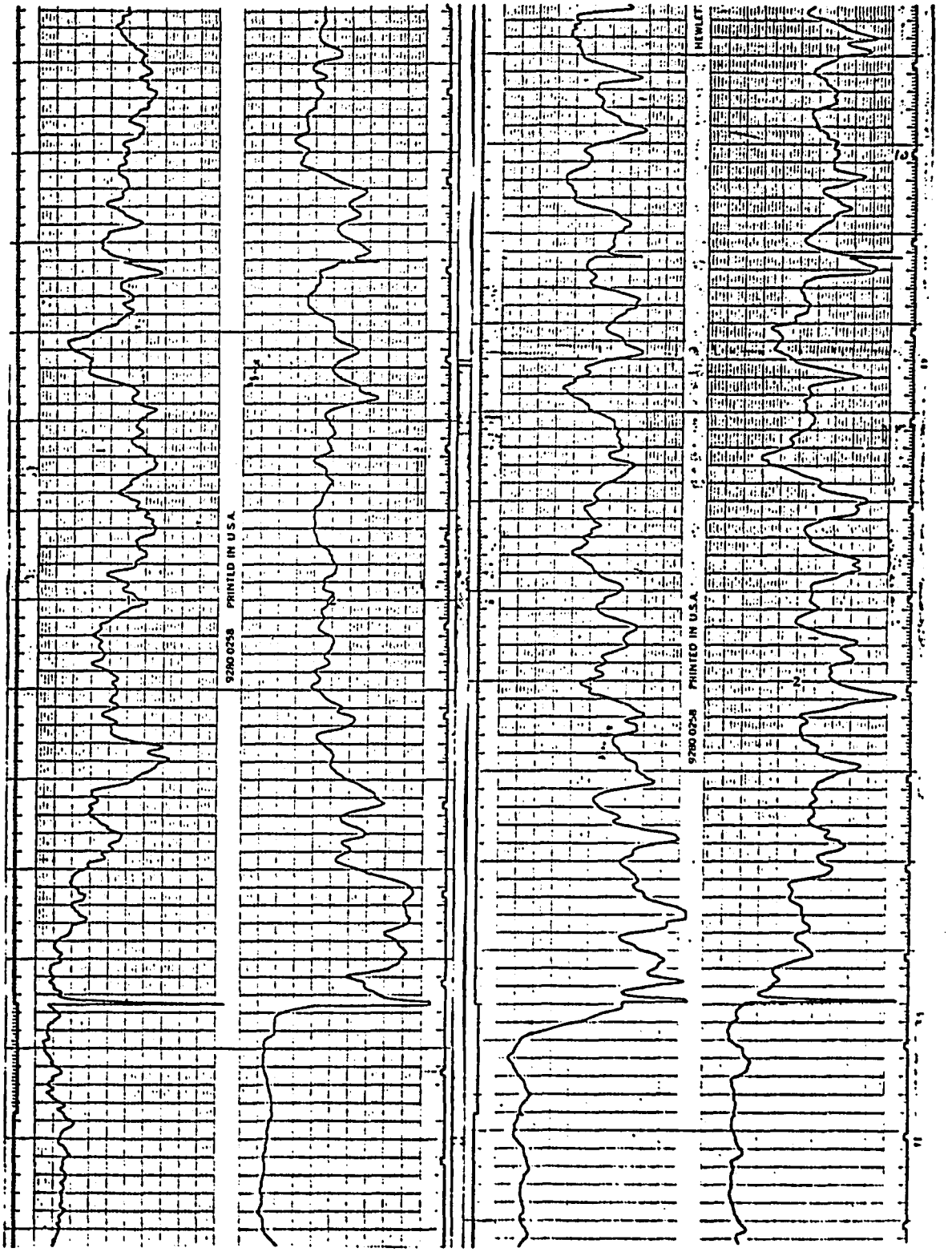

Figure 4.5 d: RUN C 6

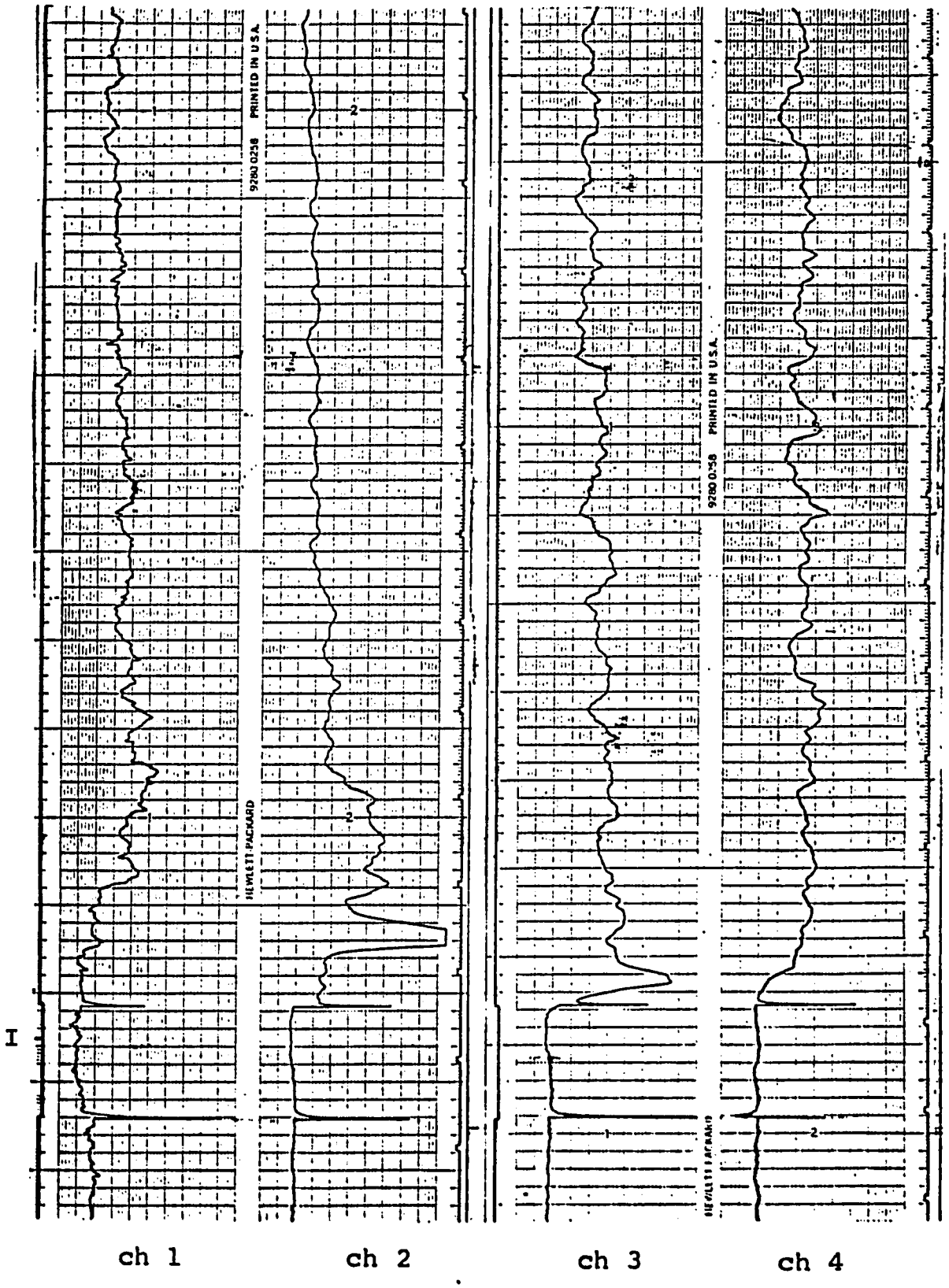

Figure 4.5 e: RUN C 9

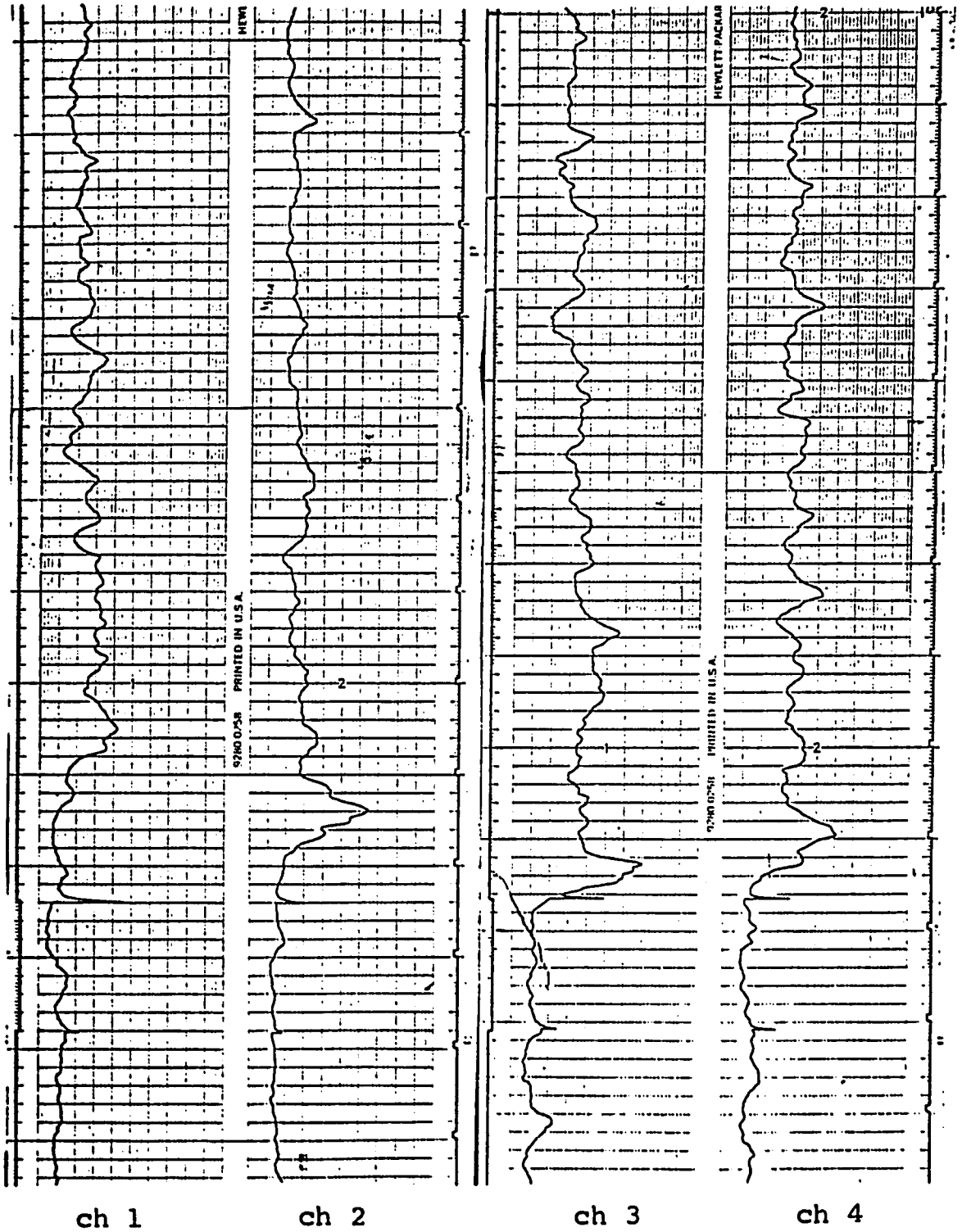

Figure 4.5f: RUN C 11

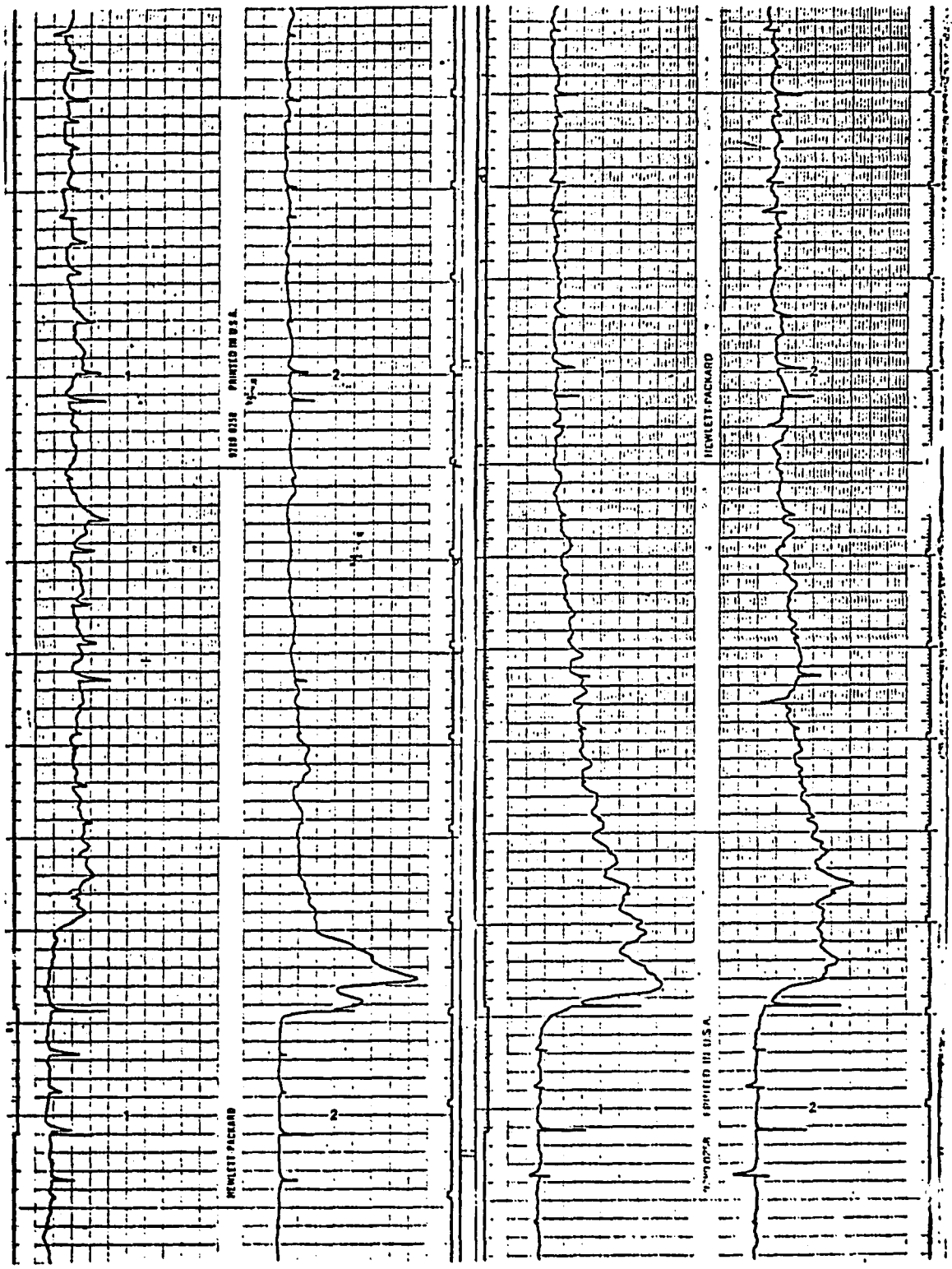

ch 1 ch 2 ch 3 ch 4

Fig. 4.5 g: RUN C 13

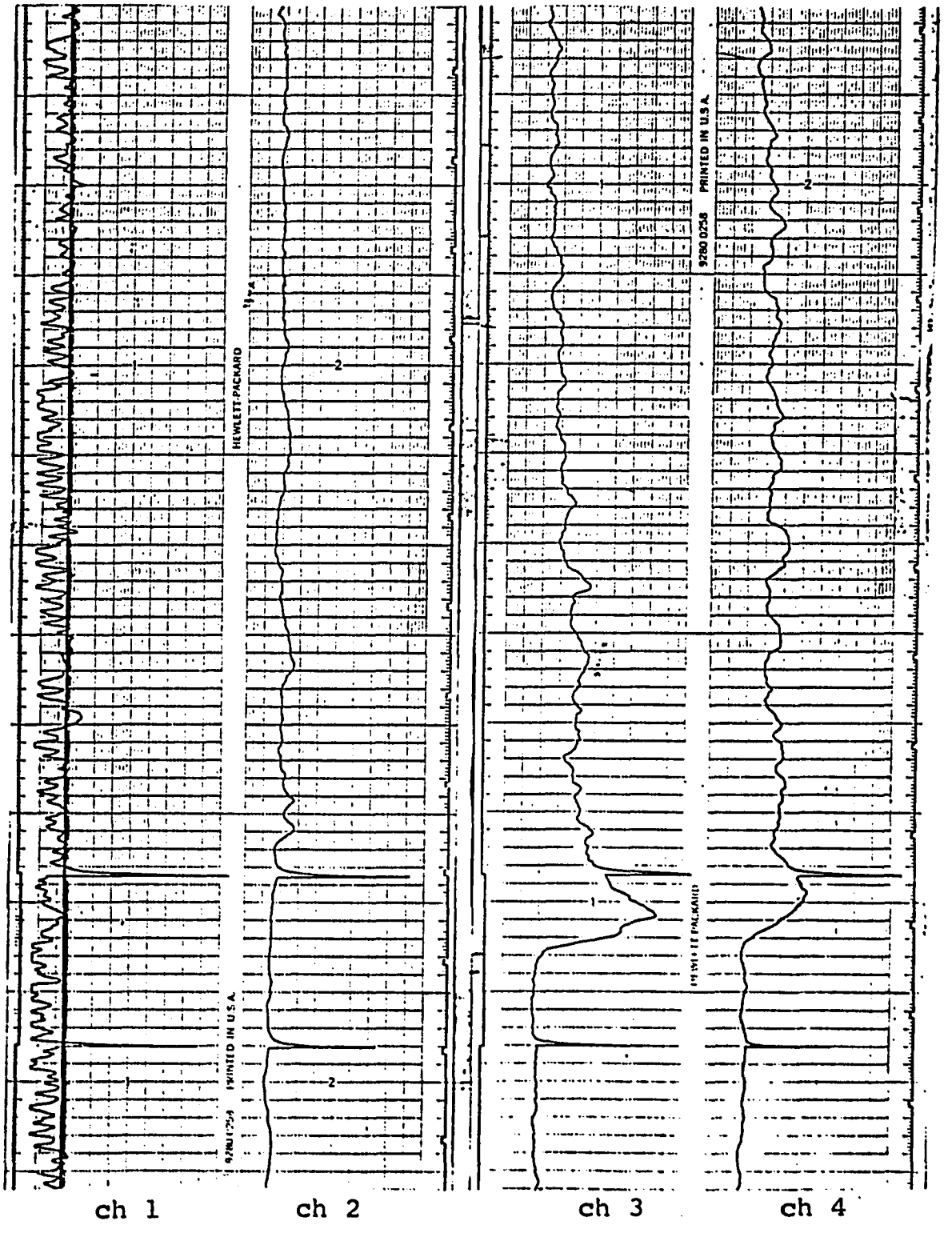

Figure 4.5h: RUN C 15

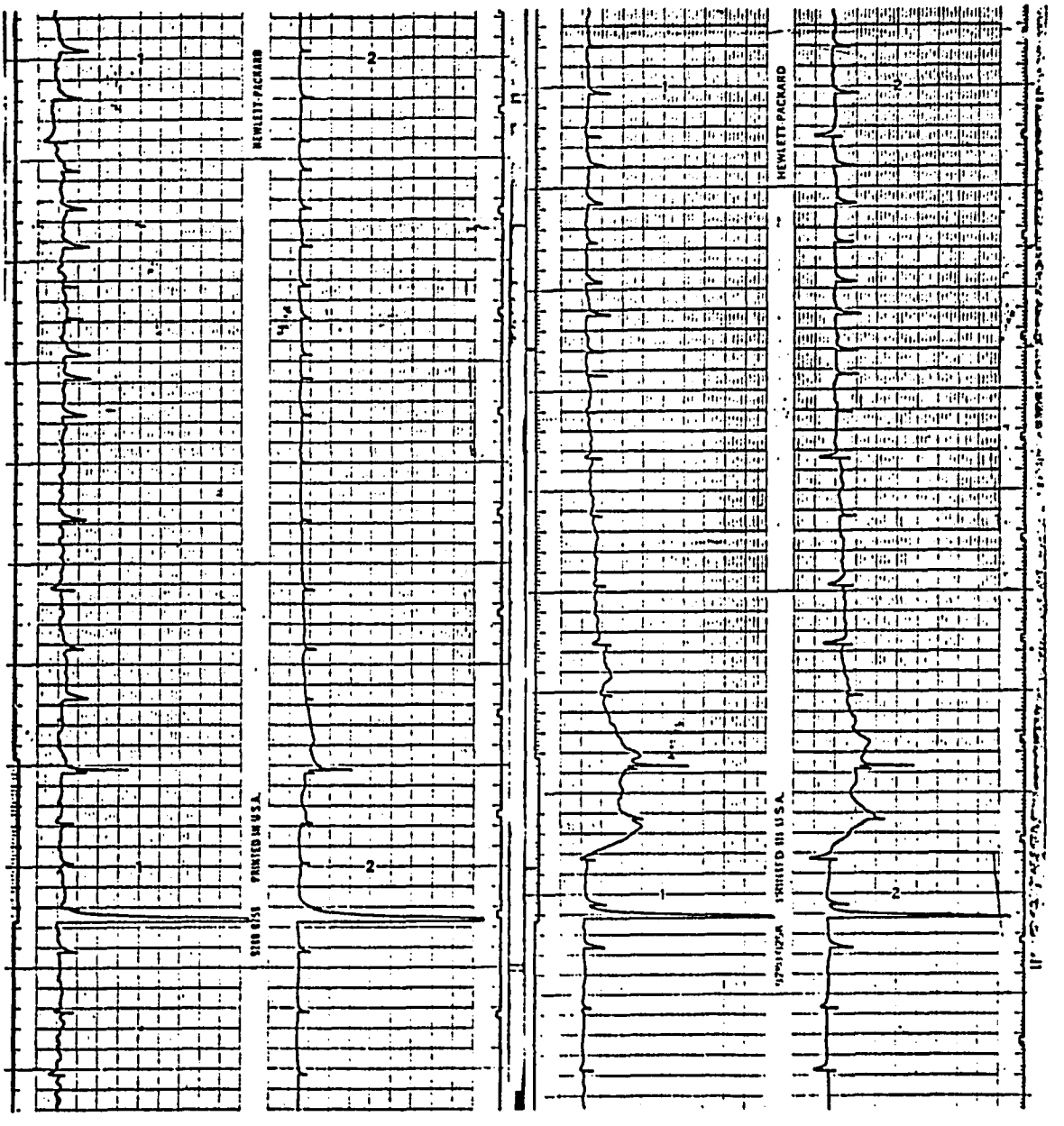

Figure 4.5 i: RUN C 18

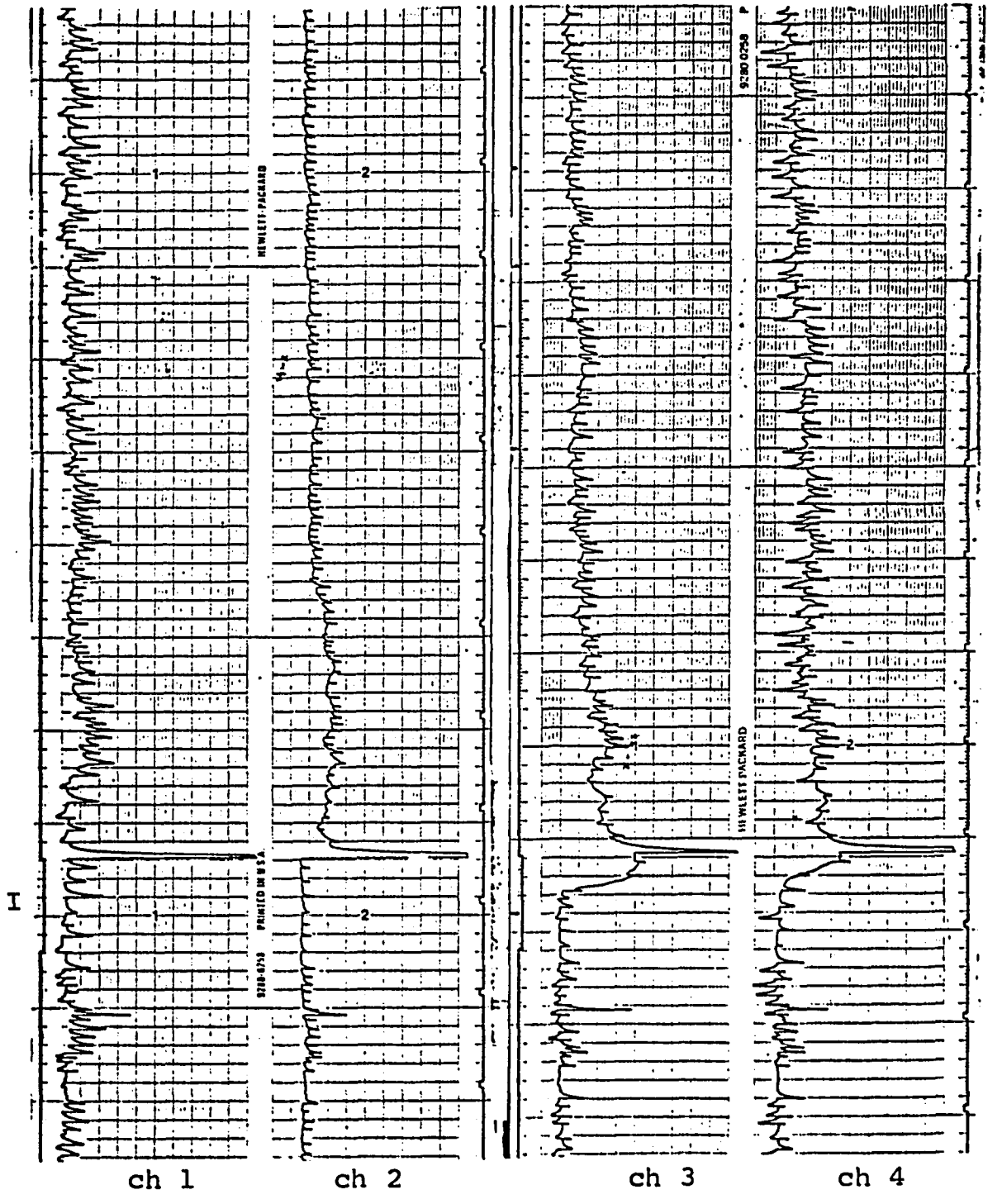

Figure 4.5 j: RUN C 19

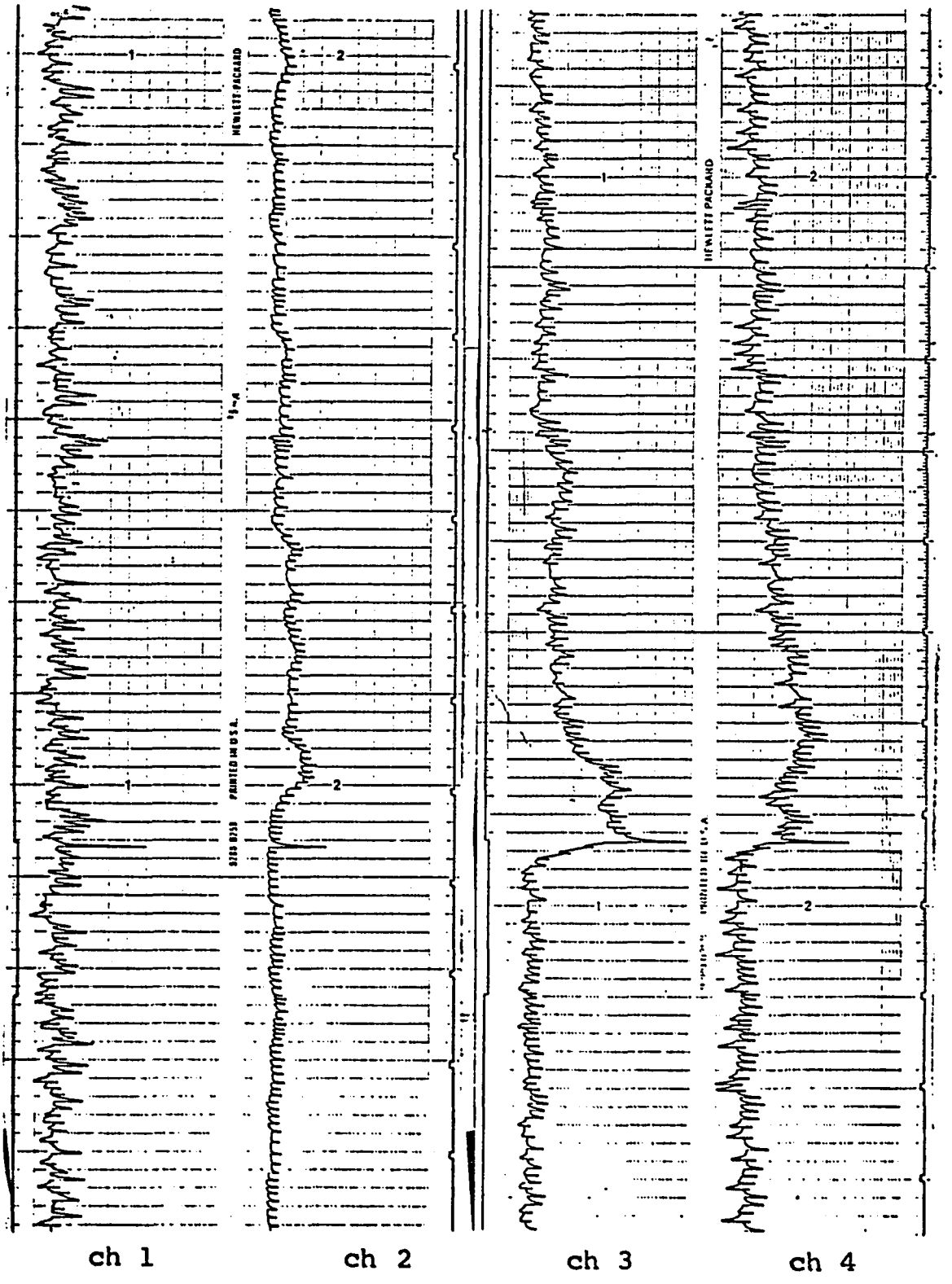

4.5 Solid Mixing Models

Various models were proposed to account for solid mixing in fluidized beds. The major models are briefly described by Potter (1971), and Levenspiel (1972). Early attempts tried simple one parameter models, either a "tanks in series" or a dispersion model. These models could not account for conversions lower than a completely mixed reactor while such a situation can be readily observed in a low velocity, shallow fluidized bed where gas flow in bubbles effectively bypasses the emulsion phase. Residence time distribution models, later modified to account for contact time distribution were also tried, but the models that came into prominence are the two-phase models. The latter fall into two major categories, the general countercurrent two-phase model (for example van Deemter, 1967) and the "bubbling" models advocated by Davidson and Harrison (1963) and Kunii and Levenspiel (1969). The simple dispersion models usually use one parameter - the effective axial diffusivity which is of interest for predicting axial heat transfer and conversion in a fluidized bed. The two-phase models use 2-6 parameters: dispersion coefficients in each phase, phase velocities, solids fraction in each phase and a solid interchange rate between the two phases. The major parameter in the Kunii and Levenspiel model is bubble size which is used to determine a score of secondary parameters.

4.6 The Two-Phase Model

The two-phase model is thoroughly discussed by Potter (1971). The van Deemter (1961, 1967) model is actually an extension of the May (1959) model where a horizontal exchange coefficient is coupled with an eddy diffusivity concept. We

have previously used this model (Cankurt et al., 1980) to account for gas mixing in high,velocity fluidized beds. The general model, both for gas and solid mixing is illustrated in Figure 4.6.

The governing equations of this model are:

$$f_g + F_g + f_s + F_s = 1 \tag{4.1}$$

$$U_g = f_g v_g + F_g V_g \tag{4.2}$$

$$U_s = f_s v_s + F_s V_s \tag{4.3}$$

Gas mixing:

$$F_g V_g \frac{dC}{dx} + k_g (C-c) = 0 \tag{4.4}$$

$$f_g v_g \frac{d}{dx} + k_g (c-C) = 0 \tag{4.5}$$

where C and c are the local concentrations of tracer in the upflow and the downflow phase, respecitvely.

The solution to equations 4.4 and 4.5 is:

$$c = \alpha + \beta e^{-k_g(r-1)x/f_g v_g} \tag{4.6}$$

$$C = \alpha + \beta r e^{-k_g(r-1)x/f_g v_g} \tag{4.7}$$

where: $$r = \frac{f_g v_g}{F_g V_g} \tag{4.8}$$

and α and β are constants.

The experimental results with FCC (Cankurt and Yerushalmi, 1978) do indeed confirm the relevance of the model. Since radial concentrations were measured, f_g and F_g can be assumed and the results can be reduced to two effective parameters, k_g and r.

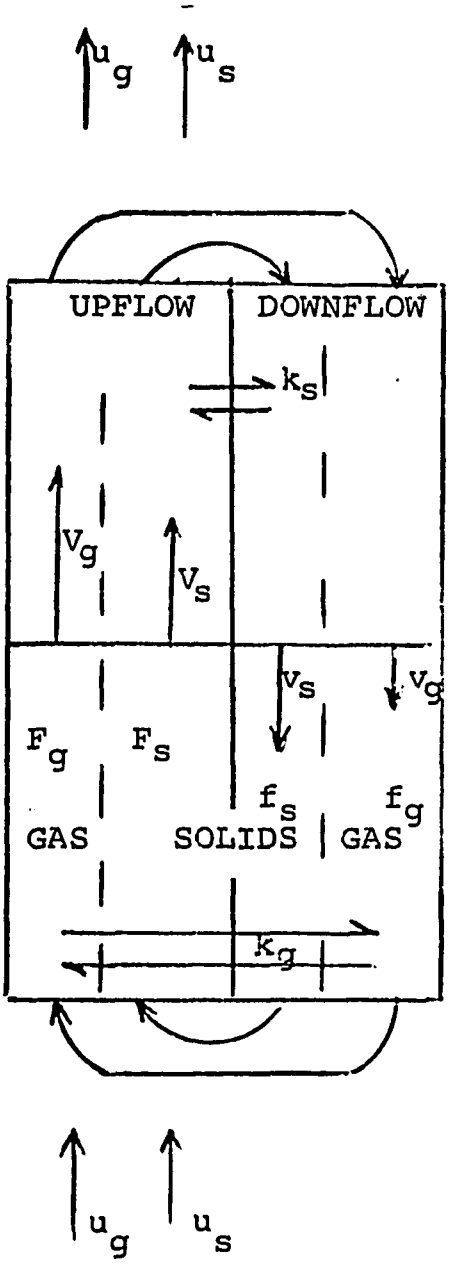

Figure 4.6: Counter-current flow model (van Deemter, 1967).

These are shown in Figure 4.7. The relative amount of backflow, r, or q/Q

$$\frac{f_g v_g}{F_g V_g}$$

seems to decrease linearly in the turbulent regime, virtually decaying to plug flow in the fast fluidization regime. The cross flow parameter k_g is shown to go through a maximum in the turbulent regime. Note that the gas mixing studies consisted of steady-state experiments.

Solid Mixing:

If c_s and C_s are the local fractions of tracer in the downflow and upflow phases, the governing equations are:

$$f_s \frac{\partial c_s}{\partial t} + f_s v_s \frac{\partial c_s}{\partial x} + k_s (c_s - C_s) = 0 \qquad (4.9)$$

$$F_s \frac{\partial C_s}{\partial t} + F_s V_s \frac{\partial C_s}{\partial x} + k_s (C_s - c_s) = 0 \qquad (4.10)$$

These equations are solved for a low velocity fluidized bed by van Deemter (1967) with the aid of an analog computer. For relatively low values of the parameter $k_s L/F_s V_s$ an oscillatory behavior is observed for both phases c_s and C_s for high values of this parameter a more damped response is observed. By assuming little carryover and for large values of time, van Deemter defines an effective diffusion coefficent:

$$D_{SA} = \frac{(f_s v_s)^2}{k_s (f_s + F_s)} = \frac{(F_s V_s)^2}{k_s (f_s + F_s)} \qquad (4.11)$$

Equation 4.11 illustrates our previously made claim that the two-phase models need some difficult to obtain parameters, as f_s and the phase velocities, to calculate the dispersion coefficient. The Kunii and Levenspiel model would lead to

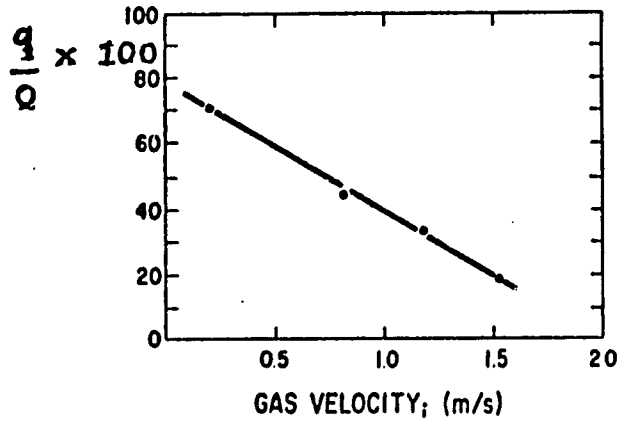

Figure 4.7a: Relative Gas mixing in the circulating system (FCC).

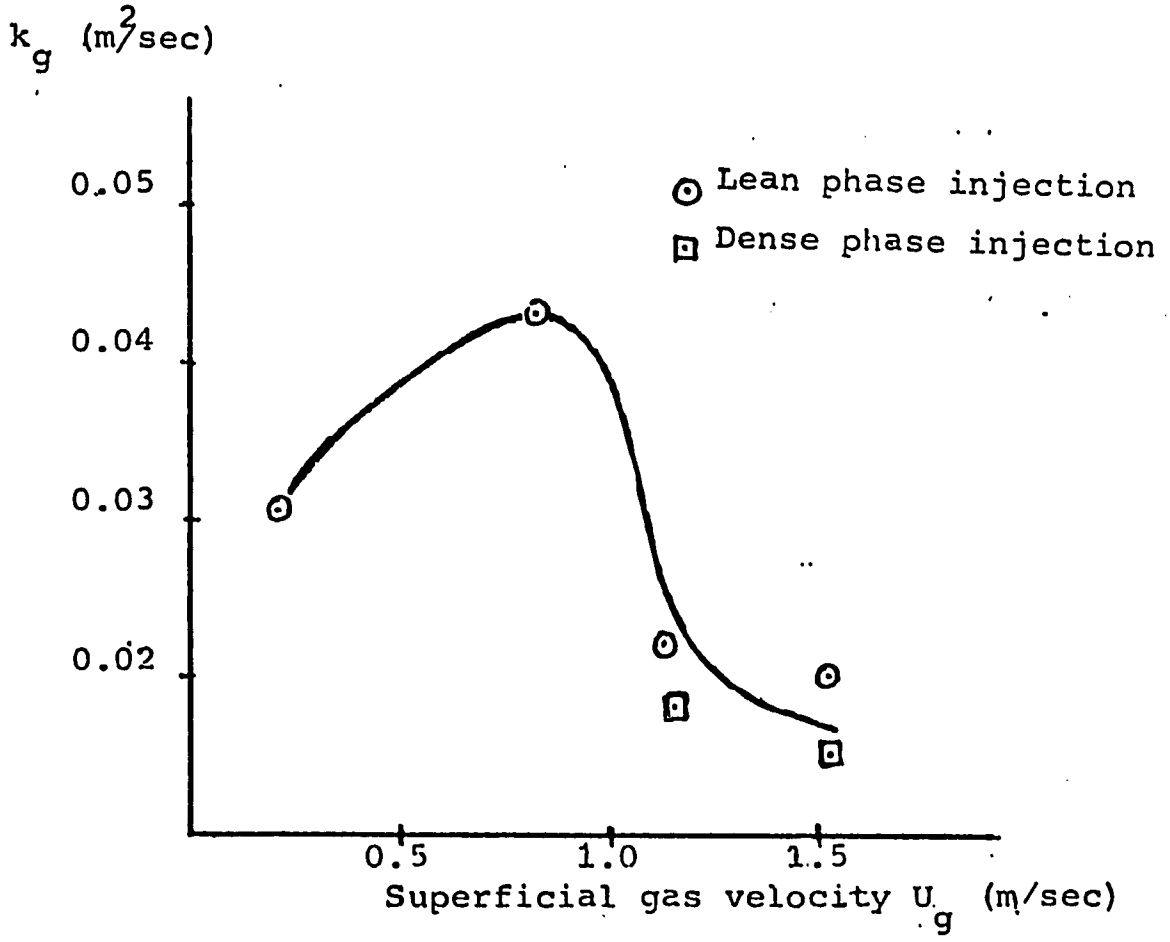

Figure 4.7b: Gas Transfer coefficient, k_g.

the following expression (Potter, 1971):

$$D_{SA} = \frac{f_w^2 \epsilon_o \epsilon_b}{3U_o} D_e U_A^2 (1-\epsilon_b) \qquad (4.12)$$

Equations (4.9) and (4.10) can be solved by the methed of characteristics by the addition of the following two equations:

$$dc_s = \frac{\partial c_s}{\partial x} dx + \frac{\partial c_s}{\partial t} dt \qquad (4.13)$$

$$dC_s = \frac{\partial C_s}{\partial x} dx + \frac{\partial C_s}{\partial t} dt \qquad (4.14)$$

To obtain the characteristic lines the determinant of these four equations is set equal to zero:

$$D = \begin{vmatrix} f_s v_s & f_s & 0 & 0 \\ 0 & 0 & F_s V_s & F_s \\ dx & dt & 0 & 0 \\ 0 & 0 & dx & dt \end{vmatrix} = 0 \qquad (4.15)$$

$$\text{or} \quad V_s v_s + \left(\frac{dx}{dt}\right)^2 - (v_s + V_s) \frac{dx}{dt} = 0 \qquad (4.16)$$

or the solution moves with velocity of the phase:

$$\frac{dx}{dt} = V_s \text{ and } \frac{dx}{dt} = v_s \qquad (4.17)$$

To get the solution along the characteristic line, the numerator is set equal to zero:

$$N = \begin{vmatrix} -k_s(c_s - C_s) & f_s & 0 & 0 \\ -k_s(C_s - c_s) & 0 & F_s V_s & F_s \\ dc_s & dt & 0 & 0 \\ dC_s & 0 & dx & dt \end{vmatrix} = 0$$

or:

$$(V_s k_s - f_s k_s)c \qquad (f_s V_s - f_s v_s)\frac{dc}{dt} = (k_s V_s - k_s v_s)C_s \tag{4.18}$$

and by taking the Laplace transform of equation (4.18) one gets:

$$\frac{\bar{c}_s}{\bar{C}_s} = \frac{1/\tau}{1/\tau + p} \tag{4.19}$$

where ps is the transformed time and $\tau = \frac{f_s}{k_s}$ (4.20)

For an impulse injection of a quantity of tracer, m, in one phase, say the upwards moving one, the solution to equation (4.19) is:

$$c(t) = \frac{m}{\tau} e^{-t/\tau} \tag{4.21}$$

This solution moves with the velocity described by equation (4.17).

The Naor, Shinnar and Katz (1972) Method:

Equation 4.21 has the same form as the solution to the dispersion model discussed later on. However, there is a difficulty in measuring v_s, the velocity of the down-moving phase. Inspection of the results from the expanded top bed (Figure 4.4) and the circulating system (Figure 4.5) shows that it is not clear how to calculate the velocity of the

phase. Some particles travel very fast, with a very small slip velocity and when enough particles get to the vicinity of the probe, it begins registering their concentration. One limitation is inherent in the fact that the probe registers a cross-sectional average, and there is no way to measure the concentration of one of the postulated phases. The introduction of an inside probe would probably disrupt the flow patterns too much. A more serious difficulty associated with all closed (the expanded top bed) and recirculating systems is that the first significant peak does not necessarily correspond to the first passage time distribution anymore. This point has been discussed by Shinnar et al. (1972) and Naor et al. (1972).

If one considers point A to be the injection point and point B the sampling point, W_B the average solid particles flow rate at point B, and $C_{AB}(t)$ as the tracer concentration history (the measured variable), the tracer quantity moving through B in an interval Δt is: $W_B\ C_{AB}\ (t)\ \Delta t$. This is the macroscopic approach. If one now considers the probability approach, the probability of a single given particle going through site B in the internal Δt is $h_{AB}(t)\ \Delta t$. If m is the quantity of tracer injected, one gets upon equating the two approaches:

$$W_B\ C_{AB}\ (t) = m h_{AB}\ (t) \qquad (4.22)$$

One cannot get the local flow rate W_B by simply integrating equation 4.22 because the integral $\int_0^\infty h_{AB}(0)\ dt$ diverges for a closed system. Note that it is equal to one for an open system, illustrating the basic difference between the two types of systems.

The renewal density, $h_{AB}(t)$ consists of the first passage distribution $f_{AB}(t)$ and the convolution of k visits of the same particle at point B because of recirculation. Naor et al. use the integral equation of renewal theory:

$$h_{AB}(t) = f_{AB}(t) + \int_o^t f_{BB}(u) h_{AB}(t-u)\,du \qquad (4.23)$$

It is clear from equations 4.22 and 4.23 that the local flux w_B is undetermined in a closed system from a tracer experiment as many distinct sets:

$$\left\{f_{AB}(t),\ f_{BB}(t)\right\}$$

may be consistent with a given renewal density $h_{AB}(t)$. Only additional information, typically external measurements of the the flow rate can solve the problem.

In their paper, Naor et al. (1972) illustrate a procedure to calculate the maximum flow rate consistent with the experimental measurements. While some of their assumptions do not apply in our case (namely: A and B are in the same flow path, or a particle leaving A cannot return to A without passing first at B, and some other assumptions) some comparison seems illustrative. For one particular example of ten stirred tanks connected in series, several first passage distributions are illustrated in Figure 4.8a. The reduced concentration, c/c_∞ consistent with all of them is shown in Figure 4.8b.

It should be noted that the Shinnar, Naor and Katz method method is independent of any detailed information regarding the underlying structure of the system since no model is used. Thus, it is very powerful and would seem to indicate that in theory at least, the two-phase model should not be used for solid mixing models as it is not clear how to obtain the two-phase velocities v_s and V_s. These velocities cannot be

a)

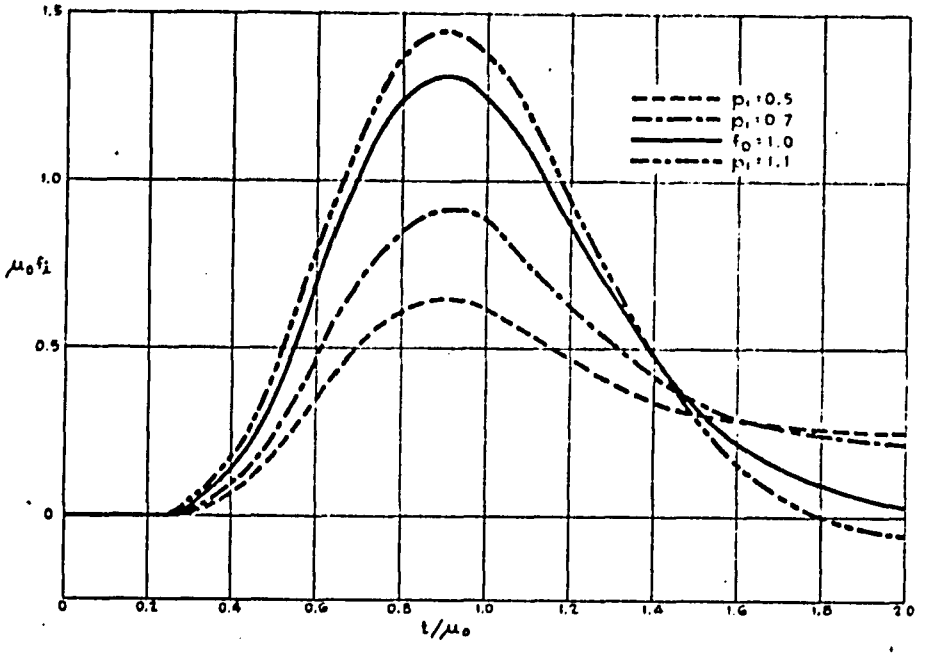

b)

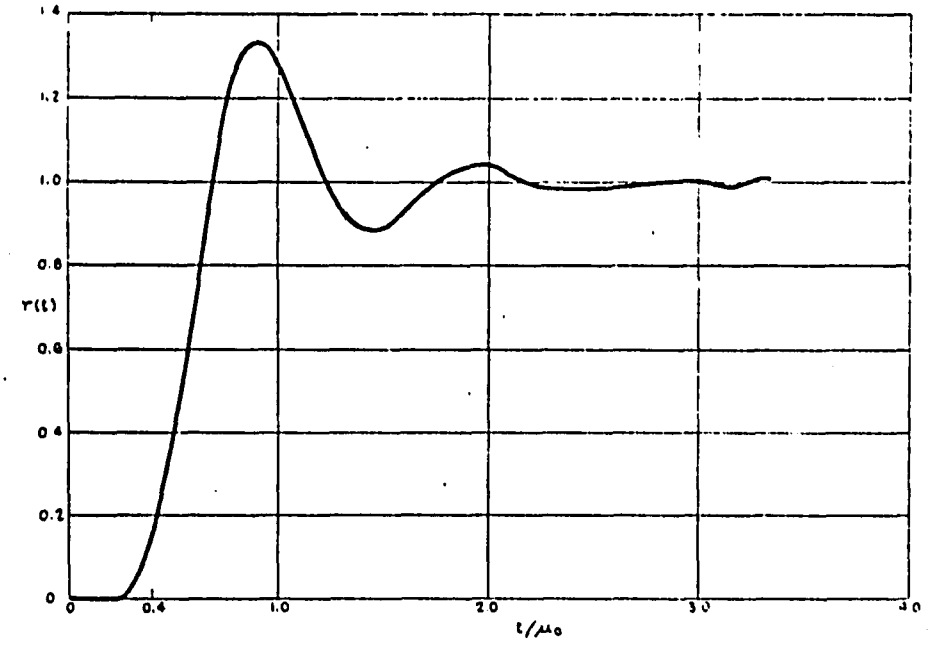

Figure 4.8: a) Dilation and contraction of the first passage time density f_0 (ten equal-size stirred tanks). b) Reduced concentration for the densities given in a (from Naor et al. 1972).

obtained, it seems, from tracer experiments.

Phase Velocities

The above objections notwithstanding*, one can claim an order of magnitude for the phase velocities, by taking the first "substantial" quantity of tracer appearing at a probe to represent this approximate velocity. The results for the expanded top system are shown in Figure 4.9 and 4.10. The upflow velocity seems to be higher than the superficial gas velocity and lower than the average interstitial, linear gas velocity in the bubbling and slugging regimes. It seems to peak at the onset of the turbulent regime and sharply decrease at superficial gas velocities higher than 0.9 m/s, where considerable downflow is forced by the expanded top. The downflow velocity slowly increases throughout the bubbling, slugging and turbulent regimes and seems to be about one half of the superficial gas velocity.

The results for the circulating system are shown in Figure 4.11. It is much harder to estimate the upflow velocity in the high velocity regimes, as the scatter of the experimental points shows. Nevertheless, it seems that the upflow velocity is of the same order of magnitude as the superficial gas velocity (or the average interstitial velociy, as the voidage is high). This confirms the trend observed in the expanded top bed, except for the maximum evident in the latter for the transition from slugging to turbulence. The circulating system is different from the expanded top bed in this region because of the different solid recirculation schemes. The downflow velocity does not increase with increasing the superficial gas velocity, and it stands to reason that it should decline at the higher gas velocities.

*See end of this subsection.

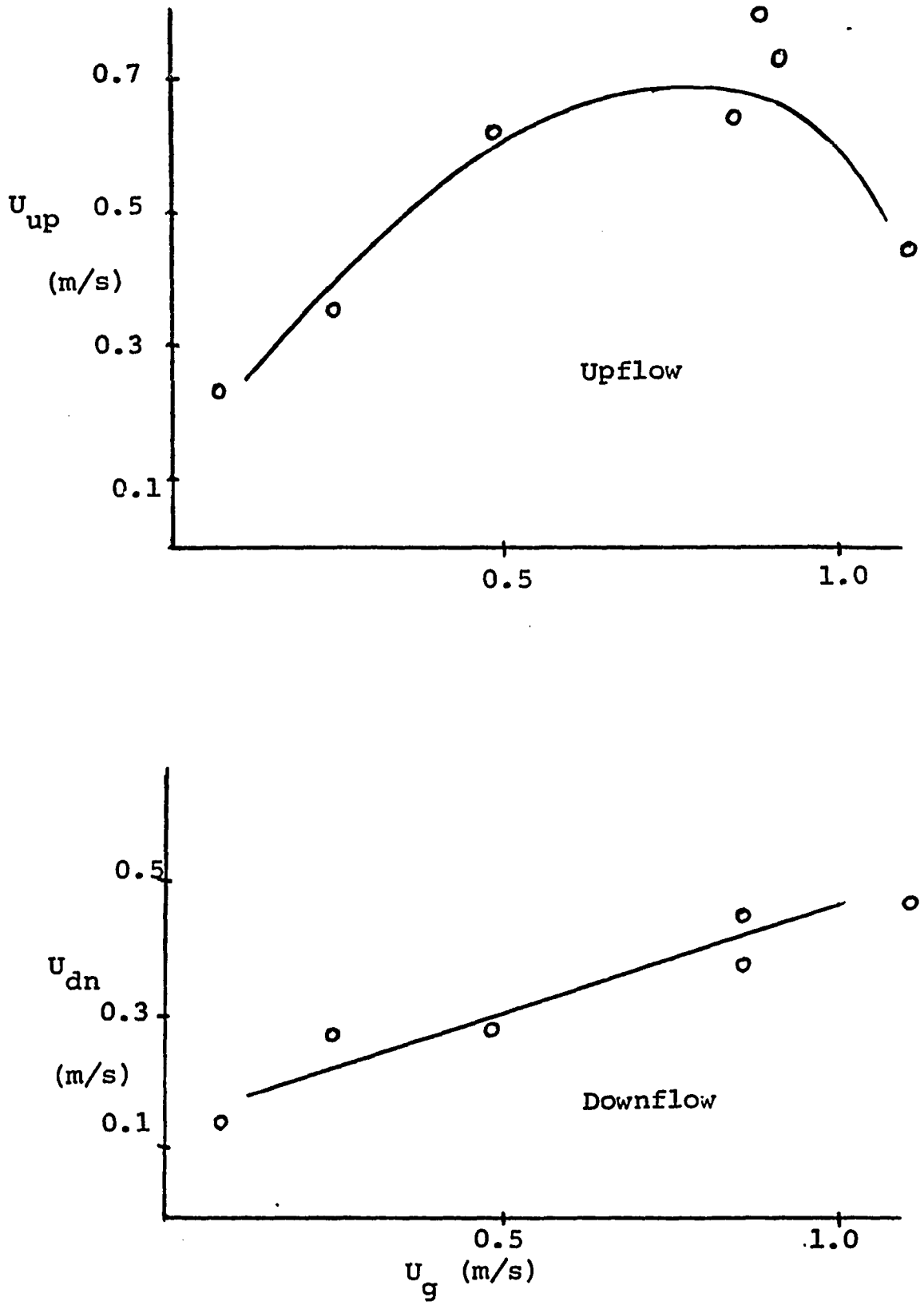

Figure 4.9: Phase Velocities in the expanded Top Bed (vs. Superficial gas velocity)

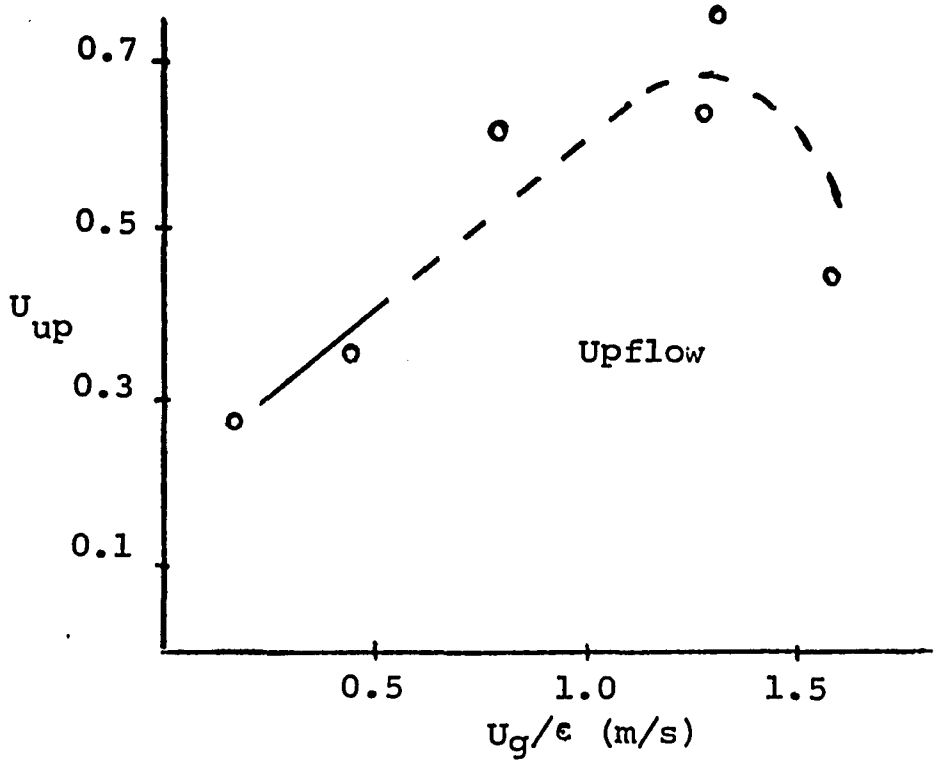

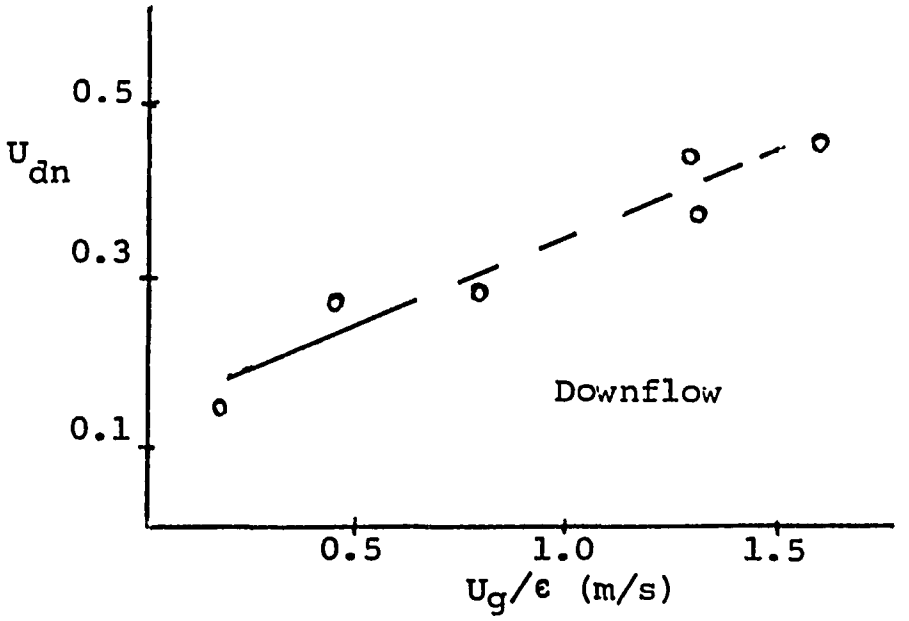

Figure 4.10: Phase velocities in the expanded top bed (vs. linear gas velocity)

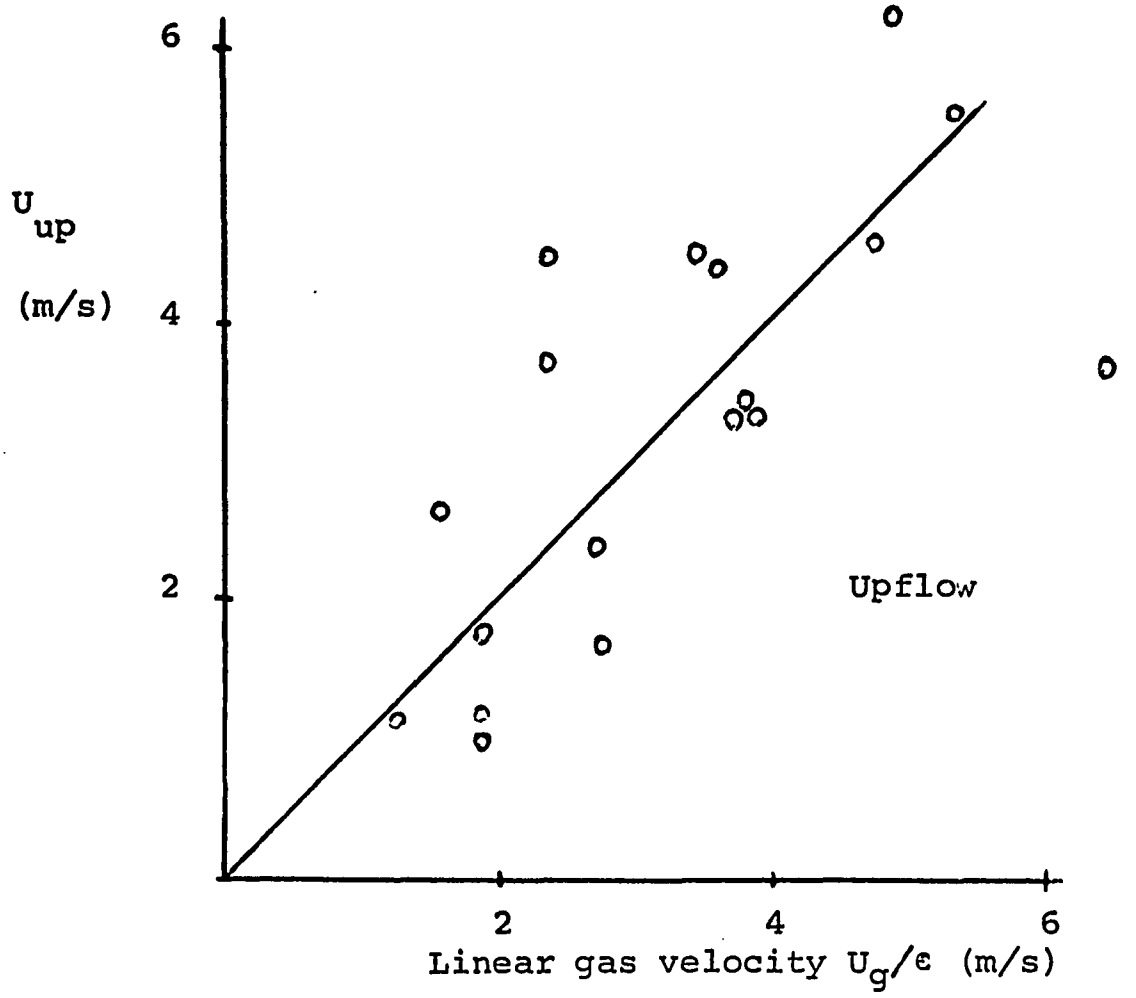

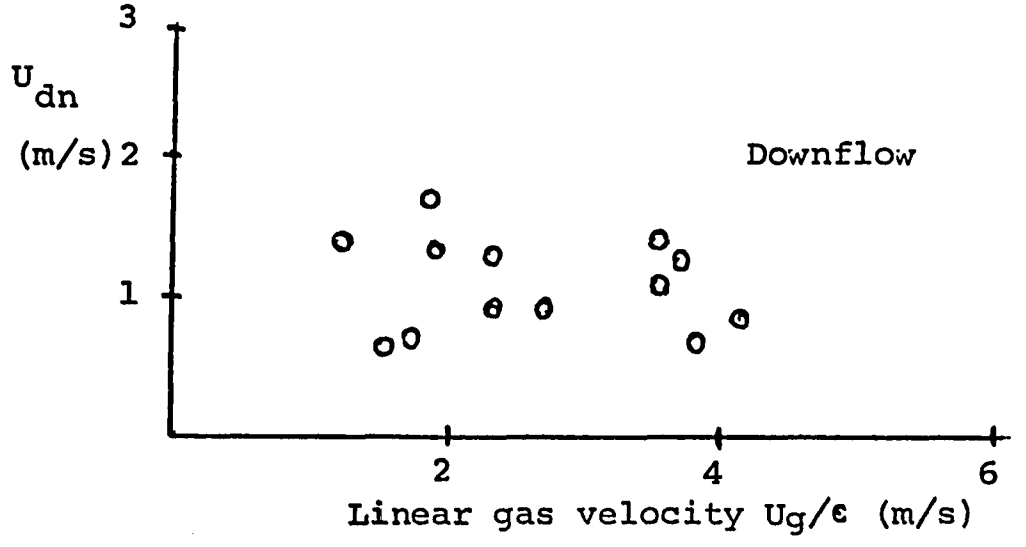

Figure 4.11: Phase velocities in the circulating system.

Van Swaaij et al. (1970) note a change in the direction of the shear stress on a riser walls from negative (downflow) to positive (upflow) at a gas velocity of around 10 m/s.

Dispersion Coefficients from the van Deemter Method

The difficulty in obtaining the two-phase model parameters presents us from analyzing our results in this fashion. For illustration purposes, some analysis is attempted for the lowest velocities in the expanded top bed. Equation 4.21 can be rewritten as:

$$\log \frac{c(t)}{m/\tau} = - {}^{t}/_{\tau} \qquad (4.24)$$

and the results plotted on a semi-log scale. The slope of the resultant curve is $-{}^{1}/_{\tau}$. Such plots are shown for the two upstream channels of run E1 in Figure 4.12. The dispersion coefficient is obtained from equation 4.12:

$$D_{sp} = \tau f_s v_s^2 \qquad (4.25)$$

where fs is taken to be 0.5, which approximates the apparent voidage at low velocities, or equivalently assumes minimum fluidization voidage for the downflow phase. Some results are shown in Table 4.3.

Table 4.3: Dispersion Coefficients from the van Deemter method

Run	Channel	τ (sec)	D_{sp} (m^2/s) X10^2
E1	1	2.04	2.04
	2	2.09	2.05
E2	1	3.33	12.14
	2	2.00	7.29

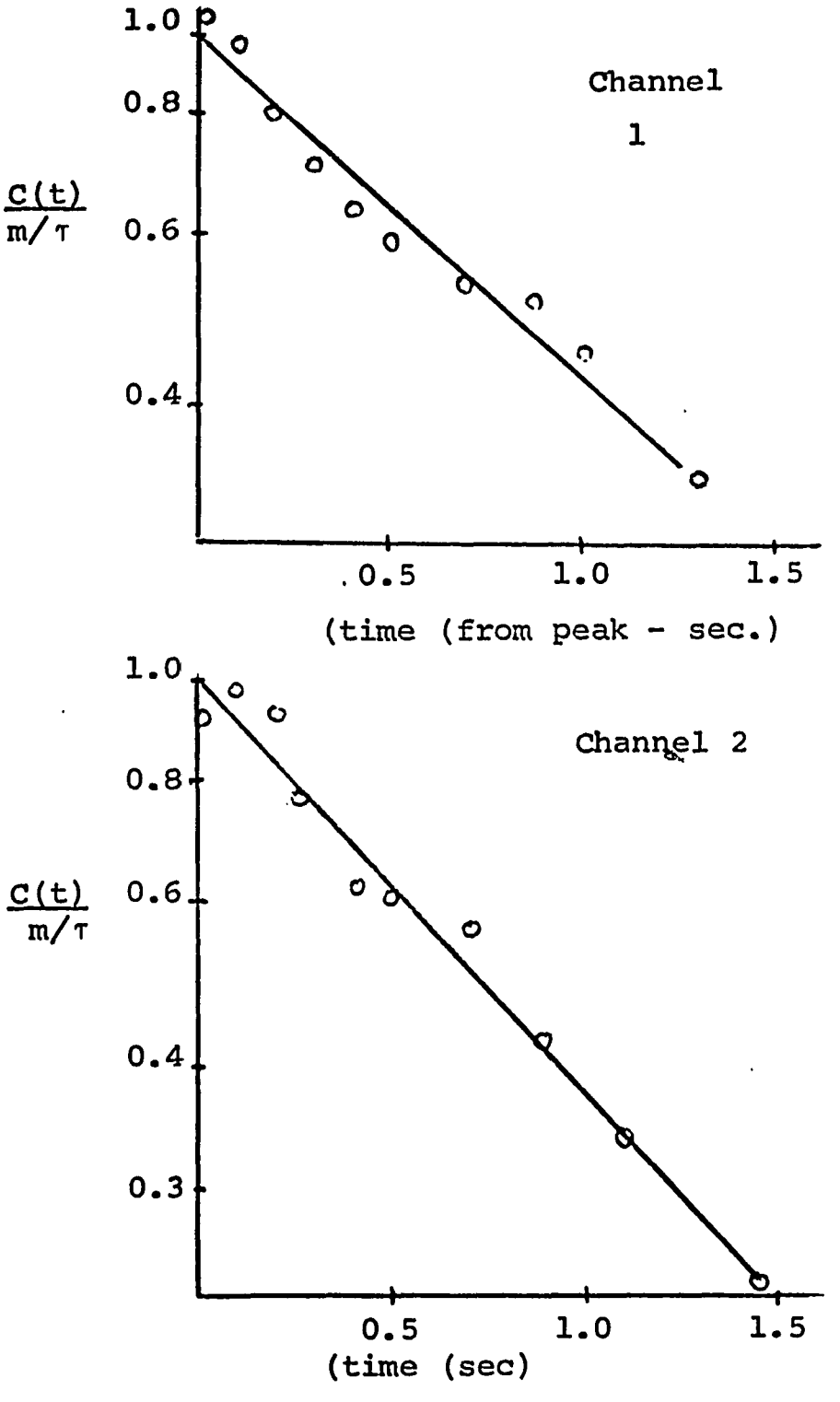

Figure 4.12: The two-phase method applied to run E1.

The results for run E1 are in the same order of magnitude as the results later obtained by the modified dispersion model, but no such agreement can be claimed for run E2. Not only are the dispersion coefficients obtained too high, but the two channels give conflicting results. We must conclude that the van Deemter approach can describe our results only at the lowest superficial gas velocity.

4.7 The Modified Turbulent Dispersion Model

A modified turbulent dispersion model has been adopted to represent our solid mixing results. Three factors seem to support this choice:

a) Visual observations of high velocity fluidized beds show a greater uniformity than low velocity beds. In the turbulent fluidization regime, for example, voids appear and disappear without travelling a long distance. This seems to indicate that mixing is taking place on a smaller length scale in the high velocity bed as compared to the bubbling bed. One can claim that throughout the turbulent and fast regimes, the turbulent eddy mixing scale is of the order of magnitude of the bed diameter. Our high velocity beds are of a much higher aspect ratio than common low velocity beds. The expanded top bed was typically operated at $L/D_t = 23$ and the circulating system at $30 < L/D_t < 50$. These dimensions are much higher than the apparent turbulent eddy mixing scale and so the continuum approach is applied to the suspension. It should be stressed that this is an apparent, or modified, dispersion model - not a molecular diffusion mechanism.

b) The main objection raised against diffusion models in a fluidized bed is the possibility of obtaining a lower conversion than a completely mixed model would predict.

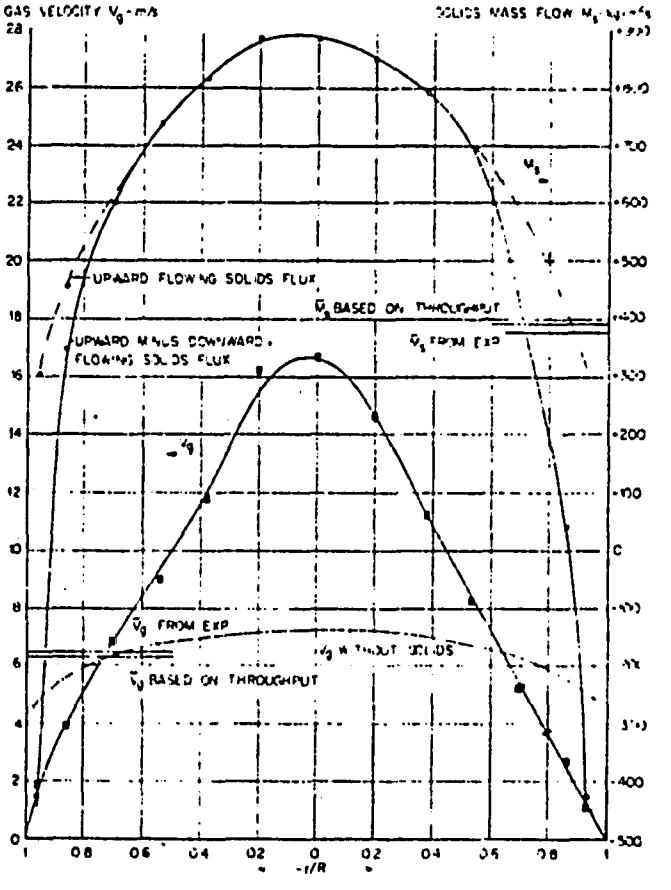

Figure 4.13. Gas velocity and solids mass flux profiles measured in a 30-cm diameter riser(van Breugel et al., (1969).

This has been observed in shallow low velocity bubbling beds, where some gas completely bypasses the dense phase. Since we claim a much smaller mixing scale, and a high L/D_t ratio this objection does not seem valid. The results of Massimilla (1971) reproduced in Figure 1.6 show a higher conversion in a turbulent bed than the slugging bed model would predict.

c) The results of van Breugel et al. (1969) reproduced in Figure 4.13 show that in a 30-cm I.D. riser the turbulent gas velocity profile in an empty tube is modified to a "laminar" flow type profile by the presence of solids. The solid flux profile also seems to resemble a parabolic profile and thus a dispersion mechanism similar to Taylor dispersion is claimed.

4.7.1 The Expanded Top Bed

The net solids flux in the expanded top bed is zero and the one dimensional diffusion equation is:

$$D_{SA} \frac{\partial^2 C}{\partial X^2} = \frac{\partial c}{\partial t} \qquad (4.26)$$

D_{SA} is the cross-sectional average solid diffusivity (based on the entire cross-sectional area) and the X coridnate is measured from the injection point. The solution for an impulse injection is:

$$\frac{C}{C\infty} = 1+2 \sum_{n=1}^{\infty} \exp\left(-n^2\pi^2 \frac{D_{SA}}{L^2} t\right) \cos \frac{n\pi x}{L} \qquad (4.27)$$

By matching the measured response curve $C/C\infty$ with equation 4.27 at the four probes it is possible to calculate D_{SA}. The results are summarized in Table 4.4 and some of the curves are shown in Figure 4.14.

Table 4.4: Dispersion coefficient in the Expanded Top Bed

Run No.	U_g (m/s)	Channel	D_{sp} (m^2/s) X10^2
E1	0.075	Bottom 1 Top 3	1.02 3.64
E2	0.24	Bottom 1 Top 4	3.27 4.09
E3	0.48	Bottom 1,2 Top 4	3.26 3.26
E4	0.48	Bottom 1,2 Top 4	2.54 3.62
E5	0.84	Bottom 1,2 Top 3,4	2.53 4.74
E7	0.86	Bottom 1 Top 4	2.50 4.74
E8	1.10	Bottom 2 Top 4	4.18 4.46

Figure 4.14 shows a generally good description of the experimental results with the dispersion model, except for the lowest velocities, where clearly the large peaks cannot be explained by a dispersion solution. This was discussed in the previous section, where the two-phase model was shown to describe this kind of behavior.

The results for the top of the bed are shown in Figure 4.15 and for the bottom of the bed in Figure 4.16. Both curves include our results as obtained from equation 4.27.

These figures also include some dispersion coefficients calculated by the Todes fluctuation method to be

a) RUN E 1

channel 3 (downstream)

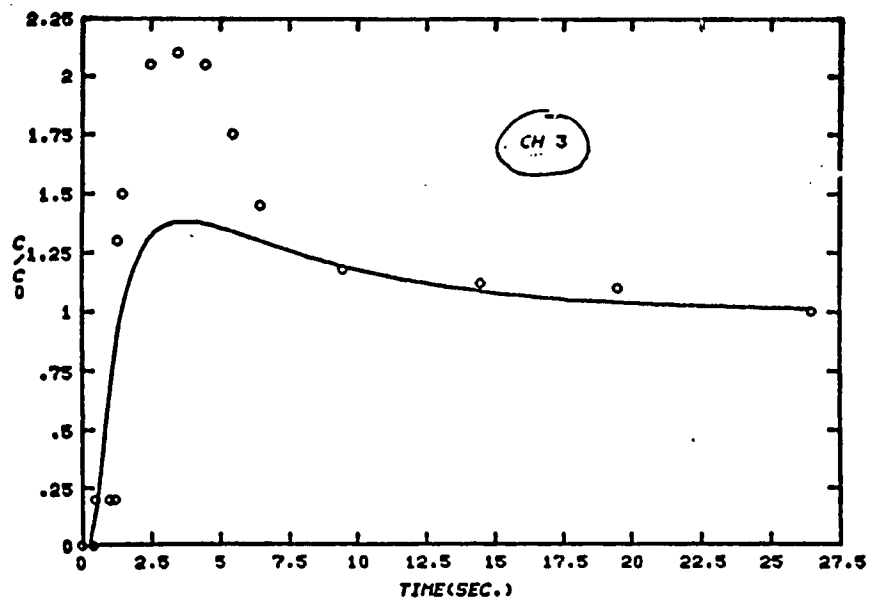

channel 1 (upstream)

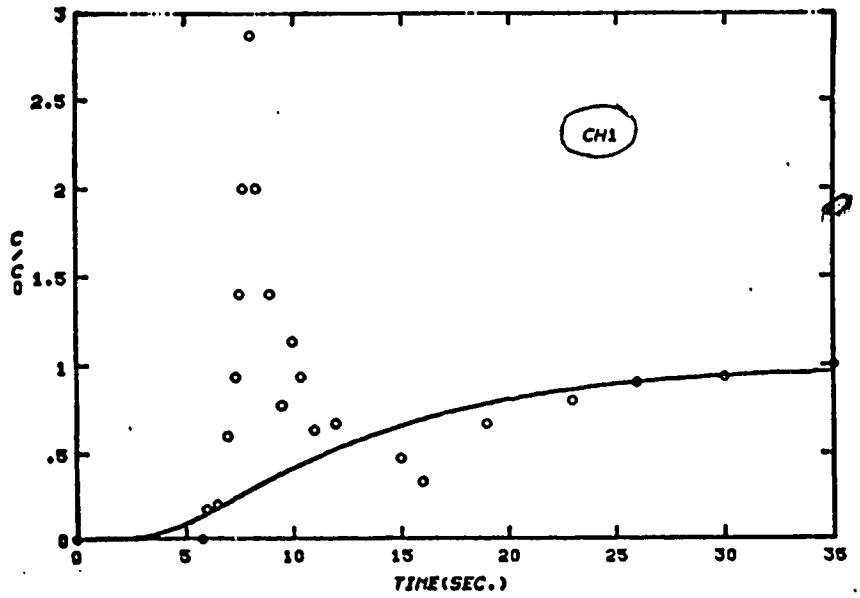

Figure 4.14 : The dispersion model fitted to the experimental results - expandedbp bed.

Figure 4.14bRUN E 2

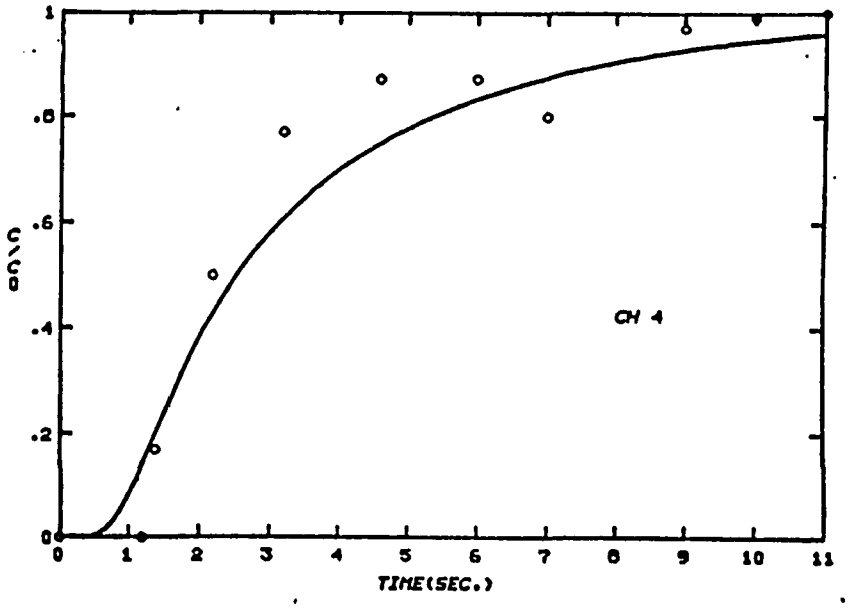

Figure 4.14 c: RUN E 3

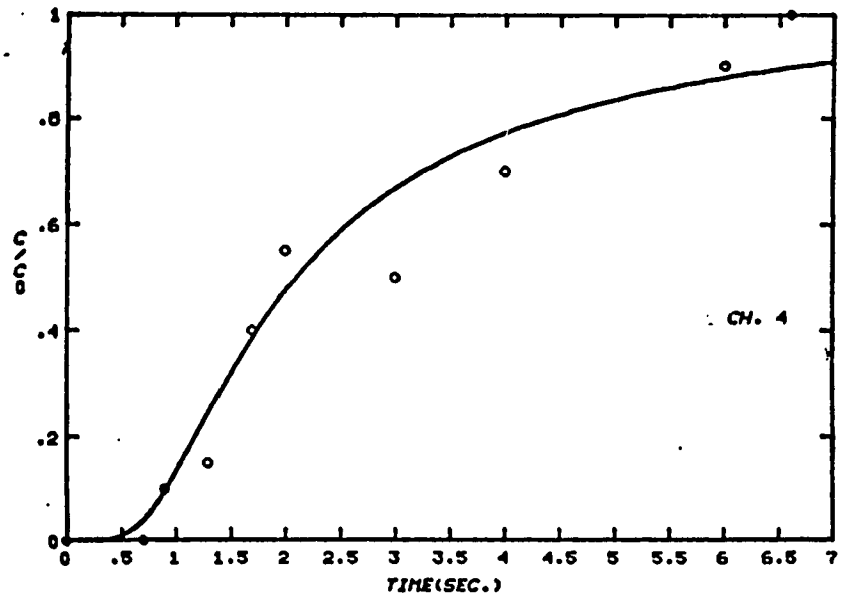

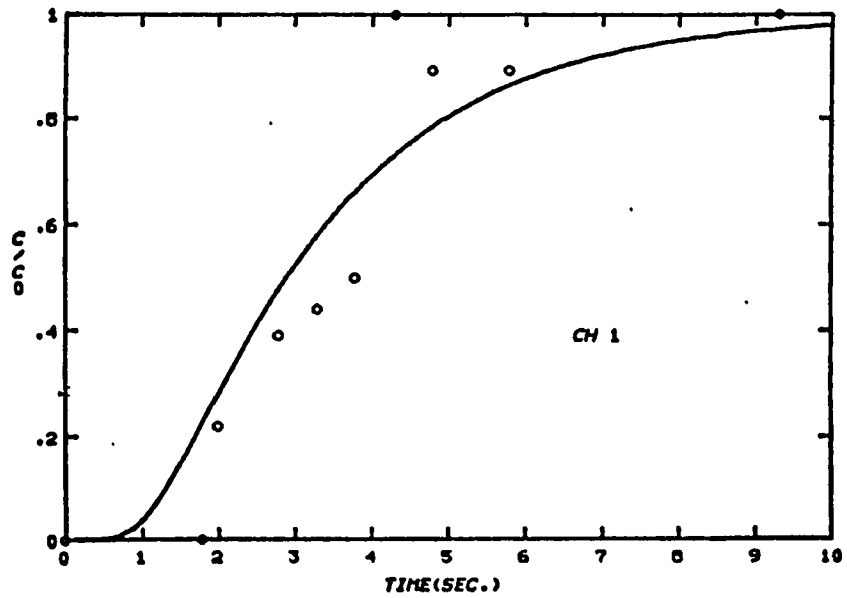

Figure 4.14 d: RUN E 4

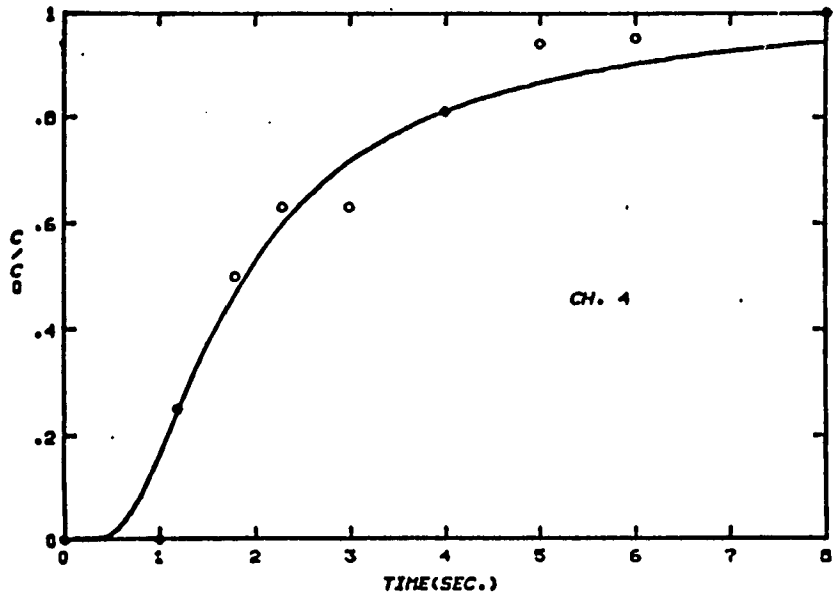

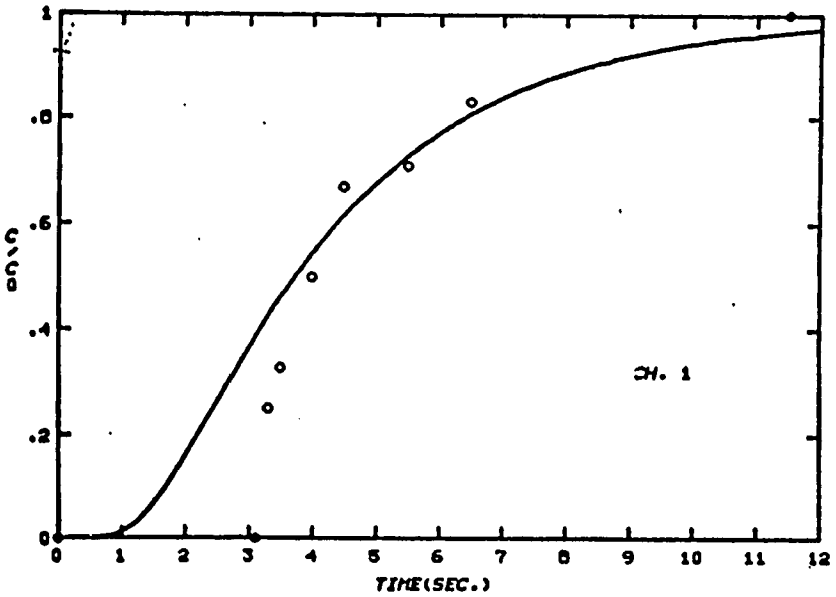

Figure 4.14 e: RUN E 7

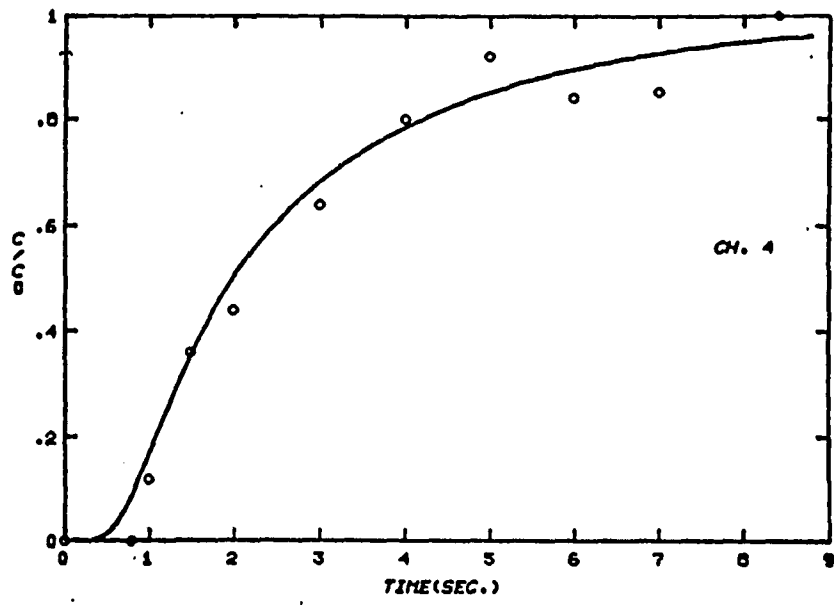

RUN E 5 ch 2

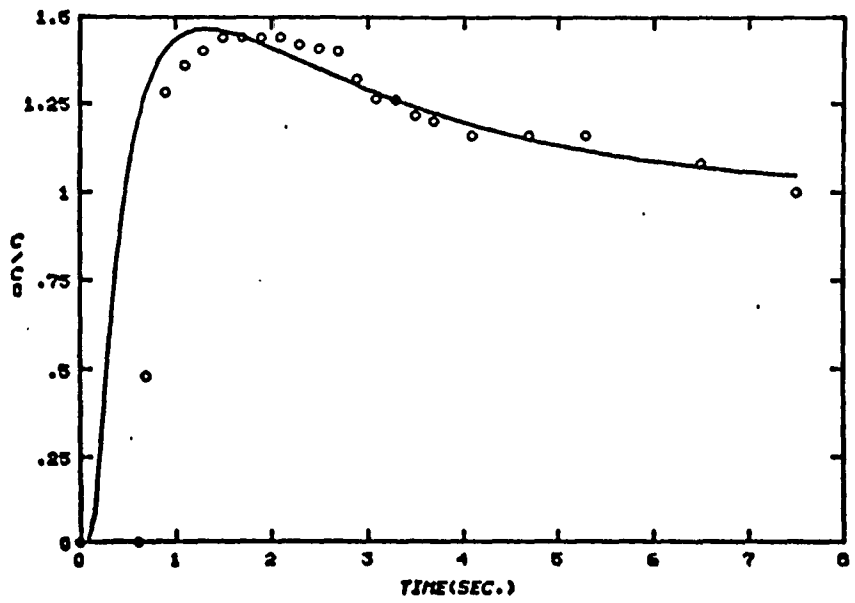

Figure 4.14f: RUN E 8

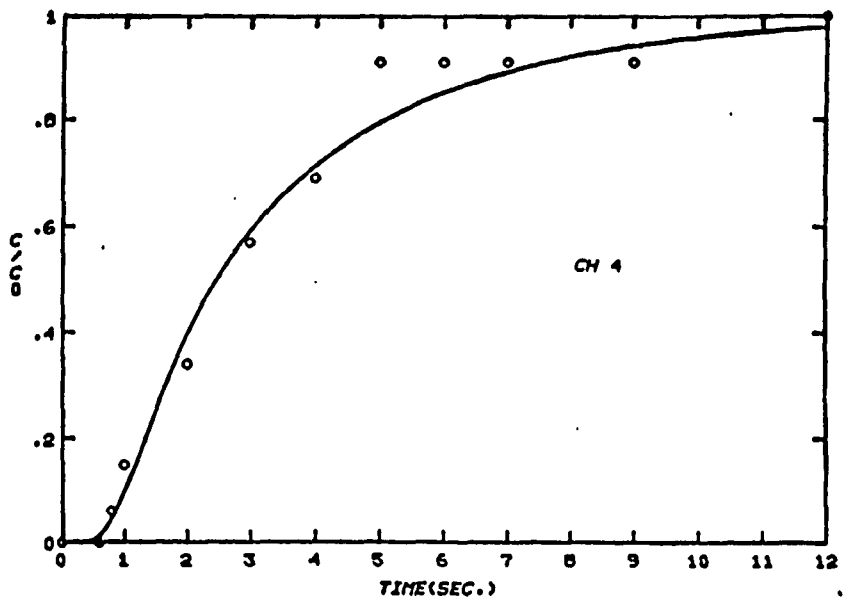

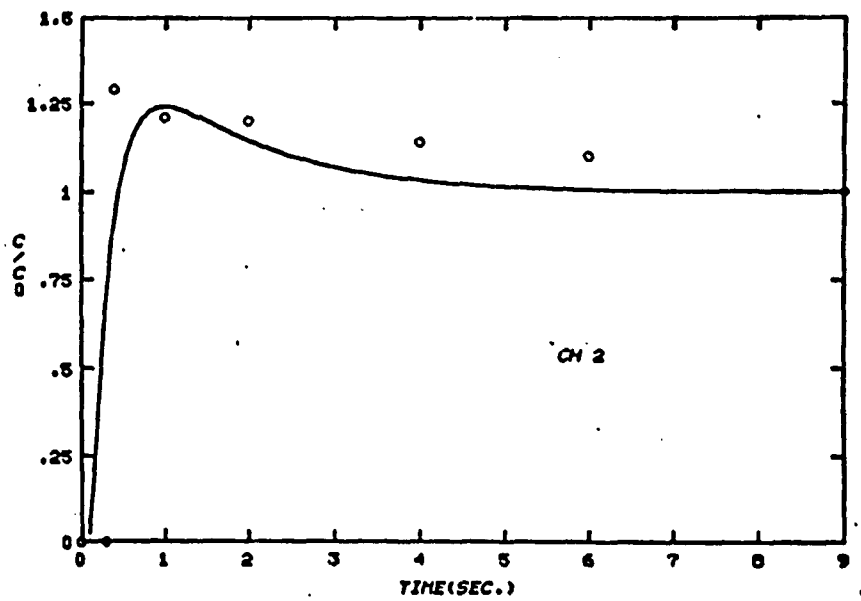

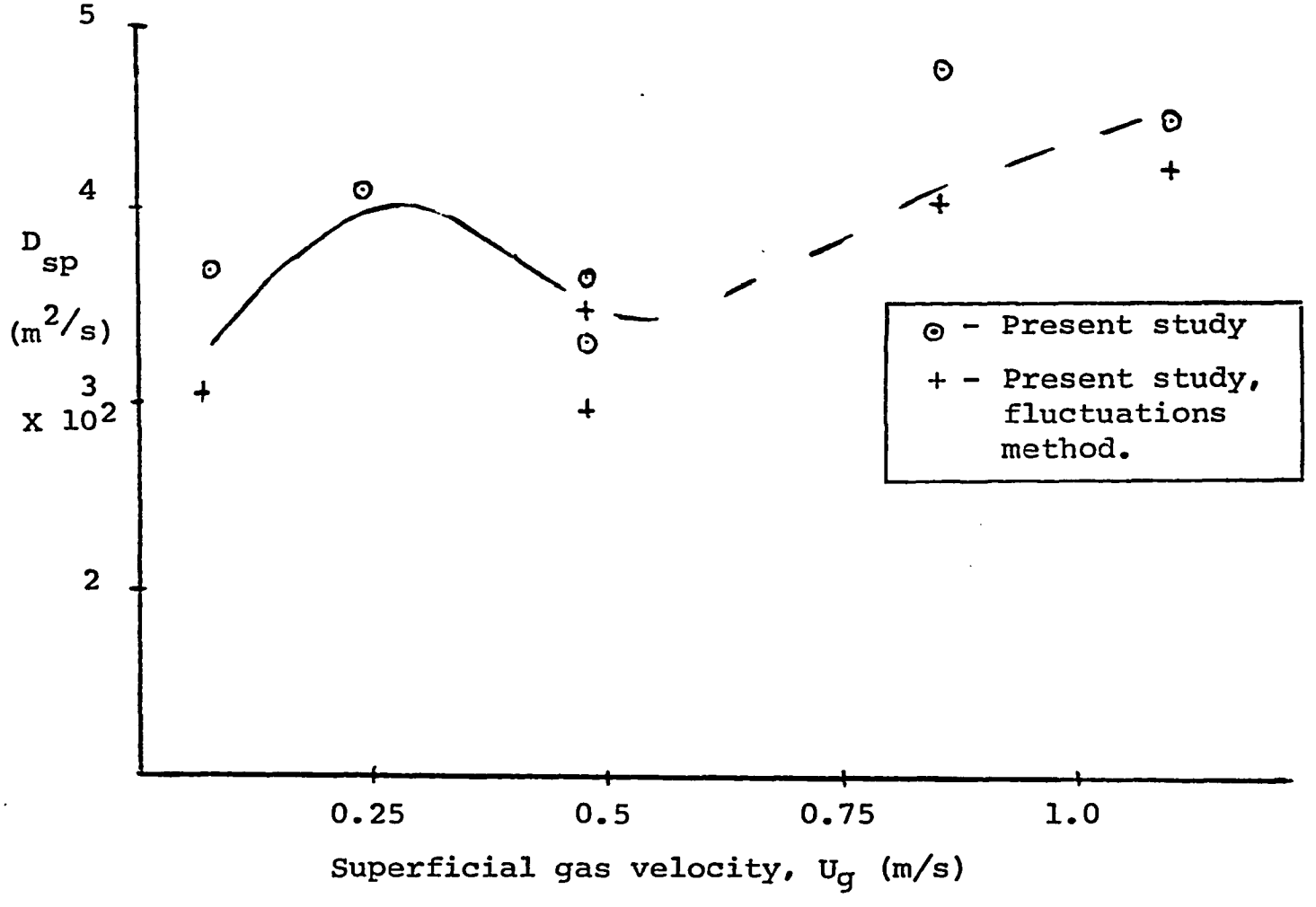

Figure 4.15: Dispersion Coefficients near the top of the Expanded top bed.

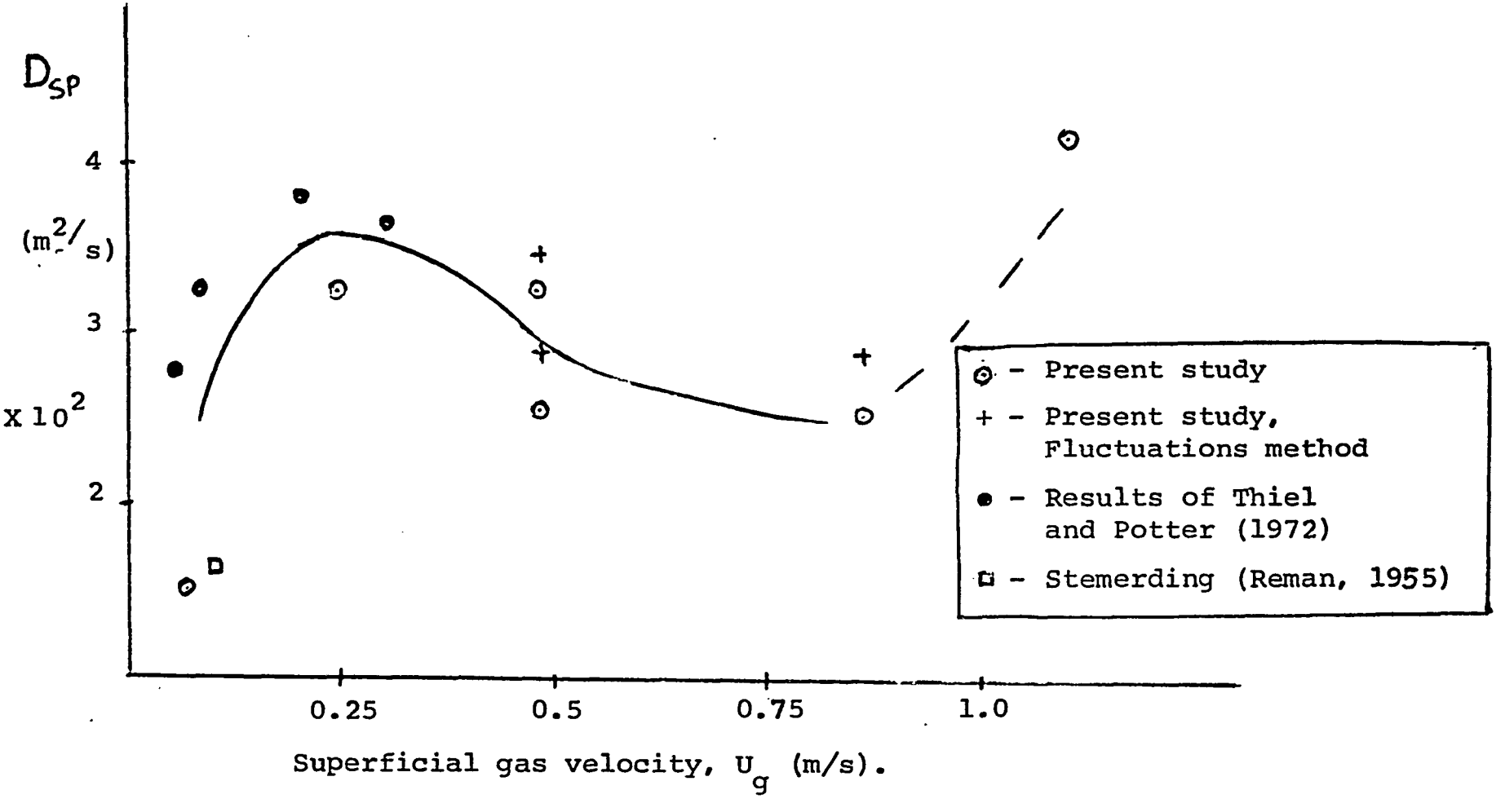

Figure 4.16: Dispersion Coefficients near the bottom of the expanded top bed.

described later on, and some data from the literature for similar powders. The data point of Stemerding (reported by Reman, 1955) is $D_{SA} \cdot \rho_s$ = 36 kg/ms, and by assuming ρ_s = 1.5 g/cm^3 we get the reported value. The data of Thiel and Potter (1978) is linearly interpolated between two of the bed diameters used by them, 0.102 m and 0.218 m. Their results indeed show a linear dependence of D_{sp} on bed diameter, an issue that will be discussed in the next section.

Both Figures 4.15 and 4.16 show that the axial solid diffusivity goes through a maximum in the slugging regime and then decreases as transition to turbulence takes place. The increase of D_{sp} with the gas velocities in the bubbling rgime has been widely observed before, and bed reaches its maximum heterogeneity has also been observed by Thiel and Potter (1978). This trend reverses itself in the expanded top bed at a superficial gas velocity of 0.9, where D_{sp} is shown to increase again. The reason for this lies in the mechanism of solid recirculation from the top. At superficial gas velocities higher than 0.9 m/s there is considerable recirculation which greatly enhances the down-the-walls, up-the-center solids movement in the bed. This indeed is the reason for the difference between the results obtained in the expanded top bed, and at comparative gas velocities in the turbulent regime, in the circulating system.

At the lowest gas velocities, the results of Table 4.4 show a considerable difference between the bottom of the bed and its top. At these velocities, examination of the results shows that bubbles are still in the coalescence stage, they are small in the lower region and coalesce to slugs in the higher sections of the bed. Thus at low gas velocities, since both

bubble size and velocities are a function of bed height, so is the axial dispersion coefficient. It is lower at the bottom of the bed and higher at the top. As the bed reaches the transition to turbulence region, this difference between top to bottom narrows down, and for all practical purposes the whole bed can be described by the same dispersion coefficient.

4.72 The Circulating System

The one dimensional conservation equation for tracer is:

$$\frac{\partial c}{\partial t} = D_{SA} \frac{\partial^2 c}{\partial x 2} - U_s \frac{\partial c}{\partial x} \qquad (4.28)$$

where D_{SA} is the axial solids diffusivity based on the entire cross-sectional area and U_s is the average linear solid velocity:

$$U_s = \frac{G_s}{\rho_s (1-\varepsilon)} \qquad (4.29)$$

If one defines a mean residence time for the solids as:

$$\bar{t} = \frac{L(1-\varepsilon)\rho_s}{G_s} \qquad (4.30)$$

and a dimensionless distance parameter z = x/L (where z=0 at the tracer injection point), one can rewrite equation 4.28 in a dimensionless,

$$\frac{\partial c}{\partial \theta} = \left(\frac{D}{U_s L}\right) \frac{\partial^2 c}{\partial z^2} - \frac{\partial c}{\partial z} \qquad (4.31)$$

where $\theta = t/\bar{t}$.

The solution to equation 4.31 for an open vessel and "through-the-wall" sampling is (Levenspiel and Smith, 1957):

$$c_\theta = \frac{1}{2\sqrt{\pi\theta (D_{SA}/U_s L)}} \exp \left[-\frac{(1-\theta)^2}{4\theta (D_{SA}/U_s L)}\right] \qquad (4.32)$$

The first and second moments are as follows:

$$\text{mean } \bar{\theta}_c = \frac{\bar{t}_c}{\bar{t}} 1 + 2 \frac{D_{SA}}{U_s L} \qquad (4.33)$$

$$\text{variance } \sigma_\theta^2 = \frac{\sigma^2}{\bar{t}^2} = 2\frac{D_{SA}}{U_s L} + 8\left(\frac{D_{SA}}{U_s L}\right)^2 \qquad (4.34)$$

For a "one-shot" tracer input Aris (1959) has shown that the dispersion coefficient can be obtained from two down-stream channels (such as channels 3 and 4 in our case) by:

$$\Delta\sigma_\theta^2 = 2\,\frac{D_{SA}}{U_s L} \qquad (4.35)$$

The Aris method and equation 4.35 are particularly powerful because they circumnavigate the difficulties of the exact amount of tracer injected and the exact shape of the injection impulse. This enables one to use the injection described here without introducing an error and it eliminates the need of calibrating the probes.

The dispersion coefficients were thus calculated from the concentration histories of channels 3 and 4 and equation 4.35. The nemesis of transient response tracer experiments can be the long decaying tails, especially when the measured variable reaches the magnitude of the measuring instrument error. To avoid introducing a large error the tails are usually cut at 10 mv. This is equivalent to fitting the experimental curve with an exponential tail from that point on. The dispersion coefficient obtained from the difference in the second moment of the two downstream channels is then compared to the exact solution in each channel (equations 4.33 and 4.34). In most cases there is a reasonable fit between the dispersion coefficients obtained. The dispersion coefficient is then fitted to the experimental data, using the exact solution (equation 4.32) as a final check. The results are given in Table 4.5 and some computer solutions are shown in Figure 4.17. In most cases the dispersion coefficients obtained from the two downstream channels are the same, leading one to speculate that they would stay constant for the rest of the downstream section. The results are not so conclusive for the upstream channels and will be elaborated upon in the next section.

Table 4.5: Downstream Dispersion Coefficients in the Circulating System

Run No.	U_g (m/s)	G_s (kg/m^2.s)	$\bar{\epsilon}$	D_{sp} (m^2/s) $_{x10^2}$
C2	1.08	5.8	0.70	0.50
C3	1.43	16.5	0.74	0.97
C4	1.46	14.3	0.74	1.09
C5	1.48	18.4	0.73	1.25
C6	2.00	47.8	0.78	5.08
C7	2.28	71.5	0.78	2.11
C8	2.39	97.9	0.79	5.25
C9	2.44	75.0	0.81	5.00
C10	3.41	76.0	0.92	6.70
C11	3.41	73.4	0.927	4.58
C12	3.35	107	0.81	8.00
C13	3.34	117	0.83	8.80
C14	3.38	112	0.81	8.80
C15	4.69	74.0	0.958	4.09
C16	4.58	84.0	0.958	3.89
C17	4.45	135	0.84	3.75
C18	4.58	134	0.84	5.20
C19	5.62	152	0.85	4.18

a) RUN C 2

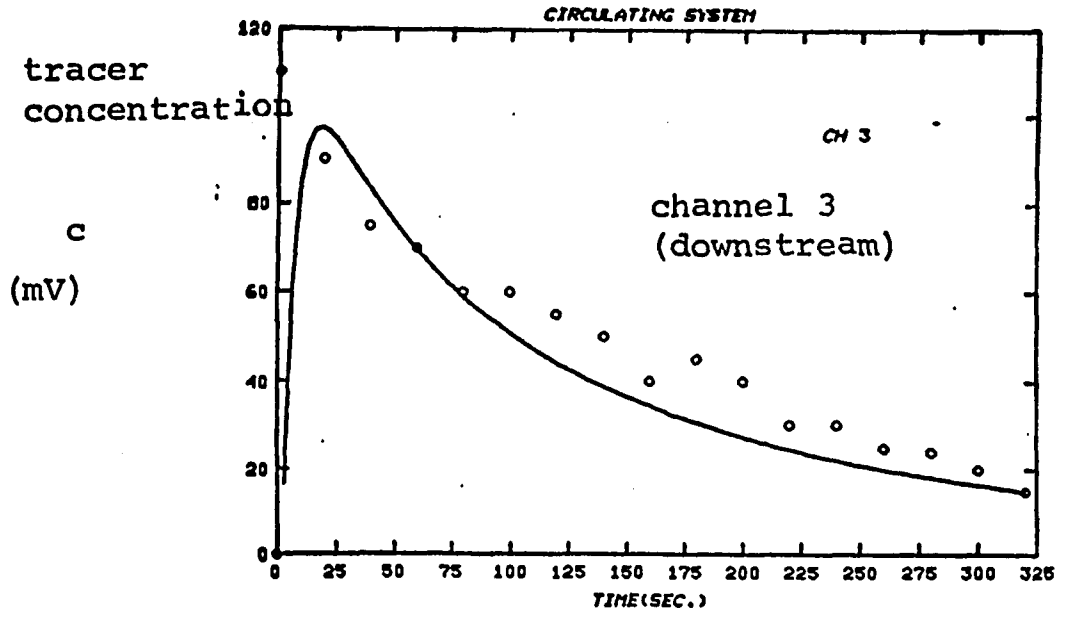

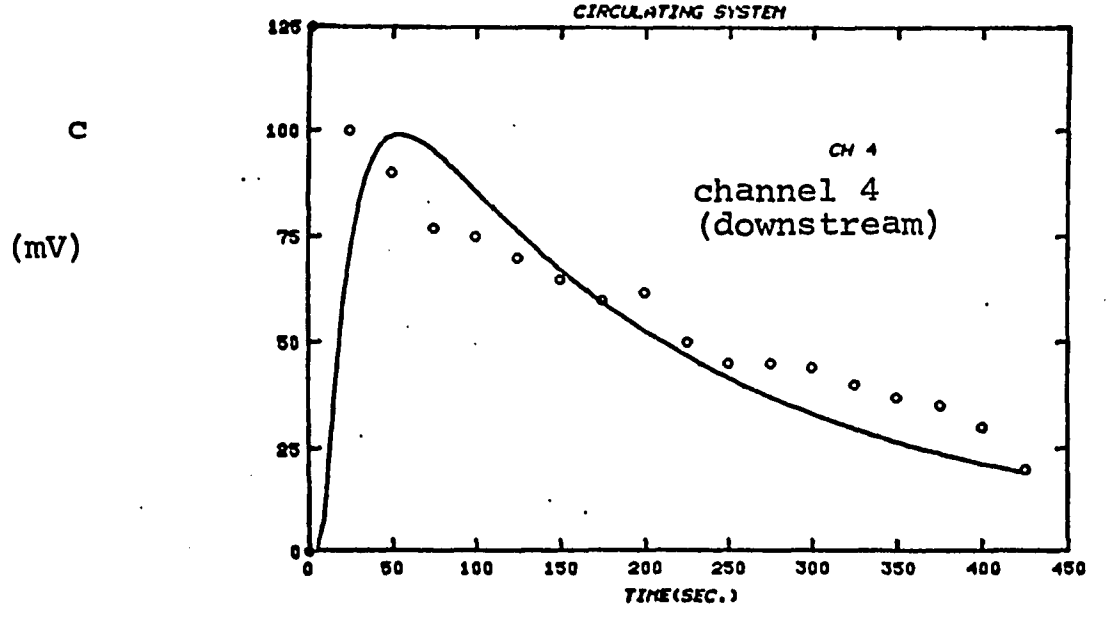

Figure 4.17: The dispersion model fitted to the experimental results - circulating system.

Figure 4.17 b: RUN C 3

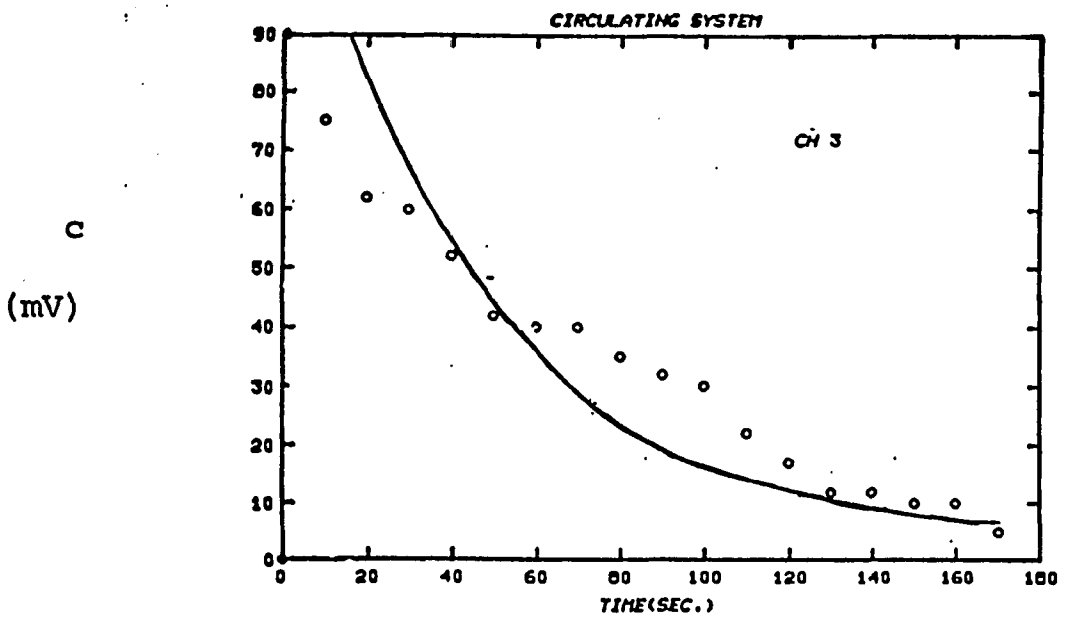

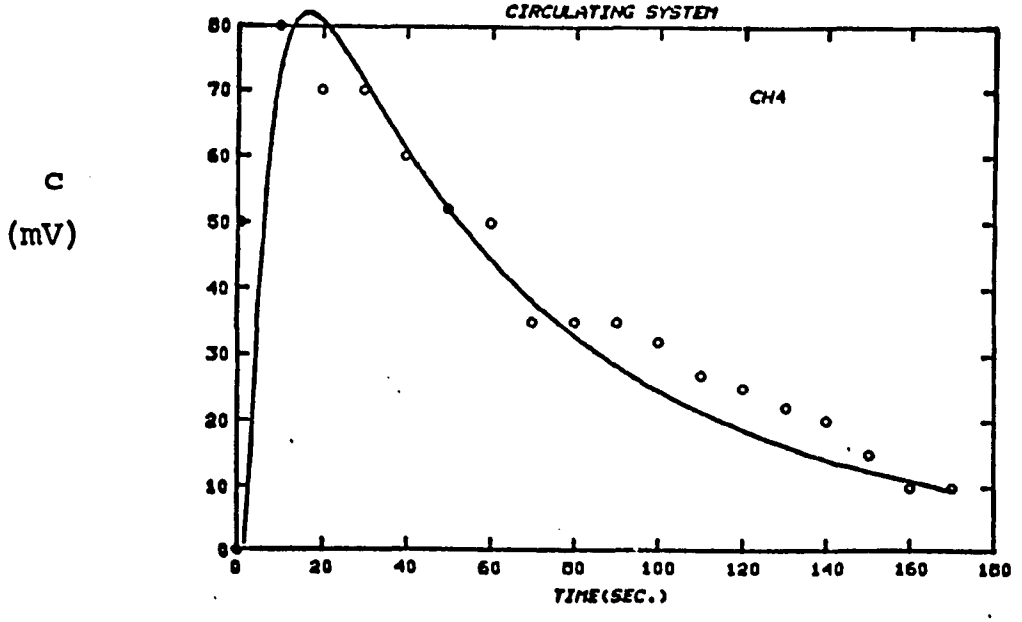

Figure 4.17c:RUN C 7

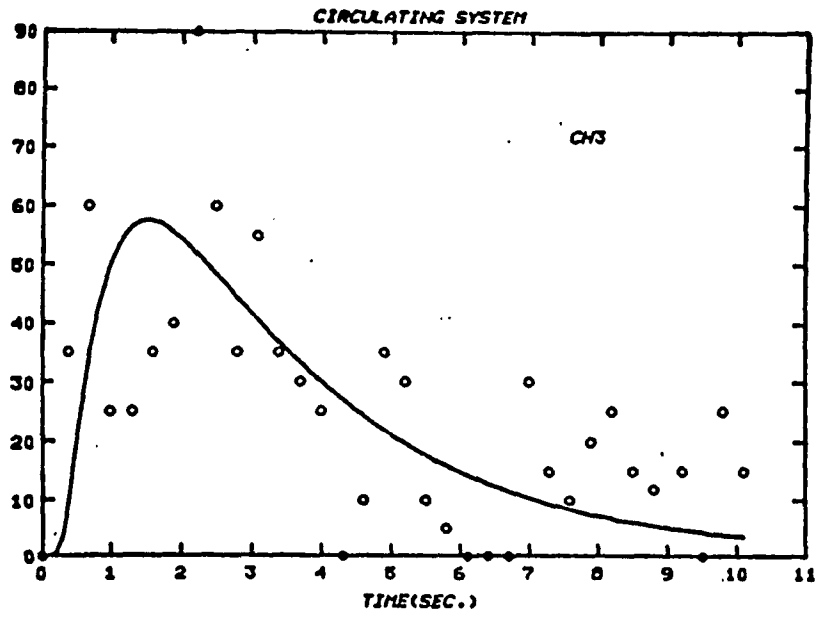

Figure 4.17 d: RUN C 13

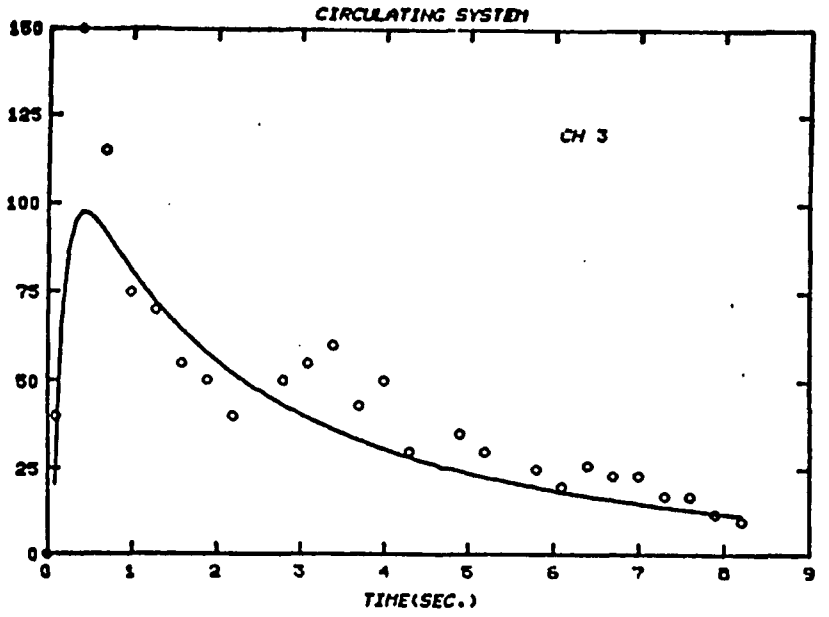

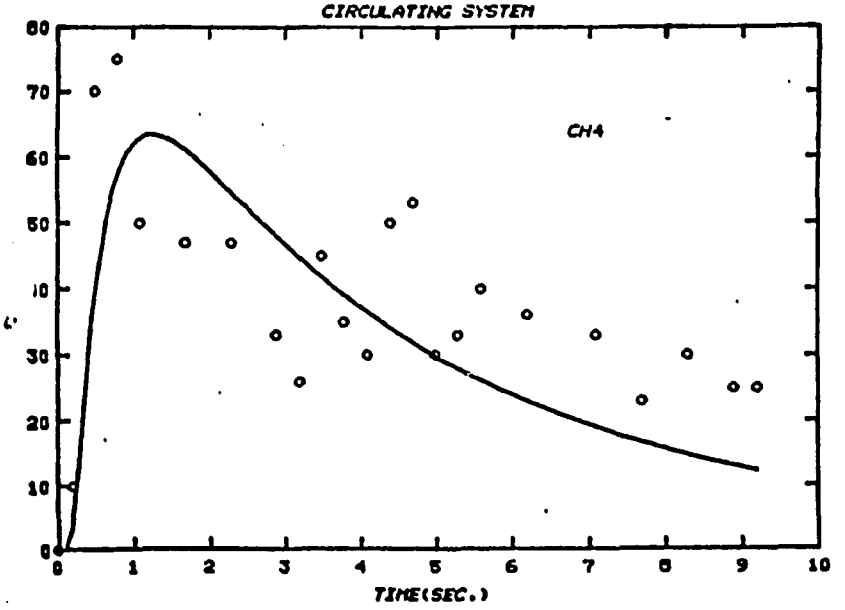

Figure 4.17 e: RUN C 14

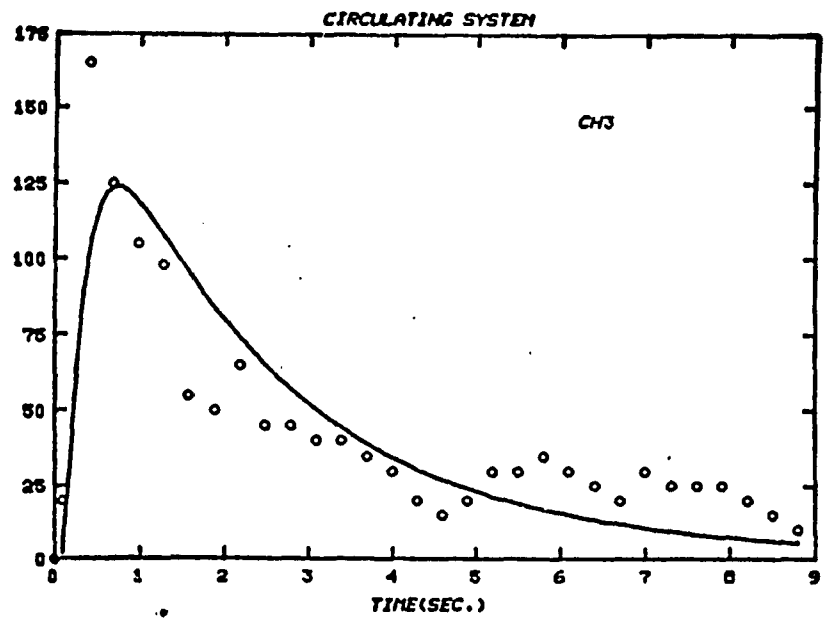

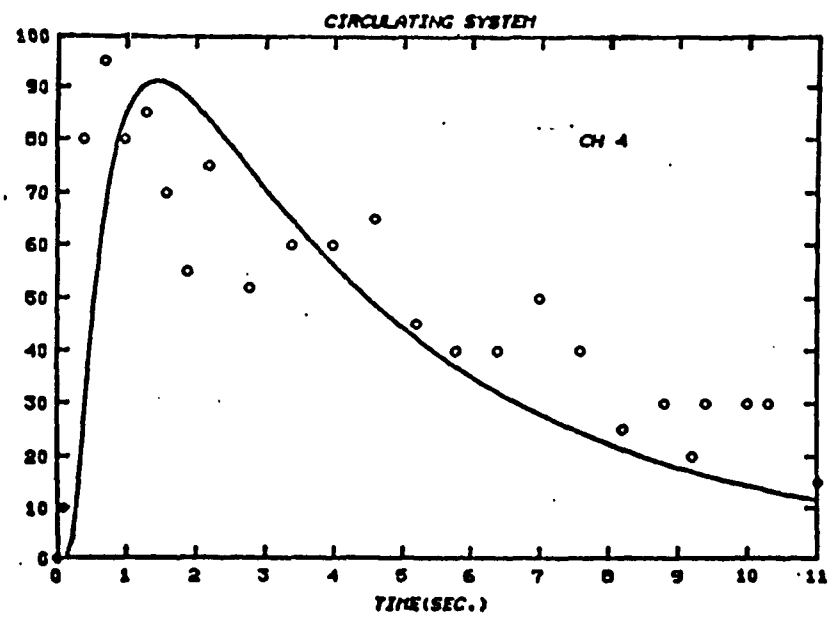

Figure 4.17 f: RUN C 15

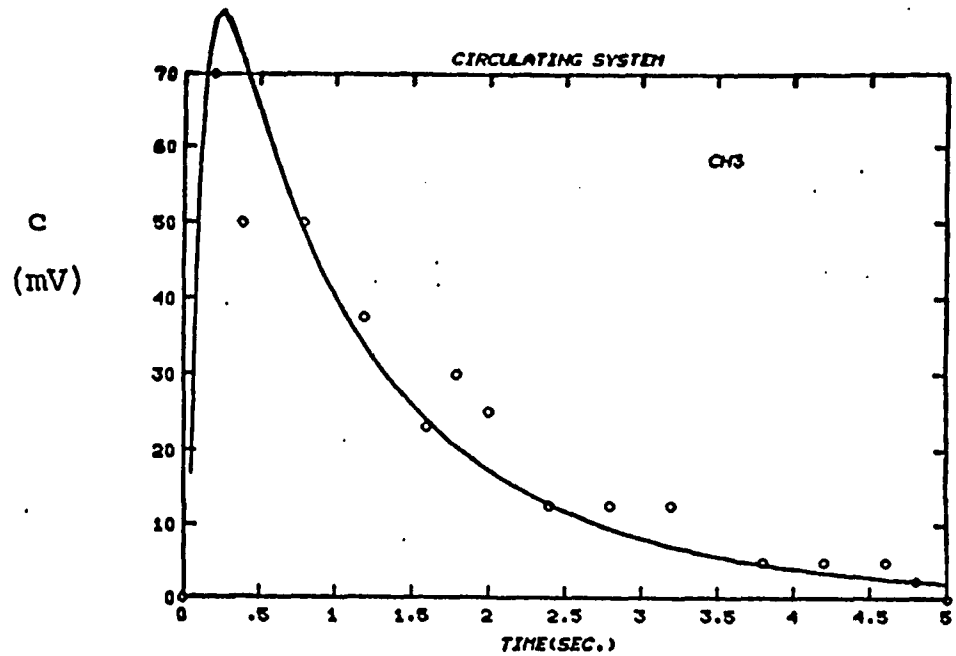

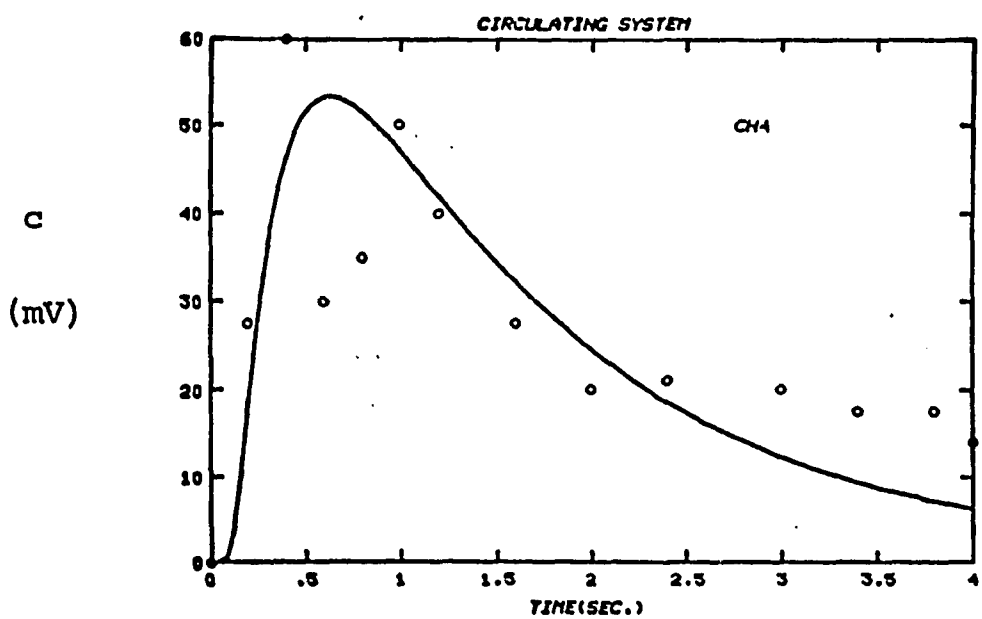

Figure 4.17g: RUN C 16

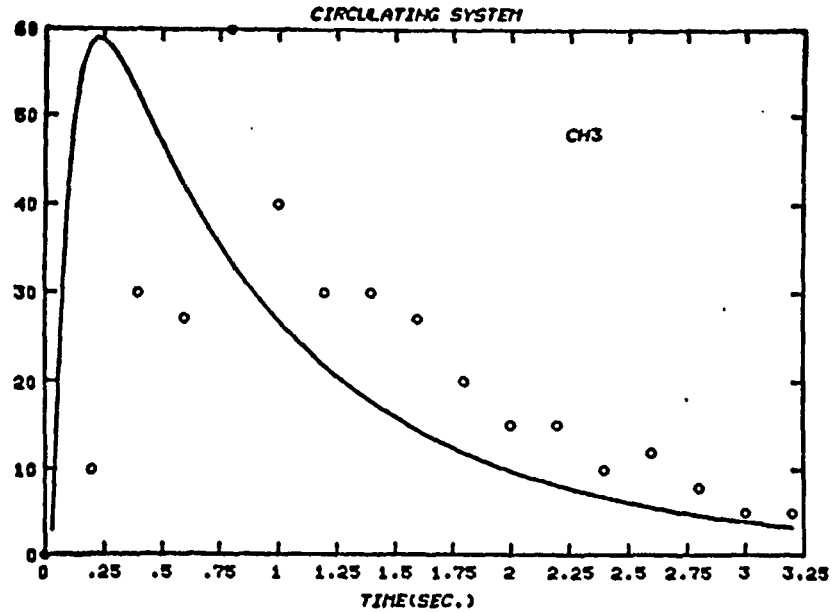

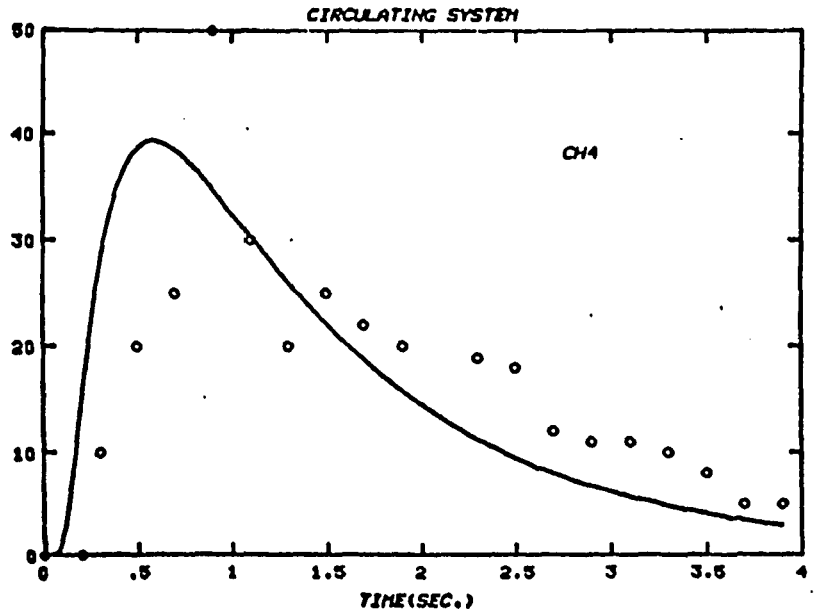

Figure 4.17 h: RUN C 19

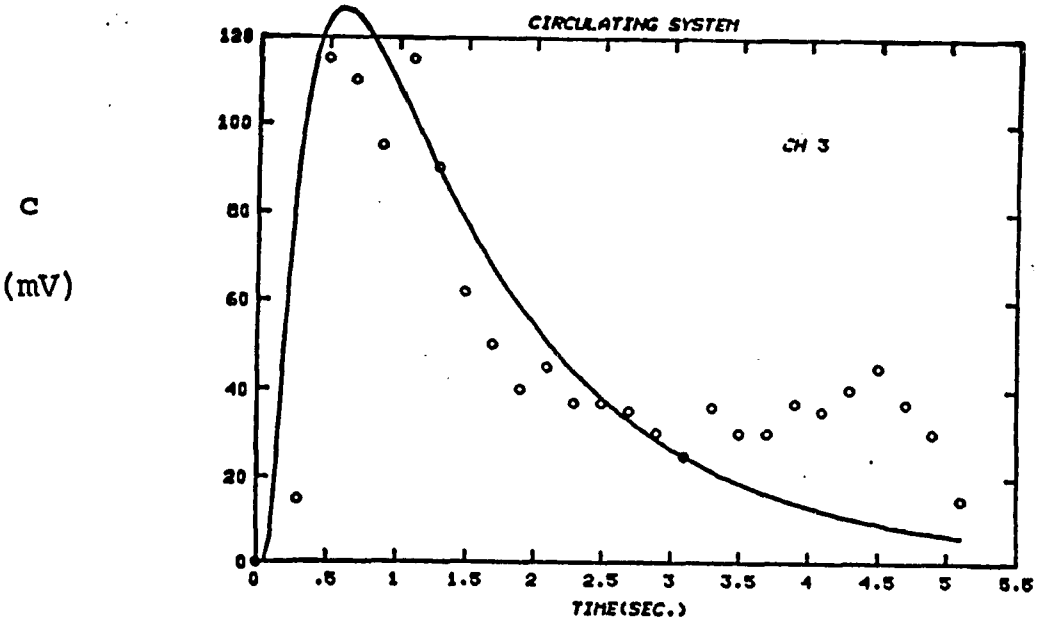

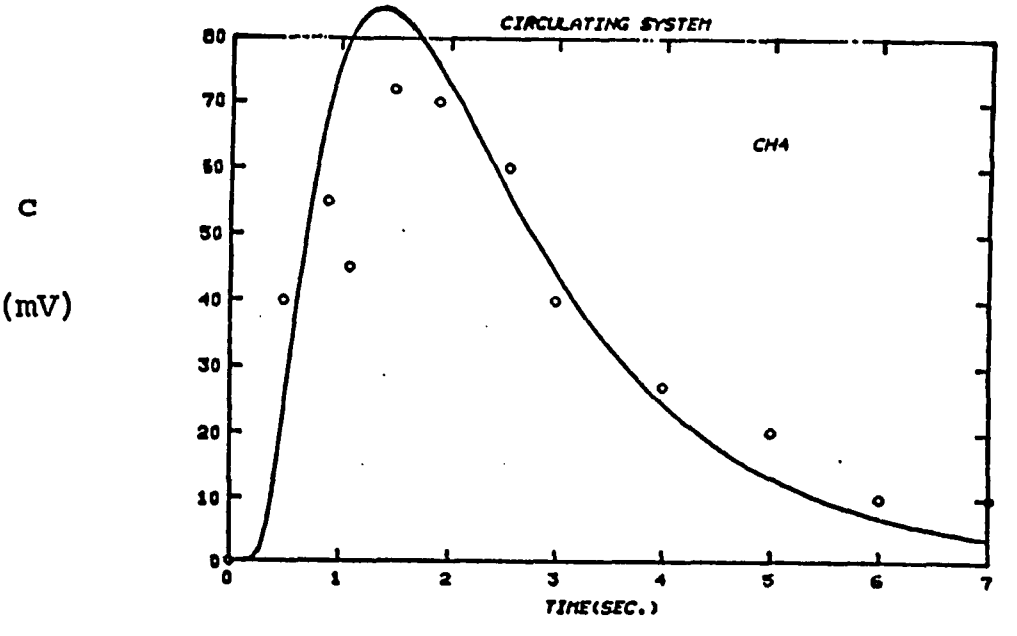

The circulating system results are summarized in Fig. 4.18. The axial dispersion coefficient rises from a value of 5×10^{-3} m^2/s for the lowest gas velocity investigated in the circulating system, 1.08 m/s, to a maximum value of $D_{sp} = 8.8 \times 10^{-2}$ m^2/s in the middle of the fast regime. The value of D_{sp} drops with the solid concentration as the superficial gas velocity is raised beyond 3.5 m/s. The following points concerning Figure 4.18 can be made:

a) The influence of solid rate is not clear and it seems not to affect the axial dispersion coefficient greatly. It is possible that a certain gas velocity, for example at $U_g = 3.5$ m/s, raising the solid rate increases D_{sp} to some extent. Kiang et al. (1975) have performed heat transfer from a heater to a fast fluidized bed experiment and they seem to indicate the same trend, beyond a superficial gas velocity of 1.5 m/s, the heat transfer coefficient does not depend on the solid recirculation rate (if that rate is not very low).

b) The dispersion coefficients at low gas velocities (1-2 m/s) in the circulating system are lower than in the expanded top bed. This feature has been elaborated on before - it is caused by the different solids recirculation modes. The expanded top bed has a higher mixing rate caused by the forced solid downflow near the walls in the turbulent fluidization regime. In the fast bed, the dispersion coefficients are higher than in the stationary expanded top bed. One should keep in mind that this dispersion is now superimposed on the external recirculation, so that the Péclet number should be considered - this will be discussed in the following section.

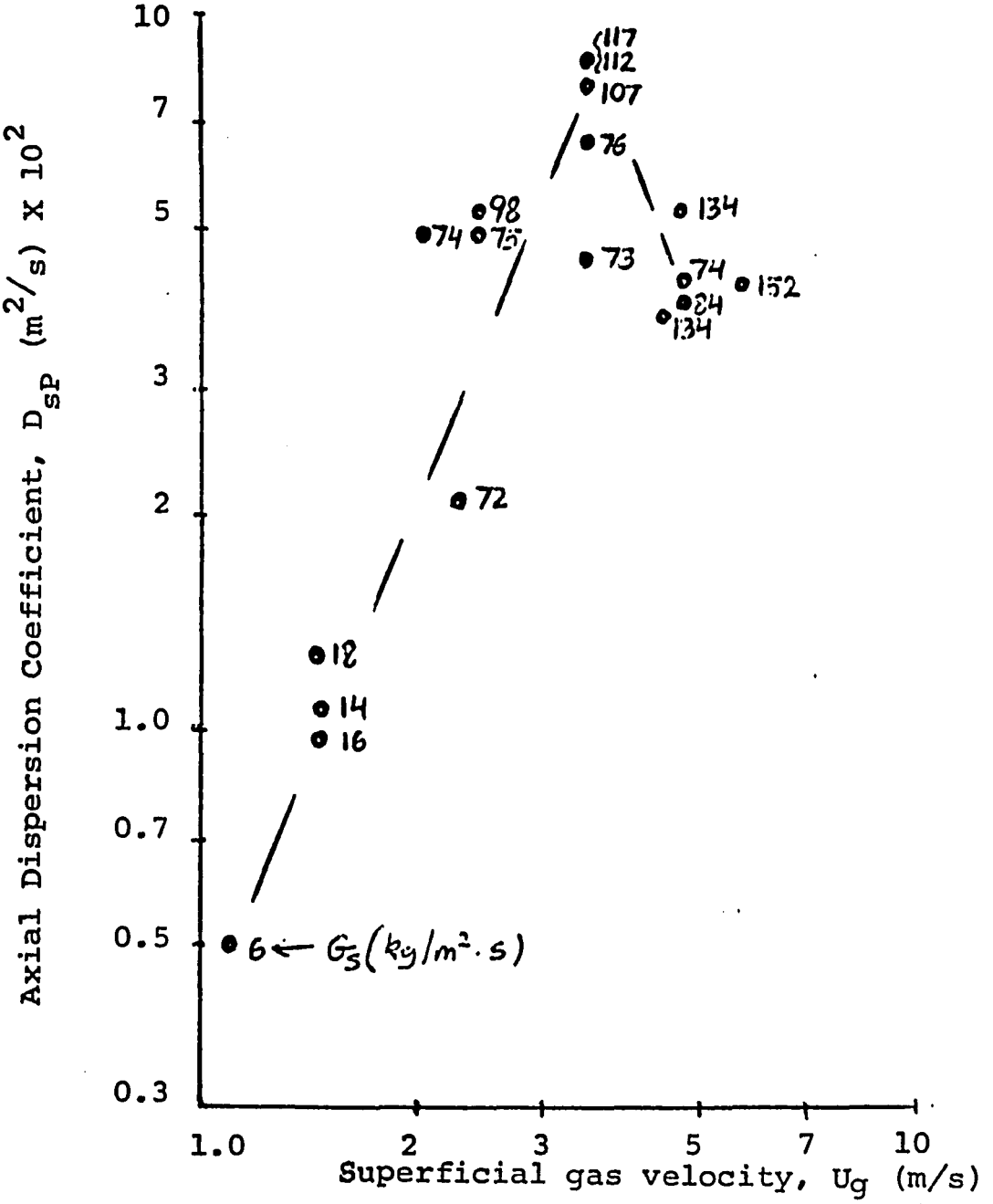

Figure 4.18: Dispersion Coefficients in the Circulating System.

4.73. Heat transfer

While no heat transfer experiments were performed, some possible implication on heat transfer in high velocity fluidized beds can be deduced. In low velocity fluidized beds, the effective thermal conductivity of the bed has often been expressed as:

$$\kappa = D_{sp}\, {}_{s}C_{p} \qquad (4.36)$$

where C_p is the solids specific heat. The results of Thiel and Potter (1978), obtained by the heat transfer method were shown to correspond to our results in Fig. 4.16. This effective thermal conductivity goes through a maximum in the slugging regime, and would probably go up again in the turbulent regime, in the expanded top bed (Fig. 4.16). It is also a function of bed height at low velocities where bubbles are still in the coalescence stage.

In the circulating system one has to consider the Péclet number, which is defined as the Prandtl number multiplied by the Reynolds number. The Péclet number indicates how important is dispersion to the mechanism of heat transfer. High Péclet numbers indicate that axial heat transfer can be described by the convective term alone, and low Péclet numbers indicate that axial dispersion predominates. The local Péclet number in the circulating system is calculated by the following relationship:

$$P_{e_L} = \frac{G_s L}{\rho_s D_{sp}} \qquad (4.37)$$

The local Péclet number at probe 4 (L = 1.42m) is shown in Fig. 4.19. Since we assume that the downstream dispersion coefficient is constant at high superficial gas velocities, the Péclet number based on the entire bed length can be

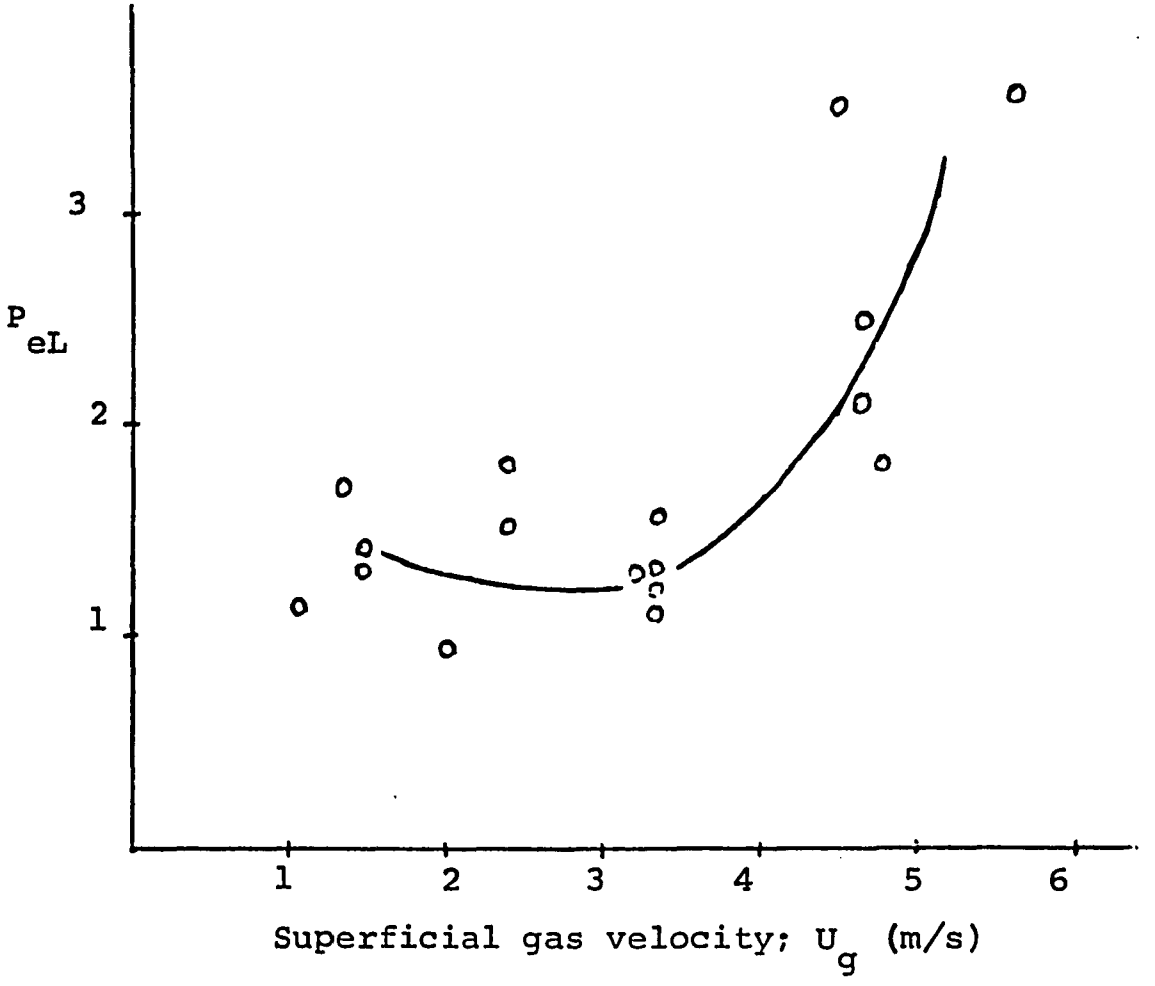

Figure 4.19: Local Péclet number in the circulating system (channel 4, L = 1.42m).

obtained by multiplying the results of figure 4.19 by a factor of 5.5. The shape of the Péclet number's variation with the gas velocity is generally the inverse of the variation of the axial dispersion coefficient. Péclet numbers between 1-2 at probe 4, and 0.5-1 at probe 3, at gas velocities of up to 4.5 m/s indicate that solid mixing and heat transfer by the dispersion mechanism is of the same order of magnitude as by the convection term. When one looks at the whole bed, one obtains Péclet numbers between 5-10 for the same velocity range. This could possibly mean that heat transfer between a combustion zone at the bottom of the bed and a section 7.5 meters above it is mostly by convection brought about by the external solid circulation, but dispersion is not negligible. When the gas velocity is raised beyond 4.5 m/s, the dispersion mechanism becomes progressively less important.

Solid mixing and heat transfer upstream:

Our experiments do not give a conclusive answer for the dispersion coefficients upstream (Probes 1 and 2). The lower velocity runs, C2 through C7, which cover the turbulent and the beginning of the fast fluidization regimes, show the same dispersion upstream as the downstream results. Runs C8 to C12, in the midst of the fast fluidization regime show tracer penetration at probes 1 and 2 but the dispersion coefficients seem slightly lower. Some of the computer results fitting equation 4.32 to the experimental results of the upstream probes are shown in figure 4.20. Runs C13-C19, in the upper velocity region of the fast fluidization regime, show little penetration of tracer upstream, except for channel 2 of run C18 (which is fitted with a dispersion coefficient slightly

a) RUN C 2

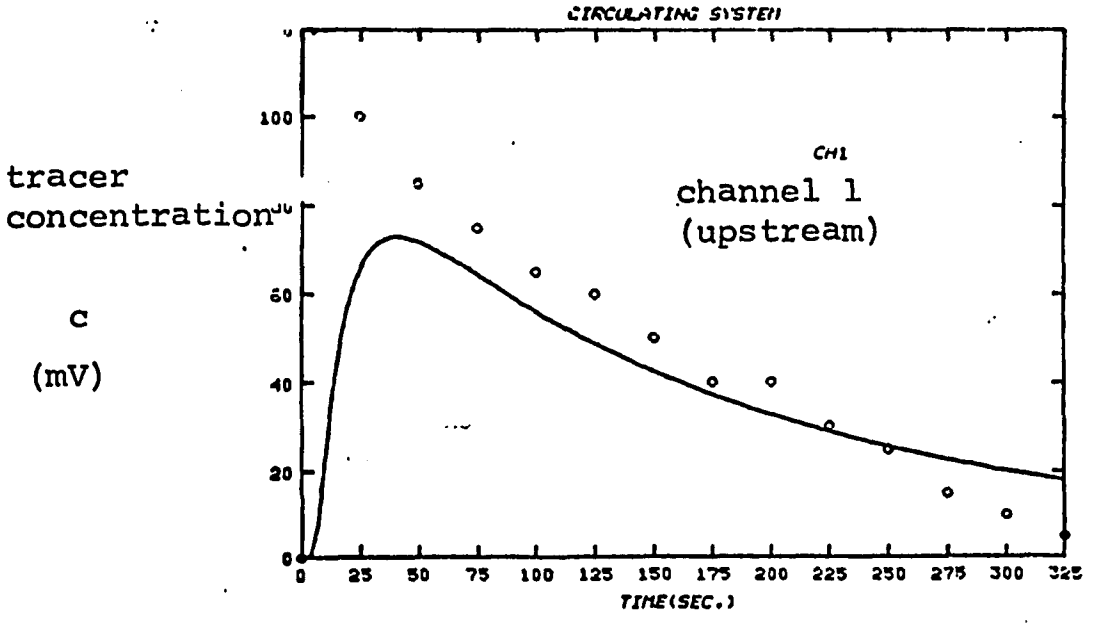

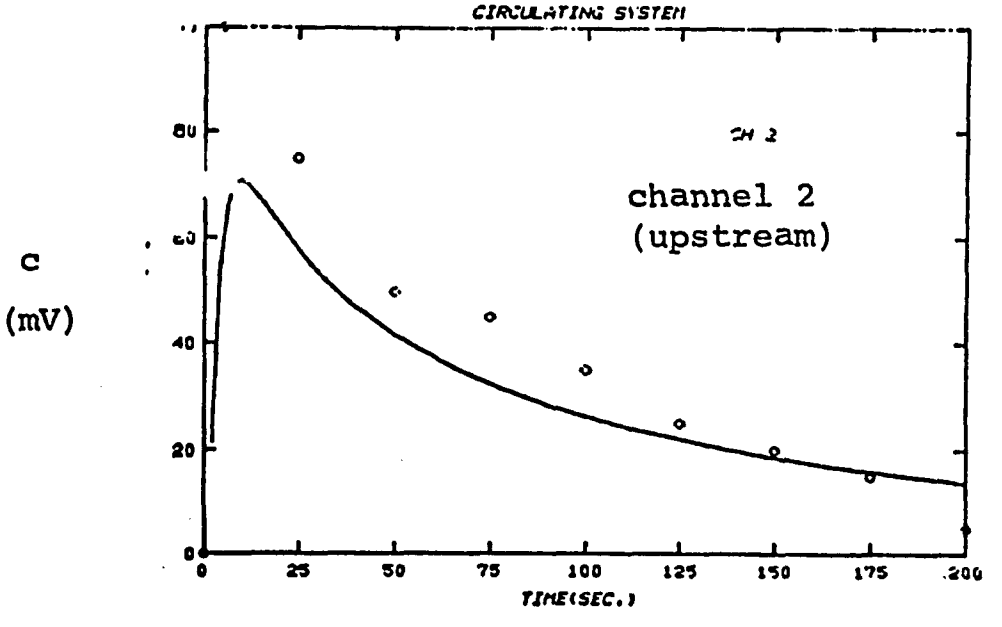

Figure 4.20: The dispersion model fitted to the eperimntal results- upstream probes, the circulating system.

Figure 4.20b RUN C 5

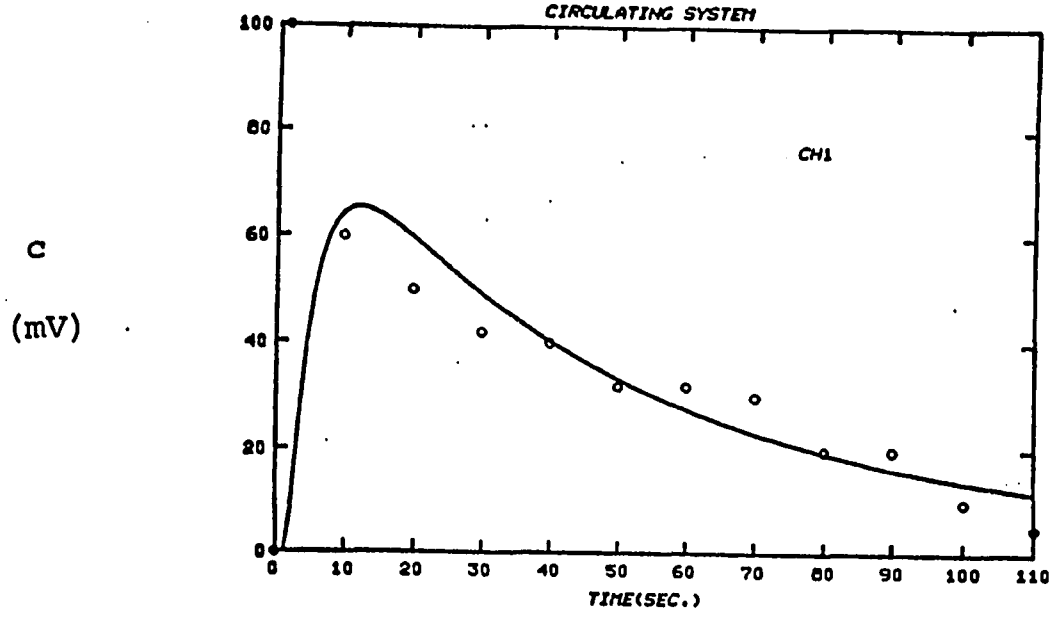

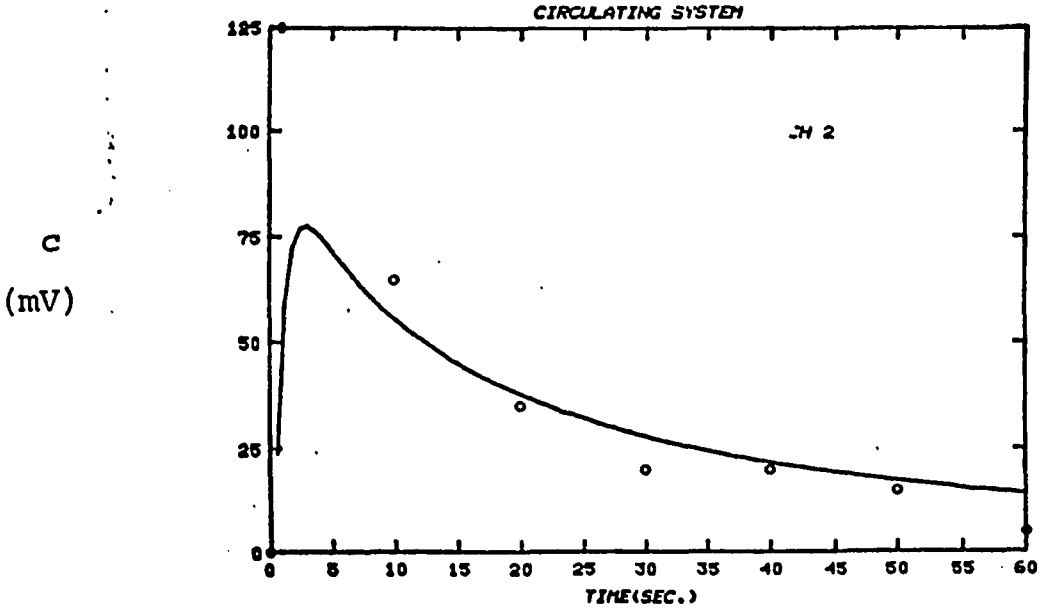

Figure 4.20 c : RUN C 7

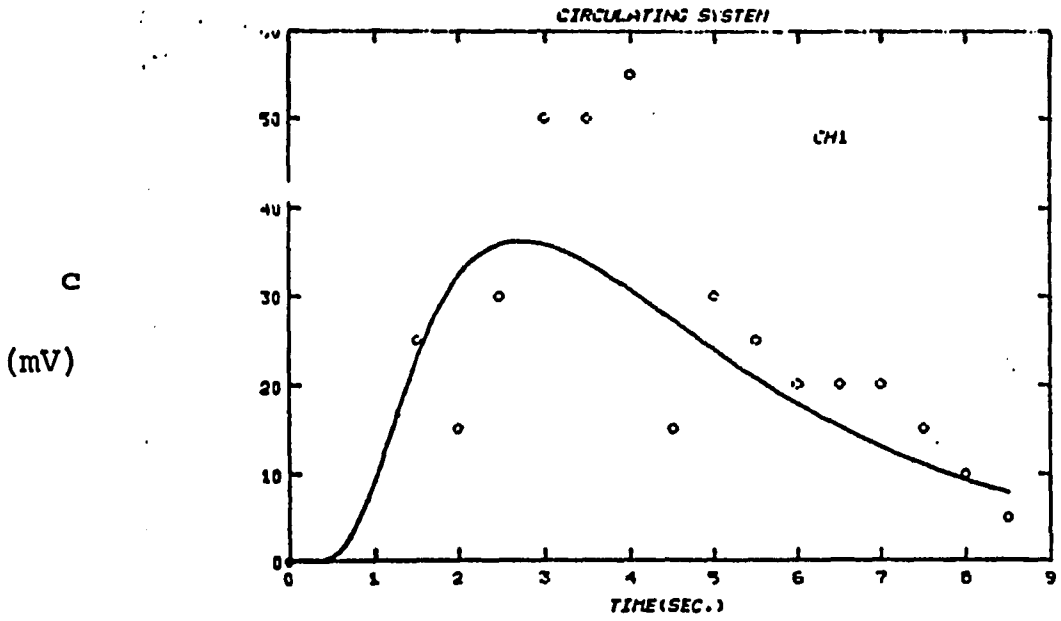

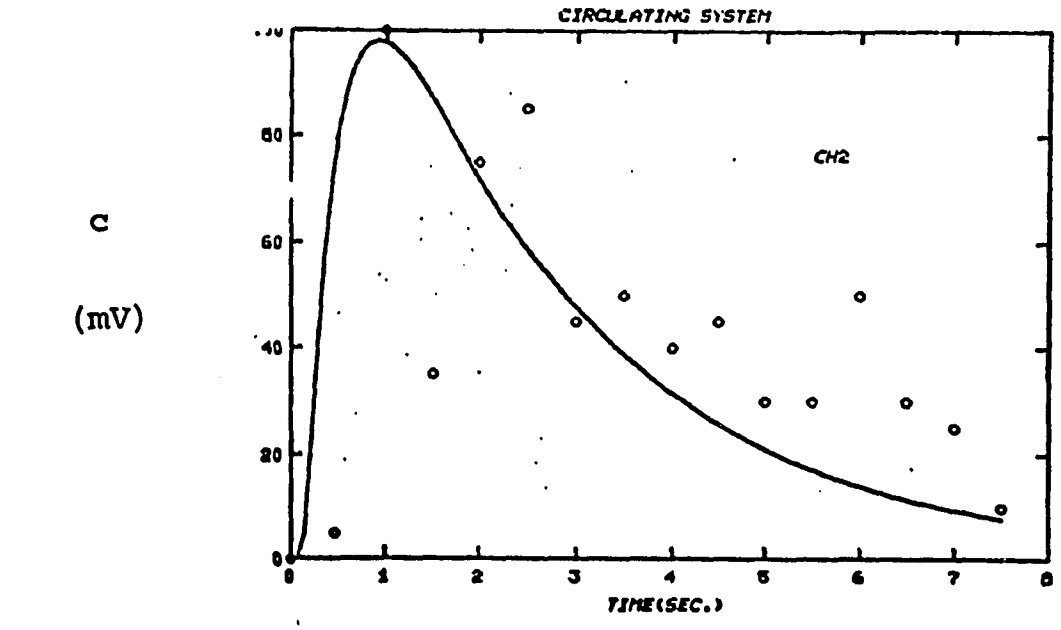

Figur 4.20 d: RUN C 11

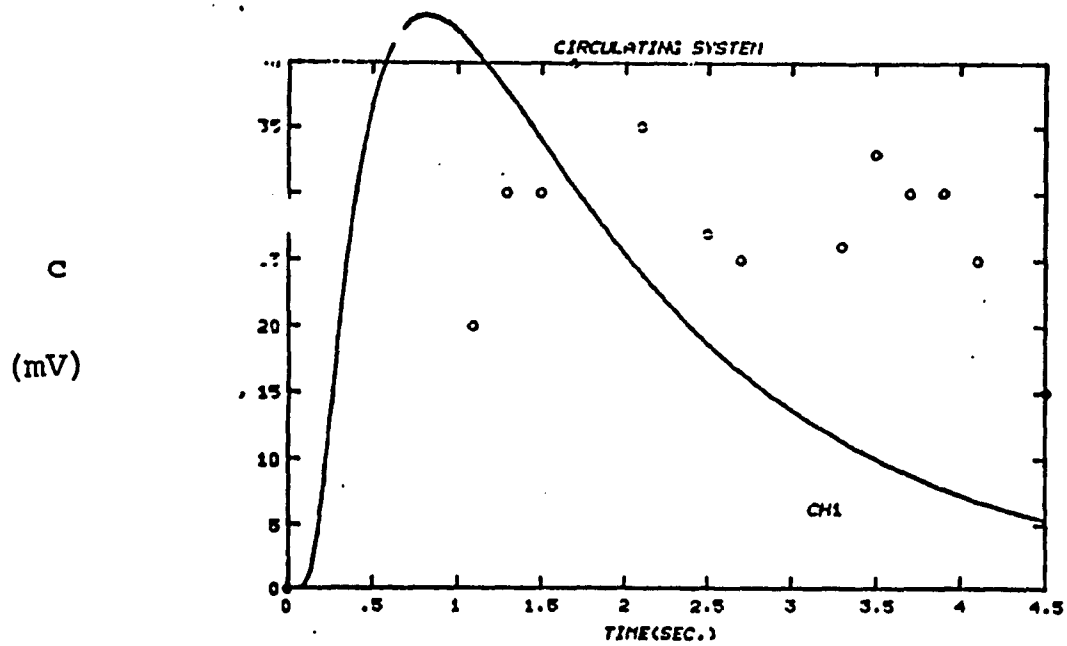

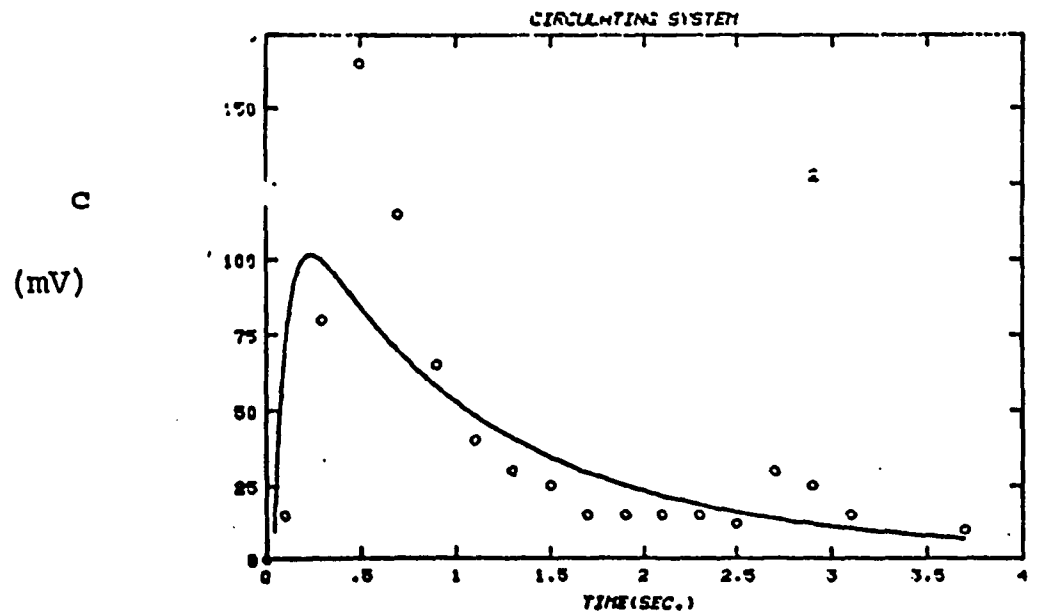

Figure 4.20e RUN C 12

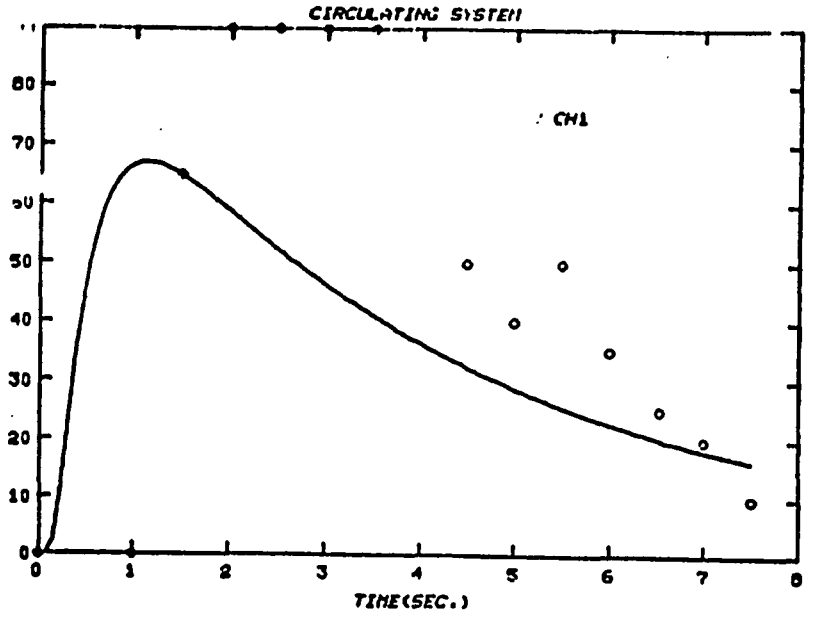

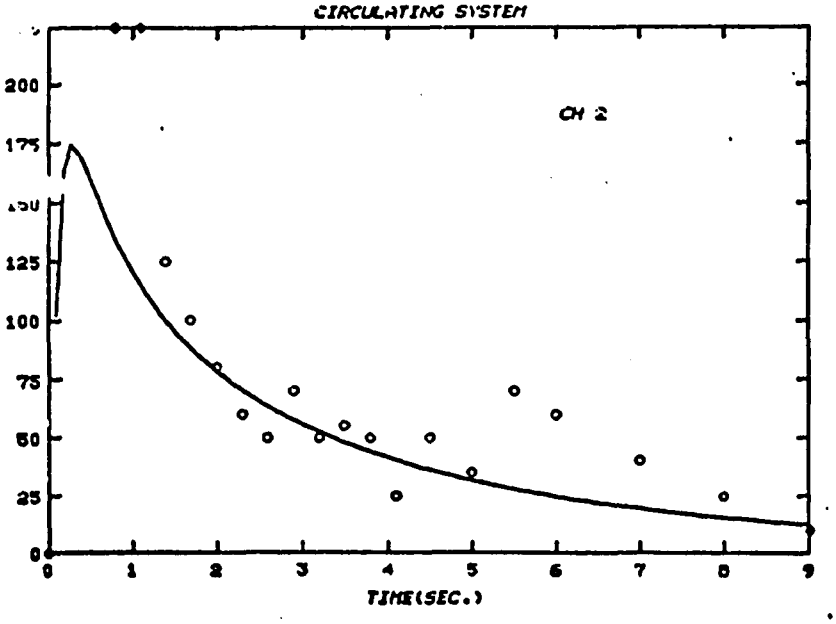

lower than the one obtained downstream). Examination of the experimental results show little response in the downstream channels too. The reason for this is the lower solid concentrations at these high velocities. It seems that larger quantities of tracer should have been used for these high velocities.

These observations can be summarized as follows:

a) In the turbulent and the beginning of the fast fluidization regimes it seems that the upstream dispersion coefficients are the same as the downstream ones.

b) In the rest of the fast fluidization regime ($3.5 < U_g < 5.5$ m/s) it is possible that the upstream dispersion coefficients are slightly lower than those obtained for the downstream probes.

c) If the preceding points are correct, then heat transfer in the turbulent bed should be the same in both the upstream and the downstream directions. In the fast bed, it is possible that the upstream dispersion coefficients are slightly lower than the downstream ones. At superficial gas velocities higher than 3.5 m/s, figure 4.19 shows the local Péclet number to rise above 1 and this raises the question of how deep a penetration does a fast fluidized bed allow for heat transfer in the upstream direction. This question can not be answered at the present. Is it possible to maintain a high temperature zone at the top of a fast fluidized bed and low temperature zone, say 10 meters below it?

The dispersion mechanism in the fast fluidized bed was described as an "effective" Taylor dispersion, caused by the solids velocity profile. The physical picture could possibly consist of particles rising in the center, being pushed to

the lower velocity wall region, and after being held up there, continue their upflow progress. This mechanism of "mixing cells" would explain the high overall slip velocity. At this point it is not clear to us if the downflow at the walls is top-to-bottom, or of the "mixing cell" type. It is also possible to speculate an additional heat transfer mechanism, from aggregates of particles in one "mixing cell" to those, say, below them, without particles actually crossing from the higher to the lower zone. It seems that the only way to answer these questions is to perform heat transfer experiments where the top of the bed will be heated up and the upstream temperature measured.

4.8 The Steady State Fluctuation Method and the Effect of Bed Diameter

The dispersion coefficients in a fluidized bed can also be calculated from the steady state density fluctuations and this method also throws some light on the effect of bed diameter on them. Following Todes et al. (1972) consider an element of volume dv', which in our case can be the effective volume that a probe senses. The transition probability of a particle from the point corresponding to the radius vector $\vec{r}$ into the volume element dv' near that point in the time t is:

$$P(\vec{r},\vec{r}',t)dv' = \exp\left[-\frac{(\vec{r}-\vec{r}')^2}{4D_{SA}t}\right]\frac{dv'}{(4\pi D_{SA}t)^{3/2}} \qquad (4.38)$$

Equation 4.38 can be recognized as a Gaussian distribution, or a three dimensional solution of random diffusion. The dispersion coefficient can be obtained from equation 4.38 by (Todes et al., 1972):

$$D_{SA} = 2\pi\ell^2(1-P)^2\left[\frac{\overline{(\Delta\nu_\tau)^2}}{\overline{(\Delta\nu_\tau)^2}_{\tau\to\infty}}\cdot\frac{1}{\tau}\right]_{\tau\to 0} \qquad (4.39)$$

where:

a) P is the probability of a particle being in the volume element considered. In our case $P<<1$.

b) ℓ is the average radius of the volume element, taken here to be $D_t/2$.

c) ν is the instantaneous number of particles in the volume element.

d) τ is the interval between successive measurements.

Here we assume that the probe reading at steady state is proportional to the number of particles in the volume element to which the probe is sensitive. We further assume that particles move in random turbulent eddies. The latter is a more questionable assumption, considering the predominant flow patterns described before.

If one considers τ to be half the period of oscillation, T, equation 4.39 can be simplified to:

$$D_{SA} = \left(\frac{D_t}{T}\right)^2 \frac{4\pi}{T} \qquad (4.40)$$

Equation 4.40 gives a simple way to calculate the dispersion coefficients if one can obtain the frequency of the fluctuations of density. Examination of the experimental results suggests that this is an easy task at the low gas velocities, especially in the slugging regime. The higher gas velocities seem to offer a multitude of frequencies, superimposed one on top of the other. This suggests a distribution of eddy sizes which is responsible for the mixing mechanism. While this conclusion is not surprising, it is not always easy to average these frequencies, or to extract the predominant one. Some dispersion coefficients were calculated from equation 4.40 and they were shown in figures 4.15 and 4.16 to agree with the dispersion coefficients calculated from the transient response. Note that equation 4.40 can be directly obtained from the theory of turbulence. The first term on the right hand side of equation 4.40 can be recognized as the eddy scale and the second term as the frequency.

In the slugging bed one can represent the frequency T as:

$$T = \frac{XD_t}{(U_g - U_o + 0.35(gD_t)^{\frac{1}{2}})} \qquad (4.41)$$

where X is the spacing between slugs divided by the bed diameter. Substituting equation 4.41 into equation 4.40 gives:

$$D_{SA} = \frac{\pi}{X} D_t (U_g - U_o + 0.35 (gD_t)^{\frac{1}{2}}) \qquad (4.42)$$

It is interesting to compare equation 4.42 to the equation obtained by Thiel and Potter (1973) on the basis of a two phase slug model:

$$D_{SA} = \frac{a^2}{2} (1-\epsilon_o) X D_t (U_g - U_o + 0.35 (gD_t)^{\frac{1}{2}}) \qquad (4.43)$$

In Thiel and Potter's equation (equation 4.43), a is the fraction of the interslug volume which is perfectly mixed, a fitted parameter. The main difference between our equation, 4.42 and equation 4.43 is the position of the parameter X. Does the interslug spacing decrease or increase the dispersion coefficient? It seems to me that the higher the value of X, the lower is the effective mixing. If this indeed is the case, equation 4.42 is of the right form.

Equation 4.42 also suggests that in the slugging regime, the axial dispersion coefficient is linearly proportional to the bed diameter. If the inverse relationship between the frequency and bed diameter holds in the higher velocity regimes as well, it is possible that the dispersion coefficient is linearly proportional to bed diameter at these velocities as well. The result of May (1959) are reproduced in figure 4.21 and they seem to confirm the linear dependence of the axial solids diffusivity on bed diameter up to bed diameters of about 1.5 m. The estimated results for 6.1 m bed clearly show that the axial solids diffusivity does not

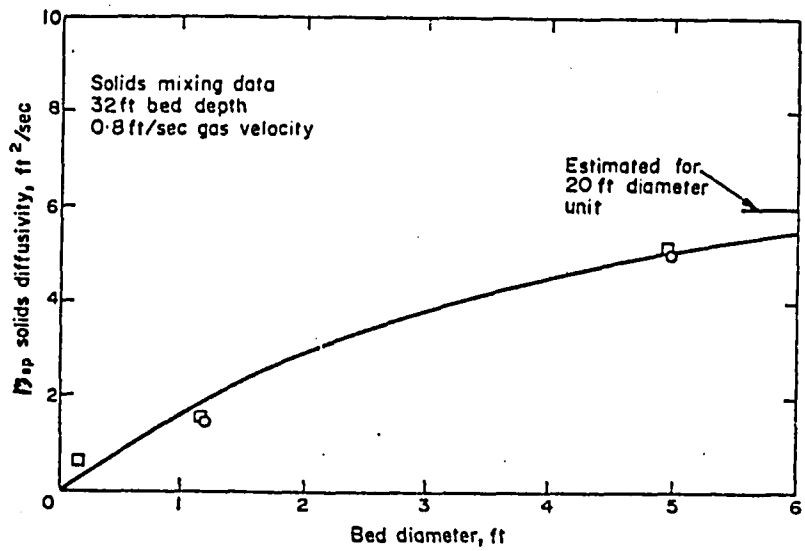

Figure 4.21: Axial solids diffusivity as influenced by bed diameter (May, 1959).

increase beyond its value at 1.5 m. This seems to agree well with our interpretation. Consider equation 4.40, where $D_t/2$ was considered as the turbulent eddy scale. One can no longer make this claim for a 6.1 m bed, where the turbulent eddys do not seem to grow to such a "monstrous" scale.

4.9 Some Qualitative Remarks on the Comparison to Liquid-solid Systems

The previous section, as well as some of the conclusions from our expansion data suggests that a high velocity gas fluidized bed of fine particles is more uniform than a two phase, aggregative low velocity bed. If the turbulent and fast fluidization regimes can be considered as "semi-particulate" some comparison to liquid solid systems is justified. Turbulence theory has been applied to such systems by Hanratty et al. (1956). They consider a turbulent field composed of a distribution of eddies ranging in size from dimensions too small to be measured to the dimensions of the container, much like the turbulent field suggested by our steady state density fluctuations. One of their interesting conclusions is that the Péclet number goes through a minimum at a value of $\epsilon = 0.70$. At this voidage they also show that the scale of turbulence goes through a maximum. This compares favorably with our figure 4.18 for the dispersion coefficient and figure 4.19 for the Péclet number, if one considers the difference between coarse and fine particles.

Consider the following analysis suggested by Al-Dibouni and Garside (1979). The solids concentration in the bed is $1-\epsilon$, and this is proportional to the particle concentration. The collision frequency is shown to be proportional to $U_g(1-\epsilon)$ and if one uses the Richardson-Zaki equation, the frequency is proportional to $\epsilon^n(1-\epsilon)$. The maximum collision frequency can be obtained by differentiating this expression, and the result is:

$$\epsilon_{max} = \frac{n}{n+1} \qquad (4.44)$$

where ϵ_{max} is the voidage at the point of maximum mixing.

For the coarse particles used by Hanratty et al. (1956), $\epsilon_{max} = 0.71$, which agrees well with their conclusions. Using a value of n = 5.2 which was shown in table 3.5 to correspond to a fast bed of FCC at a solid rate of 100 $kg/m^2 \cdot s$, we get $\epsilon_{max} = 0.84$. The observed maximum in the axial dispersion coefficient (figure 4.18) is observed to be at a superficial gas velocity of 3/5 m/s, at which point the solid rate is around 100 $kg/m^2 \cdot s$. The voidage at this point is 0.81-0.83 (table 4.2) which agrees rather well with the value predicted by equation 4.44. This comparison reaffirms our belief that the high velocity regimes are more homogeneous than the low velocity ones. The analogy between the turbulent and fast fluidization regimes and liquid systems, and the use of turbulence theory may prove very useful in further understanding these regimes.

Chapter 5 : Conclusions

1. Bed expansion of fine powders generally cannot be adequately described by the two phase theory in the slugging or turbulent fluidization regimes. The main difficulty lies in the problem of predicting bubble size and velocity, as the gas velocity is raised beyond the bubbling regime. Only one of the powders tested, FCC, gave rise to expansion behavior in line with the two phase theory predictions. The other powders tested, as well as some reported results from the literature, usually show that the slug velocity is higher than the two phase theory predicts as the gas velocity is raised.
2. The effect of particle size distribution on bed expansion was shown to be significant. "Used" catalyst, containing half the fines fraction of "fresh" ones, were shown to give rise to higher velocity slugs, thus causing larger deviations from the two phase theory predictions for bed expansion. Results from the literature for larger bed diameter beds generally show a larger deviation than small diameter beds. This can be explained by the larger degree of "freedom" the slug/bubbles have, making predictions of their sizes or velocities unreliable.
3. Upon transition to turbulence, the heterogeneous nature of the bed first peaks, and then gives rise to a condition of increasing uniformity. Thus, the high velocity regimes are treated as more homogeneous ones, or "semi-particulate", rather than aggregative, in nature. The Richardson-Zaki approach, traditionally used to describe

expansion of particulate systems cannot be applied directly because the superficial gas velocities in the high velocity fluidization regimes are higher than the single particle terminal velocity. It is shown, however, that if one takes the phenomenon of clustering - evident in fine powders - into account, a modified Richardson-Zaki approach can successfully correlate bed expansion in the high velocity regimes. A complete expansion map, spanning fluidization regimes from the slugging, to a new postulated "dense conveying" regime, is presented for one of the powders tested, FCC. This approach is also shown to give reasonable representation of the expansion of the other powders used, as well as some of the results reported in the literature.

4. All three group A powders used in this investigation can be described by the same expansion equation in the "dense conveying" regime ($0.945 < \varepsilon < 0.98$). It is possible that because of the high voidages, all group A powders show the same expansion behavior in this regime, regardless of particle properties.
5. The index n in the modified Richardson-Zaki approach is thought of as a measure of the homogeneity of a fluidized bed. It is high in the aggregative, slugging regime, and it drops to its normal value for fine powders, in the turbulent regime ($n = 10$ in the slugging regime, $n = 5$ in the turbulent regime).
6. High values of the exponent n were thought of as anomalous in the reported literature for fine powders, and Capes (1974) presented a method to explain them by considering particle aggregation. A similar approach by

Yerushalmi is shown to give estimates of cluster voidage. The cluster voidage in the turbulent regime is shown to be close to minimum fluidization voidage. In the fast bed the cluster voidage depends on solid rate and does not change much with gas velocity. "Equivalent" cluster diameters are also calculated from the exponent n and they show an order of magnitude agreement to cluster diameter calculated by other methods.

7. While the index n is not a function of size distribution, U_T^* (thought to represent the effective cluster terminal velocity) is. This effective cluster velocity, calculated from the experimental results, is shown to throw some light on the phenomenon of clustering. Clustering is shown to be a complex dynamic phenomenon. Particles move in and out of clusters rapidly and thus clusters cannot be thought of as "hard spheres" of the equivalent cluster diameter, except at the lower end of the fast fluidization regime. At the latter point the average slip velocity is shown to equal $\epsilon^n U_T^*$, thus supporting the "hard sphere" model. As the gas velocity is raised, the clusters are thought to have a higher degree of freedom and the single particle properties come into play as well, causing the average slip velocity to be lower than $\epsilon^n U_T^*$. The slip velocity peaks in the dense conveying regime and is thought to approach the single particle terminal velocity as the voidage approaches unity. A uniform suspension does not seem to form with fine powders even at very high voidages, and so instead of $U_{slip} < U_T$ (hindered settling), one always observes $U_{slip} >> U_T$. In other words, while U_T serves as the

lower limit to the slip velocity in the fast and dense conveying regimes, $\varepsilon^n U_T^*$ is the higher limit. This is thought of as representative of the dual nature of clusters: as "hard spheres" (εU_T^*) and as single particles (U_T).

8. The experimental method used to study solid mixing, the ferromagnetic tracer system, is nondisruptive of the flow patterns. It provides reasonable results at all gas velocities investigated, from the bubbling to the fast fluidization regimes.
9. The two-phase model, usually used to describe mixing in low velocity fluidized beds, does not seem to be applicable to higher gas velocities. Two problems arise:
   a) On theoretical grounds one can show that in a closed or recirculating system tracer experiments alone can not yield the local fluxes. (The method of Naor, Shinnar and Katz).
   b) Except for the lowest velocities, it is hard to obtain the two-phase model parameters, especially the phase velocities, with accuracy.
10. The objections of the preceding point notwithstanding, an order of magnitude analysis for the phase velocities shows the upflow velocity in the expanded top bed to be equal to the superficial gas velocity up until well into the turbulent regime, where it seems to go down. The downflow seems to be half the superficial gas velocity.

11. A turbulent eddy, continuum approach dispersion model is used for the results from the solid mixing experiments. It is based on the following observations:
    a) The solid velocity profile can be seen to cause "Taylor-like" dispersion.
    b) Conversion in turbulent beds is not lower than a completely mixed model would predict.
    c) The eddy mixing scale seems to be of the order of magnitude of the bed diameter, (the experiments where conducted in high L/D ratio beds).
12. The axial diffusivities (or dispersion coefficients) obtained from the expanded top bed results show the previously observed maximum in the slugging regime. The results agree with previous investigations. The dispersion coefficients seem to rise again as the gas velocity is raised into the turbulent regime because of the forced solid recirculation from the top of the expanded top bed. The dispersion coefficient seems to be dependent on the axial position in the low gas velocities (where bubbles are still in the coalescence stage), and quite uniform at the higher gas velocities.
13. The dispersion coefficients downstream in the circulating system reach a peak in the middle of the fast fluidization regime ($U_g \cong 3.5$ m/s, $G_s \cong 100$ kg/m^2.s, $\epsilon \cong 0.82$) and decrease at higher gas velocities. These dispersion coefficients are of the same order of magnitude, or higher than the dispersion coefficients in the expanded top bed, except at the lower end of the turbulent regime where the different solid recirculation mode (from the bottom) is giving much lower dispersion coefficients.

14. The local Péclet numbers seems to go through a minimum (corresponding to the maximum in the dispersion coefficient discussed before). They are of the order of magnitude of 1 for probe 4, situated 1.42 in from the injector, indicating dispersion to be important at this distance. For a bed 7.5 m long, the Péclet number is of the order of 10, and is increasing when the gas velocity is increased beyond 4.5 m/s. This could possibly indicate that for the whole bed, axial heat transfer downstream is mostly by convection induced by the external circulation, but the dispersion mechanism is not negligible. This minimum in the Péclet number (or maximum mixing) is shown to qualitatively agree with predictions from liquid-solid systems. For example, the voidage at the extremum point can be predicted.

15. Dispersion coefficients (and thus probably axial heat transfer coefficients) are the same upstream and downstream in the low velocity and turbulent fluidization regimes. They seem to be slightly lower in the fast fluidization regime for the upstream direction. The question of heat transfer from a high temperature zone at the top of the bed to the lower part is speculated upon.

16. A steady state density fluctuations method is shown to yield dispersion coefficients in the low velocity regimes, well in agreement with the previously discussed method. This method also throws some light on the bed diameter dependence of the dispersion coefficients. It is thought that the axial dispersion

coefficient increases linearly with bed diameter, at least in the slugging and turbulent regimes. This increase is arrested (the results of May, 1959) at a value of $D_t \cong 1.5$m where it is thought that the turbulent eddies reach their maximum size.

References

Adler, I.L. and Happel, J. (1962), Chem. Eng. Progr. Symp. Ser. No. 38, 58, 98.

Al-Dibouni, M.R. and Garside, J. (1979), Particle Mixing and Classification in Liquid Fluidized Beds, Trans. I. Chem. E., 57, 94-103.

Aris, R. (1959), Notes on the Diffusion-Type Model for Longitudinal Mixing in Flow (Levenspiel, Smith and van der Laan), Chem. Eng. Sci., 9, 266-267.

Avidan, A.A. (1979), Flow Patterns in High-Velocity Fluidized Beds, A Research Proposal submitted to the School of Engineering, City University of New York.

Babu, S.P., et.al. (1973), Solids Mixing in Batch Operated Tapered and Non-Tapered Gas Fluidized Beds , AIChE Symp. Series, 69.

Birkhoff, G. and Carter, D. (1957), J. Rat. Mech. Anal., 6, 769.

Brekken, R.A., et.al. (1970), Fluidization of Flows in a Stirred Aerated Bed: Part II. Solids Mixing and Circulation, Chem. Eng. Prog. Symp. Series, 105, 66.

Canada, G.S., McLaughlin, M.H. and Staub, F.W. (1976), Large Particle Fluidization and Heat Transfer at High Pressures, AIChE Symp. Series, 74, No. 176, 27.

Cankurt, N.T. and Yerushalmi, J. (1978), Gas Backmixing in High Velocity Fluidized Beds, in Davidson, J.F. and Keairns, D.C. (ed.), Fluidization, Cambridge Univ. Press.

Cankurt, N.T., Turner, D.H., Avidan, A.A. and Yerushalmi, J., The Turbulent Fluidized Bed, to be published.

Capes, C.E. (1974), Particle Agglomeration and the Value of the Exponent n in the Richardson-Zaki Equation, Powder Tech., 10, 303-306.

Carotenuto, L., Crescitelli, S. and Donsi, G. (1974), High Velocity Behavior of Fluidized Beds: Characterization of Flow Regimes, La Chimica e l'Industria (Suppl.), 10, Vol. 12, 185.

Cranfield, R.R. (1972), A Probe for Bubble Detection and Measurement in Large Particle Fluidized Beds, Chem. Eng. Sci., 27, 239-245.

Crescitelli, S., Donsi, G., Russo, G. and Clift, R. (1978), High Velocity Behavior of Fluidized Beds: Slugs and Turbulent Flow, Chisa Conference, Prague.

DeLasa, H. and Gau, G. (1973), Influence des Agregats sur le Rendement d'un Reacteur a Transport Pneumatique, Chem. Eng. Sci., 28, 1875-1884.

Fitzgerald, T., et.al. (1977), Fluidized Bed Test Facility - Report on Instrumentation, supported by EPRI, Oregon State Univ., Corvallis, Oregon.

Gajdos, L.J. and Bierl, T.W. (1978), Studies in Support of Recirculating Bed Reactors for the Processing of Coal, Topical Report to the U.S. DOE, contract #EX-C-76-01-2449.

Geldart, D. (1973), Types of Gas Fluidization, Powder Tech., 7, 285-292.

Grace, J.R. and Tout, J. (1979), A Theory of Cluster Formation in Vertically Conveyed Suspensions of Intermediate Density, Trans. Inst. Chem. Eng., 57, 49.

Hanratty, T.J., Latinen, G. and Wilhelm, R.H., (1956), Turbulent Diffusion in Particulately Fluidized Beds of Particles, AIChE J. Vol. 2, No. 3, 372-380.

Happel, J. (1958), Viscous Flow in Multiparticle Systems: Slow Motion of Fluids Relative to Beds of Spherical Particles, AIChE J. 4, 197-201.

Horsler, A.G., Lacey, J.A. and Thompson, B.H. (1969), Pressurized Fluidized Beds, Chem. Eng. Progress, 65, No. 10, 59.

Hovmand, S. and Davidson, J.F. (1971), Pilot Plant and Laboratory Scale Fluidized Reactors at High Gas Velocities, the Relevance of Slug Flow, in "Fluidization", Davidson, J.F. and Harrison, D., ed., Academic Press, London.

Kehoe, P.W.K. (1969), The Effect of Particle Size on Slugging Fluidized Beds, Ph.D. Dissertation, Cambridge Univ.

Kehoe, P.W.K. and Davidson, J.F. (1970), Continuously Slugging Fluidized Beds, "Chemeca 70", Chem. Eng. Conf., Australia, Butterworth and Co. (Australia) Ltd., 97-116.

Kehoe, P.W.K. and Davidson, J.F. (1971), Continuously Slugging Fluidized Beds, Inst. Chem. Eng. (London) Symp. Ser. 33, 97.

Kiang, K.D., Liu, K.T., Nack, H. and Oxley, J.H. (1976), Heat Transfer in Fast Fluidized Beds, in "Fluidization Technology", Keairns, D.L., ed., Vol. II, p. 471, Hemisphere Publishing Corp., Washington.

Kondubov, N.B., et.al. (1964), An Investigation of the Parameters of Moving Particles in a Fluidized Bed by a Radioisotopic Method, Int. Chem. Eng., Vol. 4, No. 1, 43-47.

Kunii, D. and Levenspiel, O. (1969), "Fluidization Engineering", John Wiley & Sons, Inc., N.Y.

Lanneau, K.P. (1960), Gas-Solid Contacting in Fluidized Beds, Trans, Inst. Chem. Eng., 38, 125.

Leva, M. (1959), "Fluidization", 1st Ed., McGraw-Hill Book Co., N.Y.

Levenspiel, O. and Smith, W.K. (1957), Notes on the Diffusion-Type Model for the Longitudinal Mixing of Fluids in Flows, Chem. Eng. Sci., 6, 227-233.

Lewis, L.W. and Bowerman, E.W. (1952), Fluidization of Solid Particles in Liquids, Chem. Eng. Progr., Vol. 48, No. 12, 603-610.

Lewis, W.K. and Gilliland, E.R. (1950), Conversions of Hydro-Carbons with Suspended Catalyst, U.S. Patent 2,490,088 (February 21).

Lewis, W.K., Gilliland, E.R. and Bauer, W.C. (1949), Characteristics of Fluidized Particles, Ind. Eng. Chem., 41, 1104.

Massimilla, L. (1971), Behavior of Catalytic Beds of Fine Particles at High Gas Velocities, AIChE Symp. Series, 128, Vol. 69, 11-13.

Matson, J.M., Hovmand, S. and Davidson, J.F. (1969), Expansion of Fluidized Beds in Slug Flow, Chem. Eng. Sci., 24, 1743-1754.

May, W.G. (1959), Fluidized-Bed Reactor Studies, Chem. Eng. Progr., Vol. 55, No. 12, 49-56.

Medies, P.J., et.al. (1973), The Velocity of Granular Material Flowing in a Pneumatic Conveyor, Pneumotransport 2, BHRA Fluid Eng. Conf., England.

Merry, J.M.D. and Davidson, J.F. (1973), Gulf Stream Circulation in Shallow Fluidized Beds, Trans. Intn. Chem. Engrs., 51.

Mogan, J.P., Taylor, R.W. and Booth, F.L. (1969), A Method of Prediction of the Porosities of High-Pressure Gaseous Fluidization Systems, The Can. J. of Chem. Eng., 47, 126-130.

Mogan, J.P., Taylor, R.W. and Booth, F.L. (1970/71), The Value of the Exponent n in the Richardson and Zaki Equation for Fine Solids Fluidized with Gases Under Pressure, Powder Tech., 4, 286-289.

Murphree, E.V., Brown, C.L., Fischer, H.G.M., Gohr, E.J. and Sweeney, W.J. (1943), Fluid Catalyst Process, Ind. Eng. Chem., 35, 768.

Murphree, E.V., Brown, C.L., Gohr, E.J., Jahnig, C.E., Martin, H.Z. and Tyson, C.W. (1944), Improved Fluid Process for Catalytic Cracking, paper presented at AIChE Meeting, St. Louis, MO, November 19-21.

Naor, P., Shinnar, R. and Katz, S. (1972), Indeterminacy in the Estimation of Flow Rate and Transport Functions from Tracer Experiments in Closed Circulations, Int. J. Eng. Sci., 10, 1153-1174.

Oki, K., et.al. (1977), The Measurement of Local Velocity of Solid Particles, Powder Technology, 18.

Potter, O.E. (1971), Mixing, in "Fluidization", Davidson, J.F. and Harrison, D., ed., Academic Press, London.

Razumov, I.M., et.al., (1968), The Flow Structure in Reactors with Concurrent Gas and Solids Flow, Khim. Prom., No. 6, P. No. 5.

Reman, G.H. (1955), Effect of Gas and Solid Mixing in Fluidized Beds on Chemical Reactions, Chemistry and Ind., Jan. 15, 46-51.

Richardson, J.F. (1971), Incipient Fluidization and Particulate Systems, in "Fluidization", Davidson, J.F. and Harrison, D., ed., Academic Press, London.

Richardson, J.F. and Zaki, W.N. (1954), Sedimentation and Fluidization: Part I, Trans. Instn. Chem. Engrs., 32, 35-53.

Rowe, P.N., Santoro, L. and Yates, J.G. (1978), The Division of Gas Between Bubble and Interstitial Phases in Fluidized Beds of Fine Powders, Chem. Eng. Sci., 33, 133-140.

Shinnar, R., Katz, S. and Naor, P. (1972), Interpretation of Tracer Experiments in Recirculating Systems: An Application of Renewal Theory, unpublished.

Stewart, P.S.B. and Davidson, J.F. (1967), Powder Tech. 1, 61.

Thiel, W.J. and Potter, O.E. (1977), Slugging in Fluidized Bed, Ind. Eng. Chem. Fund., 16, 242.

Thiel, W.J. and Potter, O.E. (1978), The Mixing of Solids in Slugging Gas Fluidized Beds, AIChE J., Vol. 24, 4, 561-569.

Todes, O.M., et.al. (1972), Eluctuation Method for Determining the Effective Mixing (Diffusion) Coefficient of the Solid Phase in a Fluidized Bed and Analogous Systems, Intn. Chem. Eng., Vol. 12, No. 2, 263-270.

Turner, D.H.L. (1978), Turbulent and Fast Fluidization, Ph.D. Dissertation, The City College, City University of New York.

van Breugel, J.W., Stein, J.J.M. and de Vries, R.J. (1969-70), Isokinetic Sampling in a Dense Gas-Solids Stream, Proc. Instn. Mech. Engrs., Vol. 184 Pt. 3C, 18-23.

van Deemter, J.J. (1967), The Counter-Current Flow Model of a Gas-Solids Fluidized Bed, in Proc. Int. Symp. on Fluidization, Drinkenburg, A.A.H. (Ed.), Netherlands Univ. Press, Amsterdam.

van Swaaij, W.P.M., Buurman, C. and van Breugel, J.W. (1970), Shear Stresses on the Wall of a Dense Gas-Solids Riser, Chem. Eng. Sci., 25, 1818-1820.

van Suillichem, D.J., et.al. (1973), Slip Velocity-Measurements by a Radiotracer-Technique in Vertical Conveying Systems, Pneumotransport 2, BHRA Fluid Eng. Conf., England.

Wallis, G.B. (1969), "One-Dimensional Two-Phase Flow", McGraw-Hill, Chapter 4.

Werther, J. (1976), Convective Solids Transport in Large Diameter Gas Fluidized Beds, Powder Tech., 15.

Yerushalmi, J. (1980a), High Velocity Fluidized Beds and Their Applications, chapter prepared for "Gas Fluidization", Geldart, D. (ed), John Wiley & Sons, Ltd.

Yerushalmi, J. (1980b), Personal Communication.

Yerushalmi, J. and Cankurt, N.T. (1979), Further Studies of the Regimes of Fluidization, Powder Tech., 24, 187-205.

Yerushalmi, J. and Cankurt, N.T. (1978), High Velocity Fluidized Beds, CHEMTECH, 8, 564.

Yerushalmi, J., Cankurt, N.T., Geldart, D. and Liss, B. (1978), Flow Regimes in Vertical Gas-Solid Contact Systems, AIChE Symp. Ser. No. 176, Vol. 74, 1-13.

Yerushalmi, J., Turner, D.H. and Squires, A.M. (1976), The Fast Fluidized Bed, I&EC Proc. Des. & Dev., 15, 47.

Zenz, F.A. and Othmer, D.F. (1960), "Fluidization and Fluid-Particle Systems", Reinhold Pub. Corp., N.Y., p. 287.